A STUDY OF DEAD-END FILTRATION ENHANCED BY ELECTRIC AND ACOUSTIC FIELDS

By Melanie Claire Smythe

A Doctoral Thesis submitted
in partial fulfilment of the
requirements for the award of
Doctor of Philosophy
of Loughborough University

February 2001

To Mom and Dad

For all the love, support and
encouragement you've given me

Abstract

This thesis describes the experimental procedure and results of an investigation into the effect of electric and acoustic fields on dead end vacuum filtration. The test suspension used was low concentration titanium dioxide. Ultrasound energy was applied tangentially and electrical energy parallel to the filter medium. Varying electric field gradients were applied to the filter cell, either alone or together with the constant frequency acoustic field. The filter cell was based on a Nutsche filter, and allowed samples of cake to be taken at the end of the filtration experiment. Electric and acoustic field strengths, suspension characteristics and process parameters could all be varied independently.

Results from the experimental programme demonstrate that the use of ultrasound across the cake surface results in different effects depending on the pH of the suspension. These effects can be attributed to the variation of zeta potential with pH. At all pHs, (when used in conjunction with a $50Vcm^{-1}$ electric field), the acoustic field appears to decrease specific cake resistance and increase filtration rates. This effect is more apparent close to the Iso-electric point (IEP), where the critical voltage required for electro-filtration is higher. This suggests that the acoustic field provides only a weak driving force in comparison to the electric field or the filtration pressure. Under lower, or zero electric field strengths, the acoustic field increases specific cake resistance, and decreases filtration rates. It has been shown that the acoustic field has little or no effect on the dewatering of suspensions of concentrations higher than 1% by volume.

The forces present in a suspension subjected to an acoustic field were not within the scope of the experimental study, but a theoretical analysis of these forces was carried out. It is shown that the experimental layout prevents detailed analysis of these forces. Indeed, due to the turbulent nature of the suspension under the influence of this type of field, it is not possible to estimate the magnitude of these forces quantitatively.

Further experiments have been carried out to investigate the effect of the acoustic field on a suspension's conductivity, and explain the synergy seen to some extent in this

study, and more clearly by other authors in cross flow filtration. In static suspensions the conductivity is greatly increased by the application of ultrasound due to both ionic and colloid vibration potentials. However this is not seen during dead-end filtration, when the suspension is constantly in motion due to the vacuum driving force. This driving force and high concentrations present in the cake region hinder particle motion, and prevent the induction of vibration potentials. In other studies, the filtration orientation differs, and pressure driving forces are less. In these cases it is likely that changes in the conductivity induced by ultrasonic irradiation affects the suspension such that application of an electrical field is enhanced, giving an equivalent electric field strength higher than that applied.

Acknowledgements

TABLE OF CONTENTS

LIST OF FIGURES

LIST OF TABLES

NOTATION

Symbols not shown in this table are defined locally.

A	Cross sectional area	m^2
a	Particle radius	m
c	Sound velocity	ms^{-1}
c_m	Mass dry solids per volume of filtrate	kgm^{-3}
d	Particle separation distance	m
D	Dielectric constant	-
E	Electrical field strength	Vcm^{-1}
ΔE_K	Kinetic energy of 'particle' in acoustic field	J
F_{drag}	Drag force	N
F_x	Drag force in x direction	N
F_{xd}	Acoustic drag force acting in x direction	N
F_{yz}	Transverse component of PRF	N
F_{zd}	Gravitational drag force	N
I	Electrical current (Chapter 2),	W
	Acoustic Intensity (Chapters 3 &4)	Wm^{-2}
I_0	Equilibrium acoustic intensity	Wm^{-2}
K	Bed permeability	m^2
k	Particle wavenumber	$radm^{-1}$
k'	Specific conductance	$mhom^{-1}$
K_1	Filtration parameter	sm^{-1}
K_2	Filtration parameter	sm^{-3}
M	Specific acoustic impedance	$kgm^{-2}s^{-1}$
m_s	Mass of sphere	kg
p	Acoustic pressure	Pa
P	Instantaneous pressure	Pa
P_0	Equilibrium pressure	Pa
$\bar{P}$	Pressure amplitude	Pa
$\bar{P}_e$	Effective pressure amplitude	Pa
Q	Volumetric flow rate	m^3s^{-1}
q	Charge on a particle	C
Q_{Ceo}	Electrosmotic flowrate through filter cake	m^3/s
Q_{Meo}	Electrosmotic flowrate through filter medium	m^3/s
R	Resistance to flow	m^{-1}

s	Mass fraction of solids in slurry	-
t	Time	s
T	Temperature	K
T_o	Equilibrium temperature	K
t_c	Time at beginning of cake electroosmosis	s
U	Sphere velocity	ms^{-1}
U_o	Equilibrium sphere velocity	ms^{-1}
u_e	Electrophoretic mobility	$ms^{-1}V^{-1}$
u_{eo}	Electroosmotic mobility	$ms^{-1}V^{-1}$
u_p	Particle velocity	ms^{-1}
V	Fluid velocity	ms^{-1}
V	Cumulative volume filtered	m^3
v'	Filtrate volume per unit area of filter	m^3m^{-2}
V'	Cumulative volume due to applied electric field and filtration	m^3
V_o	Equilibrium fluid velocity	ms^{-1}
v_{eo}	Electroosmotic velocity	ms^{-1}
v_s	Stokes settling velocity	ms^{-1}
w	Total mass of dry cake per unit area	kg
x	Horizontal co-ordinate	m
Z	Cake Thickness	m
z	Vertical co-ordinate	
z_i	Ionic valency	-

Greek letters:

ΔP	Pressure drop	Pa
E	Energy term, variants described locally	J
E	Electric field strength	Vm^{-1}
ϑ	Condensation	-
Ψ_0	Surface (wall) potential	mV
Ψ_δ	Stern potential	mV
α	Specific resistance to flow	mkg^{-1}
α_0	Specific resistance to flow at unit applied pressure drop	$mkg^{-1}kPa^{-n}$
β	Compressibility (solid or fluid, see subscript)	m^3Pa^{-1}
δ	Stern layer thickness, (Chapter 2), Viscous skin depth (Chapters 3 & 4)	m m

ε	Cake porosity	-
ε_p'	Medium permittivity	$CV^{-1}m^{-1}$
ϕ	Solid volume fraction	-
ϕ_i	Ionic concentration	$molm^{-3}$
γ	Ratio of specific heats	-
ι	Acoustic attenuation coefficient	
κ	Debye-Huckel parameter	m^{-1}
μ	Dynamic fluid viscosity	Pa.s
ρ	Density	kgm^{-3}
ρ_0	Acoustic equilibrium density	kgm^{-3}
ρ_{EK}	Kinetic energy density	Jm^{-3}
ρ_{EP}	Potential energy density	Jm^{-3}
ρ_v	Volume charge density	Cm^{-3}
ρ_E	Energy density	Jm^{-3}
σ	Ratio of solid and fluid densities	-
τ	Relaxation time	s
ω	Angular acoustic frequency	$rads^{-1}$
ξ	Displacement	m
ζ	Zeta potential	mV

The following subscripts have been used throughout the text:

A	Represents particle A
a	acoustic
AV	Average
B	Represents particle B
C	Across cake
CR	Critical
eff	Effective
f	Fluid
M	Across Medium
p	Particle
rms	Root mean square
s	Solid
x,y,z	Cartesian
Z	Across thickness, Z

1   Introduction

Solid–liquid separation (SLS) as a unit operation can comprise a variety of processes including pre-treatment, concentration, separation and post-treatment. The importance of these techniques has increased over recent years as environmental pressures, energy costs and demand for higher purity products has intensified. A major method of industrial solid-liquid separation is filtration. The production of a low moisture content filter cake can lead to a more economical process when compared with the energy costs of thermal drying, and there are advantages if the batch time for cake formation can be shortened. Conversely, if the SLS process is being used as a means of liquor purification, a higher particulate removal efficiency will be beneficial to the process, with lower transportation and waste disposal costs.

Build up of cake on a filter medium increases the resistance to flow through the filter, until eventually flow ceases. In a batch filter, this results in the need to clean the medium, which may involve dismantling the filter unit, and scraping the medium clean, or there may be a backflushing procedure to remove the solid matter from the medium. The aim of this project was to investigate whether, by the utilisation of additional fields applied to a batch dead end filter, it could be made to operate in a continuous manner, by keeping the path for fluid to flow through more open. If successful this process could reduce industrial downtime for filter cleaning, by acting as a slurry thickener rather than a cake filter.

1.1 Field Assisted Filtration

Improvements to the filtration process have been demonstrated by the exploitation of phenomena such as electrokinetic, acoustic, magnetic and centrifugal forces (Muralidhara, 1988). An applied fields approach enables limitations regarding the degree of separation, purity and yield imposed by conventional filtration to be overcome. Combinations of field may increase this effect further by increasing the driving force over and above that of conventional filtration. For example, electroacoustic dewatering (EAD) has been used on sludges as a means of producing higher solids contents than are attainable using either electric or acoustic fields

separately (Muralidhara *et al*, 1985). This technology was extended to crossflow filtration by Wakeman and Tarleton (1991).

Although the phenomena of electrophoresis and electroosmosis was probably first demonstrated by Reuss in 1808, *attempts to exploit the technology and apply it to* modern industrial situations have been, until recently, limited. In 1963 Bier filed a patent for an apparatus suitable for continuous electrophoretic separation, purification and concentration of colloidal suspensions (Wakeman, 1982) The use of electric fields to improve separations was not studied in depth until recently, by for example, Moulik (1971), Yukawa *et al* (1976, 1978) and Wakeman (1986). The processes require continuous application of electric fields and are therefore energy intensive. Electrofiltration has not been widely exploited, but advances in electrode materials have enabled the technology to be used to improve filtrate flux in crossflow filters, and as an alternative to backwashing as a method of membrane cleaning.

Ultrasonics has been shown by many authors to be a potentially economical method of removing water from products, (Kowalska, 1978) and to decrease fouling of crossflow filter membranes (Tarleton, 1992). Research suggests that ultrasonic energy is a potential aid to cake deliquoring rather than a filtration technique, but whichever it is, it is important to further understand how the mechanisms associated with ultrasound affect the suspension characteristics and behaviour. It may be that ultrasound can also provide an additional driving force, in a similar way to the electric field, *during either cake* formation or cake deliquoring operations. That is, ultrasound may facilitate a more open cake and thus improve mass transfer through the filter medium.

The study has been carried out using a dead end vacuum filter, of approximately 2 litres volume, and suspensions of titanium dioxide. Electric and ultrasonic fields could be applied in normal and parallel orientations respectively to the fluid flow. These types of fields have been shown to successfully improve filtration previously in crossflow microfiltration (Tarleton, 1988) *and so this work is a natural progression.* It was envisaged that this method of filtration enhancement has an industrial relevance, in that a reduction of filter downtime has commercial benefits. The technology has been successfully used in the dewatering of biological sludges, however its use in higher value products has not been investigated. Titanium dioxide (rutile) was used, as it is a widely used white pigment. It is used to give whiteness, opacity and protection in a wide

range of consumer products including paints, plastics, paper, printing inks, ceramics, food, cosmetics and textiles. It is easily characterised, and its small particle size results in filtration difficulties.

1.2   Scope of the Thesis

Chapter 2 briefly reviews the literature describing both the experimental and theoretical studies relevant to assisted filtration. The research completed is covered in Chapter 3 onwards. Chapter 3 introduces the experimental procedure used for the filtration tests carried out in this study, and presents the results of field assisted filtration experiments. The results are discussed within Chapter 3 to keep the different parts of the study together. In Chapter 4, the mechanisms of how acoustic fields may act within the suspension are investigated, and a theoretical analysis of the forces present in the acoustic filter is attempted. Chapter 5 returns to the experimental theme and the hypothesis that the acoustic field may increase a suspensions conductivity via the colloid vibration potential is tested experimentally and discussed. Chapter 6 gives a summary of the main findings of the work and suggests areas for further work.

2 Literature Survey

Solid-liquid separation has always been an important part of the process industries. As environmental restrictions have become more stringent, and reductions in energy usage have become important commercial considerations, the efficient separation of a contaminant from a product has become a desirable goal. The separation can be achieved in a number of ways, including filtration, centrifugation, hydrocyclones, thickening and flocculation.

The behaviour of solid-liquid systems is 'history dependent', that is they are dependent on both time and previous treatments. Parameters such as settling rate, porosity and permeability vary according to the specific treatment the slurry has previously undergone.

Solid-liquid separation is generally a combination of one or more of the following stages:

1. Pre-treatment, by changing the chemical properties of the suspension, such as pH (zeta potential), the separation may be more easily achieved. For example a suspension at its iso-electric point will have maximum particle agglomeration and particles will settle more easily.

2. Concentration of the solids content

3. Separation of the solid-liquid mixture (by any of the above methods).

4. Post treatment processes

The settling rate of a suspension is generally a good guide to the method of separation, however the desired effect can often be achieved by any number of combinations of equipment and processing aids. Rapidly settling slurries can easily be separated using gravity filtration, whereas medium or slow settling materials may require vacuum or pressure filtration. Dilute materials (less than 0.1% v/v) which produce high resistance cakes are separated using deep bed filters and particles are captured within the filter media.

2.1 Filtration fundamentals

Filtration is the separation of a fluid - solids mixture involving the passage of a majority of the fluid through a porous barrier that retains most of the solid particulates contained in the mixture. Only solid-liquid separation will be considered here. The barrier which retains the solids whilst allowing liquid to pass is known as the filter medium or septum, and may be a screen, cloth, paper or bed of solids. The liquid that has passed through is termed the filtrate.

To obtain fluid flow there must be a driving force. This force is usually achieved by gravity, vacuum, pressure or centrifugal mechanisms. The driving force which induces filtrate to flow through the filter medium may be hydrostatic head, or the application of an upstream pressure, or a downstream vacuum. The required product of the filtration unit operation may be dry solids or the clarified liquid. In a filter, the medium has a relatively low initial pressure drop and particles of the same size as the pores, or larger, partially block the openings, creating smaller channels and capturing smaller particles. Thus a cake is built up. There will often be some penetration of small particles into the medium (blinding). These types of filters are typically used for higher concentrations (over 1% v/v) because lower concentrations tend to cause greater blinding of the media. Depth filters are used for dilute suspensions (concentrations less than 0.1% v/v) and the particles are captured within the filter media. The filter cake may be compressible or incompressible.

The filtration method may vary depending on the product, with optimum solids recovery obtained by cake filtration and liquid clarification suited to either cake or depth filtration. The filter may be batch or continuous, and may function as constant pressure, constant rate or variable-pressure, variable-rate systems.

Suspension characteristics such as concentration, zeta potential and cake formation rate must all be determined in order to obtain the required product, at the required specification, economically. The nature of the solid to be handled is also an important consideration, with compressibility and particle size distribution playing a large part in the choice of filter. Very small particles ($<1\,\mu m$) are colloidal in nature and are difficult to separate from their suspending fluid. Filter performance cannot easily be predicted from theory and small-scale tests are usually carried out before process equipment is

selected and sized. Tarleton and Willmer (1997) have carried out some work on filter scale up algorithms.

2.2   Derivation of the filtration equations

2.2.1   Mass balance

A material balance based on a unit filtration area gives

$$\frac{w}{s} = \frac{w}{s_C} + \rho_f v'$$

2-1

where w is the total mass of dry-cake per unit area, v', the filtrate volume per unit area, and s, and s_C are the mass fraction of solids in the slurry and the cake. (s_C is an average mass fraction) and ρ_f is the suspending liquid density.

Rearranging for w:

$$w = \frac{\rho_f s}{1 - \frac{s}{s_C}} v' = c_m v'$$

2-2

c_m is a value which represents the mass of dry solids per volume of filtrate. If s is small compared to s_C, then equation 2-2 reduces to

$$w = \rho_f s v'$$

2-3

which is valid for most dilute slurries (Tiller and Crump, 1975). The mass of dry solids is related to the cake thickness by

$$dw = \rho_s (1 - \varepsilon_{AV}) dz$$

2-4

where z represents the incremental cake thickness and ε_{AV} is the cake porosity. Integration over the entire cake yields

$$w = \rho_s \int_0^z (1 - \varepsilon_{AV}) dz = \rho_s (1 - \varepsilon_{AV}) Z$$

2-5

where Z denotes the total cake thickness, ρ_s the solid density and ε_{AV} the average cake porosity. The mass fraction of solids in the cake, s_C is related to the average porosity by

$$s_C = \frac{\rho_s (1 - \varepsilon_{AV})}{\rho_s (1 - \varepsilon_{AV}) + \rho_f \varepsilon_{AV}}$$

2-6

Combinations of equations 2-1 & 2-5 allow a number of expressions to be calculated. For example the expression

$$Z = \frac{\rho_f s \left[\sigma(1 - s_c) + s_c \right]}{\sigma(s_c - s)} v' \qquad\qquad 2\text{-}7$$

allows the cake thickness to be calculated provided the filtrate volume is known. Here σ represents the ratio of solid and fluid densities, ρ_s/ρ_f.

2.2.2   Pumping mechanisms

To understand the filtration process further the different pumping mechanisms must be elucidated. There are 3 mechanisms:

2.2.2.1   Constant pressure filtration

Most attention has been focused in this field, and the system is well understood. For incompressible cakes, provided the pressure drop across the cake (ΔP_C) remains constant, the solids mass fraction within the cake and its average porosity will also be constant. If ΔP_C varies, the linear relationship no longer holds and the cake porosity will also vary. It is this pumping mechanism which is considered in the remainder of this study.

2.2.2.2   Constant flow rate filtration

In this case the volumetric flow rate Q, is constant and it can be shown that the pressure drop ΔP is directly proportional to the filtrate volume, V.

2.2.2.3   Variable pressure, variable rate filtration

This situation is achieved by the use of a centrifugal pump to deliver the pressure head. Calculations are complex because both filtration pressure and flow rate vary. The characteristic pump curve relating pressure and flow rate is used, and the relation between time and volume is obtained by the integral of the reciprocal flow rate with respect to V.

2.2.3   Constant Pressure Filtration

Darcy's filtration equation can be used to relate the flow rate Q of a filtrate of viscosity μ through a bed of thickness Z and face area A to the driving pressure ΔP_z:

$$Q = K \frac{A \Delta P_z}{\mu Z} \qquad \qquad 2\text{-}8$$

where K is the permeability of the bed. This can be rewritten as:

$$Q = \frac{A \Delta P_z}{\mu R} \qquad \qquad 2\text{-}9$$

Where R is the resistance to flow and is equal to Z/K. Ruth (1946) modified Darcy's law to

$$\frac{d \Delta P_z}{dw} = \mu \alpha Q \qquad \qquad 2\text{-}10$$

Where α is the specific resistance to flow. The specific cake resistance α_C and porosity ε_{Av} are thus related by (using equations 2-5 and 2-10):

$$\alpha_C = \frac{1}{\rho_s (1-\varepsilon) K} \qquad \qquad 2\text{-}11$$

The specific cake resistance is constant for incompressible cakes, but will vary with pressure drop through the cake for compressible cakes. In this case as the pressure drop increases the cake becomes 'squashed', and its resistance to flow increases as the amount of voidage in the cake (porosity) decreases.

At constant pressure drop the filtrate flow rate becomes a function of time, because the liquid is presented with two resistances in series. The medium resistance is assumed constant, but the cake resistance increases with time as the cake builds up. This assumption is based on there being no penetration or blocking of the medium. The cake resistance R_C is directly proportional to the amount of cake deposited in the case of incompressible cakes, but becomes a more complex function of pressure for compressible cakes, with a varying specific resistance α_C. Accounting for cake resistance in equation 2-9:

$$Q = \frac{A \Delta P}{\mu (R_C + R_M)} \qquad \qquad 2\text{-}12$$

2.2.4   Compressible cakes

The average cake resistance, $(\alpha_c)_{AV}$ changes with pressure drop across the cake, ΔP_C, and is defined as:

$$\frac{1}{(\alpha_c)_{AV}} = \frac{1}{(\Delta P_C)} \int_0^{\Delta P_C} \frac{d(\Delta P_C)}{\alpha} \qquad\qquad 2\text{-}13$$

If the cake resistance as a function of ΔP_C is known and thus $(\alpha_c)_{AV}$ can be calculated. An empirical expression often used over a limited pressure range is (with n denoting a compressibility index):

$$\alpha = \alpha_0 (\Delta P_C)^n \qquad\qquad 2\text{-}14$$

In this case,

$$(\alpha_c)_{AV} = (1-n)\alpha_0 (\Delta P_C)^n \qquad\qquad 2\text{-}15$$

For an analytical solution for the filtration of compressible filter cakes the pressure drops across the medium and the cake must be taken separately:

$$\Delta P = \Delta P_C + \Delta P_M \qquad\qquad 2\text{-}16$$

with

$$\Delta P_M = \frac{\mu R_M Q}{A} \qquad\qquad 2\text{-}17$$

and

$$\Delta P_C = \frac{\alpha_{av} \mu w Q}{A^2} \qquad\qquad 2\text{-}18$$

Substituting for $(\alpha_c)_{AV}$:

$$\Delta P_C = (1-n)\alpha_0 \Delta P_C^n \frac{\mu w Q}{A^2} \qquad\qquad 2\text{-}19$$

from which the basic equation allowing the special case for incompressible cakes to be derived is:

$$\frac{\mu w Q}{A^2} = \frac{(\Delta P_C)^{1-n}}{(1-n)\alpha_0} \qquad\qquad 2\text{-}20$$

2.2.5   Incompressible cakes

In the special case of incompressible cakes, α_c is constant throughout the cake and the 'average' suffix can be dropped

$$R_C = \alpha_c w \qquad\qquad 2\text{-}21$$

and equation 2-12 can be modified to

$$Q = \frac{dV}{dt} = \frac{A\Delta P}{\mu(w\alpha_c + R_M)} \qquad\qquad 2\text{-}22$$

Assuming that there is a negligible amount of solids exiting with the filtrate then the mass of cake deposited, wA is given by:

$$wA = c_m V \qquad\qquad 2\text{-}23$$

where c is the mass concentration of solids in the suspension, and V is the cumulative filtrate volume. Substituting into equation 2-22 and rearranging gives:

$$\frac{1}{Q} = \frac{\mu R_M}{A\Delta P} + \frac{\mu\alpha c_m V}{A^2 \Delta P} \qquad\qquad 2\text{-}24$$

allowing the derivation of the classic filtration equation for constant pressure filtration:

$$\frac{t}{V} = \frac{\mu R_M}{A\Delta P} + \frac{\mu\alpha c_m V}{2A^2 \Delta P} \qquad\qquad 2\text{-}25$$

Most cakes are however, compressible to a certain degree, and equation 2-13 is a better starting point. Tiller (1977) notes that these expressions are approximations which lose accuracy for filtrations with short time cycles.

2.3   Cake filters

Cake filters accumulate an appreciable amount of solids on the filter medium. The feed slurry may have concentrations between 2-40%. The filter medium will be relatively open, with pore sizes greater than the minimum particle size. The cake is allowed to build up on the medium, sometimes with the initial filtrate being recirculated to the feed, until filtrate clarity is achieved. These types of filter are used when the product is either solids or the liquor. If the filtrate is the product, the cake may be blown with air or gas to remove as much liquid as possible. To obtain solids purity the cake may be washed before the drying cycle, or mechanical expression may be used to reduce its moisture content. The cake must be easy to remove and handle; after expression it is usually quite dry and compacted.

2.4   Physical Effects of Electric Fields

The principle of electroseparation is based on the electrokinetic properties associated with the particle surface. Electrokinetics is discussed extensively by Shaw (1992), Hunter (1982, 1993), Bratby (1980) and Gregory (1993) amongst others. Negatively charged particles in a suspension move to the anode by electrophoresis, where the surface charge is neutralised and they can agglomerate. Positively charged (fluid) particles move towards the cathode by electroosmosis. If the filter medium is near the cathode, then fluid will move from the pores in the cake towards the cathode, leaving a drier cake. The negative particles will move away from the medium, which decreases resistance to flow and membrane fouling.

Other electrokinetically driven forces are streaming potential and sedimentation potential. The first is essentially the opposite of electroosmosis in so far as a field is produced when the fluid moves along a charged surface, and the second occurs when a field is created by the movement of charged particles relative to the fluid, the opposite to electrophoresis. The sedimentation potential can be used to measure the effective charge on the particles in a suspension.

2.4.1   The origins of surface charge

There are three ways in which charge can be induced on a particle surface.

1. Chemical reactions at the surface.

   Solid surfaces contain readily ionisable functional groups such as -OH, -COOH, and -OPO$_3$H$_2$. The charge of particles depends on the degree of ionisation within the suspension and thus the pH of the liquid. At low pH a positive surface charge prevails.

2. Imperfections in the solid lattice.

   This occurs in materials such as clays and SiO$_2$, if one atom happens to be replaced by, for example, an aluminium atom, which has one less electron, a negative surface charge will be induced.

3. Ion adsorption.

   London-van der Waals forces or hydrogen bonding induces the charge.

2.4.2   The Electric Double Layer

A double layer is formed when the particle is in contact with a polar (aqueous) medium, and the particle obtains a surface charge. This charge may be created either by ionisation, ion adsorption or ion dissolution and determines the distribution of the nearby ions in the medium. This leads to the formation of a double layer. Stern proposed that the double layer is made up of two regions; an immobile inner layer of counter ions, directly on the particle surface, and a diffuse region. The diffuse region is affected by the influence of electrical forces and thermal motion. Particles will begin to experience repulsive forces when their diffuse layers overlap. Gouy and Chapman's model of the diffuse region of the double layer is considered by Shaw (1992) to be the simplest, and assumes that:

1. The surface is flat, uniformly charged and infinite;

2. Ions in the diffuse region are point charges distributed according to the
Boltzman distribution;

3. The solvent only influences the double layer by the dielectric constant, which
is assumed constant throughout the double layer; and

4. The electrolyte is symmetrical, with charge number z.

The inner layer is made up of ions that are the opposite charge to those of the charged surface (counter ions). It may also contain specifically adsorbed ions, which are attached to the surface by electrostatic or Van der Waals forces. The Stern theory is a modification of the Gouy and Chapman model. The Stern plane separates the inner and outer layers, and is approximately one hydrated ion radius in size. Ions with centres outside the Stern layer are considered in the diffuse region (Figure 2-1)
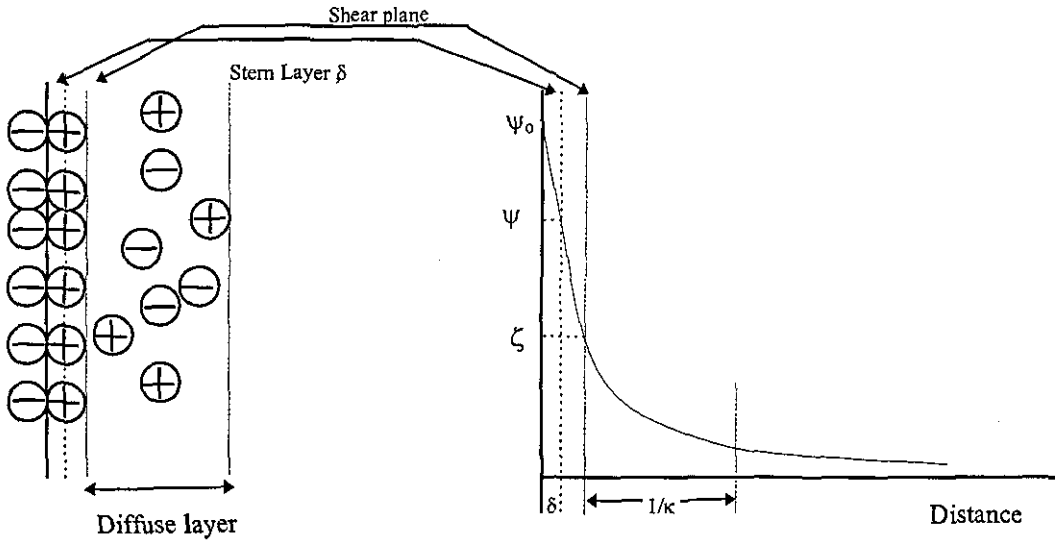
Figure 2-1: Schematic of the double layer according to Stern's theory

A radius of shear lies just outside the Stern layer, between the charged surface and the electrolyte solution. It is at this point that the zeta (electrokinetic) potential, ζ, can be measured. The electrokinetic potential at the Stern layer and at the radius of shear are assumed to be much the same, although they may differ depending on the system being considered.

The electrical potential at the surface of the particles is given by ψ_o (the surface or wall potential), and that at the Stern plane ψ_δ (the Stern potential). The potential at a point in an electric field, or in the diffuse layer is defined as the work done in moving a unit charge (of the same sign as the surface) from infinity to the point. Analysis of the exact solution is complex, but when the potential is low, the expression for the diffuse region becomes:

$$\psi_\chi = \psi_\delta \exp(-\kappa x) \qquad\qquad 2\text{-}26$$

where ψ_x is the potential a distance x from the surface, and ψ_δ is the potential at the surface. κ is known as the Debye-Huckel parameter, and is a measure of the range of the double layer. At low potentials, the potential decreases exponentially with distance from the Stern plane. Close to the charged surface, the potential is relatively high, and the approximation cannot be used, as the potential increases at a rate greater than exponential.

The Stern layer thickness is approximately one hydrated ion radius thick. $1/\kappa$ denotes the diffuse layer, the distance in the diffuse region in which the potential decreases by an exponential factor, which is known as the double layer thickness. The diffuse layer can therefore be considered as a parallel plate condenser with separation distance $1/\kappa$. In reality however the double layer extends to infinity. The double layer thickness is strongly dependent on the electrolyte concentration in the system, and for an aqueous system at 25°C is determined by (see for example Gregory , 1993)

$$\kappa = 2.3 \times 10^9 \left(\sum_i \phi_i z_i^2 \right)^{1/2} \qquad\qquad 2\text{-}27$$

where ϕ_i is the ionic concentration (mol/l) and z_i is the ion valency. The zeta potential is the potential at the position that approximately relates to the start of the diffuse region of the double layer. It is determined by measuring the velocity of the particle due to an applied electric field. When the particle has an induced velocity due to the field, the part of the double layer that is strongly bound to it remains with it as it moves. This point is the plane of shear, and the zeta potential is measured here.

2.4.3   Electrokinetic Theory

The double layer around a particle is described by the term κa. This is the ratio of the double layer radius of curvature, a, to the double layer thickness. For small κa the particle can be treated as a point of charge, and if κa is large like a flat surface. This allows different treatment according to the particle's behaviour.

2.4.3.1   Electroosmotic effect

This is defined as the movement of liquid relative to a stationary charged surface by an applied electric field. If particles are non-colloidal and are touching, then they will be unable to move when an electric field is applied. In this case the system acts as a porous medium and electroosmosis occurs. This happens on the filter medium as the cake builds up.

The theory of the electroosmotic effect was first given by Smoluchowski for large values of κa. The movement of a liquid adjacent to a large flat charged surface under an electric field applied parallel to the surface is considered. The electrical force on the liquid is opposed by a net frictional force:

$$ E\rho_v dx = -\mu \frac{dv_z}{dx^2} dx \qquad\qquad 2\text{-}28 $$

where E is the electrical field strength, ρ_v the volume's charge density, μ the liquid viscosity, x the distance from the charged surface and v_z the velocity of the liquid in a direction parallel to the wall. At the plane of shear, v_z is zero, rising to a maximum, v_{eo} a distance from the wall, where it remains constant (Shaw 1992), and the boundary conditions apply:

$$ \psi = 0, \quad v = v_{eo} \ \text{at } x = \infty $$
$$ \psi = \zeta, \quad v = 0 \quad \text{at } x = 0, \ \text{the surface of shear} $$

Integrating between a point in the bulk solution and a point in the double layer, equation 2-28 becomes:

$$ \frac{v_{eo}}{E} = u_{eo} = -\frac{\varepsilon_p{}'\zeta}{\mu} \qquad\qquad 2\text{-}29 $$

The electroosmotic mobility, u_{eo} is independent of a particle's size and shape provided the zeta potential is constant. The permittivity of the medium is given by ε'.

2.4.3.2   Electrophoretic effect

Application of an electric field across a suspension causes particles to move towards an electrode with an opposite charge. The charged particles can be made to move away from the filter medium, and form an 'open' cake. This leads to an improved filtrate rate, as there is less resistance to flow. Under the influence of an electric field the charged surface moves in the appropriate direction, with the diffuse region showing a net migration in the opposite direction, carrying the solvent with it.

The co-ordinate system used for electroosmotic theory is reversed and the movement of a solid relative to liquid considered. The solid moves with a velocity u_e equal to and opposite from that of a liquid under electroosmotic effects.

$$ u_e = -v_e = \frac{\varepsilon_p{}'\zeta}{\mu} \qquad\qquad 2\text{-}30 $$

If $\kappa a \ll 1$ the electrical forces acting on the double layer are not transmitted to the particle, which has a charge q. The electrical forces are balanced by viscous drag:

$$ qE = 6\pi\mu v_z a \qquad\qquad 2\text{-}31 $$

so

$$u_e = \frac{v_z}{E} = \frac{q}{6\pi\mu a} \qquad\qquad 2\text{-}32$$

Using the following expression to define zeta potential,

$$\zeta = \frac{q}{4\pi\varepsilon_p{}'a(1+\kappa a)} \qquad\qquad 2\text{-}33$$

and neglecting κa compared with unity, the Huckel equation is obtained;

$$u_e = \frac{2\zeta\varepsilon_p{}'}{3\mu} \qquad\qquad 2\text{-}34$$

This expression is unlikely to be applicable to particle electrophoresis in aqueous media, unless the electrolyte concentration is very low, resulting in a low value of κa. The Henry equation takes into account particle shape and size to give an equation for the electrophoretic mobility of non- conducting particles (Shaw 1992, Hunter 1981):

$$u_e = \left(\frac{2\varepsilon_p{}'\zeta}{3\mu}\right)\mathrm{f}(\kappa a) \qquad\qquad 2\text{-}35$$

The function f varies smoothly from 1 to 1.5 as κa varies from 0 to ∞. There is good agreement between zeta potentials calculated using the Huckel equation for small κa, the Smoluchowski equation for large κa, and the Henry equation. For zeta potentials over 25mV, the solution of Henry's equation becomes complex, and is improved by a more general computer aided solution by Wiersema *et al* (1966)

2.5 Physical effects of ultrasound

Two kinds of waves can travel in an unbounded medium: longitudinal (compression) waves which propagate normal to the source, and shear (transverse) waves which travel parallel to the transducer face causing shear stresses. The wave vectors can be expressed by vector functions of the form:

$$\mathbf{u} = e^{i(kx-\omega t)} \qquad\qquad 2\text{-}36$$

where k is the particle wavenumber, and ω the angular acoustic frequency. The stresses and strains can be derived from these displacement functions. Small particles move in phase with the sound field, larger ones move more slowly. If the particles collide and those collisions result in coalescence, the particle size distribution of the suspension and

hence the amplitude and phase distributions of particle motion change. This continues until the aggregated particles become too large to be affected by the frequency applied, and move out of the processing region. The magnitude of displacement will eventually become zero, and the particles will become stationary in the sound field. This phenomenon is known as a standing wave.

Standing waves can be set up in a Kundt's tube as striations. This phenomenon is the creation of alternate zones of high and low concentrations of particles, corresponding to the nodes and antinodes (or vice versa depending on the particle density). This has been modelled by Higashitani *et al* (1981). Expressions for the particle concentrations at the node and antinode are given, although it is noted that the results are difficult to reproduce using the theory proposed. The results compare well when the sources of errors are considered. Microscopic particles accumulate most readily and in the areas of high concentration there is more chance of collision. A great deal of work on separations using this phenomenon has been carried out by Benes *et al* (1993). Enderby (1951) considered the electrical effects due to sound waves in colloidal suspensions. He postulated the double layer of colloidal particles may have more effect on particle behaviour than the ions present in the bulk suspension in an acoustic field. The double layer is distorted by the fluid disturbance. This 'electro-acoustic effect' is discussed in more detail in Chapter 5. The propagation of ultrasound is further discussed in Chapter 4.

2.5.1   Mechanisms of agglomeration

2.5.1.1   Orthokinetic flocculation

Very small particles in an acoustic field move with the fluid as the elastic sound wave propagates. Particles in suspension will be affected by the energy according to the particle size distribution. In a polydisperse system smaller particles move with greater amplitudes enabling some particles to collide.. This phase impedance between the liquid and the solid can differ by a factor of between 3 and 8 (Gooberman, 1968).

2.5.1.2   Bernoulli Attraction

If particle displacement (due to the acoustic field) is much less than the fluid displacement, i.e. particle density is much greater than that of the fluid, then

hydrodynamic flow occurs. The particles cause a constriction in fluid flow past them, leading to increased flow velocity and a lower hydrostatic pressure. The Basset-Boussinesq-Oseen equation can be used to calculate the fluid force on a particle enabling the entrainment factor to be calculated for liquid systems (Shaw, 1978).

2.5.1.3 Stokes force

The local density, sound velocity and viscosity change under adiabatic compression and shear. The viscosity is larger during compression (when the temperature rises) and smaller during dilation. The overall effect is a net positive Stokes force.

2.5.1.4 Radiation Force

Each particle in the suspension causes radiation scatter and thus creates an energy density gradient. This gradient causes fluid flow in the direction of radiation propagation and return by a path of lower intensity. This is known as acoustic streaming or drifting, and can cause a microstirring action (Scott Fogler, 1971). In travelling waves the effect in colloidal systems is similar to that of gravity because the suspended particles are smaller than the wavelength, and the radiation pressure is small. In standing waves particles are pushed towards the velocity antinodes, where orthokinetic and hydrodynamic forces become important.

2.5.1.5 Oseen Force

If the pressure amplitude is finite, the pressure distribution tends to a sawtooth shape. The pressure gradient eventually becomes infinite and a shockwave results. The distorted wave shows a higher absorption than the sine wave.

The radiation force is small in colloidal systems compared to the Stokes and Oseen forces. The net sum of these forces is a directional force and will thus increase the chances of particle collisions. The particles approach under these forces, until they are close enough to be subject to other attractive forces, such as Van der Waals and surface tension. Cavitation will inhibit these agglomeration mechanisms. The amount of agglomeration achieved is not improved by an increased duration of insonation (Muralidhara 1987).

2.5.2   Sonic Dispersion

Sollner (1950) provides a full description of the methods of dispersion due to cavitation caused by high intensity ultrasonic fields and of ultrasonic aggregation. The cavitation acts as a destructive force, as the cavities collapse a mechanical hammering action occurs, and weak spots in a material may be broken. Sollner notes that sonically produced dispersions have no differing characteristics than dispersions created by conventional methods. The treatment is expensive, but has the advantage of a potential for sealed, sterile conditions.

2.6   Methods of improving the filtration process

As filter cake forms during the filtration process, resistance to flow increases, and filtrate flowrate is reduced. A number of methods can be used to reduce the effect of particles blocking the filter medium:

1. Cake removal by backflushing, or mechanical removal,

2. Crossflow filtration, with bulk flow tangential to the filter surface, reduces solids accumulation at the filter surface,

3. Reduction of cake resistance by chemical methods such as flocculation,

4. Prevention of cake formation by vibration, or by the use of electric fields.

Svarovsky (1981) gives a review of various methods for limiting cake growth such as those mentioned above, that includes chemical and mechanical methods.

2.6.1   Assisted filtration - chemical methods

Treatment of a colloidal suspension to induce agglomeration or flocculation may involve addition of chemical agents, or alteration of its pH. The enlarged particles are subsequently more easy to filter, as the degree of dispersion is reduced.

Of particular relevance to this study is the use of a D.C. voltage applied between two electrodes, one either side of the filter medium, which can also improve filtration rates. The filtration rate of fine particles is affected by their surface charge and size and the field strength applied. The field strength is affected by separation distance between electrodes, voltage, and suspension conductivity. An increase in the magnitude of the zeta potential, and the electric field strength, increases the filtration rate. The upstream

electrode has a charge opposite to that of the particles. Cake formation is limited via electrophoresis, and electro-osmosis improves filtrate flow.

2.7 Effect of electric field on membrane processes

The use of electric fields to improve separations is a well known technology. The processes require continuous application of electric fields and as such are energy intensive. Recent advances in electrode materials have enabled the technology to be used both to improve filtrate flux and as an alternative to backwashing as a method of membrane cleaning. Charges are neutralised causing agglomeration and acceleration of the dewatering rate. Also the particles will move away from the permeable electrode and cause rapid dewatering without clogging of the membrane.

2.7.1 Separation Mechanisms

The porosity of a filter cake should be increased in order to improve its dewatering rate. An electric field will allow a more open cake structure, because of the effects of electrophoresis. Wakeman (1982) studied the effects of pH and particle size on electrofiltration. An increase in the pH of the suspensions studied led to an increase in cake resistance as aggregation decreased. It was noted that the effects of pH on particle size and zeta potential need to be considered for each material. The formation of a fouling layer (in cross flow filtration) or a filter cake (in dead end filtration) reduces the filtrate volume obtained (Wakeman, 1986) as resistance to flow increases. The cross flow trajectories of particles in an electric field were considered and it was found that the electric field caused them to stay in suspension for a greater distance than when no field was applied. He suggests that only those particles fed close to the medium will contribute to fouling. Pulsing of the field improves flow through the membrane, which may be due to sudden electroosmotic flow.

Nadh Jagannadh and Muralidhara (1996) suggest the use of electric fields to prevent membrane fouling, but point out that materials with low conductivities and zeta potentials may not be affected by the electric field. Other effects due to the field occur, such as electrolysis and Joule heating, but these can be minimised. The electrical conductivity of solid-liquid suspensions varies with solids concentration (Wakeman & Holdich 1982). Hydrophobic colloids can be separated from their suspensions by

coagulation. The charge on the surface of the particles is chemically minimised and agglomeration occurs. This method fails for hydrophilic colloids, which continue to be bound to the water. Electrophoresis, however, can be used to treat both types of colloid, as it is based only on the existing surface charge of the particles

Solid-liquid separations using D.C. fields have been the most exploited. The particle surface charge in colloidal systems is utilised to make use of electrophoresis and/or electroosmosis.

2.7.2   The critical voltage

Cake formation, as seen in conventional filtration can be modified by the application of an electric field. Depending on the polarity, particles will either be attracted towards the medium and filtrate flow hindered, or under opposite polarity a more open cake can form, or in the extreme case, particles remain suspended as the fluid drag is balanced by the electrophoretic force. A critical voltage gradient is widely accepted (Moulik, 1971, Yukawa *et al*, 1976, 1978, Lee *et al* 1980, Wakeman 1981) as the field strength at which this force balance occurs and particles migrate counterflow to, and with the same velocity as, the fluid flow allowing continuous suspension of particles.

The forces acting on a particle in an electric field can be represented as in Figure 2-2, and described as follows. When $E=0$, (normal filtration), solid particles are carried to the filter surface forming a filter cake (a). If the applied voltage is increased, but is much below the critical value (b), electroosmosis occurs in the filter medium, and further increasing this causes electroosmosis in the filter cake (c). In both these cases some filter cake will form. When the applied field is equal to the critical voltage (d), the forces are completely balanced, and no filter cake is formed as the particles remain stationary. Above the critical voltage, (e), no filter cake forms and particles move countercurrent to the direction of filtrate flow.
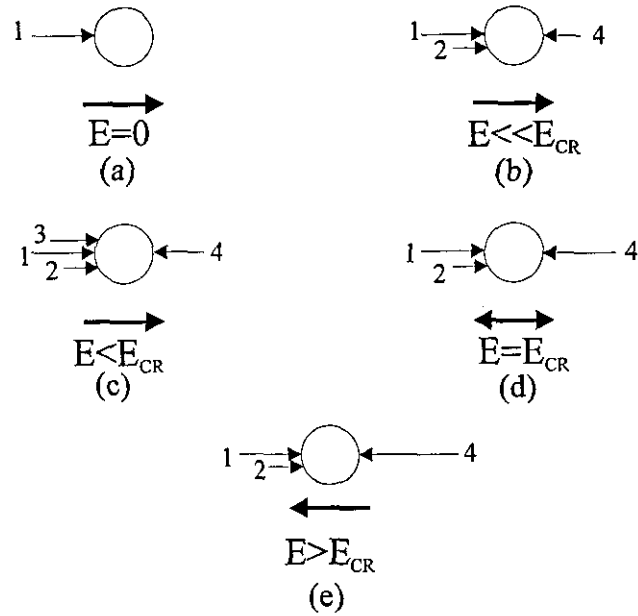
1= Normal filtration force   2= Filter medium electroosmotic force

3= Cake electroosmotic force   4= Electrophoretic force

Figure 2-2: Forces acting on colloid particles in electric fields (after Moulik , 1971)

2.7.3   Modelling of electrofiltration

Moulik, Cooper and Bier (1967) present a preliminary theory of filtration in a D.C. electric field. The Darcy equation for constant pressure filtration is modified to account for the effects on the membrane resistances as caused by the electric field. The problem of pore blocking is shown to be dramatically reduced by the application of the correct polarity (filter medium is cathode) and magnitude of D.C. electric field to the suspension. Application of the incorrect polarity can hinder or even cease filtration as the particles are forced towards the filter medium by electrophoresis and block the pores.

The physical phenomena suggested by Moulik (1971) to account for these changes are as follows:

2.7.3.1   Filter medium electroosmosis

Electroosmosis occurs in the pores of filter media in the same direction as fluid flow. The double layer between the filter pore surface and suspension controls the movement. Smoluchowski related electroosmotic flow, Q_{eo}, to zeta potential by

$$Q_{eo} = \frac{D\zeta I}{4\pi\mu k'} = C\frac{\zeta I}{k'} \qquad\qquad 2\text{-}37$$

where, k' and I represent the specific conductance of the solution and the current flowing through it. The total volume flowrate under an applied voltage is:

$$\frac{dV'}{dt} = \frac{dV}{dt} + Q_{eo} \qquad\qquad 2\text{-}38$$

Under the influence of filter medium electroosmosis, Moulik, Cooper and Bier (1967) state that the medium resistance is reduced according to:

$$R'_M = \frac{R_M}{\left(Q + C\frac{\zeta I}{k'}\right)\Big/Q} = \frac{R_M}{\left(1 + C\frac{\zeta I}{Qk'}\right)} \qquad\qquad 2\text{-}39$$

remembering that Q represents dV/dt (the mother liquor flow rate through the filter medium at zero voltage).

2.7.3.2   Filter cake electroosmosis

This phenomenon is controlled by the potential of the double layer formed between the cake pore surface and the suspension. The cake must be a certain thickness before this occurs, and so occurs after the start of filtration. A resistance correction is not possible, and so a volume correction factor is suggested (Moulik, 1971):

$$\overline{V} = V - (t - t_0)Q_{Ceo} \qquad\qquad 2\text{-}40$$

2.7.3.3   Particle Electrophoresis

If $E < E_{CR}$ filtration flow is given by the sum of the 'normal' filtration rate and that of the electroosmotic flow through the cake and membrane. At this voltage, cake will form, because particles have net flow towards the filter. Under constant pressure filtration, the rate of cake formation is controlled by a balance between the applied pressure and the voltage applied. The extent of cake deposition is proportional to

(1-E/E_{CR}), with E/E_{CR} being the fraction of cake which does not deposit (due to the action of the electric field). The cake thickness can be calculated by:

$$Z' = Z\left(1 - \frac{E}{E_{CR}}\right)$$ 2-41

Moulik (1971) proposes modification of the filtration equation (2-24) to account for these electrokinetic phenomena on filtration. When $E < E_{CR}$ the process can be described by:

$$\frac{t}{V} = \frac{t}{\{V - (t - t_c)Q_{Ceo}\}} = \frac{\mu \alpha_{av} Q_{Meo}}{2 \Delta P A^2}\left(1 - \frac{E}{E_{CR}}\right)\{V - (t - t_c)Q_{Ceo}\} + \frac{\mu R_M}{\Delta P A\left(1 + \frac{C\zeta}{k'Q}\right)}$$

2-42

At this point electroosmosis is present, however if the cake is thin, cake electroosmosis may become negligible, and (2-42) reduces to:

$$\frac{t}{V} = \left(\frac{\mu \alpha_{av} Q_{Meo}}{2 \Delta P A^2}\right)\left(1 - \frac{E}{E_{CR}}\right)V + \frac{\mu R_M}{\Delta P A\left(1 + \frac{C\zeta}{k'Q}\right)}$$ 2-43

At the critical voltage, $E = E_{CR}$ and further simplification yields:

$$\frac{t}{V} = \frac{\mu R_M}{\Delta P A\left(1 + \frac{C\zeta}{k'Q}\right)}$$ 2-44

These equations were verified experimentally, by Moulik, by plotting t/V against V for a number of suspensions representing typical wastewaters. The decrease in intercept as the applied voltage is increased is evidence of the filter medium resistance reduction theory. The applied field is seen to have a large effect on the cake resistance, but not on R_M. A similar reduction in gradient for the same conditions is an indicator of decreased filter cake build up (decreased resistance). At the critical voltage:

$$Q_{CR} = Q + Q_{Meo} = u_e E_{CR} A$$ 2-45

where u_e is the electrophoretic mobility of the suspended particles. So for any given filtration rate, a precise knowledge of u_e, A and Q_{Meo} allows calculation of E_{CR}.

Further work has been carried out by Wakeman (1982), who has confirmed that D.C. fields are useful for preventing particle deposition at the filtering surface, and also

concluded that electrolyte pH has a great effect on slurry properties and the electrofiltration process is applicable to suspensions which form high resistance deposits.

Yukawa *et al* (1976, 1978) modelled electroosmotic dewatering of sludge at constant electric current and at constant voltage. The model was based on electroosmotic flow through the particle packed bed. For the materials studied the dewatering flow rate and dewatered volume increased in proportion to the electric current density. The proposed model agreed well with the experimental results. Electroosmotic dewatering was very effective for materials which were difficult to separate by gravity, with the dewatered volume by electroosmosis being around 4 times that of vacuum dewatering.

Dewatering of sludge at constant electric current showed both primary and secondary dewatering. The distinction was made at the point where the voltage rapidly increased, requiring a large power consumption. This was due to an increase in the electric resistance of the sludge bed, as the water content of the sludge changed. Secondary dewatering showed complex phenomena and was not found to occur during electroosmotic dewatering at constant voltage.

Dewatering at constant voltage showed a terminal water content which was independent of the applied voltage for a given material. This was the sum of the volumes dewatered by electroosmosis and by gravity. Expressions for the dewatered volume by electroosmosis for conditions of constant voltage and for the power consumption were given. The electric resistance of the sludge bed increased until the dewatered volume reached a terminal value.

2.7.4   Electric fields in cross flow microfiltration

Crossflow filtration systems use high velocity flow parallel to a semi-permeable membrane. Microfiltration allows separation in ranges over 0.1-10 microns, allowing greater filtrate flux over ultrafiltration. A filter cake does not form as in dead end filtration, however particles do accumulate at the membrane surface and a gel or cake may form. This, and 'particle polarisation' are widely accepted as major causes of the loss of performance of crossflow microfiltration and ultrafiltration systems. Techniques using electric fields to minimise this fouling have been widely researched, most notably by Wakeman and Tarleton, (1982, 1986, 1987), Tarleton and Wakeman (1988) and

Tarleton (1986), but also Lee *et al* (1980),Moulik (1971) and Akay and Wakeman (1996) amongst others.

Wakeman and Tarleton (1986) calculated particle trajectories for particles introduced to a tubular filter close to and some distance from the filter septum. Those particles fed some distance from the septum showed no tendency to approach, and the conclusion was drawn that only particles fed close to the filter surface contribute to fouling in a crossflow microfilter. The application of a potential gradient enabled the particles to remain in suspension for a greater distance along the filter due to the induced electrophoretic velocity. An interesting phenomena was that under prolonged field application, particles which were deposited became re-entrained due to the hydrodynamic drag force holding particles together at the surface falling to such a level that it is smaller than the combined shear and electrophoretic effects. Pulsing of the field was seen to increase flux by inducing electroosmosis. The model presented was based on a combination of the boundary layer effect as described by Lee *et al* (1980) and the critical voltage hypothesis for dead end filtration postulated by Moulik (1971), Yukawa *et al* (1976) and Wakeman (1982). It is possible to calculate the field strength required to prevent a particle contacting the filter surface for any set of operating conditions by calculating the trajectory of a particle entering the annular space between electrodes.

Electrophoretic separation of TiO_2 has also been studied by Majmudar *et al* (1994). Their separator operates by the insertion of an electrode array into an elongated funnel. The titania particles are attracted to the anode, and a thickened slurry is intermittently removed from the bottom of the vessel. Separation seemed to be excellent, although the feed particle concentrations were very low (100 ppm). Electrode separation was small, 5mm, and voltages up to 50 V were applied. The suggested applied voltage is 15 V and a suspension flow rate of 200 mlh^{-1}.

2.8 Acoustic and Electroacoustic membrane processes

Ultrasonics has been shown to be a potentially economical means of removing water from products to relatively low levels and to decrease fouling of membranes. It is implied by Fairbanks (1967), that this is a dewatering rather than a filtration technique, and thus the mechanisms proposed focus on how ultrasound affects suspension characteristics. It may be that the ultrasonic energy provides an additional driving force,

in the same way that an electric field is considered to. That is ultrasound should be considered an aid to filtration and by facilitating a more open cake can improve mass transfer through the membrane.

Conventional dewatering removes only bulk water, but ultrasonic dewatering can also affect pore (capillary bound), chemisorbed and hydrogen bonded water. Beard and Muralidhara (1985) suggested this was a result of cavitation occurring in crevices within the particles. Fairbanks *et al* (1986) noted an effect on bound water and suggested that cavitation scrubbed particulate crevices. It was further hypothesised that the water 'gel' layer around some hydrocarbon particles could be broken by surface tension effects, which normally separate particles on settling and that this is removed and replaced by a thinner water layer. Fairbanks (1973) stated that this led to a drier cake formation, and would allow filtration of high viscosity slurries. Fairbanks and Cheng (1969) studied liquid flow through porous media using acoustic energy and noted an increase in flow rate which can be governed by the intensity of the ultrasound applied.

The advantages of ultrasonic fields in separation processes are a faster dewatering rate, lower process temperature and the maintenance of product integrity (Beard and Muralidhara, 1985). Dewatering is aided by the reduction of viscosity and surface tension of the suspension brought about by the use of ultrasound. Further work by Muralidhara *et al* (1987) suggested that particle agglomeration released both interstitial and surface water and increases the average particle size, which caused less blinding of the media. This reduction in media fouling may facilitate conventional separation methods in cases where they would be otherwise impracticable. At low ultrasonic intensities, coagulation was rapid as cavitation did not occur.

The main mechanism proposed by many authors for improved filtration effects was particle agglomeration, followed by conventional dewatering mechanisms. Reviews of agglomeration mechanisms in suspensions are given by Gooberman (1968) and Muralidhara *et al* (1987). The principal mechanisms of particle agglomeration are thought to be orthokinetic and hydrodynamic interactions (See 2.5.1.1. & 2.5.1.2). It should be noted that the models proposed for this agglomeration by Shaw (1978) and Chou *et al* (1991) are based on models of acoustic agglomeration of aerosols and may not be applicable to liquid filtration. The models are based on an agglomeration volume in which each large particle acts as a collector and sweeps a certain volume in which it

may collect smaller particles moving with different amplitudes, as described previously. Scott Fogler (1971) suggests that it may be secondary mechanisms of ultrasound, such as acoustic streaming and cavitation, that are responsible for improvements in processing operations.

Mason (1996) noted the increased particle agglomeration effect caused by sonication. The vibrational energy kept the particles suspended, leaving more channels for the solvent to pass through. The water content of various materials can be reduced by around 50% of its initial value by using a belt filter aided by ultrasound. Matsumoto *et al.* (1996) observed that in the crossflow filtration of bovine serum albumen, the flux can be made four to six times greater by the use of ultrasound. Acoustic fields seemed to be effective for removing the cake layer deposited on a membrane surface and prevented the plugging of membrane pores. They suggest that the ultrasonic waves have a washing effect on the membrane, however other authors (Scott Fogler, 1971, Fairbanks and Cheng, 1969) attributed the prevention of cake build up and an improvement in mass transfer as being due to the turbulent effect induced by ultrasound.

Crossflow microfiltration can be enhanced by the combination of a D.C. electric field and an acoustic field as noted by Tarleton and Wakeman (1990). The enhanced separation effect has also been studied by Muralidhara *et al* (1985,1986).

A number of benefits are achieved by the use of electric, and acoustic fields:

1) A higher degree of dewatering eliminates the need for extensive thermal drying of a solid product;

2) Enhanced product recovery if the product is the supernatant;

3) Dewatering of solid wastes which may reduce disposal costs;

4) Faster dewatering rates, which may allow smaller equipment;

5) A technique which can be retrofitted to existing processes.

A review of the principals involved in EAD is given by Chauhan *et al.* (1986). The electroacoustic process is intended to be used in addition to vacuum filtration, centrifuges and screw presses, but the majority of work has been carried out in the field of vacuum dewatering. EAD is more effective than mechanical dewatering and has a wide applicability in process industries such as food, biotechnology and paper. The

major cost is electricity, but this is an order of magnitude less than that for evaporative drying because of the preliminary liquid removal.

The mechanisms of separation of EAD proposed by Muralidhara *et al* (1986) can be categorised as:

1. **Mechanical-** Wave propagation, cavitation, inertial forces, heat transfer. These mechanisms are predominant in the solid/liquid separation process. The surface tension and bulk viscosity of the liquid medium are reduced by the radiation forces caused by acoustic energy. This reduction aids electroosmosis and vacuum filtration. The difference in inertial forces of two materials of differing densities will enhance vacuum filtration by reducing adhesion.

2. **Chemical-** Cavitation leads to surface energy changes.

3. **Thermal -** Ultrasonic energy is absorbed in the medium and converted to heat.

2.9   Ultrasonic Transducers

Ultrasonic transducers work either by fluid current interruption or as a piston device. These transducers can be mechanical and act as a low frequency source, or electrical to produce higher frequencies.

High frequency ultrasound is produced by electromagnetic, piezoelectric or magnetostrictive transducers depending on the system being used. Performance criteria are available for the application of electroacoustic transducers. These are (Wilson 1988):

> Linearity- The output is a linear function of the input
>
> Passivity- All the output energy is obtained from the input energy
>
> Reversibility- The device is able to convert energy in either direction.

2.9.1   Piezoelectric Transducers

The piezoelectric effect can be described as a redistribution of charge as a result of a deformation in the material, or, alternatively, as a deformation due to a redistribution of the charge. Figure 2-3 demonstrates how this redistribution of charge comes about on deformation.

High frequency electric oscillations are transformed into mechanical oscillations. The ultrasound frequency corresponds to that of the electric field applied. The material will

rupture at low frequencies, limiting the lower usable frequency. Blitz (1971) stated that an increased amplitude is achievable if the transducer is excited at its resonance frequency. Synthetic transducer materials have been developed for use in these transducers. A commonly used alternative material is barium titanate. This has the advantage of an ability to be shaped, and so the restrictions of the crystal shape are
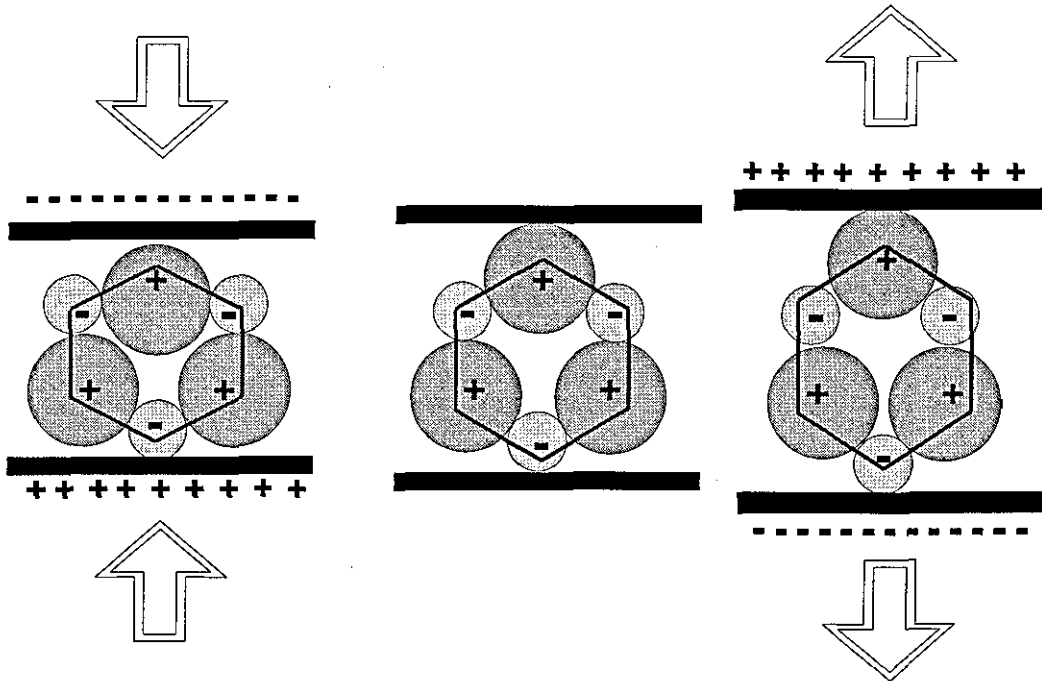
Figure 2-3: Re-distribution of charge in a piezo-electric material

removed but it is less efficient than quartz crystals. Polycrystalline ceramics (e.g. lead-zirconate-titanate mixtures) can be used at high temperatures and their piezoelectric properties are superior to those of barium titanate (Wilson, 1988). Large transducers made of several quartz plates have not been successful in colloid work as found by Sollner (1950). The main advantage of piezoelectric transducers over magnetostrictive is a wider efficient output range, and higher power outputs.

A schematic of a typical piezoelectric transducer is shown in Figure 2-4. Application of a high frequency electric field across the piezoelectric disk causes changes in the disk's dimensions. These are absorbed on one side by a backing material, such that waves propagate in one direction only. The matching layer acts as a coupling medium between the disk and the wear plate and allows good propagation of the wave to the wear plate. This plate acts to protect the transducer from damage.

The main types of piezo transducers are immersion, contact , angle-beam, array and air borne. They can be categorised by the following characteristics: coupling, matching, damping, steering and focusing. The transducer which has the highest ratings in all these categories is the immersion transducer, which can, as its name suggests, be immersed in a water bath to allow good coupling between the sample and the transducer. These types are easy to steer and focus the wave exactly at the desired position and so are popular for uses such as non destructive testing. Contact transducers are placed directly onto the sample, but a coupling medium must be between the device and sample to allow waves to pass into it.
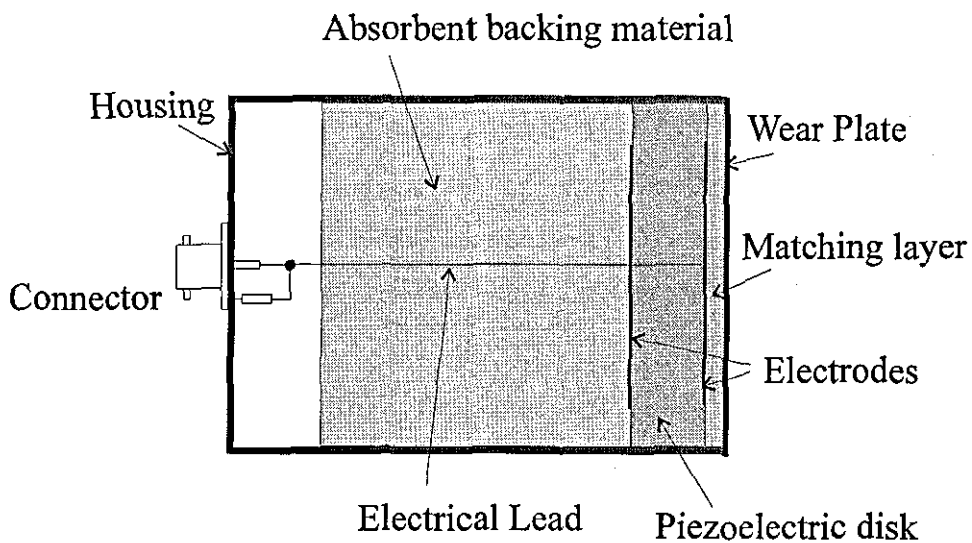
Figure 2-4: Typical Transducer Design

2.9.2   Magnetostrictive Transducers

The magnetostriction effect is utilised to create mechanical vibrations from a magnetic field. Resonance between the natural elastic period of the oscillator and the frequency of the field increases the amplitude of the mechanical vibrations and improves the energy transformation efficiency. The rod of ferromagnetic material decreases or increases in length depending on the material, its treatment and the applied field strength. The length change does not depend on the direction of the magnetic field. The material must be initially magnetised to ensure that the average movement is greater in one direction . This initial magnetisation is provided by the use of a coil or permanent magnet around the material. The amptitude of the length change can be made large under the correct

conditions, by making the frequency of the oscillatory current the same as that of the natural frequency of the rod.

Magnetostrictive transducers are highly suitable to industrial use because they possess many advantageous properties. These are (Brown & Goodman 1965):

1. Rugged construction

2. High power outputs

3. Efficient operation in certain ranges (5-40 kHz)

4. Ability to drive high impedance loads, such as solids and liquids.

5. Several transducers can be used together in large installations

2.9.3   Electromagnetic Transducers

These consist of a heavy steel membrane actuated by an electric field at the resonance frequency. At high frequencies energy losses occur because of eddies. These types of transducers require a constant application of a steady magnetic field, and as such have only been used in a few instances in liquid systems (Sollner, 1950).

Hanel *et al* (1996) have worked on the design and optimisation of high frequency piezoelectric transducers, by attempting to simulate the transducer characteristics prior to its construction.

3   Experimental Procedures & Analysis- Filtration

Experiments were designed and carried out to investigate the effects of different combinations of electric and acoustic fields on dead end filtration of low concentration rutile suspensions. The suspension was fully characterised and initial tests carried out to establish suitable values of the variables being studied. These tests included study of the effect an acoustic field on suspensions of different concentrations, the effect of electric field strength alone on filtration and the effect of electric field strength when applied together with the acoustic field.

A series of filtration experiments were then performed across a range of pHs, utilising a number of field combinations, as described in later sections.

3.1   Zeta potential

It is important to fully characterise for both zeta potential and particle size any suspension being studied because the effective charge on a particle (that which is 'seen' by other particles) will differ depending on the particles surface chemistry, the nature of the supporting medium and whether any surface active agents are present. Although titanium dioxide is well known and is well characterised in the literature, use of the surfactant MIPA to aid dispersion alters the characteristic zeta potential curve and shifts the iso-electric point to close to pH 4 (Figure 3-2.).

The zeta potential was measured using a Malvern Zetasizer 3000. This machine uses microelectrophoresis; inducing a particle velocity by application of an electric field. The particle velocity is measured using a light scattering technique, which makes use of the Doppler effect. The velocity is measured at a point in the cell where the electro-osmotic velocity is zero and the measured velocity is the true electrophoretic velocity. Two laser beams cross at this stationary point and cause interference fringes which interact with particles within the volume to scatter light. The frequency of the scattered light depends on the speed of the particles and is correlated to calculate the velocity, electrophoretic mobility and finally the zeta potential.

A dilute suspension of MIPA dispersed rutile was made up according to the same procedure used for the filtration experiments. Small samples were taken and the pH altered to cover the wide range of pHs used in this study. These samples were placed in

clean cuvettes and placed within the Zetasizer in the path of the laser beams. The equipment is computer controlled, allowing a number of readings to be taken from the same sample for accuracy.

3.2   Particle size

The particle size distributions of the rutile suspensions were measured using a Malvern MS20 Mastersizer. This allowed determination of surface charge effects on particle agglomeration. During the experimental programme particle size measurements were used to ensure adequate dispersion, as indicated in the experimental procedure.

The equipment utilises a light scattering technique to determine particle size distributions. A laser is fired at the suspension and the particle size distribution is calculated from the light received at the sensor, the scattering characteristics of the material and the focal length of the lens. The parameters used in this study were a presentation factor of 2209 and a 45mm lens. The stirrer speed within the sample vessel was set at 80%, and the feed pump to 60 %. These have been used by other authors using the same material, (Marchant, 1998).

3.3   Characterisation Background Study

3.3.1   Electrical interactions

Electrostatic interaction between two particles occurs when their diffuse double layers penetrate one another. Particles in aqueous suspensions carry surface charges, and the distribution of ions around a charged particle is determined by electrical interaction with the surface (along with random thermal motion). The electrical potential at the inner boundary of the diffuse layer is of interest to study these interactions. This cannot be measured directly, but is believed to be closely related to the measurable zeta potential. As shown in Figure 3-1, the ionic strength has a marked effect on the thickness of the double layer. A large diffuse layer, as shown in Figure 3-1(a) results in repulsion when particles are separated by a greater distance than that given by a more compact diffuse layer (Figure 3-1 (b)). This means that, at higher ionic strengths (extremes of pH) particles can approach more closely before repulsion.

(a) Low ionic strength   **(b) High ionic strength**
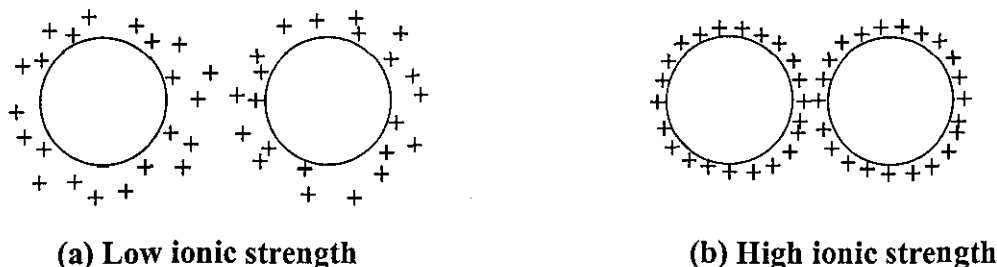
Figure 3-1: The effect of ionic strength on double layer thickness.

Measurement of the zeta potential allows the electrical interaction energy per unit area to be derived. The general expression for this repulsive energy between particles A and B is complex (Bratby 1980), but can be expressed as:

$$E_E = \frac{4\pi a_A a_B}{a_A + a_B} \varepsilon \zeta_A \zeta_B \exp(-\kappa d) \qquad\qquad 3\text{-}1$$

Within the DLVO (Deryagin-Landau & Verwy-Overbeek) theory other interactions are neglected (Shaw, 1992). These include hydration effects (hydrated surfaces must become dehydrated if true contact is to occur), hydrophobic interaction (water confined in a gap between two hydrophobic surfaces will tend to migrate to the bulk water, to facilitate hydrogen bonding and become more structured), steric interaction (stability is caused by polymers which adsorb onto the particle, but parts of these extend into the aqueous phase, the overlap of which leads to particle repulsion (by dehydration)) and polymer bridging. This does not imply however that these other interactions are unimportant, indeed steric interaction is thought to play an important part in the stability of natural inorganic colloids (Gregory 1993), which often have adsorbed layers of natural organic material which act as a structural mechanical barrier allowing particles to approach only up to a certain distance. Expressions for this interaction have been proposed, but the effect is complex and so is not considered here. Suffice to say that it acts as an extra repulsion energy, increasing the energy barrier which particles must overcome to agglomerate.

In the DLVO theory electrical double layer repulsion and van der Waals interaction are assumed to be additive and are combined to give the total energy of interaction between particles in a colloidal suspension as a function of separation distance. The Deryagin approximation is used to enable the force of interaction to be written as a function if the interaction energy, both of which are functions of the particle's separation distance. The

assumption is that two interacting spherical bodies which are very close essentially act as two parallel plates. This only holds if the bodies are very close, so that most of the contribution to interaction comes from the region where the surfaces are parallel. For this to hold, both the range of interaction (double layer thickness) of the bodies and their separation distance, should be small compared with their radius of curvature.

3.3.2   van der Waals interaction

The attractive force that occurs between colloidal particles can be explained using the concept of dipoles. A temporary dipole induces another temporary dipole on a neighbouring molecule, which is always in the direction such that the molecules attract one another. Water molecules, with their permanent dipole moment, attract each other strongly because the dipoles align themselves so that molecules are attracted rather than repulsed; this lowers the free energy of the system and gives the water 'structure'. The van der Waals force can act over longer distances in colloidal particles than in molecules because all of the atoms of one molecule can interact with all the atoms of a second one. Thus in colloidal suspensions, the van der Waals force acts over several hundred nanometers (Gregory, 1993), and its range is comparable to that of the electrostatic force. The temporary nature of the dipoles provide a possibility that, if they meet in the correct orientation, attraction will occur, until the time that the dipole's nature changes.

It is common to use the Hamaker (1937) approach to calculation of van der Waals interactions, which is based on the summation of the bodies' molecular interactions.

The interaction energy per unit area according to Hamaker is

$$E_A = -\frac{A_{12}}{12\pi d^2} \qquad\qquad 3\text{-}2$$

A_{12} denotes the Hamaker constant for interacting media 1 and 2. Convention dictates that this expression has a negative sign to indicate an attraction. The notation A_{12} is used for Hamaker constants relating to two media in a vacuum, and a modification is necessary if a third medium is suspending the particles. For example for the interaction of media 1 and 2 through medium 3 we have

$$A_{132} = A_{12} + A_{33} - A_{13} - A_{23} \qquad\qquad 3\text{-}3$$

Using a geometric mean assumption $A_{12} \approx \sqrt{(A_{11}A_{22})}$ and assuming that similar particles are interacting in the third medium, the Hamaker constant can be given by

$$A_{131} \approx \left(A_{11}^{\frac{1}{2}} - A_{33}^{\frac{1}{2}} \right)^2 \qquad\qquad 3\text{-}4$$

Thus for similar materials, the Hamaker constant will always be positive and so the negative interaction energy dictating inter particle attraction will always occur. Hamaker constants are much lower for aqueous dispersions than in a vacuum, leading to smaller interaction energies and thus less attraction. This is shown in Table 3-1, where the Hamaker constants for two particles of the same material are clearly smaller when a further medium is present between them. It is interesting to note that Titanium dioxide, TiO_2, has a Hamaker constant in water of a similar order to those given for substances in a vacuum, and orders of magnitude higher than other substances shown. This suggests that the van der Waals interaction between TiO_2 particles in water is strongly attractive, in comparison to other substances.

Material	Hamaker constant in a vacuum A_{11} x 10^{20} J	Hamaker constant in water A_{121} x 10^{20} J
Water	3----6.4	-
Oxides	10----15	1.7----4.1
Metals	7.5----45	0.7----3.3
Hydrocarbons	4.6----10	0.08----0.4
SiO_2	8.6----50	0.3----0.94
TiO_2	11----31	2.5----10

Table 3-1: Typical Hamaker constants (after Bernhardt, 1994)

3.3.3   Colloidal stability

The total interaction energy is calculated by the summation of van der Waals and electrostatic interactions, E_H and E_E . The shape of the total interaction curve for a solution is very important when considering colloid stability. If $E_H \gg E_E$ then the total energy, E_T is totally negative and the particles attract one another. This causes an unstable suspension in which particles can adhere each time they collide.

Provided that there are situations where the zeta potential of the particles and the ionic strength are such that repulsion outweighs attraction there will exist an energy barrier. It is the height of this energy barrier that enables the stability of the suspension to be maintained. Any particle having enough energy to overcome it would lose that energy by the actual act of overcoming the frictional resistance of the solvent before it could surmount the barrier. However, the particles are undergoing Brownian motion and there is a small probability that two particles will be knocked close enough together to overcome the energy barrier.

Once particles have agglomerated they are held in the deep primary minimum, from which it is difficult to escape, and they are unlikely to separate.

3.3.4   Discussion of characterisation results

Increasing the salt concentration of the Titania suspension used in this study (Figure 3-2), both reduces the zeta potential and increases the ionic strength resulting in a reduction in the energy barrier (because this reduces the electrical attraction). This effect is shown by the particle size data of Figure 3-3; at extremes of pH, the magnitude of the zeta potential is reduced and the size data clearly shows an increase in the mean measured particle size.

This particle agglomeration occurs as a result of a reduction in the total interaction energy and so contact of the particles can occur more readily, resulting in adhesion. As the energy barrier is lowered, the point at which the maximum just touches the abscissa is termed the critical coagulation concentration and it is at this point that rapid coagulation occurs. The greatest surface charge (approx. −50 mV) occurs at pH 9 and the iso-electric point (IEP) is approximately at pH 3.4. Between pH 6-10 the zeta potential remains approximately constant, at -45mV, reducing in magnitude slightly as pHs over 10 are reached. Particle sizes associated with these pHs show that a stable, well dispersed suspension is formed in this region, with a mean particle size of around 0.30μm (Figure 3-3).
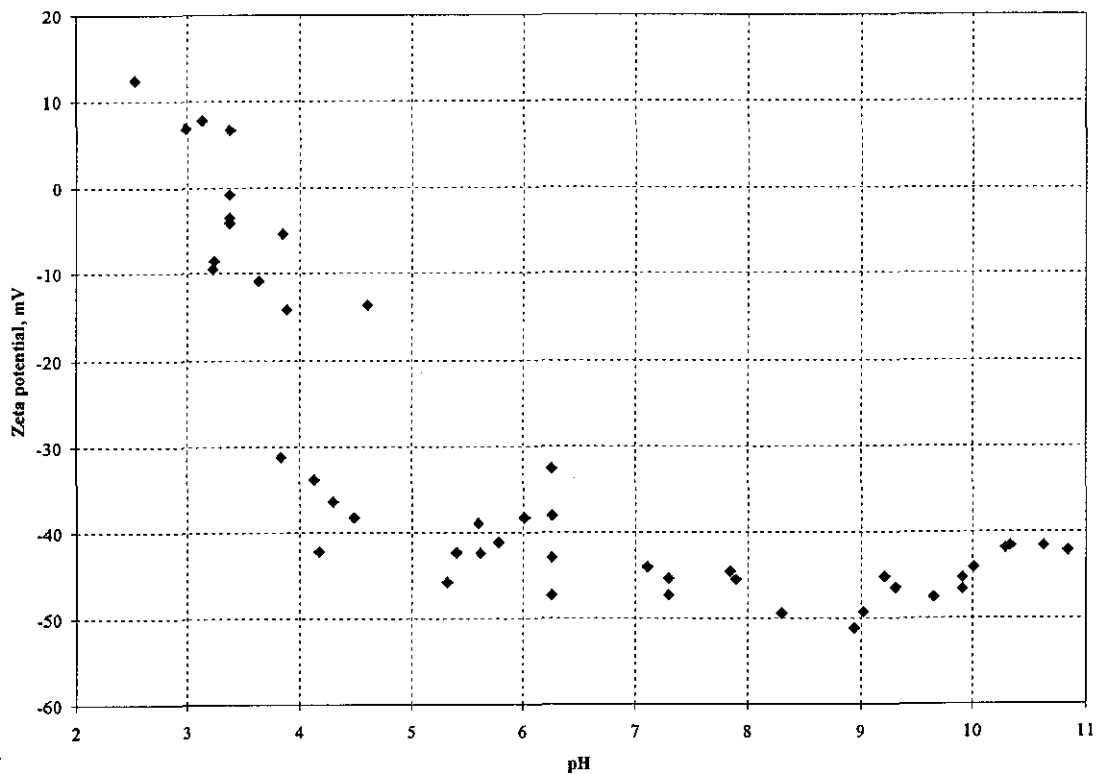
Figure 3-2: Zeta potential of Titanium Dioxide
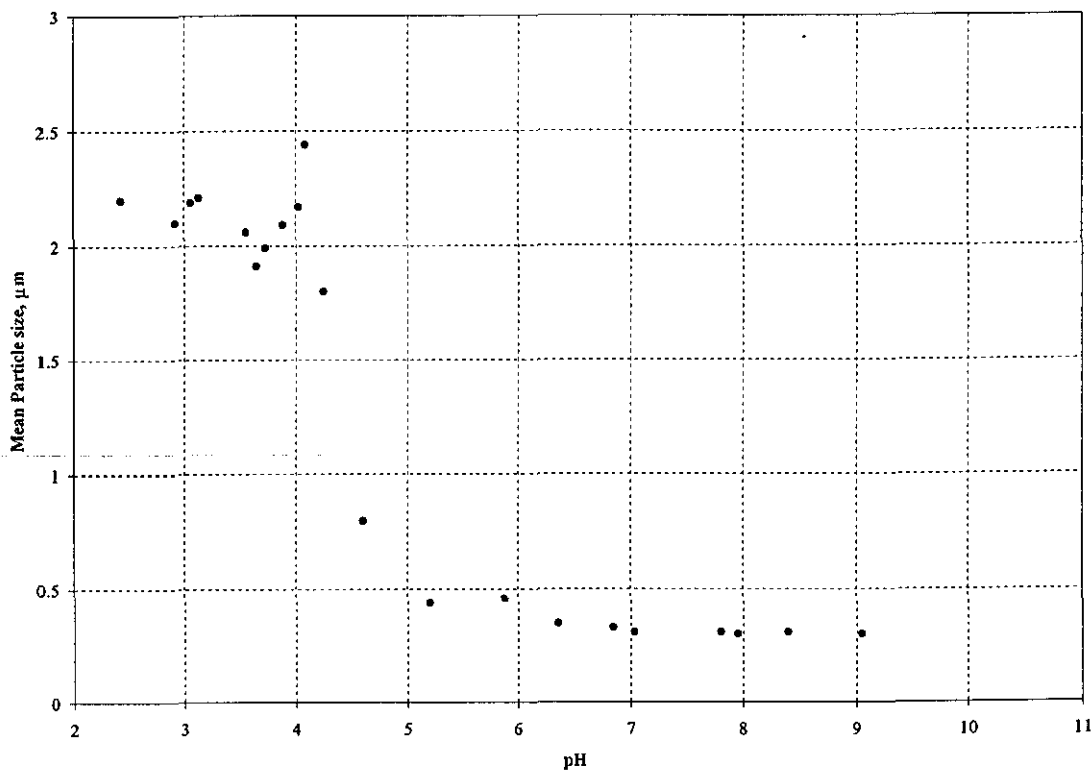
Figure 3-3: Particle size distribution of Titanium Dioxide

Around the IEP, low or zero zeta potential implies that there are few interparticle repulsive forces, and van der Waals forces dominate, resulting in particle agglomeration. This is confirmed by the increase in particle size seen as the suspension pH is reduced and poorer dispersion is achieved, with a mean particle size of 2 μm. As the pH is reduced further the zeta potential becomes positive and increases in magnitude. There is no corresponding rapid increase in mean particle size, suggesting that particles have become trapped in the deep primary minimum and a large increase in potential energy would be required to overcome this and re- disperse the particles.

Figure 3-3 follows a similar shape to that in Figure 3-2. Maximum particle sizes are seen between pHs 3-4 and minimum sizes are consistent between pHs 6-10. This suggests the zeta potential has a marked effect on particle agglomeration and can be explained by electrical interactions between particles.

3.4   Acoustic Power Supply

The ultrasonic generator used in this study is a Telsonic NSM 220 module supplied with an MG-300 –x-22 module. It is sold for use as a generator for ultrasonic baths, but has been modified for use with a transducer for the experimental programme. A summary of the acoustic properties of the generator is given in Table 3-2.

Property	Value
Supply	220V, 50/60 Hz ±10%
Current Consumption	1.5A (max)
Output Frequency	23 kHz
Output Power	300 W (rms), 600 W (peak)
Transducer area	91.68 cm^2

Table 3-2: Acoustic generator properties (Telsonic Ltd, 1999)

The generator converts mains frequency (50/60 Hz) into high frequency electrical signals. An ultrasonic converter converts the electrical energy into mechanical energy with the same frequency, as described in Section 1.9. The mechanical waves are then transmitted through the suspension, which is in contact with the converter.

The output frequency is double half wave operation (pulsed at 100 Hz) and frequency modulated ±3 kHz.

3.4.1   Sound velocity

An expression to derive the velocity of sound in liquids is given by Kinsler and Frey (1962) as

$$c = \sqrt{\frac{\gamma B}{\rho_0}}$$
                                                                    3-5

where B is the isothermal bulk modulus, an elastic modulus which gives an indication of the compressibility of a liquid, and γ the ratio of specific heats. All the quantities in equation 3-5 vary with pressure and temperature, however, and so it is necessary to measure the velocities or use empirical equations such as that given below for distilled water at one atmosphere:

$$c = 1403 + 5T - 0.06T^2 + 0.0003T^3$$
                                          3-6

where T is the temperature of the water in ° C (valid between 0-60 ° C) and c is the wave speed (ms^{-1}). Pressure and the presence of salts increase sound velocities such that the speed of sound in sea water is taken to be approximately 1500 ms^{-1}. The sound speed used in this study is that found from equation (3-6) of 1481 ms^{-1}.

3.4.2   Energy density

The energy involved in the propagation of acoustic waves through a fluid medium consists of the kinetic energy of the moving particles and the potential energy inherent in a compressed fluid. The energy density is a measure of this energy caused by the sound field, and can be calculated by summing the kinetic and potential energies. A volume element of thickness dx, (see Figure 4-1), such that all particles within the element have the same velocity u, and have kinetic energy, ΔE_K given by:

$$\Delta E_K = \frac{1}{2}\rho_f u^2 Adx$$
                                          3-7

As the fluid is compressed and expanded, the volume of the element, V_e, varies according to

$$V_e = Adx\left(1 + \frac{\partial \xi}{\partial x}\right)$$
                                          3-8

where Adx is the volume of the element in the undisturbed fluid. The change in potential energy is given by

$$\Delta E_P = -\int p \, dV_e \qquad \text{3-9}$$

Potential energy increases as work is done on the fluid when its volume is decreased by the action of a positive acoustic pressure p. Substituting equation 3-7 and differentiating the expression for V_e, and substituting into the integral expression for potential energy gives

$$\Delta E_P = \frac{A dx}{\rho_0 c^2} \int_0^p p \, dp = \frac{1}{2} \frac{p^2}{\rho_0 c^2} A dx \qquad \text{3-10}$$

The total acoustic energy ΔE_{AC} is the sum of the kinetic and potential terms and the energy density, ε is given by

$$\varepsilon = \frac{\Delta E_{AC}}{A dx} = \frac{1}{2} \rho_0 \left(u^2 + \frac{p^2}{\rho_0^2 c^2} \right) \qquad \text{3-11}$$

This is simply twice the expression for kinetic energy density ρ_{Ek}, because $p = \rho_0 c u$, as defined by the expression for wave speed, see Chapter 4.

3.4.3 Acoustic Intensity

The acoustic intensity of a sound wave is defined as the average rate of flow of energy through a unit area normal to the direction of wave propagation. The intensity of a wave travelling in the positive x direction can be defined as (Kinsler and Frey, 1962):

$$I = \frac{P^2}{2M} \qquad \text{3-12}$$

I_0 is the specific acoustic impedance of the medium,. Impedance is a measure of how difficult it is to make the fluid move, and is defined as the ratio of acoustic pressure and associated particle velocity. It can be shown (Hall 1993) to be equal to the product of the medium density and the wave speed $(\rho_0 c)$ in the case of a plane travelling wave. The impedance of water at 20 ° C is 1.48×10^6 kg m^{-2} s^{-1}. The impedance of air is much lower than that of water, 415 kg m^{-2} s^{-1} at the same conditions, because both the density and particle speed are lower. The impedance is a property of both the media and the wave type and geometric position (Hall 1993). $\overline{P}$, the pressure amplitude is often replaced by $\overline{P_e}$, the effective pressure amplitude or root mean square (rms)

$$\overline{P}_e = \frac{\overline{P}}{\sqrt{2}} \qquad\qquad 3\text{-}13$$

For example, the sound intensity can be defined using the effective pressure amplitude

$$I = \frac{\overline{P}_e^2}{\rho_f c} = \frac{\overline{P}_e^2}{M} \qquad\qquad 3\text{-}14$$

The rms power output of the generator used in the study is known, along with the transducer area. Thus the effective intensity of the acoustic wave in the water is 300 W / 100 cm^2 i.e. 3Wcm^{-2}. Substitution into equations 3-13 and 3-14 gives a peak pressure amplitude of 3 x 10^5 Pa and an effective (rms) amplitude of 2.1 x 10^5 Pa. The energy consumption based on the available area of the transducer (91.68 cm^2) is 275 W.

3.4.4 Sound intensity levels and acoustic parameters

Knowledge of the frequency and power level of an ultrasonic source can allow calculation of any parameter required:

The sound intensity level, *SIL*, is given by

$$SIL = 10\log_{10}\frac{I}{I_{ref}} \qquad\qquad 3\text{-}15$$

where I_{ref} is a mutually agreed reference intensity. The sound pressure level, *SPL* (more often used for liquids), can be defined in a similar form and is given by

$$SPL = 20\log_{10}\frac{\overline{P}_e}{P_{ref}} \qquad\qquad 3\text{-}16$$

For water $\overline{P}_{ref}$ is 1 µPa, although older sources use 20 µPa or 0.1 Pa, (Hall 1993) so it is important to specify which reference pressure is used. Now the rms density fluctuation ρ_e is defined as

$$\rho_e \approx \frac{\overline{P}_e}{c^2} \qquad\qquad 3\text{-}17$$

the rms displacement ξ_e,

$$\xi_e \approx \frac{\overline{P}_e}{c\omega\rho_f} \qquad\qquad 3\text{-}18$$

and the rms velocity amplitude, u_e

$$u_e = \omega\xi \qquad \qquad 3\text{-}19$$

the average kinetic energy density, ρ_{EK}

$$\rho_{EK} = \frac{\overline{P_e}}{2\rho_f c^2} \qquad \qquad 3\text{-}20$$

with the total energy density, ρ_E

$$\rho_E \equiv 2\Delta E_K \qquad \qquad 3\text{-}21$$

The acoustic parameters are summarised in Table 3-3.

Acoustic Parameter	Value
Wave frequency	23 kHz
Angular frequency	144513 rads^{-1}
Effective intensity	3×10^4 Wm^{-2}
Peak pressure amplitude, P	298295 Pa
Effective Pressure amplitude, P_e	210927 Pa
SPL, dB (P_{ref}=1μPa)	226.5 dB
ρ_e	0.096 kgm^{-3}
ξ_e	9.8×10^{-6} m
v_e	1.42 ms^{-1}
ΔE_K	4.8×10^{-5} J
ε	9.6×10^{-5} Jm^{-3}

Table 3-3: Acoustic parameters for ultrasonic source with power output of generator 300 W, transducer area 100 cm^2

3.5 Electrical Power supply

A stabilised D.C. power supply (Sorensen model DCR 150-12B) provided an electric field gradient. The D.C. power supply allowed application of a constant, stabilised voltage across the electrodes. The field gradient was varied from one experiment to the next by altering the separation distance between the electrodes or by applying a different voltage. Energy consumption was below 5W in all the experiments carried out (Wakeman and Smythe, 2000).

3.6   Experimental Procedures

The experimental programme consisted mainly of filtration experiments, using rutile as the test material. During each experiment, the conductivity was monitored using a WPA portable conductivity meter, together with an epoxy resin conductivity probe.

3.6.1   Test Suspension

The test suspension used was uncoated rutile, which was dispersed using monoisopropanolamine (MIPA) at a concentration of 0.15% by weight (based on the mass of TiO_2). MIPA is a surfactant which has a number of effects. Initially, it reduces surface tension, allowing the liquid phase to penetrate the finer interstitial voids betwen particles, thus resulting in a better dispersed suspension. Once dispersed, it also enables the suspension to maintain its dispersed state.

The dispersion method used was that developed by Marchant (1998) for the same type of MIPA dispersed Titania suspensions. To disperse particles down to approx 0.3 microns, it is necessary to prepare a 50% vol. solids suspension, as this concentration has been shown to give the best dispersion. The close proximity of particles in the suspension aids dispersion.

The suspension was homogenised using a Ultra Turrax T25 homogeniser. This high shear mixer was used for 8 minutes at 2000 rpm to homogenise up to 200 ml of feedstock at a time. The 50 % vol feedstock was placed in a plastic beaker, sized to cover the homogeniser's rotor, and following mixing was covered with clingfilm to minimise water loss through evaporation. Malvern MS20 Mastersizer was used to ensure a mean particle size of 0.3 μm. The suspension is made up at 50% (w/w) of TiO_2 in ultrapure water, obtained from a Millipore MilliRX20 water purification system. This is a method which simulates industrial conditions (Marchant 1998).

When an experiment took place, the 50% feedstock was diluted using ultrapure water, and the procedure given in Figure 3-6 followed.

3.6.2   Membranes

The filtration experiments reported use Sartorious cellulose nitrate membranes, with a pore size rating of 0.2 μm. These membranes have been extensively characterised previously, (Tarleton & Wakeman 1994) and show a negative zeta potential in the pH

range 3-12. They have a measured mean pore size of 0.51 μm, and a thickness of 130 μm. A new membrane was used for each filtration test.

3.6.3   Experimental Rig

An experimental rig was designed and built based on a conventional dead end vacuum filter (Figure 3-5).
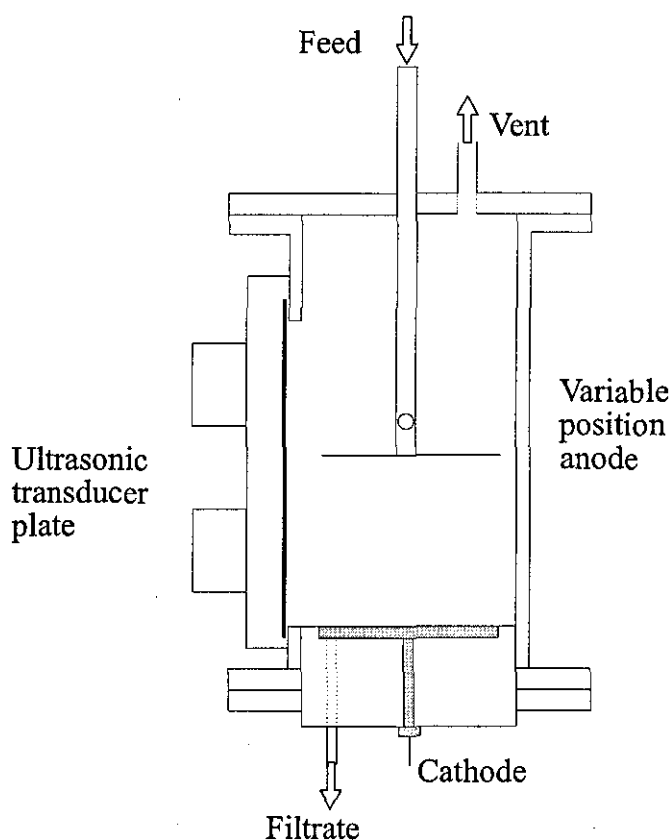
Figure 3-4: Filter cell detail

In these experiments the filter medium support acted as a cathode. A variable position anode was suspended parallel to the support, and the separation distance could be varied. The electric field was thus applied normal to the filter surface. The ultrasonic transducer was attached to one side of the filter cell and ultrasonic energy applied tangentially to the filter surface. The ultrasonic transducer position could not be altered and has the properties described in Table 3-2 and 3-3. The filter cell is shown in detail in Figure 3-4 below

The experimental apparatus (Figure 3-5) comprised a feed reservoir with recirculation pump to ensure the feed is completely mixed. The feed flowed into the filter cell and the pressure drop across the cell was monitored by pressure transducers. The system was controlled by a host computer which controlled the vacuum held in the filtrate tank in order to control the pressure difference across the filter. Experimental runs were carried out at constant vacuum. The pressure drop across the cell was recorded and the filtrate volume collected was measured at different filtration times. As the initial effects of the fields were most significant run lengths were between 30 and 60 minutes, greater than the cake formation time of most industrial filters.
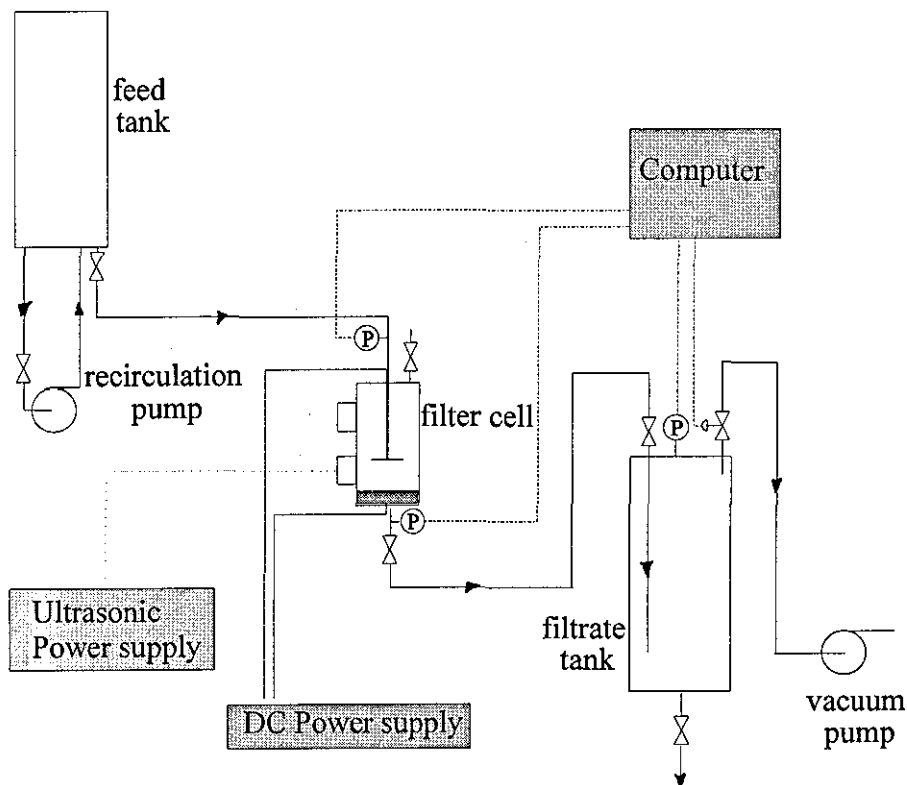
Figure 3-5: Experimental rig

3.6.4   Experimental Procedure

Before commencing a filtration experiment a test suspension was made to a known concentration by dilution of the suspension described above with ultrapure water. The suspension was re-circulated around the flow circuit until a homogenous mixture was achieved. The pH of the resulting suspension was monitored, and if necessary altered to the desired value using dilute hydrochloric acid or sodium hydroxide. A sample of the suspension was then taken for particle size analysis. The initial conductivity and

temperature was noted. At commencement of the experiment, the feed cell valve was opened and the suspension allowed to fill the filter cell. At this point the fields required for the particular test were switched on, such that the suspension was under the influence of the fields for the entire duration of the experiment. This procedure is summarised in Figure 3-6.

3.7 Field Effects on Filtration

The first filtration experiments carried out attempt to 'characterise' the filtration process, such that the parameters chosen were within the limitations of the experimental rig. This was especially important in light of the great synergistic effect seen by other authors, for example, Muralidhara *et al* (1985), Wakeman and Tarleton (1991).

Results are plotted in the form often used to report filtration data, either as filtrate collected with time or Ruth plots from which an effective specific cake resistance can be calculated. This calculation method however, has limitations, in that the derivation of the Ruth equation makes use of certain assumptions that may not hold in this case. For example the derivation of equation 2-25 assumes constant feed concentration and filtration pressure. The application of external fields may alter the effective feed concentration. Rushton *et al* (1978) have shown that specific cake resistance is altered by both the feed concentration and velocity. This suggests that cake resistances calculated under these conditions using the traditional method of analysis will not hold. For these reasons the following method of comparing experimental results has been used.

Following the simplifications used by Yukawa *et al* (1976) to derive a relationship for electrofiltration, a similar equation can be formed to include the effects of ultrasound. The result of modifying the classical filtration equation based on Darcy's law is simply expressed as equation 2-25:

$$\frac{1}{Q} = \frac{\mu R_M}{A \Delta P} + \frac{\mu \alpha c_m V}{A^2 \Delta P} \qquad \qquad 2\text{-}25$$

In these experiments the electrical and/or acoustic forces change the effective concentration, c_m, of the suspension that actually forms the filter cake so that it is different from that of the slurry feed. The pressure across the filter, $\Delta P'$, is given by the sum of the pressure differences across the cake and the medium; this includes
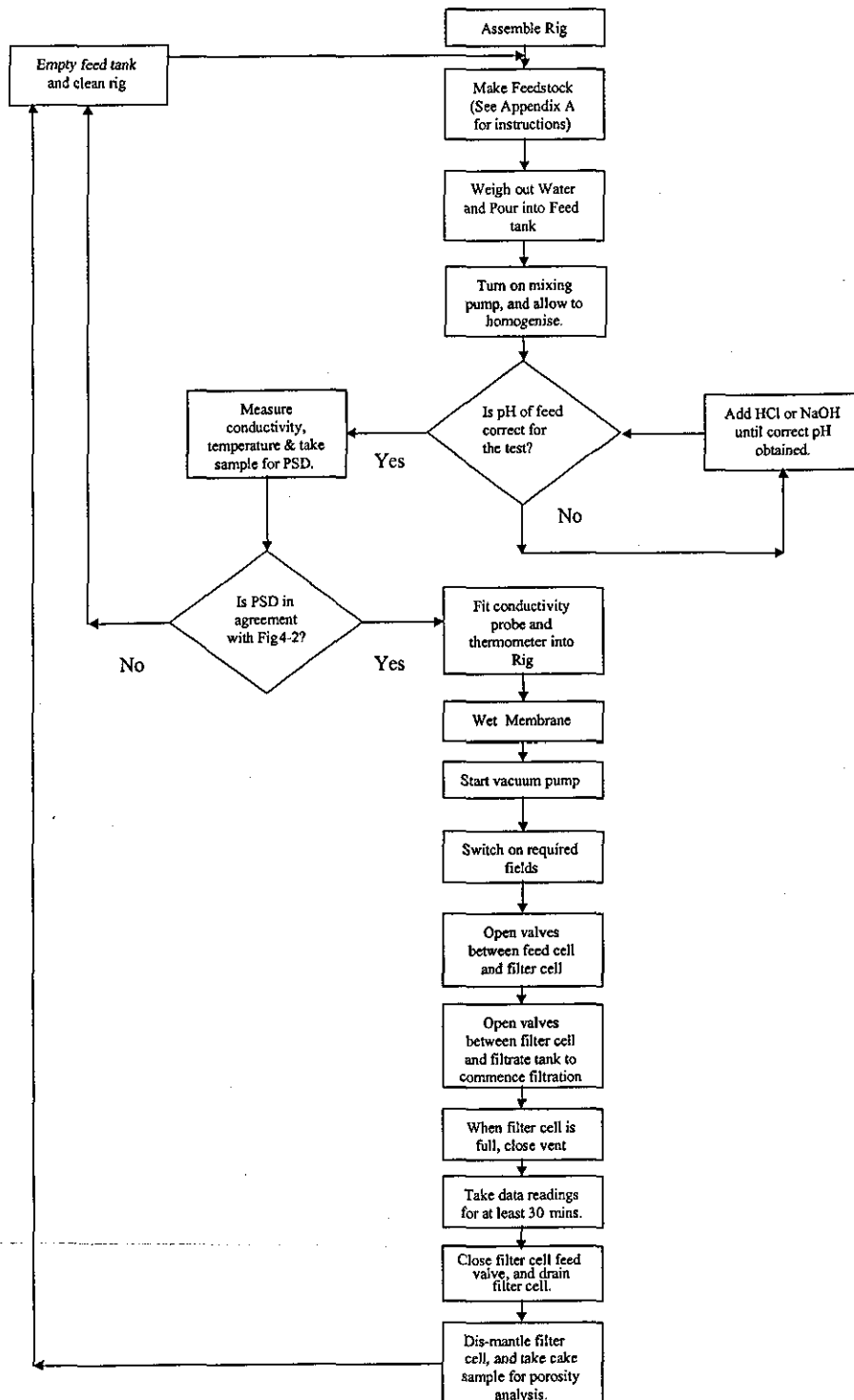
Figure 3-6: Summary of experimental procedure

contributions from the hydraulic (p_h), electroosmotic (p_e) and acoustic (p_a) pressures, that is:

$$\Delta P' = \Delta p_h + \Delta p_e + \Delta p_a \qquad\qquad 3\text{-}22$$

The electroosmotic pressure difference arises from electroosmotic flow of liquid through the filter medium and any cake or thickened suspension that is formed; assuming this and the acoustic pressure difference are small compared with the hydraulic pressure difference derived from the vacuum, Δp is constant to a first approximation and equation 2-25 can be integrated at constant pressure difference to give:

$$\frac{t}{V} = \frac{\alpha_{av} c_m \mu}{2 A^2 \Delta P'} V + \frac{\mu R_M}{A \Delta P'} = K_1 V + K_2 \qquad\qquad 3\text{-}23$$

In the results that follow, K_1 is often quoted as it not only represents the gradient of the Ruth plot, but also indicates the relative magnitude of the specific cake resistance, although this cannot be calculated explicitly as the pressure is not, strictly speaking, constant during acoustic filtration due to the cyclic nature of the wave.

3.7.1   Effect of concentration on acoustic filtration

Suspensions of different concentrations were filtered, with and without the acoustic field activated. The suspensions ranged from 0.01% to 5% by volume of MIPA dispersed rutile. These concentrations are typical of those found in the dewatering of industrial suspensions, and can be considered at low enough concentration that, in the bulk suspension at least, the particles are separate enough that the assumptions used in DVLO theory hold.

The result of no field filtration at different concentrations is shown in Figure 3-7, and of acoustic filtration in Figure 3-8. The experiments were carried out at pH 8, with a filtration pressure of 750 mBar vacuum. These values were chosen because the particle size distribution at this point is constant, at its minimum, and the suspension is at its most stable because of the high magnitude of the zeta potential (Figure 3-2). The pressure drop was chosen arbitrarily, under the assumption that the largest pressure drop would yield the largest volumes of filtrate. Study of Figures 3-7 and 3-8 initially seems to indicate that filtration is less successful or the same under the application of acoustic fields at all concentrations. At higher concentrations ($\geq$ 1%v/v), filtration rates are

similar, regardless of whether or not the acoustic field is applied. The presence of large numbers of particles attenuates the acoustic field. At 5% v/v filtration appears to occur in the same manner as if the field was not present. This is in agreement with the multiple scattering theory proposed by Harker and Temple (1988) and discussed in Section 3.7.1.4. At lower concentrations (0.5%v/v and below), the volumes collected under acoustic filtration are consistently lower than under conventional filtration. This suggests that, when used alone, the acoustic field has the opposite effect to that seen by other authors during crossflow microfiltration (Wakeman and Tarleton, 1991). It is likely then that this may be due to the orientation of the acoustic field relative to the filter medium combined with flow normal to, rather than parallel with the medium. Tarleton (1988) saw similar results in his work on assisted filtration. In his work, the orientation of the sound field with the filter septum differed from the experiments carried out here, with the ultrasonic horn located parallel to the filter membrane. For china clay, a reduction in filtrate volume was always seen when the acoustic field was applied, and whilst gains were seen during the acoustic filtration of anatase, they were not large. It would seem then that the orientation of fluid flow normal to the medium may not be suitable for filtration enhancement by acoustic methods.
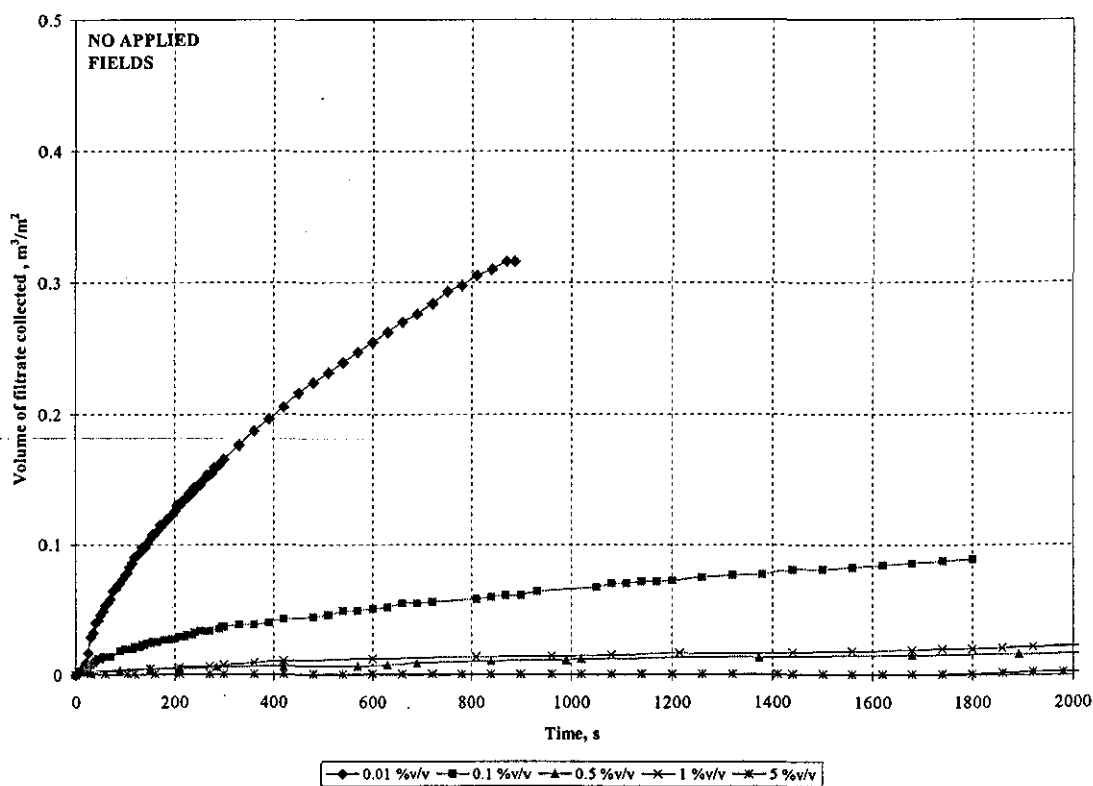
Figure 3-7a: Dead end filtration of various concentration rutile suspensions
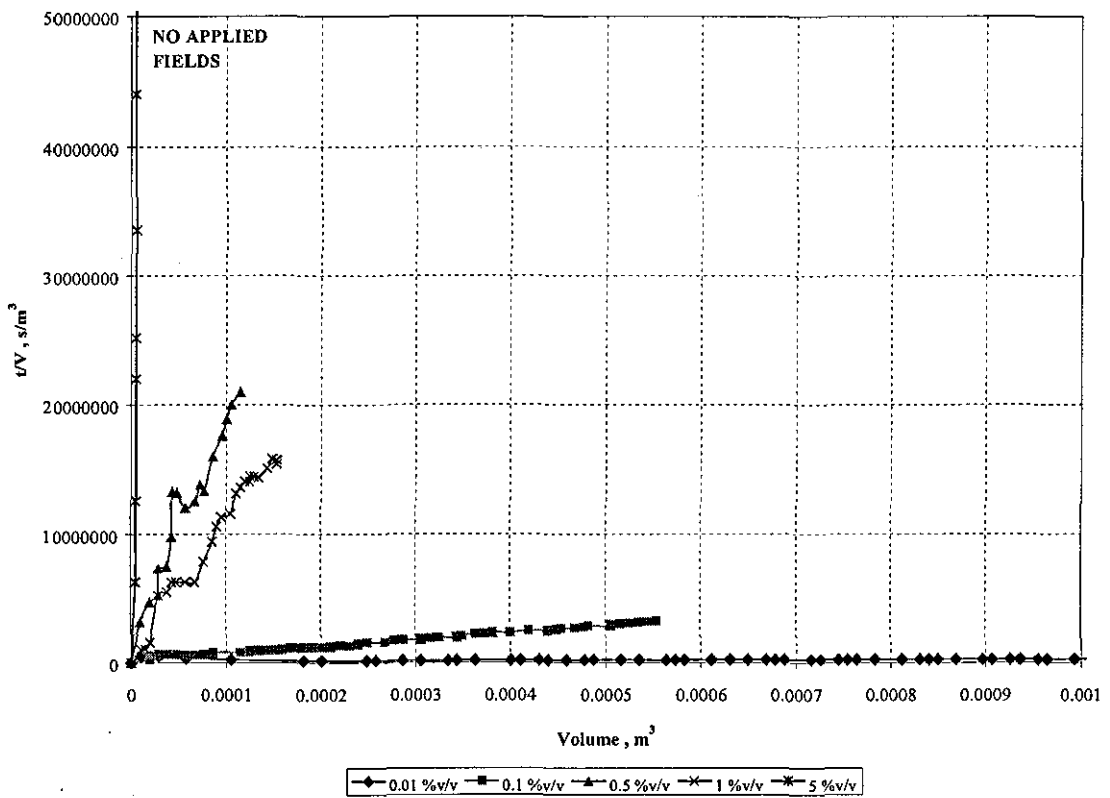
Figure 3-7b: Dead end filtration of various concentration rutile suspensions
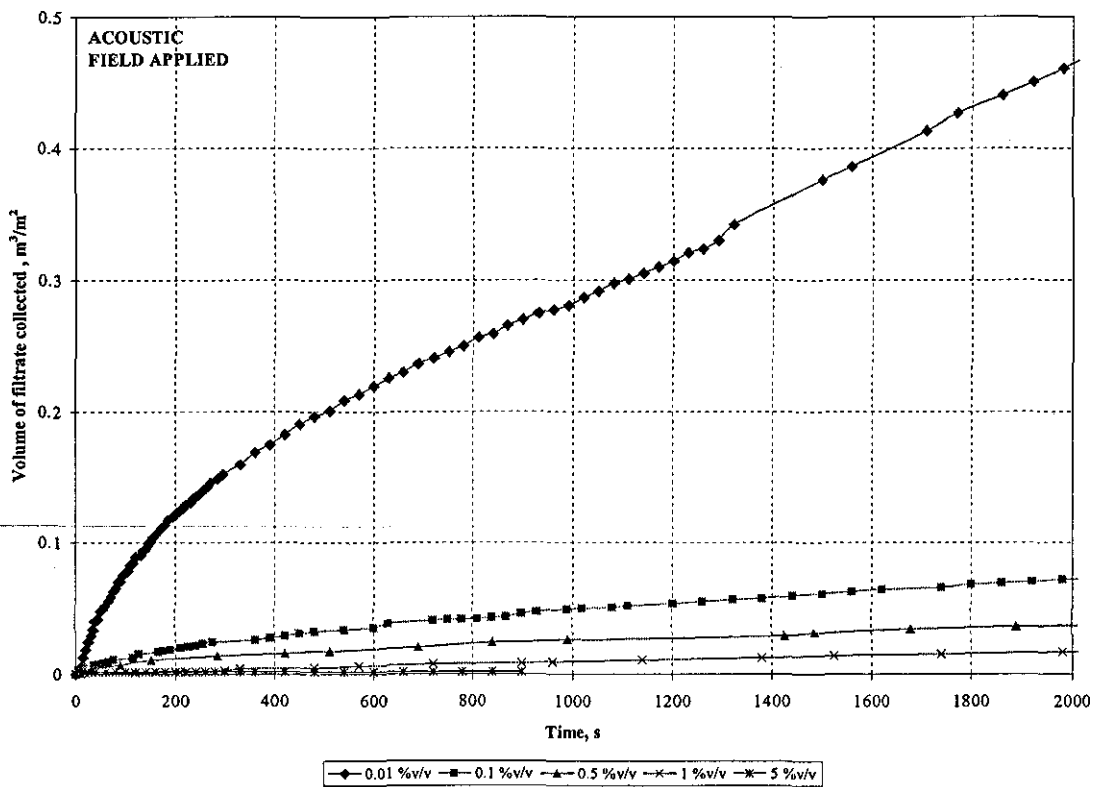
Figure 3-8a: Dead end acoustic filtration of various concentration rutile suspensions
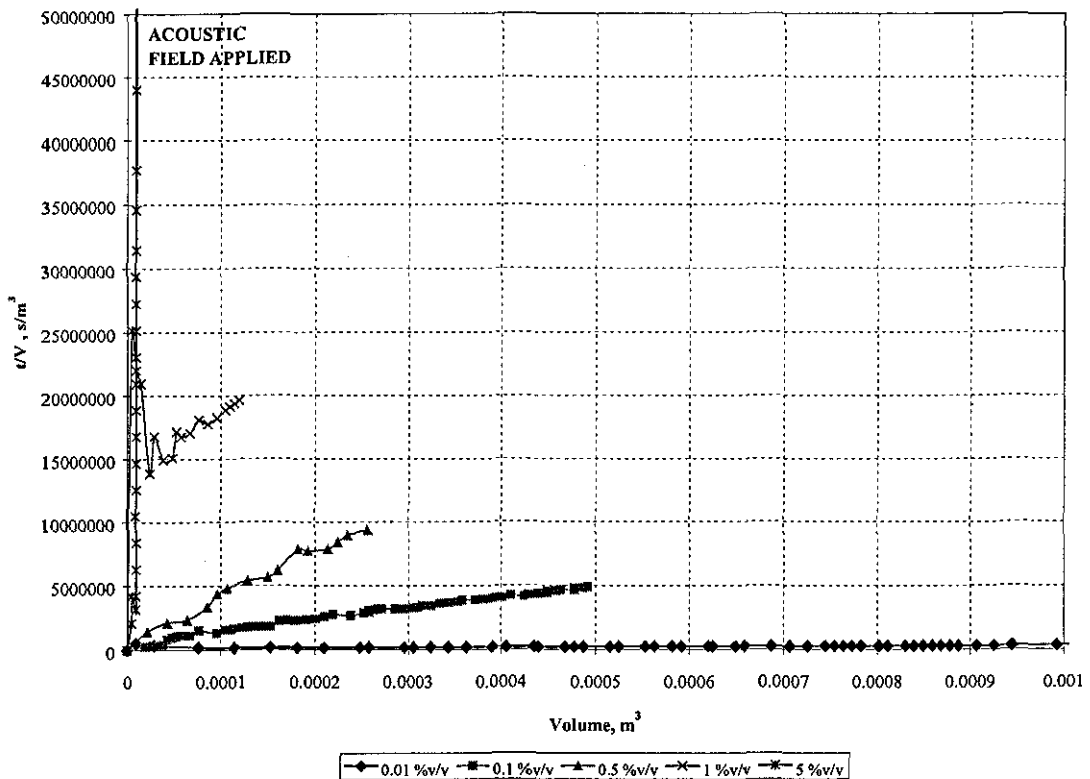
Figure 3-8b: Dead end acoustic filtration of various concentration rutile suspensions

In crossflow microfiltration however, such as that studied by Wakeman & Tarleton (1991), fluid flow is tangential to the medium, and the acoustic field appears to have a positive effect on filtration.

Study of Figure 3-9 indicates a possible reason for the results seen in Figures 3-7 and 3-8. A plot of K_l vs. concentration yields some interesting results; whilst at low concentrations the function $\dfrac{c_m \alpha \mu}{\Delta P'}$ is similar irrespective of the type of filtration, it is reduced considerably for acoustic filtration over 0.1%. It is not possible at this stage to hypothesise the mechanisms behind this change, suffice to say that, at higher concentrations, the nature of the suspension is changed in some way by the acoustic field. This conflicts with the evidence in Figures 3-7 and 3-8 that suggest that it is more likely to be at low concentrations that the suspension properties are changed. Rushton *et al* (1978) have shown that for the inorganic materials they studied, the values of α in a constant pressure experiment go through a maximum with increasing concentration. This effect is seen quite clearly by plotting K_l against concentration in Figure 3-9; for the no fields situation, the maximum occurs at a concentration of approximately 0.55 % v/v. At concentrations below the maximum low cake resistance is attributable to

high initial fluid velocities which are likely to produce open cake structures. Rushon et al (1978) explain the low cake resistances seen at higher concentrations by short cake formation times. It is of interest to note that a similar effect is not seen under acoustic filtration conditions. In fact K_1 continues to increase with increasing concentration suggesting that the cake resistance does not go through a turning point in these types of tests, at the concentrations studied. The ultrasound consolidates the cake as it forms, irrespective of the feed concentration. Thus at high concentrations, although the cake may be formed more rapidly, the consolidation effect prevents formation of a structure which differs from that formed at low concentrations. The slight increase in K_1 can probably therefore be attributed to the increase in the concentration term within K_1.

At low concentrations values of K_1 are similar whether or not the acoustic field is present. The increase in K_1 for acoustic filtration appears to be less. This phenomena would suggest that the acoustic field facilitates a more open cake than conventional filtration, with a lower cake resistance, although the variables within K_1 means that the effect could also be due to decreases in effective concentration, or increases in pressure. Table 3-1 shows the effective pressure amplitude of the acoustic wave to be 2.1 Bar,
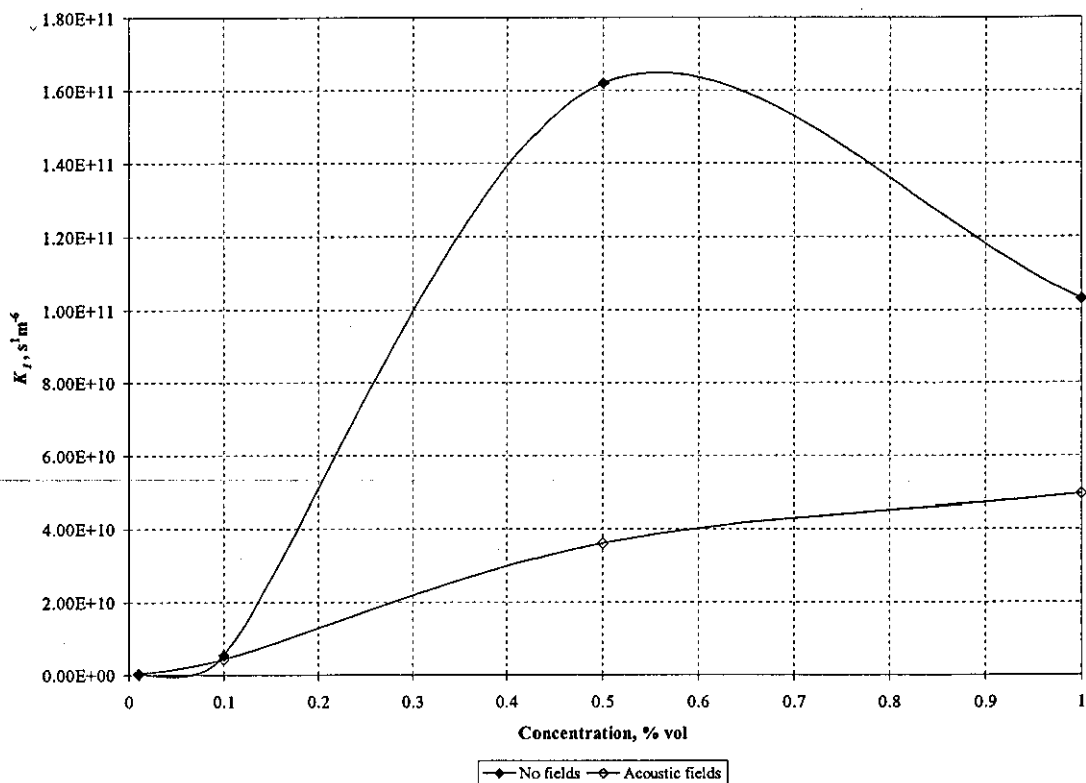
Figure 3-9: Concentration effects on the slope of the conventional Ruth Plot
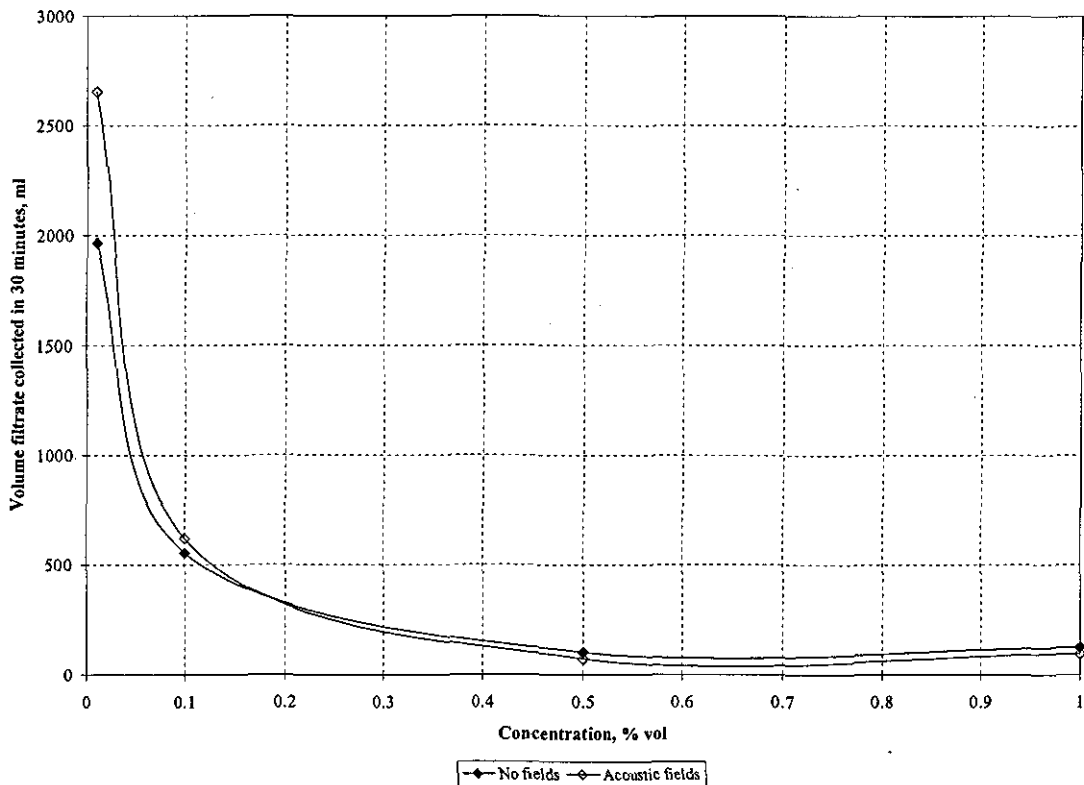
Figure 3-10: Concentration effects on filtrate volumes.

with a peak of 2.9 Bar. So acoustic pressure, although cyclical, is at times much larger that the applied vacuum, and no conclusion as to the true effect on specific cake resistance can be drawn.

The volume of filtrate collected in a given time period allows direct comparison of the field effect on filter performance. Much higher volumes are collected at low concentrations, but there is no great difference between conventional and acoustic filtration, suggesting that the application of an acoustic field alone is unlikely to be a viable method of filtration enhancement.

Following these experiments, a concentration of 0.1% v/v was chosen, as volumes obtained at this concentration most easily facilitated experimentation, based on the rig design.

3.7.1.1   The absorption attenuation coefficient

The majority of work into the absorption of sound in suspensions of one material in another has been carried out in the field of atmospheric aerosols. Initially Sewell (1910) considered small immobile particles in a sound field, and applied this to the propagation of sound in fogs and cloud. This assumption however is not valid at frequencies below

one Megahertz, or aqueous suspensions, because under these conditions the particles move with the fluid. Lamb (1945) extended the theory to rigid, incompressible particles which are free to move in the sound field. The work yields the well-known expression for the intensity absorption coefficient, ι.

$$I = I_0 \exp(-2\iota x) \qquad\qquad 3\text{-}24$$

$$2\iota = (4/9)k^4 a^4 \cdot \pi a^2 + (4\pi H'/k^2) \qquad\qquad 3\text{-}25$$

Where H' is the real part of a complex function of the particle and fluid densities ρ_s and ρ_f, the particle wavenumber, k, and the viscous skin depth, δ. The viscous skin depth is the characteristic thickness of the fluid layer around the sphere over which viscous coupling of the phases occurs, defined as

$$\delta = \sqrt{\frac{2\mu}{\omega\rho_f}} \qquad\qquad 3\text{-}26$$

Urick extended this work, to account for a number of particles in a suspension, by treatment of a dilute suspension as a series of independent Rayleigh scatterers. The attenuation expression becomes:

$$2\iota = \phi\left[\frac{1}{6}k^4 a^3 + k(\rho_s/\rho_f - 1)^2 \frac{s}{s^2 + (\rho_s/\rho_f + \tau)^2}\right] \qquad\qquad 3\text{-}27$$

where

$$s \equiv \frac{9\delta}{4a}\left(1 + \frac{\delta}{a}\right) \qquad\qquad 3\text{-}28$$

$$\tau \equiv \frac{1}{2} + \frac{9\delta}{4a} \qquad\qquad 3\text{-}29$$

The first term in equation 3-27 is the scattering loss produced by the small rigid particles which are free to move in the sound field, and shows a redistribution of the sound energy. The second term is a frictional loss due to the viscosity of the suspending fluid, under the conditions limiting Sewell's result, this term accounts for nearly all the absorption (Urick , 1948).
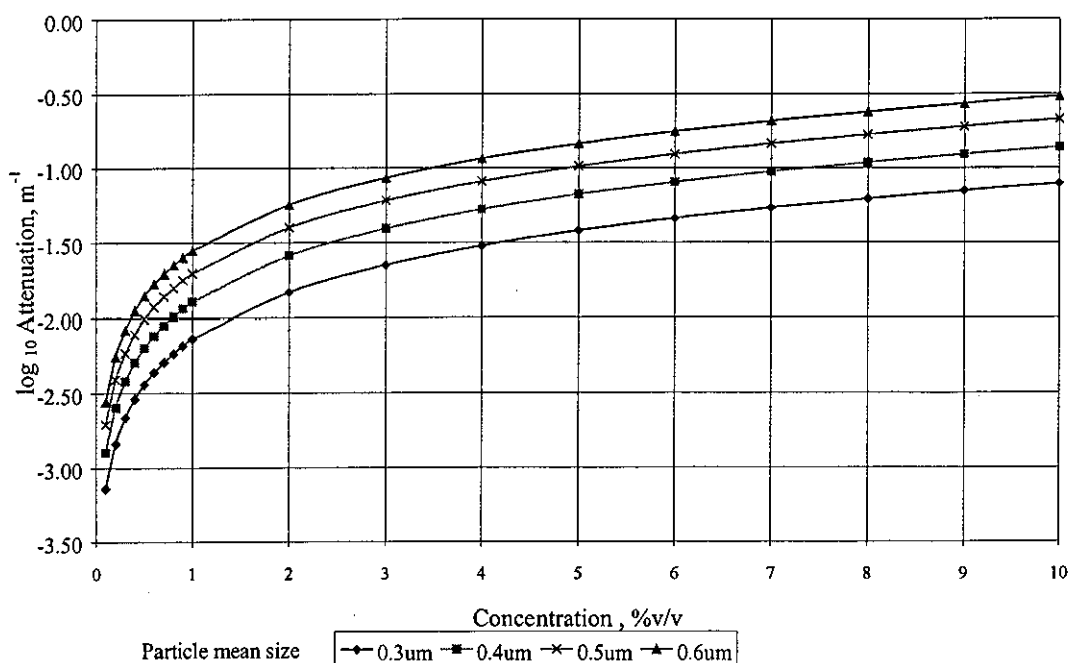
Figure 3-11: Attenuation calculated for sub-micron particles of density 4260 kgm⁻³,
according to Urick's expression for attenuation coefficient (1948)

At larger particle sizes, the effect of suspension concentration on the attenuation is greater, as shown in Figure 3-11. The work has been furthered and reviewed by many authors (Epstein and Carhart (1953), Chow (1964), Allegra & Hawley (1972)). Additionally Blue and McLeroy (1968), and Ahuja & Hendee (1978) have studied the effect of particle shape and orientation on the propagation of sound. Figure 3-12 and Figure 3-13 show how a particle's shape and orientation in the sound field may affect the attenuation and relative velocity. It is clear that the difference between particle and fluid velocity can be large for some shapes. However the discrepancy at low concentrations such as those used in this study is small, and these effects can be neglected.

3.7.1.2   Multiple Scattering

Epstein and Carhart's (1953) work on the attenuation of sound in aerosols can be extended to dispersions (Allegra and Hawley,1972). There are several minor and one fundamental difference between these works; the stress-strain relation used by Allegra and Hawley is appropriate to isotropic elastic solids, rather than fluids. The equations of mass, (continuity), momentum (Navier Stokes), and energy conservation are used,

together with the elastic isotropic stress tensor and two thermodynamic equations of state.
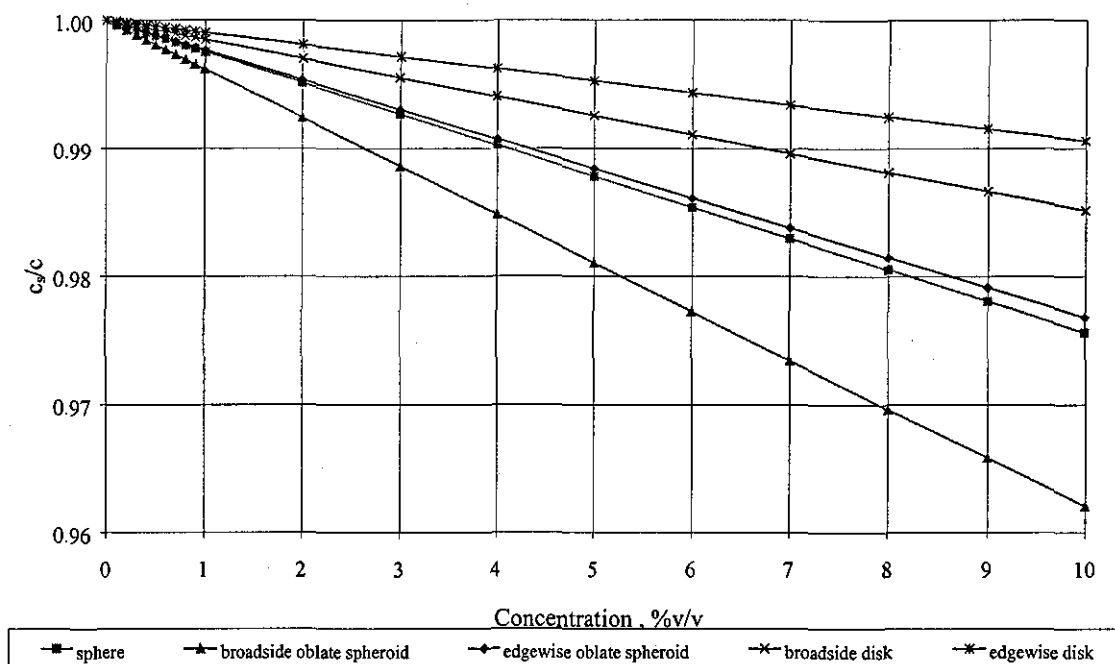
Figure 3-12: Effect of particle shape on the relative velocity of solid and fluid, according to Ahuja, 1978. Each particle has a volume equal to the sphere of radius 2.75 μm.
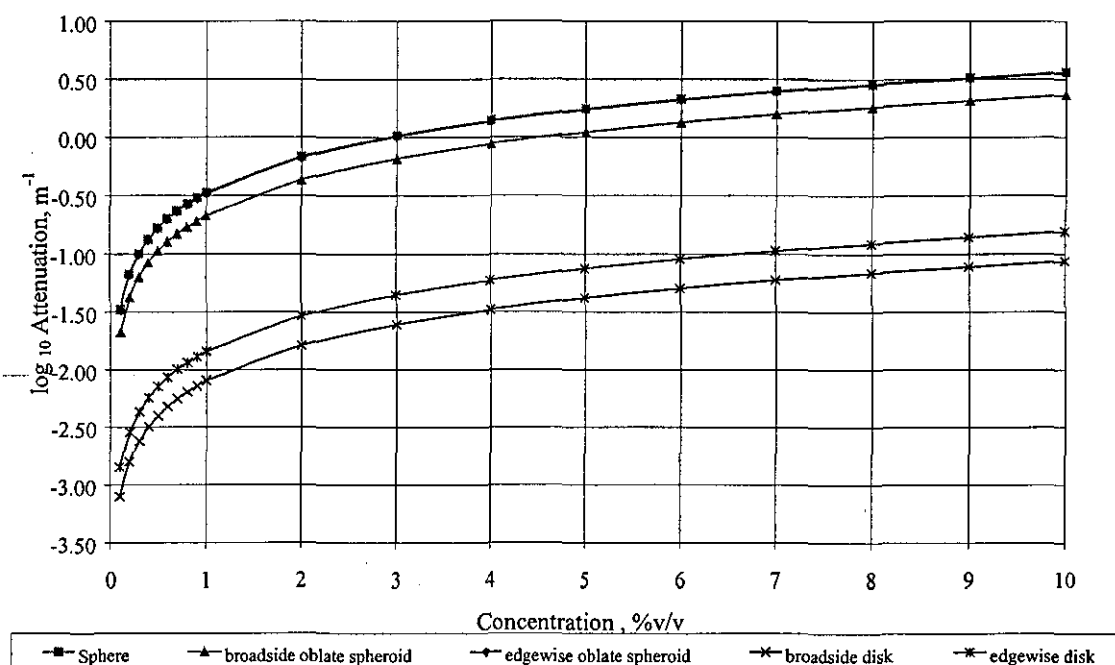
Figure 3-13: Effect of particle shape on the attenuation coefficient, according to Ahuja, 1978. Each particle has a volume equal to the sphere of radius 2.75 μm.

Davis (1979) reproduces Allegra and Hawley's work, to obtain six general equations for a solid particle suspended in a fluid medium. If the particles in a suspension are regarded as spherical scatterers, as a suspension becomes more concentrated the scatterers become more closely spaced and may no longer be treated as independent. Interference between the scattered wave functions will no longer be negligible, and compressional wave coefficients can no longer be added linearly. An averaging technique is used to calculate the field in a suspending medium containing a number of scatterers. This multiple scattering field calculation yields a complex propagation constant κ^* in the function:

$$\left(\frac{\kappa^*}{k^2}\right) = \left[1 + \frac{3\phi f(0)}{2k^2 a^3}\right]^2 - \left[\frac{3\phi f(\pi)}{2k^2 a^3}\right]^2 \qquad \textit{3-30}$$

where the scatterer amplitudes $f(0)$ and $f(\pi)$ are given by:

$$f(0) = \frac{1}{ik}\sum_{n=0}^{\infty}(2n+1)A_n$$

$$f(\pi) = \frac{1}{ik}\sum_{n=0}^{\infty}(-1)^n(2n+1)A_n$$

The sound attenuation is then evaluated by obtaining the coefficients A_n. A_n represents various attenuation coefficients, with n denoting the order of the particular coefficient. The zero and first order coefficients, A_0 and A_1 are given by Allegra and Hawley for solid particles. A_0 is known as the coefficient of thermal attenuation (Epstein and Carhart, 1953); it has two components, the first is identified by Allegra as being simply the difference in attenuation between the case where the volume fraction ϕ is occupied by scatterers and that when the particles are absent. The second component is the thermal conduction loss term, the magnitude of which can be determined by the thermal dilation, density and specific heats.

Similarly A_1 is the coefficient of viscous attenuation and depends on the shear viscosity of the suspending fluid. The magnitude of the thermal and viscous parameters denotes which coefficient dominates the absorption.

Comparison of expressions for single scattering (Davis, 1979) and multiple scattering (Allegra and Hawley, 1972) show that a second order correction factor is present in the

multiple scattering expression. For this term to dominate (and multiple scattering to be important) the following conditions apply.

- The suspension must be highly concentrated.

- A_0 and A_1 must be of equal magnitude- this must hold if the expression for attenuation is not to be reduced to the trivial case involving a single, dominating coefficient (thermal or viscous).

Multiple scattering only becomes important if both of these statements are true. In general viscous losses will dominate all other effects unless the density of the suspending fluid is close to that of the particles and multiple scattering can be neglected.

3.7.1.3   The effect of suspension concentration on the acoustic attenuation coefficient.

An expression for calculating the velocity and attenuation of ultrasound in a suspension can be obtained by a number of methods, as reviewed in this thesis and by Harker and Temple (1988). A simple quasi-phenomenological approach can be used, where the effective velocity is dependent on an effective suspension density and compressibility and the attenuation is given by the volume concentration multiplied by an average scattering factor.

Another method is to treat the suspension as a fluid saturated porous medium (as described in 3.1.1.2), and consider the scattering effect of particles within this system. The form of a scattered wave for small particles ($\kappa a < 1$) is given and it is suggested by these authors that multiple scattering effects dominate for solids volume fractions over 0.35, and are significant for volume fractions above 0.1. At volume fractions less than 0.15, for small particles (diameter below 50 μm) scattering can be neglected at low frequencies (less than 50 MHz). The conditions given in 3.7.1.2 also suggest that multiple scattering unlikely to have a large effect where the density difference is great, as is the case for solid-liquid suspensions.

The small particles and low concentrations being used in this work are unlikely to be affected by scattering effects, and Harker and Temple's hydrodynamic approach to finding the velocity and attenuation can be used.

3.7.1.4   Calculating the attenuation coefficient using Harker and Temple's approach

A number of assumptions are made in order to simplify the problem. The vertical (gravitational) forces are assumed to be much smaller than any force due to the acoustic field and we can assume that the effect of the gravitational field is small. Thus any force variations are in the x direction only.

The low volume concentrations (much less than 10% v/v) and frequency (23 kHz) being considered allows us to neglect multiple scattering effects according to Harker and Temple's suggestions, and Davis' requirements for the correction term to dominate.

Particle spacing is much less than the scale of x; particles are much closer together than the distance across the filter. The volume of fluid under consideration is far from any boundaries and the particles are sufficiently far apart not to have drag effects one another. That is, wall effects can be neglected. The boundary layer around each particle can be considered laminar.

The major energy damping is due to the forces between the solid and fluid, rather than due to the fluid. Harker and Temple also assume that the compressibility of the suspension is equal to an average of the solid and the fluid.

Momentum and continuity of the phases are balanced with the drag of one phase on the other, and Stokes expression for the force on a sphere oscillating steadily in a fluid is used to obtain expressions for the conservation of momentum for each phase.

A further assumption is that the compressibility of the suspension is equal to the average of the solid β_s and the fluid β_f. This arises from the change in densities of the components due to the compression effect of the wave. The component densities are dependent on their compressibility and pressure.

$$\rho_f = \rho_{f0} + \rho_{f0}\beta_f p \qquad\qquad 3\text{-}31$$

$$\rho_s = \rho_{s0} + \rho_{s0}\beta_s p \qquad\qquad 3\text{-}32$$

The equations are solved for a wave like solution of u_s, u_f, ρ_f, ρ_s, p and ϕ. An expression for each of the unknowns is written in a wave form,

$$u_f = \overline{u_f} \exp\left[\mathrm{i}(kx - \omega t)\right] \qquad\qquad 3\text{-}33$$

$$u_s = \overline{u_s} \exp\left[\mathrm{i}(kx - \omega t)\right] \qquad\qquad 3\text{-}34$$

$$p = \bar{p}\exp\left[i(kx - \omega t)\right]$$

3-35

$$\rho_f = \rho_f^0 + \overline{\rho_f}\exp\left[i(kx - \omega t)\right]$$

3-36

$$\rho_s = \rho_s^0 + \overline{\rho_s}\exp\left[i(kx - \omega t)\right]$$

3-37

$$\phi = \phi^0 + \bar{\phi}\exp\left[i(kx - \omega t)\right]$$

3-38

The solution is derived in two ways by Harker and Temple (1988). Their non-trivial solution for the wavenumber is:

$$k^2 = \omega^2\left[(1-\phi)\beta_f + \phi\beta_s\right]\left\{\frac{\rho_f\left[\rho_s(1-\phi+\phi R)+\rho_f R(1-\phi)\right]}{\rho_s(1-\phi)^2 + \rho_f\left[R+\phi(1-\phi)\right]}\right\}$$

3-39

Where $R = Q + is$

and

$$Q = \frac{1}{2}\left(\left(\frac{1+2\phi}{1-\phi}\right)+2\tau-1\right)$$

3-40

with s defined by equation 3-28.

The attenuation, ι is given by the imaginary part of k, and the effective wave velocity by the real part of (ω/k). These are denoted by $\Im(k)$ and $\Re(k)$ respectively. Hence

$$\iota = \Im(k) = \sqrt{|k|}\sin\left(\frac{\Psi}{2}\right)$$

3-41

where

$$k = \frac{T}{W^2 + X^2}\left\{(UW + VX) + i(VW + UX)\right\}$$

3-42

and

$$\Psi = \tan^{-1}\frac{(VW + UX)}{(UW + VX)}$$

3-43

T, U, V, W and X are defined below.

$$T = \omega^2 \left(\beta_f (1 - \phi) + \phi \beta_s \right)$$

3-44

$$U = \rho_f \left(\rho_s (1 - \phi + \phi Q) + \rho_f Q (1 - \phi) \right)$$

3-45

$$V = \rho_f \left(\rho_s \phi R + \rho_f R (1 - \phi) \right)$$

3-46

$$W = \rho_s (1 - \phi)^2 + \rho_f \left(Q + \phi (1 - \phi) \right)$$

3-47

$$X = \rho_f R$$

3-48

Attenuations are calculated up to the point where multiple scattering may begin to dominate (in this case 10 % v/v). The wave propagation velocity, c, given by $\Re(\omega/k)$, can be calculated in a similar manner using

$$\Re(k) = \sqrt{|k|} \cos\left(\frac{\Psi}{2} \right)$$

3-49

Then

$$c = \Re\left(\frac{\omega}{k} \right) = \frac{\omega}{\Re(k)} = \frac{\omega}{\sqrt{|k|} \cos\left(\frac{\Psi}{2} \right)}$$

3-50

At the low concentrations where this theory is valid the following curve is obtained.

The sound propagation velocities shown in Figure 3-15 are of a similar order to that calculated in 3.4.1 (1481 ms^{-1}). The velocities shown are slightly less than that, but this merely shows the effect of the particles present in more concentrated suspensions, as the empirical equation given was for distilled water.

The results given by this analysis can be used to explain the decline in acoustic filtration performance as seen in Figure 3-7 and Figure 3-8. Whilst multiple scattering does not dominate the attenuation in these low concentration suspensions, there is certainly an attenuation effect, and a reduction in wave velocity. As the concentration increases the energy damping between the solid and the fluid increases, and the acoustic field is less effective.
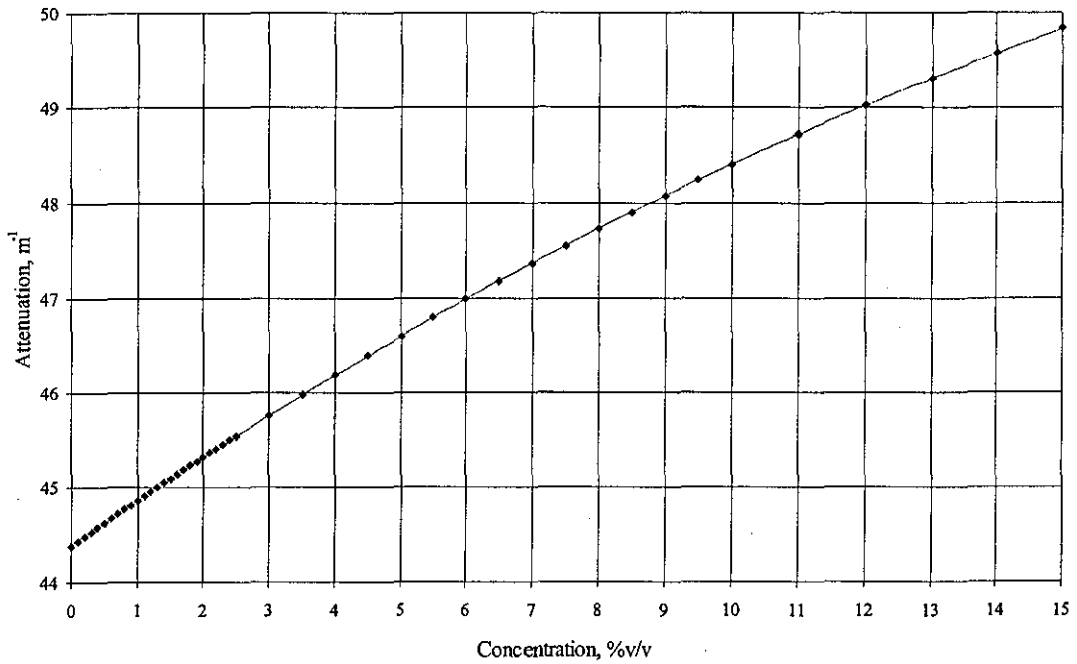
Figure 3-14: The effect of concentration on attenuation using Harker and Temple's expression. Attenuation calculated for a 0.3μm particle of solid density 4260 kgm⁻³. (The titania properties used in the experiments reported in this thesis)
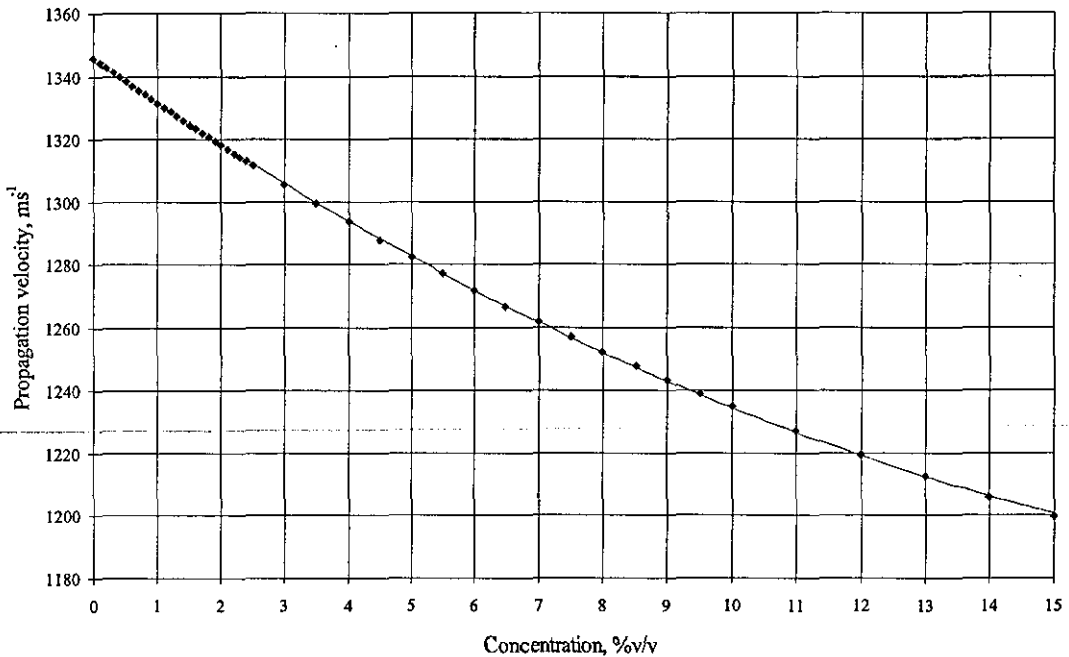
Figure 3-15: Calculation of propagation velocity in a suspension (as described in Figure 3-14).

3.7.2   Effect of applied voltage on field assisted filtration

Typical filtrate volume versus filtration time curves measured for dead-end filtration of 0.1%v/v rutile suspensions at pH 8 under various applied field strengths are shown in Figure 3-17. Each experiment was carried out at constant voltage, although this was varied between experiments. The overall rate of filtration increases as the electric field gradient is increased. As the electric field strength is increased, the rate of decline in filtrate flux is reduced.

This reduced decline in flux is a result of reduced cake formation due to electrophoresis, an effect that has previously been observed by Moulik *et al* (1967, 1971) and Wakeman (1982). It has been shown that a critical voltage gradient exists at which point the induced electrophoretic velocity v_e is equal and opposite to the local fluid velocity, v_b, and suspended particles become stationary, assuming zero slip between the liquid and suspended solids. This critical voltage gradient E_{CR} is given by

$$E_{CR} = \frac{3\mu v_b}{2\varepsilon_0 D\zeta} \qquad\qquad 3\text{-}51$$

Where ε_0 is the permittivity of a vacuum and D the dielectric constant of the suspending media. The initial filtrate velocity (based on the first 200 s of filtration) at pH 8 is 130 μms^{-1}. To avoid deposition altogether, a field of 56 Vcm^{-1} would need to be applied. This analysis based on the Henry equation assumes that all the particles are flowing normal to the membrane surface as the approach it, and that all particles in the suspension have identical surface properties.

Although it is stated in the literature (Section 2.4.3) that solutions to the Henry equation are complex for zeta potentials over 25 mV the theory of electrofiltration and a critical field gradient is upheld by the results shown in Figure 3-16. Whilst an improvement in filtration rate is seen when a 20 V cm^{-1} field is applied, this is markedly greater as voltages close to the critical field gradient are applied. As the duration of the experiment increases, flux levels drop and the critical field strength to suspend particles is reduced, resulting in an almost constant velocity of 28 μm s^{-1}.
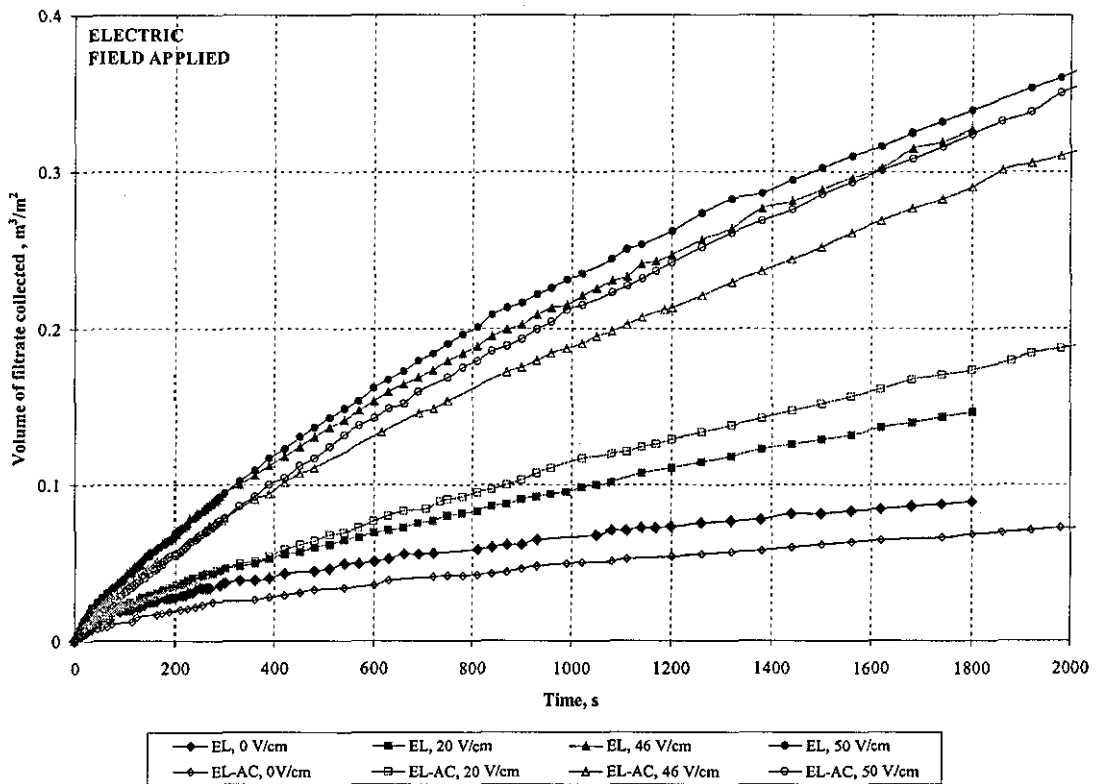
Figure 3-16: The effect of various applied voltages on assisted field filtration
Suspension concentration 0.1 %v/v, pH 8.
(Notation: EL- electric field only; EL-AC, electric and acoustic fields applied)

The application of an ultrasonic field to the electrofiltration appears to reduce the filtrate flux under most conditions. At higher field strengths, where the applied field is close to the critical field strength, the acoustic field may be forcing particles which would otherwise be suspended via the balance of electrophoresis and fluid flow, towards the filter medium and cake. It may also be causing particulate agglomeration, resulting in increased gravitational settling. Chapter 4 discusses acoustic forces and how they may affect suspension behaviour. The theory for E_{CR}, based on the assumption that particles approach the medium normally, no longer holds as the turbulent effect of the ultrasound may move them axially across the filter. The velocity imparted to the particles is likely to be large (see Chapter 4 and Wakeman & Bailey 1998), so the critical field gradient is greater and a lesser effect of the electric field is seen.

Ultrasound is rapidly attenuated in suspensions of concentration greater than 0.1%, so if electrothickening does proceed the ultrasonic effect is likely to become less apparent. This is shown by the electro- and electroacoustic curves following one another for the

initial part of the filtration (up to 300s). The improvement by application of the acoustic field at lower voltage gradients cannot be explained at this stage.

3.7.3   Effect of pressure on field assisted filtration

The effect of pressure on filtration rate is shown in Figure 3-17. There is a small pressure effect, with volumes collected at 250 mBar vacuum being lowest in both cases. It does not appear that variation of filtration pressures in this range has a great effect on the filtration although in general increasing the pressure drop increases the filtrate volume collected over time slightly. It is interesting to note that the conventional filtration behaviour at 250 mBar is similar to the acoustic at 750 mBar, implying that the acoustic field may actually reduce the effective pressure drop.

K_1, sm^{-1}	No Fields	Acoustic Field	Electric Field, 50Vcm^{-1}	Electro- Acoustic Field, 50Vcm^{-1}
250 mBar (vac)	9.3×10^9	1.3×10^{10}	2.0×10^8	1.8×10^8
500 mBar (vac)	5.44×10^9	6.5×10^9	2.5×10^8	1.8×10^8
750 mBar (vac)	5.5×10^9	8.6×10^9	2.2×10^8	1.8×10^8

Table 3-4: Effect of pressure on K_1 values for field assisted filtration

Similarly there does not appear to be a great effect of pressure on electrofiltration (Figure 3-18). The pressure effect can be more clearly seen by considering K_1. Table 3-4 clearly shows that at all pressures studied, the application of an acoustic field actually increases K_1. For electrofiltration, K_1 is reduced considerably, and the acoustic field used with electrofiltration results in K_1 values being reduced further. There is no pressure effect for electroacoustic filtration. Tarleton (1986) carried out some similar work to study the effect of applied pressure gradient and electric field strength.. He showed that the electrokinetic effects have a greater influence on the filtration process when the applied field is lower. This effect is duplicated to a certain extent in this study, with the improvement shown at 250 mBar greater than that at 500 or 750 mBar. The application of the electric field resulted in similar filtrate volumes at all pressures, and this too is supported by Tarleton's work (1986), suggesting that the effect on the filtration rate that the electric field has is greater than the effect of an increase in pressure . In order to carry out a filtration more quickly then, electric fields may be a suitable method of reducing the required hydraulic pressure.
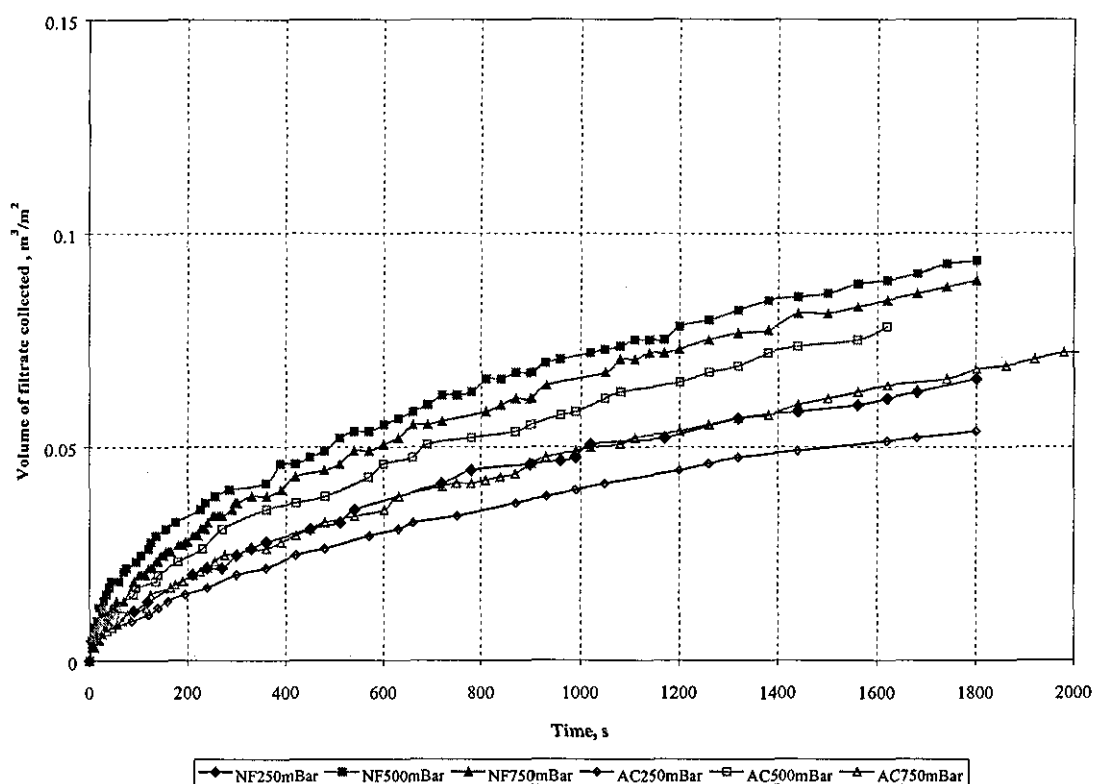
Figure 3-17: Effect of applied vacuum on acoustic field assisted filtration,
Suspension concentration 0.1% v/v, pH 8
(Notation: NF- No fields; AC- Acoustic field applied)

3.7.4   Effect of pH on field assisted filtration

Filtration experiments were carried out to investigate how assisted field filtration performed at different pHs. Table 3-5 shows that the suspension behaved differently as pH varied. A phenomena which should be mentioned here is that of electrode dissolution, reactions occur at the electrodes releasing gas and ions into the permeate or feed streams. The most likely cathode reactions are

$$2H_2O + 2e^- \rightarrow H_2 + 2OH^- \quad \text{and} \quad M^{n+} + ne^- \rightarrow M$$
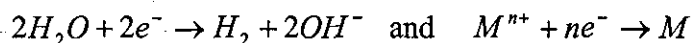
where M represents a metal. The most likely anode reactions are

$$M_a \rightarrow M_a^{n+} + ne^- \quad \text{and} \quad 6H_2O \rightarrow O_2 + 4H_3O^+ + 4e^-$$
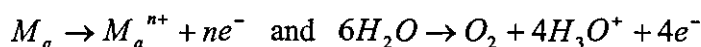
where M_a represents the anode metal. Therefore during electrically assisted filtration gases will be evolved which may act to alter the formation of cake, by allowing a more porous cake to form, and reducing the specific cake resistance. The ions released will act to alter the pH in the region of the electrodes, which will also affect cake formation, by

changing the zeta zeta potential of the particles. For example at the anode, electrode dissolution will cause a more acidic environment, reducing zeta potentials and causing particle agglomeration. This in turn allows more open cake formation as the effective particle size is larger. Similar results were seen by Akay & Wakeman (1996), in which the porous electrode was the anode, and an increase in the pH of the permeate was observed upon application of an electric field.

Volume filtrate after 1800s, ml	No Fields	Acoustic Field	Electric Field 20Vcm^{-1}	Electro-Acoustic Field 20 Vcm^{-1}	Electric Field 50 Vcm^{-1}	Electro-Acoustic Field 50 Vcm^{-1}
pH 4	916	1126	1222	1098	1957	2344
pH 6	702	883	1279	1346	1842	2043
pH 8	554	425	912	1079	2109	2014
pH 10	453	506	1370	1413	2479	2925

Table 3-5: Filtrate volumes collected after 1800s of assisted field filtration
Suspension concentration 0.1%v/v, pressure drop 750mBar

The effect of pH is shown in Figure 3-19 as a percentage gain, with conventional filtration being taken as the zero point.

At pH 4, (close to the IEP), where zeta potentials are small, the gain is close to zero for acoustic and electrofiltration when the applied voltage is low. Filtrate gains of over 50% are achieved by higher voltage application, as the higher induced electrophoretic velocity is able to prevent more of the particles from settling. This effect is more pronounced at the lower pHs, because the particles have a much wider particle size distribution and a larger mean particle size. The larger particles have higher Stokes settling velocities and require higher electric field gradients in order to keep in suspension. Figure 3-20 shows that there is little difference between conventional, acoustic and low voltage electrofiltration and similar gradients (K_1) are obtained. It was noted during experimentation at pH 4 that a large amount of settling took place during residence in the filter cell, with aglommerates collecting on top of the anode, which acted as a primary sieve. Fewer particles reached the region of the filter medium, and so an effectively lower concentration suspension challenged the media.
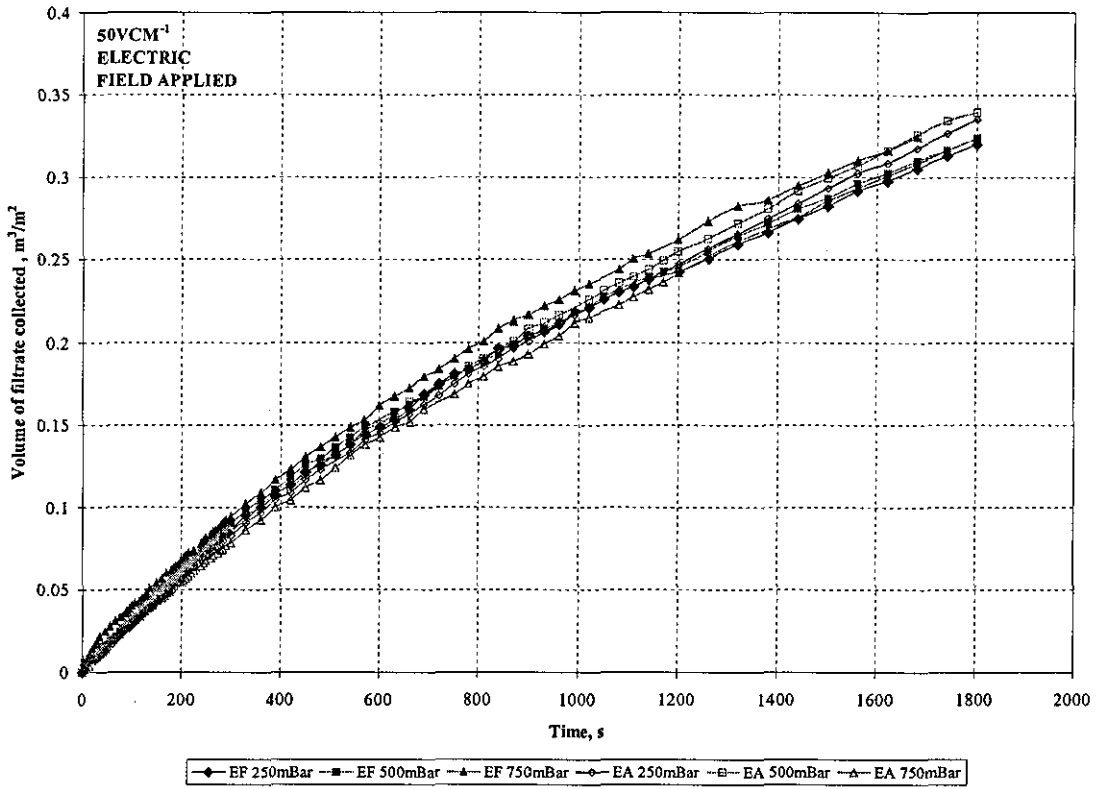
Figure 3-18: Effect of applied vacuum on acoustic field assisted electrofiltration,
Suspension concentration 0.1%v/v, pH 8
(Notation: EF-Electric field, EA-Electro-Acoustic field applied)
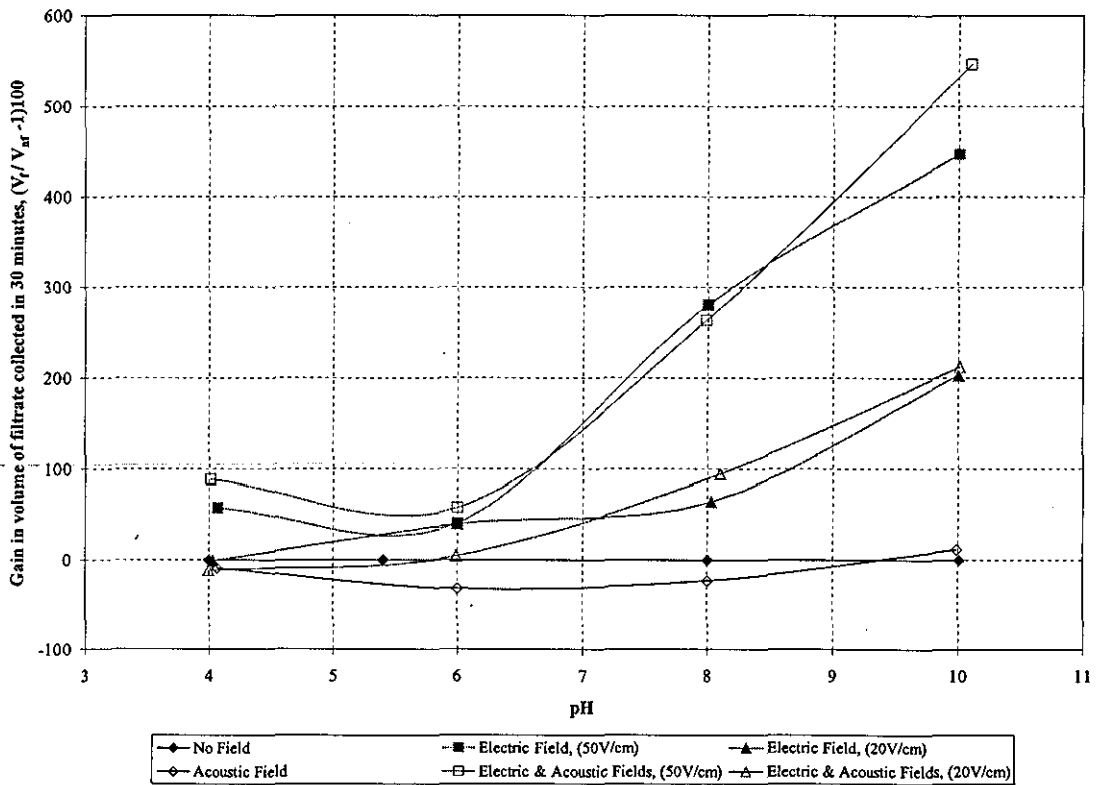
Figure 3-19: Gains in filtrate volume as a result of pH changes of the test suspension
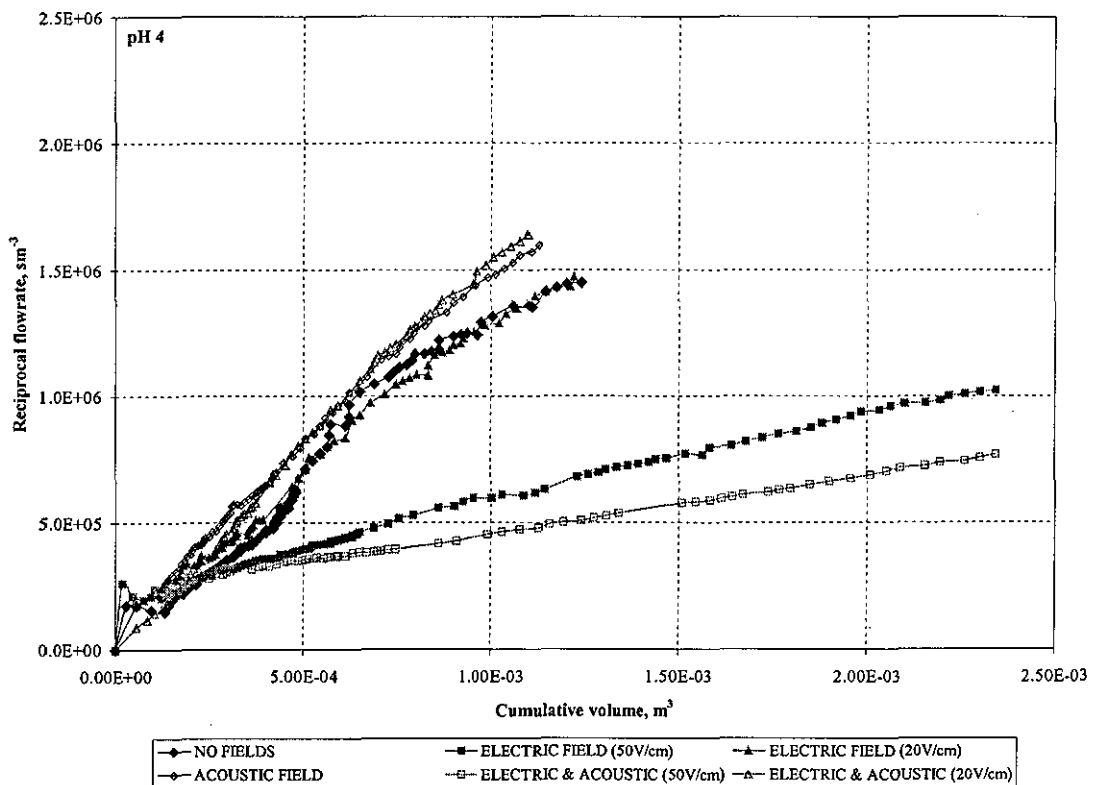
Figure 3-20: Field effects on filtration at pH 4
Suspension concentration 0.1% v/v, Pressure drop 750mBar

At pH 6, which represents the steep part of the zeta potential curve, the magnitude of zeta potential is greater and so lower electric field gradients are required. The higher magnitude field does not have as pronounced an effect as at pH 4. Application of the ultrasonic field alone reduces the filtrate volume, suggesting that the irradiation increases the specific cake resistance (shown by an increase in the gradient on Figure 3-21). This is supported by Kowalska *et al* (1979) who studied the changes of properties of sonated sludges, and found that ultrasound always increased the specific resistance of the sonated sludge, The mechanism suggested of the ultrasound further reducing particle size by breaking down flocs could be applied here in considering that the ultrasonic energy may have broken down some of the larger agglomerates to discrete particles.

Higher pHs show the most pronounced effects of the applied fields. At pH 8 a 20 Vcm^{-1} applied electric field provides the same gain in filtrate as 50 Vcm^{-1} at pH 4. The highly negative zeta potential together with a smaller particle size reduces E_{CR} and electrophoretic flow takes place directed away from the filter medium. The gain is higher at 50 Vcm^{-1} because of the greater difference between the applied and critical voltages. However the acoustic field still appears to be having little effect on the

filtration performance. At pH 10 the gain doubles again to 200% at low voltages, but there is no difference between electro- and electroacoustic filtration. At higher voltages however the gain in filtrate volume is in the region of 500%. It is unclear why the acoustic field appears to benefit the filtration under these conditions. It could be that pH 10 is the turning point on the zeta potential curve, and is thus the location where a minimum of agglomerates exist. Figure 3-23 would suggest that cake resistances were similar under both conditions. The ultrasound may work with the electric field, but the mechanism is not understood at this stage.

Again, Tarleton's (1988) work on assisted filtration shows similar results. For anatase a slight gain in permeate volume is seen when the acoustic field is applied together with the electric field, however for china clay, the ultrasound again has a negative effect when compared with the electric field alone. This suggests that the effect of ultrasound on the filtration performance is dependant on the material being studied, and at this stage empirical results would have to be used to predict an assisted filter's performance.
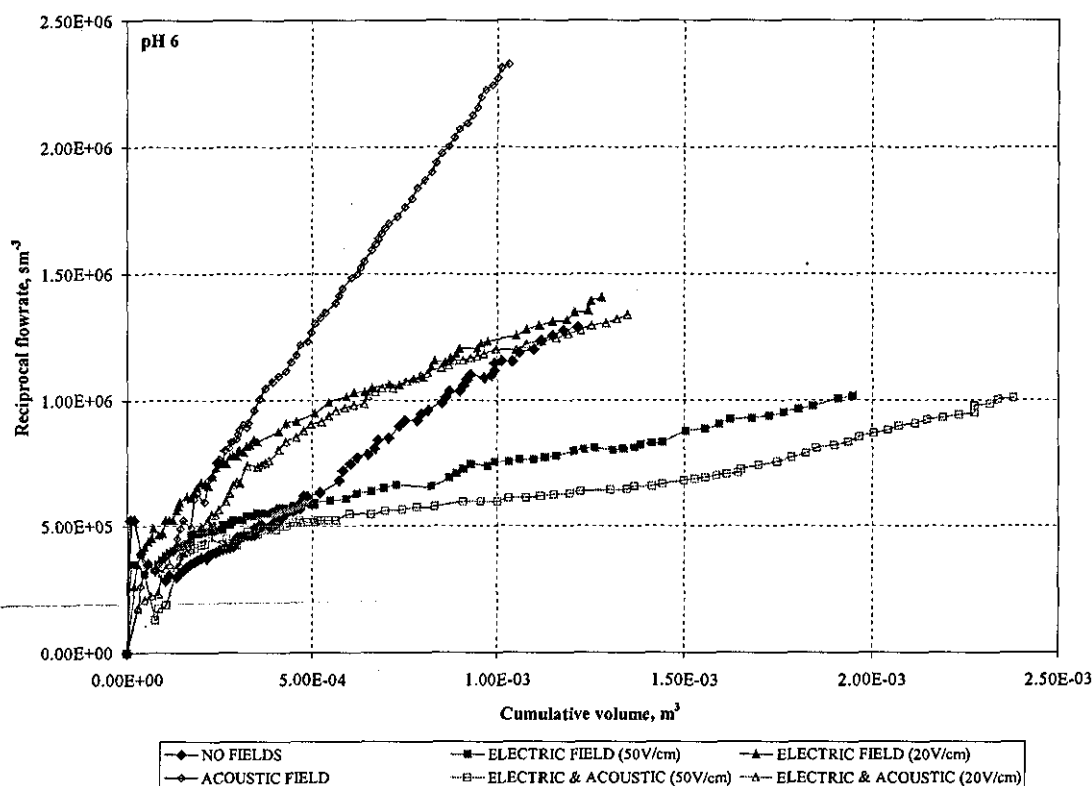
Figure 3-21: Field effects on filtration at pH 6
Suspension concentration 0.1% v/v, Pressure drop 750mBar
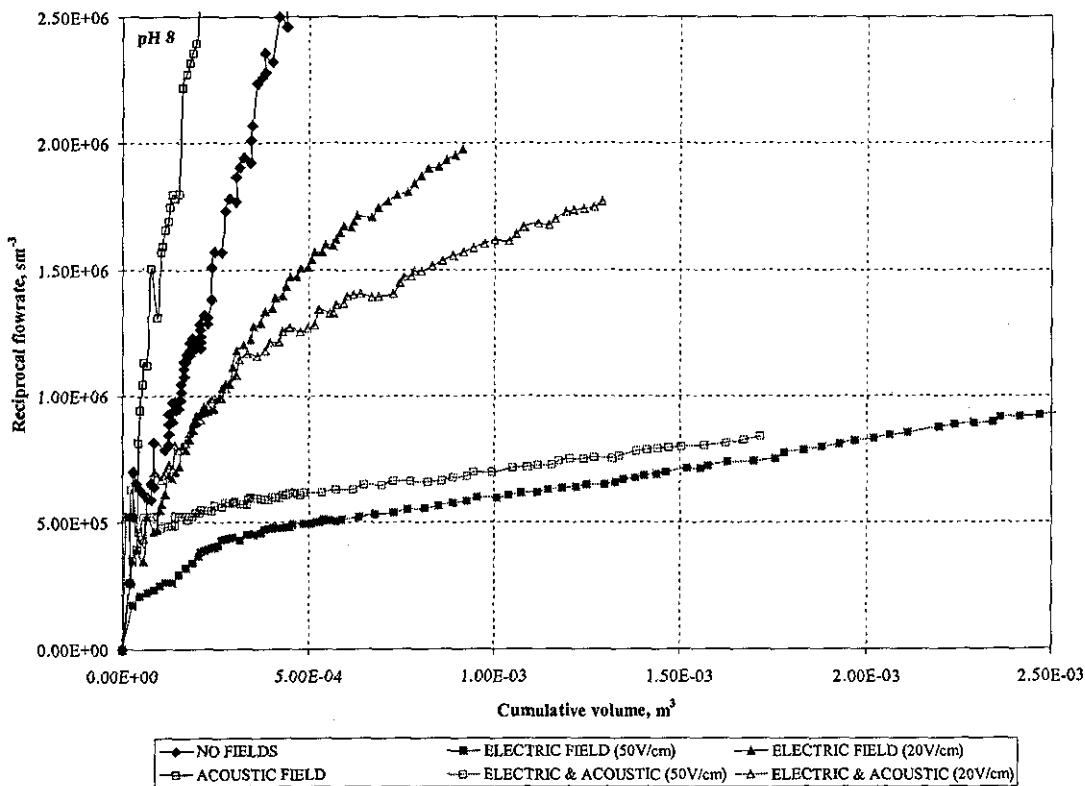
Figure 3-22: Field effects on filtration at pH 8
Suspension concentration 0.1% v/v, Pressure drop 750mBar
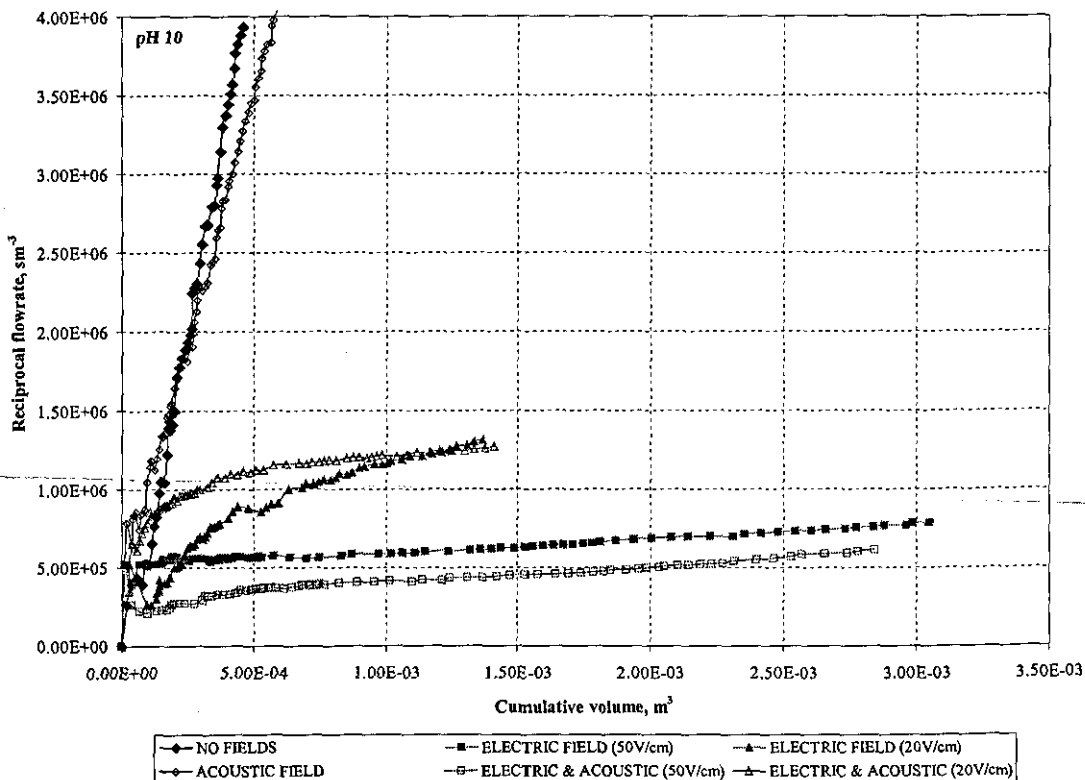
Figure 3-23: Field effects on filtration at pH 10
Suspension concentration 0.1% v/v, Pressure drop 750mBar

3.7.4.1   The variation of porosity due to the application of fields

Cake samples were taken following every filtration, and the porosity measured by drying as described in Section 3.7.4.1.1

3.7.4.1.1   Cake Sampling

A technique was developed for the removal of samples of cake from the filter medium, in order that the moisture content of the cake could be calculated. It should be noted that this technique gives only an indication of the cake porosity, as the nature of the filter cell construction means that the cake will always be disturbed to a certain extent prior to a sample being taken. In addition, the low suspension concentrations resulted in only thin cakes being formed, increasing the difficulty of obtaining a representative sample.

The method developed was as follows:

1. Following the completion of a filtration experiment, close the valve between the filter cell and filtrate tank.

2. Close the feed vessel valve to the filter tank and drain feed vessel. Begin to dismantle filter cell by removing the lid (which removes the anode and allows access to residual suspension in the cell).

3. Syphon the remaining suspension form the cell. Care should be taken when carrying out this operation that the cake is not disturbed by the syphon pipe. Due to this, a small amount of fluid will remain in the bottom of the cell, just covering the filter cake.

4. The body of the filter cell can now be removed, leaving the filter medium support with the membrane attached standing proud of the unit base.

5. The cake sample can be carefully scraped from the membrane onto a dish of known mass, which is suitable for oven drying.

6. The dish and sample are weighed, dried, and then weighed again, to calculate the moisture content of the sample. The cake concentration is calculated by the ratio of dry to wet volumes, and the volumetric porosity obtained.

This method of cake sampling is far from ideal, and has numerous limitations due to the design of the filter cell. In any further work that is carried out, the location of the filter membrane and its ease of removal should be carefully considered, in order that more

representative sampling could be carried out. The porosity results given in this thesis give an indication of the field effects when backed up by the filtration results in the form of K_l.

3.7.4.1.2   Porosity results

At all pHs except pH 4 the porosity obtained by conventional filtration was around 0.6   . No conclusion can be drawn regarding whether this is due to the limtations of the sampling method, or due to the fields. However the method used was consistent throughout the tests and it is reasonable to assume thet the results discussed are due to the applied fields. Porosity was higher at pH 4 due to the presence of agglomerates causing looser packing. In agreement with the filtration results, there is little difference in cake porosity at pH 4 suggesting that the cake structure was not changed considerably by the application of fields. However at other pHs the cake structure does appear to have changed, particularly at pH 6.
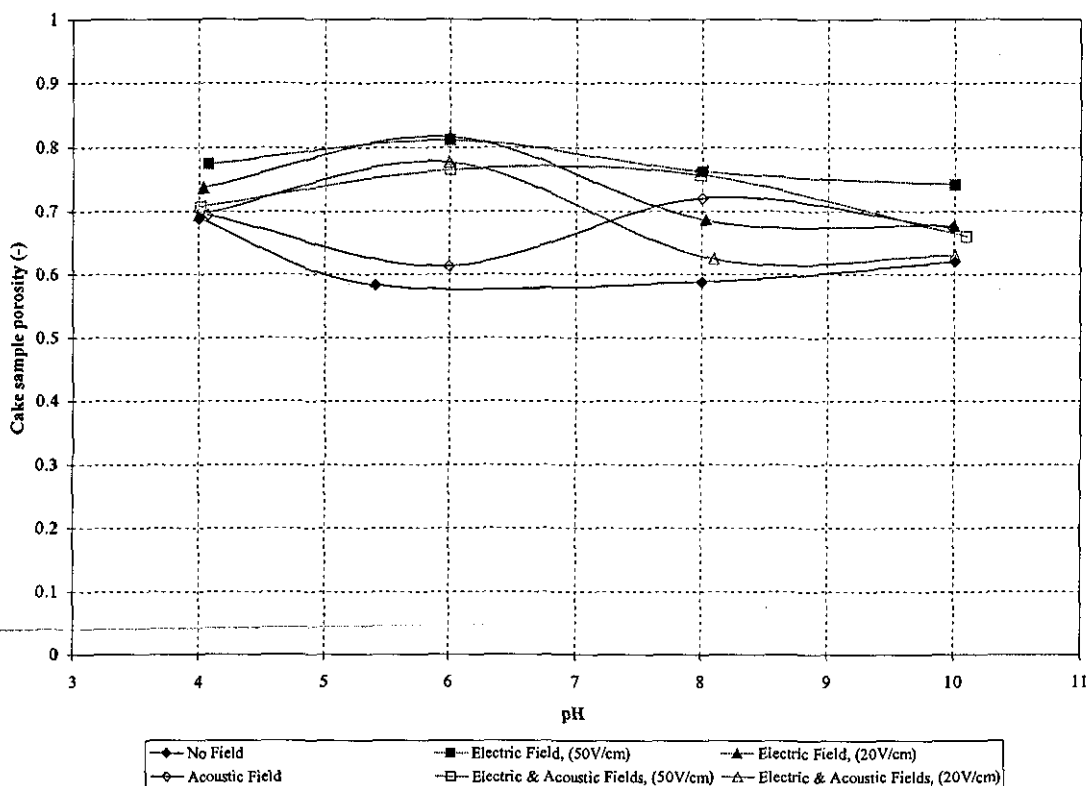
Figure 3-24: Field effects on sampled porosity of filter cake
Suspension concentration 0.1% v/v, Pressure drop 750mBar

We have established that the ultrasound is likely to increase cake resistance (Kowalska *et al*, 1979), so these changes can be attributed to the electric fields applied. This is

supported by the porosity result for acoustic field alone, whilst it is not lower than conventional filtration it is certainly lower than other combinations of applied fields.

At pH 8 the difference between the field strengths is clear. Electrophoretic flow results in a more open cake, particularly at high field strengths.

At pH 10 the range of porosities becomes closer again. This is due to electrophoretic flow actually reducing the amount of cake formed, so that whilst the porosity remains similar, the mass of cake is less, and a thickening process occurs.

3.7.5   Energy Consumption

Energy consumption of the processes studied has been considered, in order to assess whether the processes under investigation are economically viable. Experiments were carried out under constant voltage, and typical values of current are given in Table 3-6

pH	Electric Field (50 V/cm)	Electric Field (50 V/cm) + Acoustic Field 23 kHz
4	42.5	72
6	74	-
8	47	33.4
10	58	57.6

Table 3-6: Typical value of current during filtration experiments

The power consumptions corresponding to the experiments described in section 3.7 are shown in Tables 3.7 and 3.8 below. Because of the differing filtrate flow rates obtained under different conditions, for comparative purposes it is most appropriate to look at specific energy consumption figures. These show that least energy is consumed by conventional filtration at all pH values; the addition of either field increases the energy consumed, with the greatest amount being taken by the ultrasonic field.

Total Power Consumption, W	pH 4	pH 6	pH 8	pH 10
No fields	0.8	0.9	0.3	0.2
Acoustic Field (23 kHz)	275.8	275.6	275.2	275.3
Electric Field (50 V/cm)	4.5	6.3	4.4	5.3
Electric Field (50 V/cm) + Acoustic Field (23 kHz)	5.4	280	278.3	278.8

Table 3-7: Power consumption data for the experiments described in this Chapter.

In making these comparisons, the increased filtrate rates need to be considered as this affects either the time to accomplish a given filtration, or the size of the equipment needed to achieve the separation. This is given in Table 3-5, for the full length of the experiments. The increased flux as a result of adding the fields is apparent, but the data also indicates that the electric field is more effective at increasing the filtration rate than the acoustic field. In some applications it may be acceptable to consider using the electric field as a way of shortening the filtration time, albeit with the penalty of an increased energy consumption. But for industrial use it is unlikely that ultrasound would be considered to increase filtration rates as the penalty in energy consumption would always be too high.

Specific Energy consumption, kWhm^{-3}	pH 4	pH 6	pH 8	pH 10
No fields	0.02	0.02	0.02	0.02
Acoustic Field (23 kHz)	7.5	10	22.3	16.8
Electric Field (50 V/cm)	0.08	0.13	0.08	0.09
Electric Field (50 V/cm) + Acoustic Field (23 kHz)	2.4	4.7	4.7	3.3

Table 3-8: Specific energy consumption data for the experiments described in this Chapter.

3.7.6   Experimental reproducibility

The data given in this chapter is experimental, and therefore subject to errors. The following section attempts to quantify these, by looking at the scatter between repeated experiments. In the first stages of the research, the experimental technique was optimised, although this was always constrained by the design of the rig.
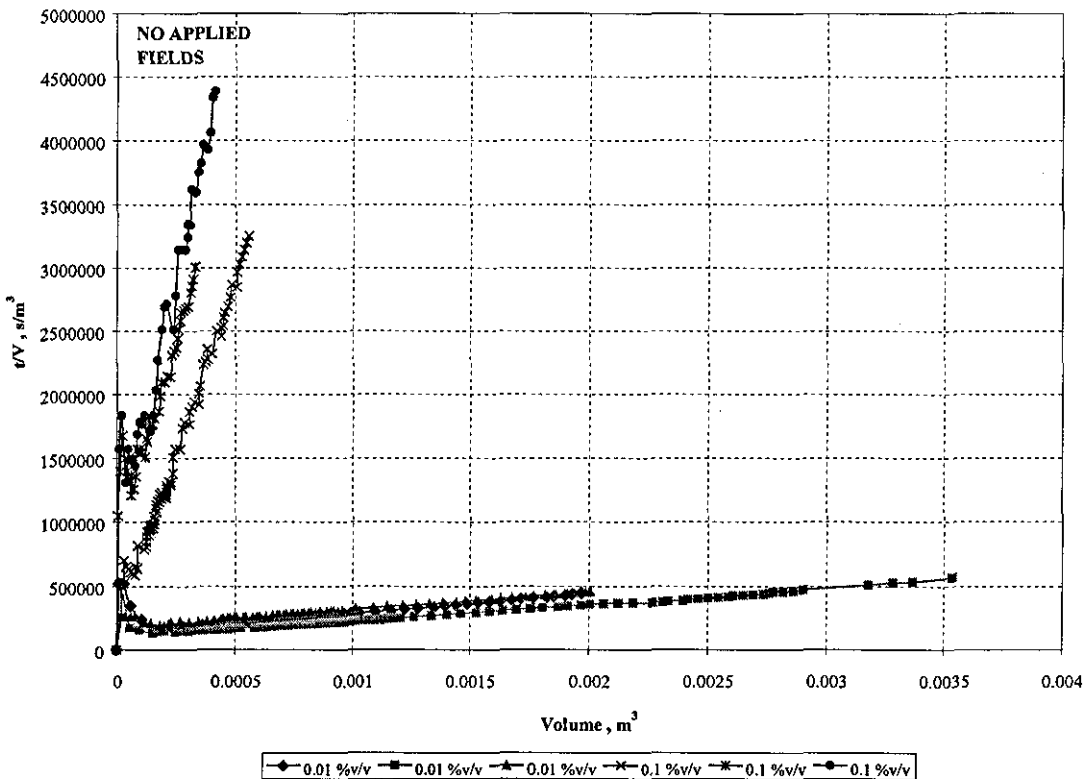
Figure 3-25: Examples of reproducibility of concentration tests (pH 8, 750 mBar)

The data shown in Figure 3-25 and Figure 3-26 give an indication of the levels of reproducibility of the experimental technique. The data appears to be somewhat scattered, however, it is important to note that the parameter of interest in these t/V plots is the slope, which indicates K_I. As previously discussed, consideration of K_I has enabled some indication of the field effects on specific cake resistance. In all repeated tests, examples of which are shown in the following figures, a plot of the reciprocal flowrate against volume has yielded lines with similar gradients for identical experiments. The figures for comparing the actual slopes are given in the data sheets in the appendix, but are not quoted here. The values of the slope are dependent on the method of analysis, and can be greatly altered by the data points between which the

gradient of the line is taken. These results were borne out through other sets of experiments. In summary then, whilst the experimental data reported here can indicate trends, further work is required to establish a more robust experimental design, enabling more accurate calculation of K_I and ε.
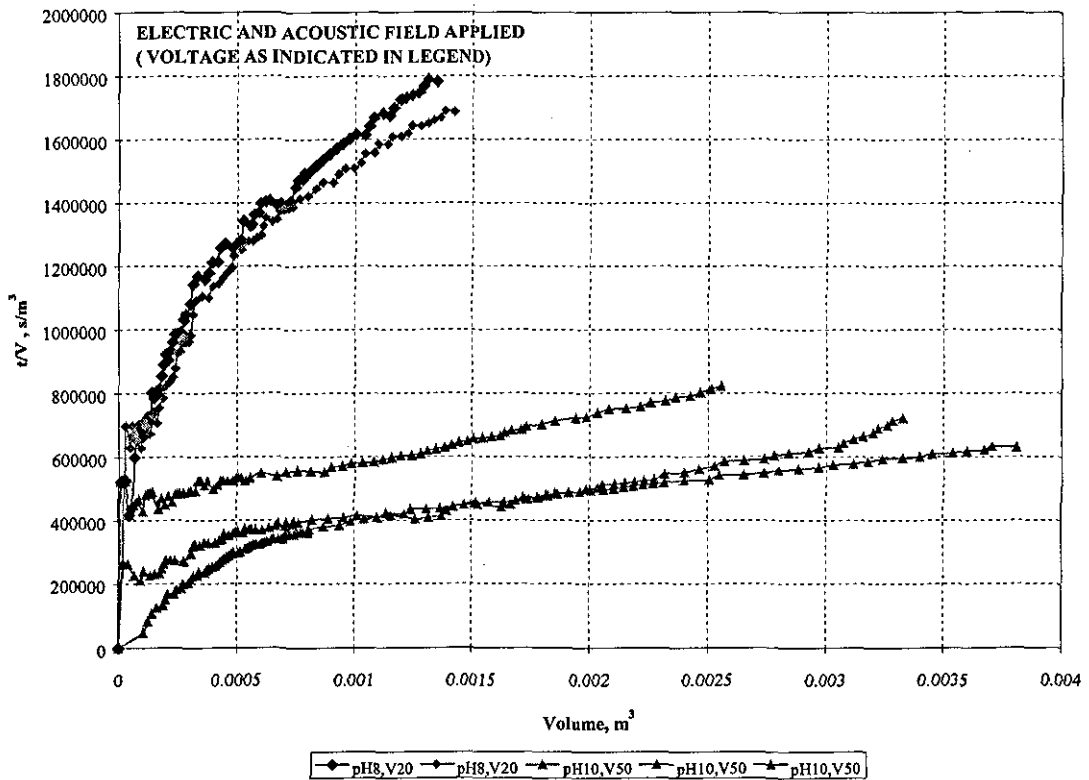
Figure 3-26: Examples of reproducibility of pH tests (concentration 0.1% v/v, 750 mBar)

4   Acoustic Force Analysis

Following the experimental filtration programme, it became clear that more insight into the acoustic effects within the filter was necessary to fully understand the results. This chapter analyses the filter system theoretically, comprising a background study, followed by an analysis of the forces present during acoustic wave propagation through the suspension. Cavitation was also investigated, as it may provide an explanation for the effects seen. The frequency and power of the transducer are well within the ranges under which cavitation can occur.

4.1   Background Study

The propagation of an acoustic wave through a fluid results in various effects, the nature of which is dependent on, amongst other parameters, the fluid viscosity. Thus, as the acoustic effects discussed here are relevant to liquids, viscosity plays an important role. The presence of particulate matter also has quite a large effect on the fluids behaviour; there are more sites for acoustic scattering effects (increasing attenuation), a larger number of nucleation sites for cavitation and the particle associated double layer is also free to move due to the acoustic field.

4.1.1   Acoustic wave propagation

Acoustic waves in fluids are complex because they are able to propagate in three dimensions. They are longitudinal: the molecules transmit the wave move back and forth in the direction of its propagation, rather than crests and troughs as would be produced by transverse waves. The wave is propagated via a force created by compression of the fluid. The simplest type of wave motion is that of plane waves, which are characterised by properties such as acoustic pressures, 'particle' displacements and density changes. In a plane wave these properties have common phases and amplitudes at any point perpendicular to the direction of wave propagation. It should be noted that the term 'particle' used here represents a 'pocket' of fluid, a volume element large enough to be considered a continuous fluid, yet small enough that the pressure, density and velocity can be assumed to be constant throughout the pocket. A further point must be made to differentiate between c, the signal speed or velocity of

propagation of a wave (which is a function of the ratio of specific heats, the isothermal bulk modulus, and the equilibrium density) and u_p the velocity of a fluid 'particle', given by the differential of the 'particle' displacement. The fluid velocity $\partial \xi / \partial t$ is always much less than the signal speed in ordinary sound waves (Hall, 1993).

The simplest treatment of waves is for the special case of a monochromatic plane wave, because of the simple functions for the velocity potential which describe it, *sin ωt* and *cos ωt*. A monochromatic wave is one in which the pressure, velocity *etc.* depend only on time through functions of the angular frequency, ω. Monochromatic waves can be summed to describe waves that are more complex with a more general time dependency. In the analysis of plane waves given by Kinsler and Frey (1962), gravity forces are neglected, allowing the equilibrium values of density and pressure to be considered constant throughout the medium. The medium is also assumed to be homogeneous, isotropic and perfectly elastic such that there are no dissipative forces arising from viscosity or heat conduction. The derivation is limited by assuming waves of small amplitude in order that any changes in density are small compared to its equilibrium value ρ_0.
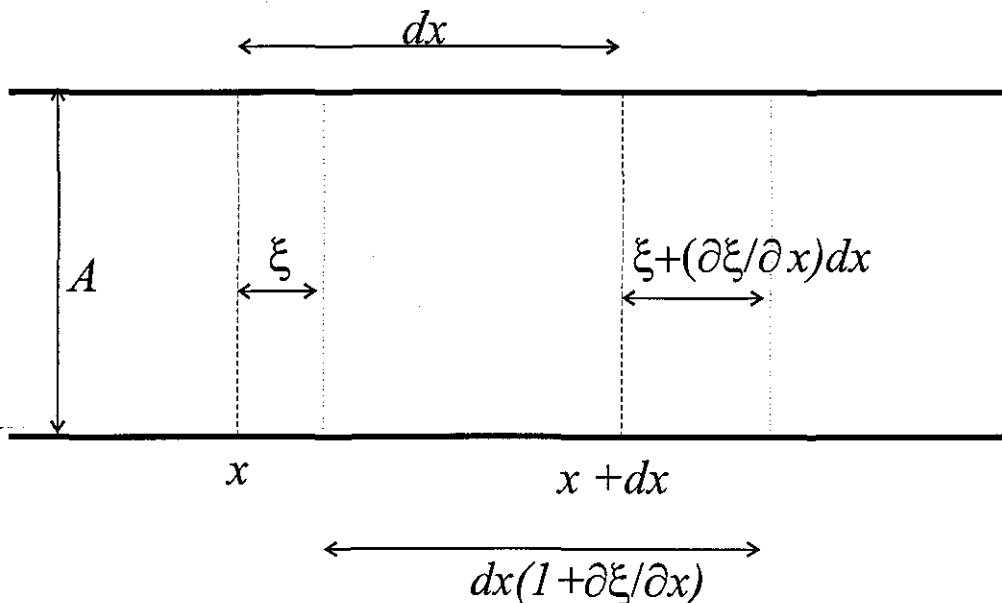
Figure 4-1. Longitudinal displacements in a plane sound wave.

Consider a cross sectional area A, of fluid positioned between planes at positions x and $(x + dx)$. On propagation of a sound wave the plane at x is displaced a distance ξ to the

right, and similarly the plane at $(x + dx)$ is displaced to $\xi + (\partial\xi/\partial x)dx$, as shown in Figure 4-1.

A mass balance yields:

$$\rho A dx\left(1 + \frac{\partial\xi}{\partial x}\right) = \rho_o A dx \qquad 4\text{-}1$$

The condensation at any point is defined as ϑ:

$$\vartheta = \frac{\rho - \rho_0}{\rho_0} \qquad 4\text{-}2$$

Density changes and molecular displacements are assumed small, such that the product of ϑ and $\partial\xi/\partial x$ can be neglected, and the equation of continuity is derived:

$$\vartheta = -\frac{\partial\xi}{\partial x} \qquad 3$$

To summarise, the planes are now separated by a distance $dx\ (1+\partial\xi/\partial x)$ greater than their equilibrium separation, dx, the quantity $\partial\xi/\partial x$ is positive, and the density of the fluid is reduced.

4.1.1.1   Thermodynamic description

As well as a relation between ξ and x, a thermodynamic equation of state, relating the excess (or acoustic) pressure at any point, p, defined by

$$p = P - P_0 \qquad 4\text{-}4$$

where P and P_0 are the instantaneous and the (constant) equilibrium pressures respectively. The instantaneous density at any point, ρ, and temperature, T are also required for the thermodynamics calculations. The compressions can be assumed to be adiabatic (Hall, 1993). The compression of a fluid by the wave requires work, which is converted into heat energy. The propagation of acoustic waves causes temperature gradients between adjacent compressed and expanded volume elements, however these are relatively small and little heat is transferred from compressed elements before they begin to expand. Thus the process can be assumed nearly adiabatic, and is certainly adiabatic for frequencies below 500 MHz for air and 10^6 MHz for water. To produce a

general derivation (for all fluids) the adiabatic process is represented by $P=P(\rho)$.
Differentiation of this equation gives:

$$dP = \left(\frac{dP}{d\rho}\right)_0 d\rho \qquad\qquad 4\text{-}5$$

The incremental pressure change dP can be replaced by the acoustic pressure, p, and the
incremental density change $d\rho$ by $\rho_0 s$.

Defining c:

$$c^2 = \left(\frac{dP}{d\rho}\right)_0 \qquad\qquad 4\text{-}6$$

we have:

$$p = -\rho_0 c^2 \frac{\partial \xi}{\partial x} \qquad\qquad 4\text{-}7$$

4.1.1.2   The equation of motion.

If a volume element is deformed as described previously, the pressures on each of the
faces will be slightly different, producing a net force F_x, which will accelerate the
element. The net force acting on the element is the sum of the pressure on each face, in
the positive x direction. Forces caused by the equilibrium pressure P_0 can be ignored
since they cancel, with only the incremental pressure changes contributing to the net
force:

$$dF_x = \left[pA - \left(p + \frac{\partial p}{\partial x} dx \right) A \right] = -\frac{\partial p}{\partial x} dx A \qquad\qquad 4\text{-}8$$

The net force is equated with the product of the elements mass, $\rho_0 A dx$ and acceleration,
$\partial^2 \xi / \partial t^2$.

$$-\frac{\partial p}{\partial x} = \rho_0 \frac{\partial^2 \xi}{\partial t^2} \qquad\qquad 4\text{-}9$$

Hence, the wave equation for one-dimensional motion can be derived, by combination
of equations 4-7 and 4-9.

$$\frac{\partial^2 \xi}{\partial t^2} = c^2 \frac{\partial^2 \xi}{\partial x^2} \qquad\qquad 4\text{-}10$$

Other forms of this equation can be obtained by simple manipulation of the previous equations.

Hall (1993) gives a comprehensive derivation of the equations of motion in three dimensions. The unequal relative movement of the planes in the x direction is repeated in the y and z planes, although the displacements are not necessarily of the same magnitude. The simple wave equation (equation 4-10) is then of the form:

$$\frac{\partial^2 \xi}{\partial t^2} = c^2 \nabla^2 \xi \qquad\qquad 4\text{-}11$$

4.1.2   Cavitation

The majority of literature regarding acoustically induced cavitation is found in the sonochemistry literature, where it is commonly accepted to be the major mechanism causing sonochemical effects (Suslick 1989). For example, Young (1989) states

"The bubble collapse in liquids results in an enormous concentration of energy from the conversion of the kinetic energy of liquid motion into the heating of the contents of the bubble. The high local temperatures and pressures, combined with rapid cooling, provide a unique means for driving chemical reactions under extreme conditions".

Cavitation is defined as the formation and activity of bubbles (or cavities) in a liquid. The word 'formation' refers to the creation of a new cavity or the expansion of an existing one. The bubbles may be trapped in the liquid, may be in cracks at the liquid's boundary surface, or in solid particles suspended in the liquid. These minute bubbles can be expanded by reducing the ambient pressure by static or dynamic means. They may contain gas or vapour or a mixture of both. For a bubble containing gas, expansion could be due to diffusion of dissolved gases from the liquid into the bubble, or by reduction in pressure or a rise in temperature. If the bubbles contain mostly vapour, reducing the ambient pressure at constant temperature causes an 'explosive' vaporisation into the cavities, which is cavitation. This can be compared to raising the ambient temperature causing the vapour bubbles to grow, and causing boiling. Both cavitation and boiling have a threshold, below which they do not occur.

There are four types of cavitation, all of which have the same mechanism, but are caused in different ways. Hydrodynamic and acoustic cavitation are results of tensions in the liquid. Both types are brought about by pressure variations in the liquid, either due to the geometry of the system or by sound waves. Optic and particle cavitation are achieved by local deposition of energy, photons of light or other elementary particle rupturing a liquid.

Of interest to this study is acoustic cavitation. Sound waves travelling through a liquid impose a sinusoidally varying pressure on the steady ambient pressure. If the amplitude of the pressure variation is great enough to bring the local pressure to below the vapour pressure of the liquid and produce zero, or even negative, pressures then tensions occur and bubble growth is increased. The sound field must overcome the attractive forces holding the liquid molecules together. For pure liquids with no impurities or dissolved gases the negative pressures required to do this are prohibitively high. However, most liquids contain some impurities which reduce the tensile strength, and it is gas within crevices on the surface of these contaminants which allows bubbles to form as a result of gaseous expansion as a sound wave passes.

4.1.2.1 Stable and Transient motion

Stable cavities are bubbles which oscillate (non-linearly) about some equilibrium size for many cycles of the sound field. They are relatively permanent and although they do not collapse violently (unless they become transient during their lifespan), they cause effects such as microstreaming and surface oscillations and the integrated effect of a number of stable cavities can be great. Stable cavities can evolve into transients by bubble growth due to either heat or mass transfer, or by coalescence of a number of bubbles. The pressure amplitude where these transfer processes commence is known as the threshold for rectified diffusion, P_T. Stable cavitation can occur at pressures below P_T if there are suitable bubbles already existing in the solution.

Transient cavities, which exist for less than one cycle (during which time they expand to at least double their original radius), collapse violently at a pressure known as the transient cavitation threshold. They often form a number of smaller bubbles, which may be stable or transient; thus, cavitation is a cyclical process. Cavitation is a non-linear process; the changes in bubble radius are not proportional to the sound pressure. A great

deal of potential energy is obtained from the sound waves when the bubbles expand, due to the high compressibility of the gas. This is converted to kinetic energy on bubble collapse. The energy is concentrated into very small volumes and produces the high temperatures and pressures responsible for sonochemical reactions, sonoluminesence and the erosion of surfaces.

Either type of bubble may contain gas (usually air) or vapour. In transient cavities it is normal to assume that there is no time for mass diffusion into or out of the bubble, although condensation and evaporation of vapour can occur. A gas filled transient that collapses has a constant gas content over its lifetime, and this gas cushions the collapse. A vaporous transient contains vapour which varies in mass, but remains at or near to its saturation pressure, and the collapse can be very violent due to the absence of the residual gas cushion. The lifespan of stable cavities is longer, and both mass diffusion of gas and thermal diffusion causing condensation or evaporation can occur.

At the moment cavitation commences, the medium's properties change; it has greater acoustic losses and is more compressible. An effective acoustic impedance, z_e, must be defined, because the assumption that the liquid motion is linear used in defining impedance is no longer valid. In general cavitation increases the acoustic impedance of the medium. The presence of stable cavities causes greater scattering because the absorption scattering cross section is much greater for a bubble than for a liquid or solid particle of equivalent size (Young, 1989).

4.1.2.2   Bubble nucleation

Once the sound pressure amplitude reaches a certain value, and the cavitation threshold is reached, cavitation can commence by nucleation in one of three ways: (i) in water, a large number of minute spherical gas bubbles exist; (ii) solid particles in the liquid may have gas trapped inside them; (iii) gas may be trapped in tiny crevices within the vessel walls, or on the filter surface.

Any of these can be represented by Figure 4-2 (a). If the liquid pressure is reduced (Figure 4-2 (b)) the liquid gas interface retreats from the solid and a bubble can form.
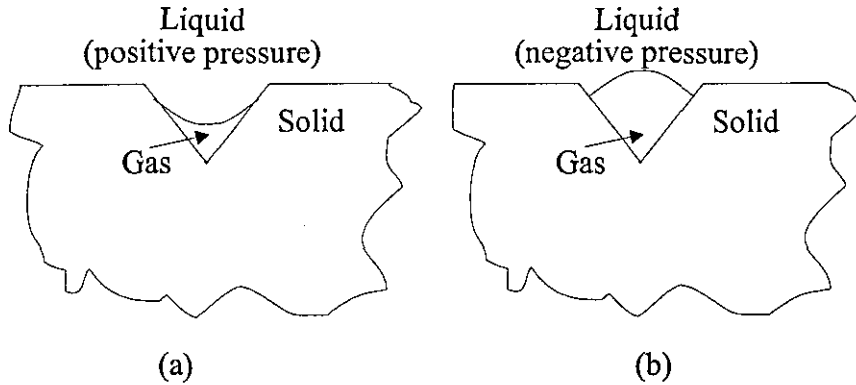
Figure 4-2: Cavitation bubble nucleation

Once the bubbles are in the bulk liquid, they are inherently unstable and absorb energy from the sound field.

4.1.2.3   Cavitation thresholds and bubble behaviour

If a cavity is released from a crevice as shown in Figure 4-2 (b) it will grow in a sound field by rectified diffusion. A good review of this is given by Crum (1984) and a brief explanation follows:

During the positive pressure half cycle of the sound field, the bubble is compressed and gas diffuses outwards from the bubble to the liquid. During the negative pressure cycle, the opposite occurs and gas diffuses inwards. During this time, the bubble surface area is greater, and so the bubble gains gas over a complete cycle.

When the bubble contracts, the shell of liquid surrounding it increases in thickness, and the gas concentration near to the outer bubble wall is reduced. Thus the concentration gradient between the gas in the bubble and gas in the shell is increased and the gas diffusion rate away from the bubble is greater than when the bubble is at its equilibrium radius.

When the bubble expands, the shell thickness contracts, the concentration of gas near to the bubble is increased and the rate of gas diffusion towards the bubble is again greater than the equilibrium rate. The bubble surface area is now greater leading to a net gas inflow and bubble growth.

The point at which rectified diffusion commences is called the threshold for rectified diffusion. The transient cavitation threshold is the threshold at which the cavity becomes transient and expands in an unstable way.
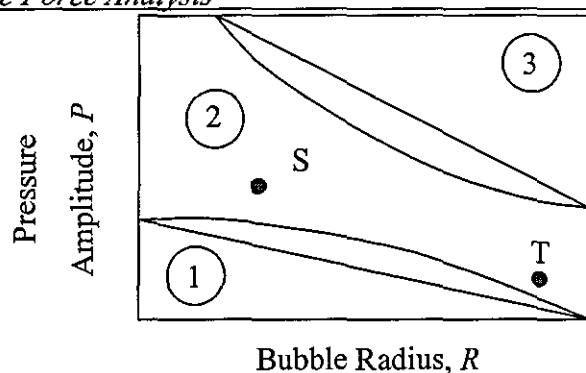
Figure 4-3: Cavitation and bubble thresholds

At a given pressure amplitude and frequency a nucleus will only grow into a transient cavity provided its radius is greater than the threshold radius. Similarly at a given frequency a cavity of radius R_0 will only become transient if the acoustic pressure is greater than the threshold for rectified diffusion. This is illustrated in Figure 4-3 (Neppiras 1980). Zone 1 is below the threshold for rectified diffusion (AB), the bubbles cannot grow by rectified diffusion and either slowly dissolve away or become stable at a small radius. A cavity within zone 2 at position S in Figure 4-3 will grow by rectified diffusion and reach the transient threshold CD where it will immediately expand (zone 3) and collapse. The small bubbles created either go into zone 1 or increase in size once more if they remain in zone 2. A cavity at position T in zone 2 will also grow by rectified diffusion, but it is unlikely to reach the transient threshold, and so will continue to grow until it becomes buoyant and leaves the system in this way.

Once the cavity has experienced rapid expansion, it can no longer efficiently absorb energy from the sound waves. Without this energy input, the bubble cannot sustain itself and liquid rushes in causing implosion. The dynamics of the bubble collapse depend upon the type of medium, as bubble dynamics near a solid surface are very different to that in a homogenous liquid.

The majority of studies concerning bubble behaviour and cavitation focus on spherical bubble studies. Dassie & Reali (1996) present a physico-mathematical model for the dynamic behaviour of a spherical gas/vapour bubble under an acoustic field. The model is shown to be valid whenever flow velocities are much smaller than the instantaneous velocity of sound in the bubble. The model allows a large range of thermodynamic parameters to be considered. As Blake (1999) points out, this spherical bubble

assumption is likely to be an over-simplification, as the experimental studies by Ohl *et al* (1999) and Prosperetti (1997) have confirmed. Blake suggests that the interactions with the acoustic pressure field, hydrodynamic interactions with other bubbles and buoyancy forces leads to asymmetric behaviour, with consequences such as high speed jets forming within the bubbles on collapse, leading to higher pressures and strain rates, and better mixing. In particulate suspensions, the jet travels through the bubble from the side furthest from the solid particle, and strikes the other side of the bubble and the particle if it is close enough. It is this 'liquid hammer' that causes the erosion and pitting seen on the surface of solids in a cavitating acoustic field. High temperatures occur within the bubble due to adiabatic heating, providing yet another possible reactive environment to account for chemical changes- the 'hot spot' theory.

The point at which the intensity of the ultrasound just causes cavitation to begin is known as the cavitation threshold. Whilst it is important in sonochemistry to be above this intensity, in medical uses of ultrasound, intensities lower than the cavitation threshold are required. It can be determined in a number of ways; the formation of cavitation bubbles is accompanied by a rapid increase in measured attenuation, weak light which can be detected (sonoluminescence) is emitted and chemical reactions can be initiated, for example Fe^{3+} is oxidised to Fe^{2+}.

4.1.2.4   Predicting bubble behaviour

A series of cavitation charts have been made by authors such as Neppiras (1980). These charts show the various thresholds applicable to air bubbles in various sound frequencies and gas saturations. The diagrams can be interpreted in a similar way to Figure 4-3 above, as they show the thresholds for rectified diffusion and the lower transient threshold (where an initially stable cavity becomes transient) and the transient threshold as functions of bubble radius for fixed values of ambient pressure and frequency. The tendency of a bubble to collapse is frequency dependent, and collapse is more likely to occur at lower frequencies where the length of the compression cycle is greater.

4.1.2.5   Sonochemical effects of cavitation

The chemical effects of ultrasound (Suslick (1989), Mason and Cordemans (1996)) have been widely discussed and a number of mechanisms proposed for the effects. The

chemical effects of ultrasound have been explained as the consequences of localised hot spots caused by cavitation since the 1950s.

4.1.2.6   The Hot Spot theory

The implosion of cavitation bubbles generates an intense, but short lived hot spot, as the low energy density sound is converted into high energy density of a collapsing bubble. If the collapse occurs in a homogenous liquid, the compression of the gas is almost adiabatic, because the compression is rapid. The localised hot spot can have temperatures in the region of 5200K in the gas phase and 1900K in the surrounding liquid phase. Pressures can reach hundreds of atmospheres. The presence of surfaces near to the cavities cause asymmetric bubble behaviour and a moving jet of liquid is directed at the surface, causing surface erosion as previously explained. For an aqueous solution the maximum temperature and pressure can be estimated using the following expressions (Neppiras, 1980):

$$T_{max} = T_0 \left\{ \frac{P_0(\gamma - 1)}{P_v} \right\} \qquad\qquad 4\text{-}12$$

$$P_{max} = P_v \left\{ \frac{P_0(\gamma - 1)}{P_v} \right\}^{\left(\frac{\gamma}{\gamma - 1}\right)} \qquad\qquad 4\text{-}13$$

T_0 is taken to be the ambient (experimental) temperature and P_v is the gas pressure inside the bubble at its maximum size, which is equivalent to the vapour pressure of the liquid at T_0. P_0 here is the liquid pressure at the point of the bubbles transient collapse, equal to the ambient pressure, and γ is the ratio of specific heats. Values for T_{max} and P_{max} can be calculated for pure water and for electrolytes. The addition of colloidal particles to an aqueous solution will not significantly alter its vapour pressure, and values for T_{max} and P_{max} will be of the same order as those of the solution. Addition of a solute however lowers the vapour pressure, which raises T_{max} and P_{max}. For water at 20 °

C, with γ taking a value of 1.33, at an ambient pressure of 1atm, T_{max} is shown to be 4135 K and P_{max} 1000 atm.

These expressions have been derived for transient cavities, which are produced by sources of intensity greater than $10Wcm^{-2}$ (Mason and Lorimer, 1988). Stable cavities, as previously stated, are more likely to contain gas and have less violent implosions. The cavitation threshold and effects vary greatly depending on the conditions of acoustic irradiation.

4.1.2.7   Factors affecting cavitation

A number of environment and system conditions can affect the cavitation threshold, and its sonochemical effects, although much of the use of ultrasound in sonochemistry is not optimised, because the chemistry is difficult to control.

Frequency

As frequency increases the length of the rarefaction phase shortens, and the amplitude (power) must be increased to attain the same cavitational effects. Cavitation will occur at frequencies below 10^4 kHz if the intensities are greater than 1 Wcm^{-2}, but can begin at intensities as low as 0.3 Wcm^{-2} in water under ambient conditions .

In the megahertz region, the rarefaction time is shorter than the time required for the liquid to be pulled apart sufficiently to create a bubble. Transducers that operate at high frequencies are mechanically unable to produce high power and thus cavitation.

Solvent Viscosity

Cavitation is more difficult to produce in viscous fluids where cohesive forces within the liquid are large.

Solvent Surface Tension

Addition of a surfactant facilitates cavitation

Solvent Vapour Pressure

More volatile solvents ease cavitation, but when more volatile solvents are used, more vapour enters the cavity, and the collapse is cushioned and hence less violent.

Temperature

An increase in temperature raises the vapour pressure of a medium (see above). Approaching the boiling point of a solvent a large number of bubbles are produced, and these act as a barrier to sound transmission.

Bubbled gas

Dissolved gas acts as a provider of cavitation nuclei, and as the sites are used up, the cavitation rate decreases. Gas can be bubbled through the medium to maintain a constant amount of dissolved gas, and uniform cavitation.

External pressure

An increase in applied pressure will require an increase in power supplied, as more energy is required to induce cavitation. At higher pressures however, the intensity of collapse is greater and the sonochemical effect is greater. At any frequency there is an optimum pressure which facilitates a maximum sonochemical reaction.

Intensity

The energy input to a system cannot be increased indefinitely. This is for a number of reasons; limitations of the transducers, increasing dimensional changes will eventually cause fracture. Decoupling may occur, and contact is lost between the source and the liquid. An increasing number of cavitation bubbles will be produced, and will at a certain intensity begin to coalesce, dampening sound and removing small bubbles that would otherwise have collapsed.

Attenuation

The extent of attenuation in a system is inversely related to frequency, therefore a higher power would be required for a higher frequency source to prevent attenuation.

A summary of the effects of changes in conditions is given in Table 4-1 below.

An increase of	causes a .... in cavitation threshold
dissolved gas saturation	decrease
hydrostatic pressure	increase
surface tension	decrease
temperature	decrease
solids concentration	decrease
particle size	decrease
dissolved ion concentration	increase (at low concentrations)

Table 4-1: Factors affecting cavitation threshold (Wakeman and Tarleton, 1991)

4.1.3   Acoustic Forces

A number of forces act on solids dispersed in a fluid. The presence of solid particles means the system is much more complex than in a pure medium, with a number of forces now acting on any volume element. Solid particles with a density higher than the liquid's are pushed in the direction of propagation by the radiation force. Bernoulli's force is caused by hydrodynamic flow around the particles. A Stokes force is caused by local variations in viscosity due to thermal gradients caused by localised adiabatic compressions. This is a steady net positive force. An Oseen force can be caused by the distortion of high amplitude waves if the suspended particles are much smaller than the wavelength. The major force acting on finely dispersed solids in solid-liquid suspensions is the orthokinetic force, which governs the relative velocity of particles and of the liquid. The magnitude of this force is dependent on the suspended materials density and size, the ultrasonic frequency and liquid viscosity. Bolt and Heuter (1955) give an expression for the magnitude of the relative displacement between the fluid and the particle as:

$$\frac{\xi_p}{\xi_f} = \left[1 + \left(\frac{2\rho_s \omega a^2}{9\mu} \right)^2 \right]^{-\frac{1}{2}} \qquad\qquad 4\text{-}14$$

As particle size diminishes the magnitude of the ratio tends to unity. This implies that if the particle is small enough it will move with the fluid 'particles' analysed in the previous section. Figure 4-4 represents the test system being used in this study, titanium dioxide (rutile) in de-ionised water. It is clear that any particles below one micron in the suspension will essentially move with the fluid, and any expressions used for fluid

'particle' velocity in a liquid can be used to describe the motion of solid particles in the suspension under these conditions. In a monosize dispersion, if all particles move with the liquid then no collisions occur due to the ultrasonic wave. The particle size distribution causes some particles to move out of phase with the fluid, especially at extremes of pH when the double layer is small and particles tend to agglomerate leading to a wider size distribution.
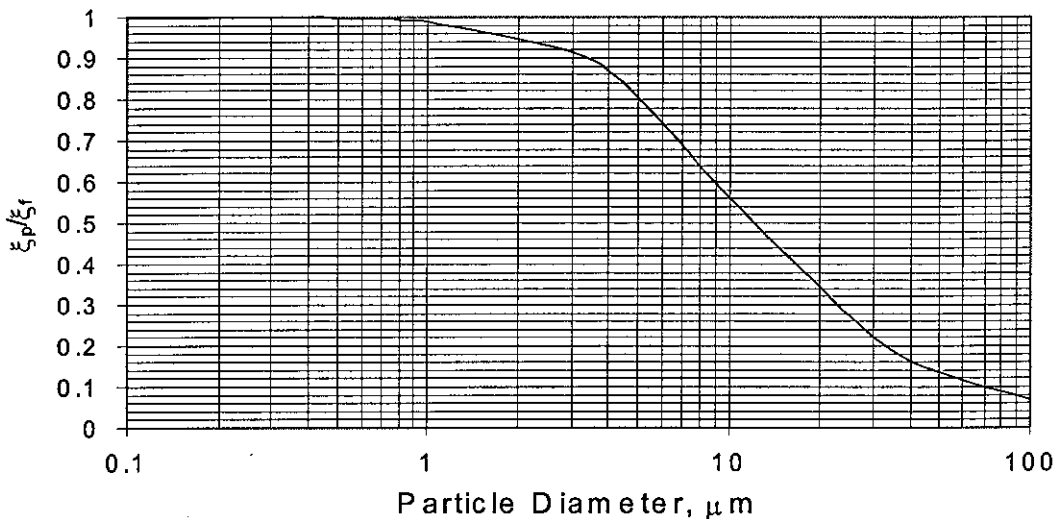
(Calculated from equation 4-14 for the filtration experiments in this work: Acoustic field of 23 kHz applied to a suspension containing particles of density 4260 kgm^3, and a fluid viscosity of 10^{-3} Nsm^{-2}).

Figure 4-4: The magnitude of the ratio of relative particle displacement to fluid displacement,

4.1.3.1   Hydrodynamics of a spherical particle oscillating in a viscous fluid.

An expression for the total force exerted on an oscillating sphere in a fluid was first obtained by Stokes. The drag force acting on a sphere of radius a executing a simple harmonic oscillation along a straight line with angular frequency ω in an incompressible fluid is

$$F_{drag} = -6\pi a \mu \left(1 + \frac{a}{\delta}\right) U - \frac{2}{3}\pi a^3 \rho_f \left(1 + \frac{9\delta}{2a}\right)\frac{dU}{dt} \qquad 4\text{-}15$$

with δ, the viscous skin depth, defined by equation 3-26.

This derivation has a number of provisos and limitations, which are detailed below in a brief review of the derivation. These conditions impose limits on the force balance and it is important to understand under what circumstances this derivation is valid.

Polar co-ordinates, r, θ and ϕ are used in the derivation of this expression, with the line of oscillation being the polar axis $(\theta = 0)$. The velocity U of the sphere along this axis is a function of time t, and is of the form $A \cos (\omega(t-t_0)+\alpha)$, where A is the amplitude of oscillation, t_0 is the time origin and α is the phase angle. To ease calculation U is expressed as terms of $exp^{(-i\omega t)}$ because

$$e^{i\omega t} = \cos \omega t + i \sin \omega t \qquad 4\text{-}16$$

The real part of the expression corresponding to U can be written as

$$U = \text{Re}\left(U_0 e^{-i\omega t}\right) \qquad 4\text{-}17$$

Provided only linear operations are carried out on U, the Re symbol can be omitted and calculations can proceed as if U were a complex function, and the real part of the result taken.

The velocity vector U is then

$$U = U_0 e^{-i\omega t} \qquad 4\text{-}18$$

where U_0 is a constant vector lying along the axis $\theta = 0$.

The governing equations for the pressure P and fluid velocity V in an incompressible viscous fluid are the continuity equation

$$\nabla \bullet V = 0 \qquad 4\text{-}19$$

and the Navier- Stokes equation

$$\rho_f\left[\left(\frac{\partial V}{\partial t}+\frac{\partial U}{\partial t}\right)+(V \bullet \nabla)V\right]=-\nabla P + \mu\nabla^2 V \qquad 4\text{-}20$$

The term involving the sphere's velocity, U, arises from the choice of the sphere as the frame of reference for the system. The gravitational force is omitted from the Navier-Stokes equation because it is assumed small compared with hydrodynamic forces. Assuming that the convective acceleration term $(V\bullet\nabla)V$ is small in comparison with the

rest of the terms in the Navier stokes equation and may be neglected equation 4-21 becomes

$$\rho_f \left(\frac{\partial V}{\partial t} + \frac{dU}{dt} \right) = -\nabla P + \mu \nabla^2 V \qquad 4\text{-}21$$

This assumption is valid provided

$$\omega >> \frac{\eta}{a^2}$$

where $\eta = \mu/\rho$, is the kinematic viscosity of the fluid, and the amplitude of the oscillation is much less than the particle radius.

The boundary conditions that the velocity of the fluid and of the sphere are equal at the surface of the sphere ($V=0$ at $r= a$) and the fluid is at rest at infinite distances from the sphere ($V=-U$ at $r=\infty$) are used to solve the equations, resulting in equation 4-22, the expression for the drag force on the sphere as derived by Stokes.

$$F_{drag} = -6\pi\mu a \left(1 + \frac{a}{\delta} \right) U - \frac{2}{3}\pi a^3 \rho_f \left(1 + \frac{9\delta}{2a} \right) \frac{dU}{dt} \qquad 4\text{-}22$$

This drag force consists of both velocity and acceleration terms arising from the sphere's motion, and this formula reduces to the inviscid result when $\mu=0$.

$$F_{drag} = -\frac{2}{3}\pi a^3 \rho_f \frac{dU}{dt} \qquad 4\text{-}23$$

By comparison of the viscous and inviscid results the effects of viscosity on the fluid motion are clear, one of them being to increase the added mass coefficient of dU/dt. As frequency increases the thickness of the oscillating viscous layer, δ, decreases and this increase in the added mass coefficient diminishes as δ tends to zero. Another effect is the presence of the first term in 4-22, which is proportional to the size, and instantaneous velocity of the sphere. In the low frequency limit, the equation reduces to Stokes law for the drag on a sphere moving uniformly through a viscous fluid and at high frequencies when the viscous skin thickness is small the drag becomes

$$F_{drag} = -\left(3\pi a^2 U \sqrt{2\mu\omega\rho_f} \right) - \left(\frac{2}{3}\pi a^3 \rho_f \frac{dU}{dt} \right) \qquad 4\text{-}24$$

Thus even at high frequencies the fluid viscosity retains an effect on the drag proportional to the instantaneous velocity of the sphere. This result is only valid

however when the viscous layer is very thin, or $\kappa a \ll 1$, and so there will be an upper limit of δ/a at very high frequencies where this result is incorrect.

This result was extended by Temkin (1981) who considered the opposite problem of a sphere set in motion by an oscillating fluid, as in the example of a sound wave travelling through the fluid. Provided the frequency is not too large the result given in 4-24 can be adapted to this problem because the flow field close to the sphere is essentially incompressible.

In equation 4-24 the value of U, representing the sphere velocity, must be replaced by $(U-V)$, representing the relative velocity between the sphere and fluid. An additional force must be added to the expression to take into account the acceleration of the frame of reference (which is now the fluid). If we consider a situation where the sphere moves with the fluid, the expression for the force vanishes, since the fluid is accelerating with velocity V, a force must be acting on any volume of fluid according to Newton's second law. If we take the volume to be equivalent to that of a sphere, then the accelerating force is *4/3 ($\rho_s \pi a^3$ (dV/dt))* and the total force acting on the sphere is:

$$\frac{4}{3}\pi a^3 \rho_s \frac{dU}{dt} = \frac{4}{3}\pi a^3 \rho_f \frac{dV}{dt} - 6\pi a\mu\left(1+\frac{a}{\delta}\right)(U-V) - \frac{2}{3}\pi a^3 \rho_f\left(1+\frac{9\delta}{2a}\right)\frac{d(U-V)}{dt}$$

$$4\text{-}25$$

Assuming that the fluid velocity V is of the form

$$V = V_0 e^{-i\omega t} \qquad\qquad 4\text{-}26$$

Defining τ as the relaxation time for the sphere's motion,

$$\tau = \frac{2a^2\sigma}{9\eta} \qquad\qquad 4\text{-}27$$

and σ as the ratio of fluid and particle densities, ρ_s/ρ_f. The substitution in 4-25 for U and V and their differentials with respect to time (from 4-18 and 4-26) allows the complex ratio of velocity amplitudes U_0/V_0 to be obtained

$$\frac{U_0}{V_0} = \frac{\left(1-\frac{a}{\delta}\right) - i\omega\tau\left[\frac{1}{\sigma}\left(\frac{3}{2} + \frac{9\delta}{4a}\right)\right]}{\left(1-\frac{a}{\delta}\right) - i\omega\tau\left[1 + \frac{1}{\sigma}\left(\frac{1}{2} + \frac{9\delta}{4a}\right)\right]} \qquad 4\text{-}28$$

Clearly when $U_0/V_0 = 1$ the sphere moves with the fluid, in other cases, the sphere oscillates with the same frequency as the fluid, but with a different amplitude and velocity phase. When the density of the sphere approaches that of the fluid $U_0/V_0 \to 1$ and the sphere's motion is identical to the fluid's. By imposing limits on this expression, simple forms can be obtained. For example, for small spheres in a low density fluid, $\sigma \ll 1$ such that

$$\frac{U_0}{V_0} = \frac{1 + \frac{a}{\delta} - i\left(\frac{2a}{3\delta}\left(\frac{a}{\delta}+1\right)\right)}{1 + \frac{a}{\delta} - i\left(\omega\tau + \frac{a}{\delta}\right)} \qquad 4\text{-}29$$

This makes use of the identity

$$\omega\tau = \frac{4}{9}\frac{a^2}{\delta^3} \qquad 4\text{-}30$$

Now if the sphere radius is small compared with the viscous skin depth, then $a/\delta \ll 1$ and

$$\frac{U_0}{V_0} = \frac{1 - i\frac{a}{\delta}}{1 - i\left(\omega\tau + \frac{a}{\delta}\right)} \qquad 4\text{-}31$$

Then if $\omega\tau \ll a/\delta$ then $U_0 = V_0$ for all a/δ, conversely if $\omega\tau \ll a/\delta$

$$\frac{U_0}{V_0} = \frac{1}{1 - i\omega\tau} \qquad 4\text{-}32$$

which is easily derived from Stokes law

$$F = 6\pi\mu a(U - V) \qquad 4\text{-}33$$

This derivation dictates the conditions under which this can be applied to a sphere in an acoustic wave. As compressibility effects were neglected in Stokes original derivation, $ka \ll 1$. The values of $1/\sigma$ and a/δ were assumed small, with the relative magnitude of

these being given by $a/\delta \ll \omega\tau$. As $(a/\delta)^2 \ll a/\delta$ when $a/\delta \ll 1$ and $(a/\delta)^2 = 9\omega\tau/4\sigma$ these restrictions can be written

$$a/\delta \ll \omega\tau \ll a\sigma/\delta$$

A 0.3 micron sphere in a 23kHz sound wave in water at standard temperature and pressure yields the parameters detailed in Table 4-2 that are used to assess the validity of the derivation in this study.

Condition	Value in this study	Valid in this study?
$ka \ll 1$	1.46×10^{-5}	Yes
$1/\sigma \ll 1$	0.235	Yes
$a/\delta \ll 1$	$4.03\ 10^{-2}$	Yes
$\omega\tau$	3.08×10^{-3}	-
$a/\delta \ll \omega\tau$	-	No
$a/\delta \gg \omega\tau$	-	Yes
$a\sigma/\delta$	0.172	-
$\omega\tau \ll a\sigma/\delta$	-	Yes

Table 4-2:Confirmation of validity of derivation

The calculation of parameters shows that, although the derivation is valid for the filtration system being considered, in fact $a/\delta \gg \omega\tau$ which dictates that the particles will indeed move with the fluid, as predicted by Bolt and Heuter (1955).

4.1.3.2   The Basset Boussinesq Oseen Equation

The velocity U of a sphere translating unsteadily in a viscous, incompressible fluid is described by

$$m_s \frac{dU}{dt} = \delta m_s \frac{dV}{dt} + 6\pi a\mu(V-U) + \delta \frac{2}{3}\pi a^3 \rho_f \frac{d(V-U)}{dt} + 6a^2\left(\pi\mu\rho_f\right)^{\frac{1}{2}} \int_{-\infty}^{t} \frac{d(V-U)}{dz} \frac{dz}{\sqrt{t-z}}$$

4-34

which is known as the BBO equation. The last term is a history term, and is dependant on the past history of the motion. For a constant wavelength (monochromatic time dependence), this equation can be solved to give the result of equation 4-25.

4.2   Analysis of the filtration system

The trajectory of a particle of radius a across the filter can be calculated by considering the forces acting upon a particle suspended in a fluid. A frictional force due to the gravitational acceleration F_z is given by Stokes law:

$$F_z = \frac{4}{3}\pi a^3 \left(\rho_s - \rho_f\right)g \qquad\qquad 4\text{-}35$$

Derivation of Stokes law is subject to certain assumptions. Particle motion is assumed to be extremely slow; this is always true for colloidal particles in filter systems. The suspension is considered to be very dilute such that the liquid medium extends an infinite distance from the particle and the nearest particle is sufficiently far away to have no effect on the one being considered. The medium is also considered to be continuous when compared with dimensions of the particle.

A further assumption is implied from the above. That is, separation distances between particles will be large and are thus unlikely to be close enough to cause interparticle forces. At low concentrations hydrodynamic and interparticle forces can be neglected. The system is defined in cartesian form, with x and z representing horizontal and vertical planes respectively.

Suspension concentrations are lowest farther away from the filter cake surface. It is assumed that there is no slip at the particle surface and that the particle velocity is equal to the mean pore velocity of the fluid. The suspension thickens as it approaches the filter medium and here a differential velocity between the particle and the fluid develops. The no-slip assumption no longer holds. Considering a particle in the bulk suspension away from the cake surface.

$$v_z = v_b = \frac{dz}{dt} \qquad\qquad 4\text{-}36$$

where v_b is the bulk fluid velocity.

The Reynolds number, Re, is given by

$$\mathrm{Re} = \frac{2v_b a \rho_f}{\mu} \qquad\qquad 4\text{-}37$$

The downward fluid velocity in the cell is around 2×10^{-4} ms^{-1}. The maximum drag would occur when the fluid velocity is zero at the particle surface, when Re $= 0.6 \times 10^{-4}$; in this case the Reynolds number is much less than 0.2, the limit for purely laminar flow, and the gravitational fluid dynamic drag force, F_{zd}, is given by Stokes' Law:

$$F_{zd} = 6\pi\mu a v_b \qquad\qquad 4\text{-}38$$

The Stokes settling velocity v_s can hence be calculated by equating drag and acceleration forces to give

$$v_s = \frac{2a^2 \left(\rho_s - \rho_f \right) g}{9\mu} \qquad\qquad 4\text{-}39$$

If an acoustic field is applied to the suspension, the forces acting on the particle are as shown in Figure 4-5, where F_x and F_{xd} are the acoustic force and the drag acting on the particle as a result of the acoustically induced particle velocity respectively.
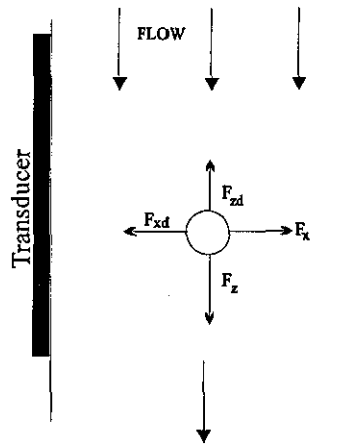
Figure 4-5: Forces acting on a particle in an acoustic field

The forces acting horizontally on particles (in the x direction) are assumed to be much greater than those acting vertically due to bulk fluid flow. Justification for this is given in Section 3.3.

4.2.1 Estimation of the acoustic radiation force

Gor'kov, 1962 showed that the acoustic potential energy of a single particle in a standing wave field is given by

$$E = m_s \left[\frac{\beta_f - \beta_s}{\beta_f} \langle E_P \rangle - \frac{3(\rho_s - \rho_f)}{\rho_f + 2\rho_s} \langle E_K \rangle \right] \qquad\qquad 4\text{-}40$$

where $\langle E_P \rangle$ and $\langle E_K \rangle$ represent the time averaged potential and kinetic energies. Expressions for the incident primary field pressure and the first order incident fluid velocity vector can be used to derive the force on a particle in a standing wave. Since $F = -\nabla E$, the primary radiation force (PRF) can easily be derived.

Expressions for the PRF are given by many authors including the theories proposed by Yoshioka and Kawashima (1955) for compressible spheres and King (1934) for incompressible spheres. (See also Hager and Benes, 1991). For a spherical particle in a standing wave the axial component of the radiation force F_x is given by:

$$F_x = -\frac{4\pi}{3}a^3 k \rho_E G \sin(2kx) \qquad\qquad 4\text{-}41$$

where r is the particle radius, ρ_E the average acoustic energy density, k represents the particle wavenumber and G a constant given by

$$G = \left(\frac{3(\rho_s - \rho_f)}{2\rho_s + \rho_f}\right) + \left(\frac{\beta_f - \beta_s}{\beta_f}\right) \qquad\qquad 4\text{-}42$$

G gives an indication of a particle's behaviour within the standing wave. If $G > 0$, for example mammalian cells in culture liquid, the cells collect at the pressure nodes of the wave. If however $G < 0$, for example bubbles, the pressure antinodes of the wave become the collection zones.

The transverse component of the PRF, F_{yz} on a single particle in a standing wave is given by Woodside *et al* (1997)

$$F_{yz} = \frac{4}{3}\pi a^3 \nabla \rho_E \left(\frac{3(\rho_s - \rho_f)}{2\rho_s + \rho_f}\cos^2(kx) - \frac{\beta_f - \beta_s}{\beta_f}\sin^2(kx)\right) \qquad\qquad 4\text{-}43$$

It is this transverse force which causes particles which have been moved to a pressure node or antinode by the axial PRF to agglomerate at the local energy density maximum. The secondary radiation force (SRF), F_{sec}, acts on a particle due to the interaction between its own scattered field and the total scattered field arising from neighbouring particles. It is strongly dependent on the particle radius and separation distance

$$F_{sec} = a^6 \left[p^2 \frac{f(\beta_s, \beta_f)}{d^2} + v^2 \frac{f(\rho_s, \rho_f)}{d^4} \right] \qquad\qquad 4\text{-}44$$

In this case the dependence on the sixth power of the radius and utilising the assumption that particles are far from one another (Stokes law), along with the statement that multiple scattering is negligible (See Chapter 3) means that the SRF can be neglected.
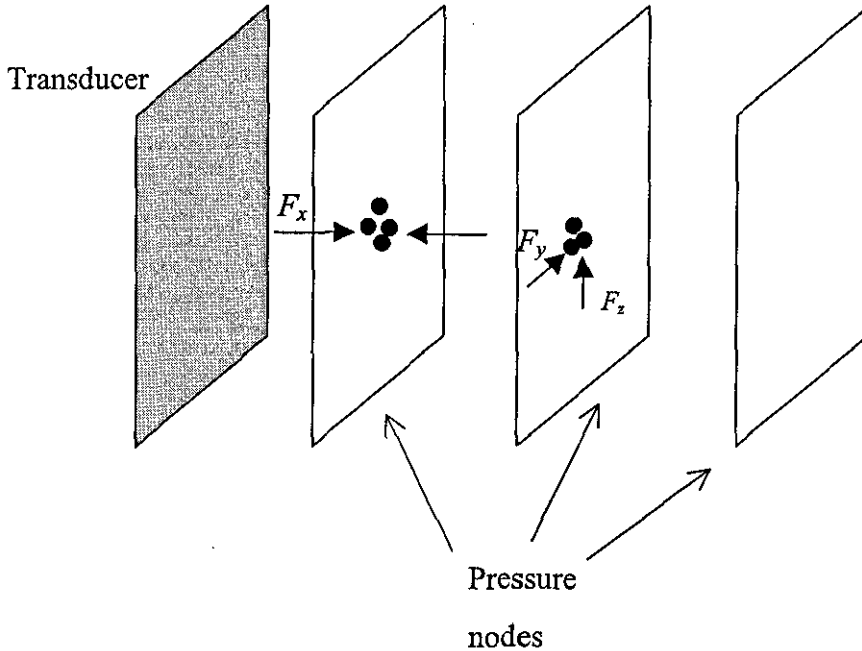
Figure 4-6: Axial (F_x) and transverse (F_y, F_z) primary radiation forces

Woodside *et al* (1997) have carried out velocity measurements of polystyrene spheres in such a standing wave, and by neglecting diffusion, the SRF, double-layer and hydrodynamic interactions obtain the following expressions for the axial and transverse PRF. The results are based on the assumption that observed particle velocities in a standing wave field are proportional to the applied ultrasonic forces, and that a particle in an acoustic field is subjected to primary and secondary radiation forces as well as gravitational, fluid dynamic drag and interparticle forces.

$$F_{yz} = 6\pi\mu a v - \frac{4}{3}\pi a^3 (\rho_s - \rho_f) g \qquad\qquad 4\text{-}45$$

Gravitational forces act parallel to the transverse force in Woodside's work, thus the gravity component is retained in the force balance.

Woodside *et al* (1997) apply a curve fitting procedure by calculating the axial forces using equation 4-45, and then obtain a nonlinear least squares fit of the form

$$F_x = A\sin(2k(x - \Phi)) + B \qquad\qquad 4\text{-}46$$

This is based on equation 4-41 but has been modified to include both a phase shift and offset. The phase shift accounts for the arbitrary origin of data and the offset Φ quantifies the magnitude of bulk fluid flows at the time of measurement. During the procedure, only data for which B was less than 10% of A was retained.

Although these expressions are strictly only true for standing wave fields, they may go some way to allow the particle motion in the filter to be analysed. In a method similar to Woodside *et al*'s, equation 4-46 is modified to include a phase shift and offset. To account for the resonant wave system and the altered geometry in the experimental set up equation 4-46 is modified to

$$F_x = A\cos(2k(x - \Phi)) + B \qquad\qquad 4\text{-}47$$

with

$$A = \frac{4\pi}{3}a^3 k\rho_{\mathrm{E}}G \qquad\qquad 4\text{-}48$$

The cosine function is present because in this case it is assumed that the maximum force will be at the transducer surface ($x=0$)

A force balance in the x direction gives:

$$F_x - F_{xd} = 0 \qquad\qquad 4\text{-}49$$

$$A\cos(2k(x - \Phi)) + B - 6\pi\mu a v_x = 0 \qquad\qquad 4\text{-}50$$

The sonic force is equated to an acoustic drag force using the assumption that the flow around the particle is predominantly laminar (Particle Reynolds number, Re' <10).

Equation 4-50 becomes

$$A\cos(2k(x - \Phi)) + B - 6\pi\mu a\frac{dx}{dt} = 0 \qquad\qquad 4\text{-}51$$

Rearranging Equation 4-51

$$\frac{dx}{dt} = A*\cos(2k(x - \Phi)) + B* \qquad\qquad 4\text{-}52$$

and

$$A^* = \frac{2a^2 k \rho_{\text{E}} G}{9\mu} \qquad\qquad 4\text{-}53$$

$$B^* = \frac{B}{6\pi\mu a} \qquad\qquad 4\text{-}54$$

4.3   Approximating an order for the acoustic force

A method for obtaining the velocity of small particles in an acoustic field has also been developed by Bailey and Wakeman (1998). The method can be briefly described as follows. Dispersed particulate suspensions are placed in a graduated cylinder in front of a high speed camera. The cylinder is illuminated using a high intensity light source. An ultrasonic probe is placed in the top of the cylinder, with its tip immersed in the suspension. On application of the acoustic force from the transducer, the movement of the particle away from the probe tip is recorded, and timed over a specified distance to give a particle velocity.

Particles below 1 micron cannot be seen using the video technique used to measure the velocity; thus it was not possible to use a similar video technique to study the titania used in the filtration experiments described in Chapter 3. For this reason, data for the velocity of calcite particles in a similar acoustic field (Bailey and Wakeman 1998) has been used in an attempt to predict how rutile particles may behave under acoustic irradiation. Data for the velocity profile of 1, 4 and 8 μm particles were used to plot the variation of particle velocity with particle size, for varying distances, x, from the transducer.

This data has been used in a curve fit procedure in order to elucidate the motion present in the filtration system investigated in this thesis. The form of equation 4-52 with A^* and B^* as defined in 4-53 and 4-54 was used. A commercial curve-fitting package (Jandel sigmaplot) was used in an attempt to fit the velocity data in Figure 4-7 to the equation. Bailey and Wakeman's data (1998) claims high particle velocities at the transducer surface. Initially the data given for the transducer surface was disregarded, as the apparently high velocities at this point gave an inappropriate bias to the results. The

acoustic wavenumber, k, was allowed to vary during the fitting procedure, as this varies the wavelength of the fitted curve.

Now by inspection of 4-52 it is clear that, $A*$ and $B*$ must be of the same order as one another and as the measured v_x. The first term of 4-52 can vary only between $\pm A*$ because the _cos_ function varies between ± 1. $B*$ serves purely to move the curve up or down the ordinate, and if it is much larger than $A*$ will dominate the curve.
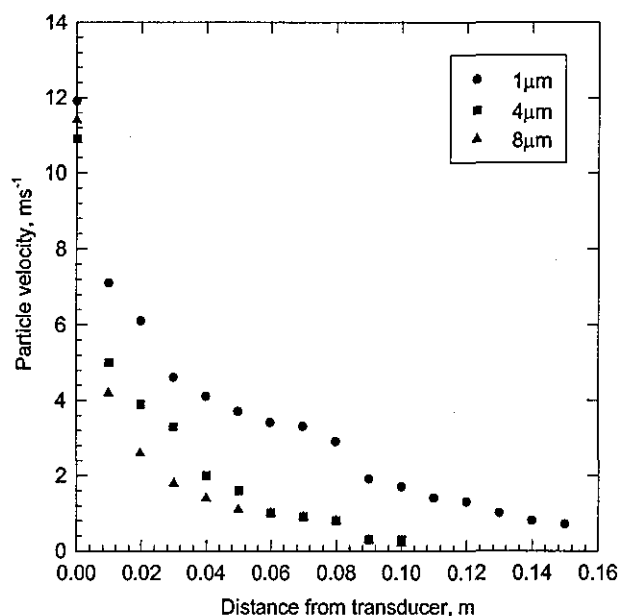
Figure 4-7: Particle velocity data given by Wakeman and Bailey (1998) for calcite particles in a 20 kHz, 0.32Wcm^{-2} acoustic field.

Conversely if $B*<<A*$ then $A*$ dominates and the curve oscillates with an amplitude of $A*$. The acoustic energy density and wavenumber defining $A*$ can be calculated using the sound frequency and power, as given in Table 4-3.

Particle size, μ	$A*$ ms^{-1}		$B*$ ms^{-1}	k radm^{-1}		φ
	Curve fitted	Calculated		Curve fitted	Calculated	
1	2.17	8.04 x 10^{-3}	4.12	16.32	83.77	0
4	2.16	0.129	2.43	18.70	83.77	0
8	1.48	0.515	1.79	18.74	83.77	0

Table 4-3:Curve fitted and calculated values for experimental data

The fitting procedure was unsuccessful for a number of reasons. During all curve fittings, k was consistently a factor of 2π lower than expected from ω/c. The major problem however was the order of the velocity. As already mentioned, the velocities quoted by Bailey & Wakeman (1998) were high, and it would be expected, by inspection of equation 4-45, that particle velocities for rutile would be even higher. $A*$ can be calculated by knowledge of the ultrasonic parameters being used (given in Chapter 3). The velocities quoted are an order larger than those expected from equation 4-53 which yields a value for $A*$ of the order of 10^{-1}. While the calculated values for $A*$ increase with particle size, the opposite happens to the fitted values. $B*$ cannot be calculated or estimated theoretically, as it is unknown, although it is likely to be a function of acoustic power, suspension viscosity and particle parameters. It is interesting to note that during their fitting procedure, Woodside *et al* (1997) discounted any results which gave B as greater than 10% of A as above this value the measured particle velocities are likely to have been distorted by excessive attenuation, caused by particle accumulation at the nodes. In the case in question here $B*$ is always greater than $A*$ which suggests that the bulk flow in the axial direction is much larger than in Woodside's experiments.

The above expressions and results give an insight into the factors affecting the forces on small or neutrally buoyant particles in a standing wave. The forces in this study, and that of Wakeman and Bailey (1998), will arise from similar factors, but the extent to which these factors influence particle motion is different for various reasons. The standing wave assumption is invalid; motion in the filter cell is subject to recirculation currents, and wave reflection from the filter cell walls, which may slow or divert the particles. Particulates suspended, although very small, have densities significantly greater than the

liquid, $\sigma \gg 1$, and the momentum of particles which have been imparted a velocity will cause a relative motion between fluid and solids.

By considering the forces transmitted to the particles more of an insight may be possible. Firstly, calculation of Stokes settling velocities and associated drag forces settling velocities shows that gravitational forces can be neglected in the remainder of the analysis. The velocities shown in Figure 4-7 are much greater than those given in Table 4-4, suggesting that the acoustic force will dominate the particle motion. In the experimental layout used in this thesis, gravitational forces act perpendicular to the direction of the acoustic force, thus there is no vertical component in the force balance.

Particle diameter, microns	Stokes settling velocity, ms^{-1}	Stokes drag force, N
0.3	9.47×10^{-8}	2.68×10^{-16}
1	1.05×10^{-6}	9.91×10^{-15}
4	1.68×10^{-5}	6.34×10^{-13}
8	6.73×10^{-5}	5.08×10^{-12}

Table 4-4: Gravitational settling velocities and drag forces for calcite particles of density 2930 kgm^{-3}.

The velocities measured by Bailey and Wakeman (1998) acted in the same direction as gravity, but due to the small Stokes forces are assumed to be equivalent to those that would act horizontally.

Considering only the horizontal acoustic forces, the expression for the acoustic drag force need only consider the measured velocity because as shown in Table 4-3 and previously in Section 4.1.3 and, there is very little or no relative displacement between the particle and fluid. The maximum particle Reynolds number at 1cm from the transducer surface for 1, 4 and 8 micron particles is 7.1, 20 and 33.6 respectively, thus the flow around the particle can be considered predominantly laminar and the acoustic drag force is given by

$$F_{xd} = -6\pi\mu a v_x \qquad\qquad 4\text{-}55$$

In the x direction, the rate of change of particle momentum is given by

$$\frac{4}{3}\pi a^3 \left(\rho_s + \frac{\rho_f}{2} \right) \frac{dv_x}{dt} = F_x + F_{xd} \qquad\qquad 4\text{-}56$$

Assuming that the ultrasonic force, F_x is constant and integrating with respect to t with the following boundary conditions

$$t = 0 , \ v = v_x$$

$$t = t , \ v = v_\infty$$

we obtain

$$\frac{v_x}{v_\infty} = 1 - \exp \left[\frac{-6\pi\mu t}{\frac{4}{3}\pi a^2 \left(\rho_s + \rho_f / 2 \right)} \right] \qquad\qquad 4\text{-}57$$

Thus, the time to 99% of the maximum velocity can be calculated as of the order 10^{-7}s. The time to reach maximum acoustic particle velocity is short, and $\frac{dv_x}{dt}$ can be assumed to be zero. Substituting in equations 4-55 and 4-56

$$F_x = -F_{xd} = 6\pi\mu a v_x \qquad\qquad 4\text{-}58$$

The acoustic force F_x of a 1 micron calcite particle is 1.12×10^{-7} N at the transducer surface, and 1.6×10^{-8} N at a distance of 10 cm away. These forces are considerably larger than the gravitational forces previously calculated, and the assumption that those vertical forces are negligible holds.

The use of Equation 4-58 allows the variation of acoustic radiation force with distance from the transducer to be plotted.

Wakeman and Bailey (2000) have taken a slightly different approach to the curve fitting, by fitting two curves, of the form of 4-59 and 4-60 to data calculated using expression 4-58, yielding two sets of values for A, A_1 and A_2. A critical distance from the transducer surface, x_c denotes which equation is used.
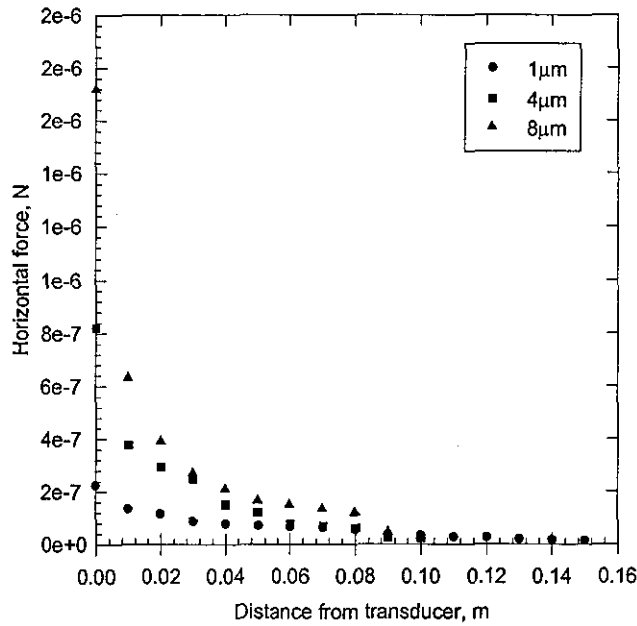
Figure 4-8: Calculated force on particles positioned across the filter

$$F = A_1 \cos(B_1 x) \qquad \text{for } x < x_c \qquad\qquad 4\text{-}59$$

$$F = A_2 \cos(B_2 x) \qquad \text{for } x > x_c \qquad\qquad 4\text{-}60$$

These equations go some way to address the problems with the curve fitting procedure which have been highlighted in this study. However there are still some discrepancies, with A_1 an A_2 increasing with particle size, but not with frequency, as the authors expected by inspection of 4-59 and 4-60. In this case, A_1 and A_2 are of the orders 10^{-7} N and 10^{-8} N respectively, considerably larger than the 10^{-22} N calculated using the acoustic parameters. Although A_1 and A_2 are not expected to be comparable to A^*, comparison may suggest whether this procedure has any validity. Differences of this order of magnitude suggest that although a first approximation has been made, a more rigorous model of particle motion in travelling waves is required, and until better understanding of the recirculation and reflection from the vessel is available only qualitative analysis is possible.

4.4 Conclusions

Although primary radiation forces have been previously calculated by authors such as Woodside *et al* (1997) these are for stationary waves. The methods cannot be used to assess the forces present in this study due to the largely different waveforms being used. The large amounts of reflection and recirculation occurring in the filter cell cannot at this stage be quantified, to allow comparison between the waves present in this study and those used by Woodside *et al* and therefore the forces present.

Analysis of waves of a more similar nature was carried out by Wakeman and Bailey (1997, 1998). A fitting procedure carried out on their data was found to be unsatisfactory as both A^* and k were found to be far from the values expected by the direct calculation of these parameters.

5   Experimental Procedures & Analysis- Conductivity Effects

In order to further investigate the effects described in Chapter 4 and the synergy seen by other authors, the physical effects of ultrasound on the suspension have been studied. The hypothesis that the synergistic effect could be explained by the ultrasound effecting an increase in a suspension's conductivity was investigated experimentally, even though this was only seen under certain conditions during this study.

5.1   Background study

Electric fields can be generated in a colloidal suspension by the application of an ultrasonic field. The fields arise from the electric charge on the colloidal particles. Sound waves passing through the suspension generate relative motion between the particles and the liquid. The magnitude of this motion depends on the particle and suspending liquid density differences, particle size and shape, and the sound wave frequency (Bolt and Heuter 1955).

5.1.1   Vibrational effects of ultrasound

As a result of the relative motion described above, the diffuse layer around the colloidal particle distorts, resulting in a displacement of the centre of charge away from that of the particle (in the same way as the electrophoretic relaxation effect). Each particle generates an alternating electric field, and an overall effect occurs in the form of a macroscopic electric field, alternating at the frequency of the soundwave. The field generated is dependant on the same suspension parameters as the magnitude of particle-liquid displacement, and also the geometry and type of ultrasonic device.

This idea of sound waves generating electric fields was first noted by Debye (1933). In 1951 Enderby studied a dilute suspension of weakly charged spheres in an electrolyte, and presented a method for obtaining the potential difference when the ratio κa is small (double layer thickness small when compared to particle radius), which is valid for low zeta potentials. An exact expression is also given for large κa. Enderby obtained the macroscopic field by summing the dipole field produced by individual particles. Calculations have been limited to the dilute case, or particular effects, until more recently. O'Brien (1988, 1990) has taken Booth and Enderby's (1952) work further,

correcting the assumptions, and allowing calculation of any electroacoustic effects in suspensions of arbitrary concentration, provided the particles are small compared to the sound wavelength. Equations describing microscopic variations in ion density, electric potential, velocity and pressure are used to produce a set of macroscopic equations which describe the electric field generated by a sound wave. Sound waves generated by an electric field, a phenomenon discovered by Cannon *et al* (1985), are also described. O'Brien and White (1978) give the initial detailed mathematical derivations, which are solved for a dilute suspension by O'Brien (1988), and for arbitrary concentrations at a later date (1990). The mathematical derivations provided by the authors are not within the scope of this study, however the phenomena involved may provide an explanation for the ultrasonic effects seen in the filter cell.

Jossinet *et al* (1998) suggested that the conductivity changes of aqueous solutions were primarily due to changes in acoustic pressure inducing changes in the solvent viscosity, thermal effects due to the adiabatic compression-expansion cycle and the bulk compressibility of the medium. A decrease in the viscosity of a solution as it increases in temperature causes an increase in ionic mobility. It is pointed out by O'Brien (1990) that ionic mobilities of electrolytes and particles are typically of the same order, so the electrolyte contribution is only significant if the electrolyte mass is comparable to the mass of particles, thus in most cases the particles provide the dominant electroacoustic effect.

5.1.2   The Ionic Vibration Potential (IVP)

IVP's occur when ultrasonic waves are propagated through simple electrolyte solutions, generating relative motion between the ions and the liquid. The effect occurs because differences in the effective masses and frictional coefficients of the solvated anions and cations cause differences in their amplitudes and phases of displacement of the ions.

Electrodes placed at positions A and B in Figure 5-1 will receive an A.C. signal with a frequency equal to that of the acoustic wave. Although this phenomenon was first suggested by Debye (1933), it was not until 1949 that the effect was shown experimentally (Zana and Yeager, 1982). A standing wave technique allowed the acoustically produced signal of the order of 10^{-6} V to be distinguished from the electromagnetically induced signals used to generate the ultrasonic wave.
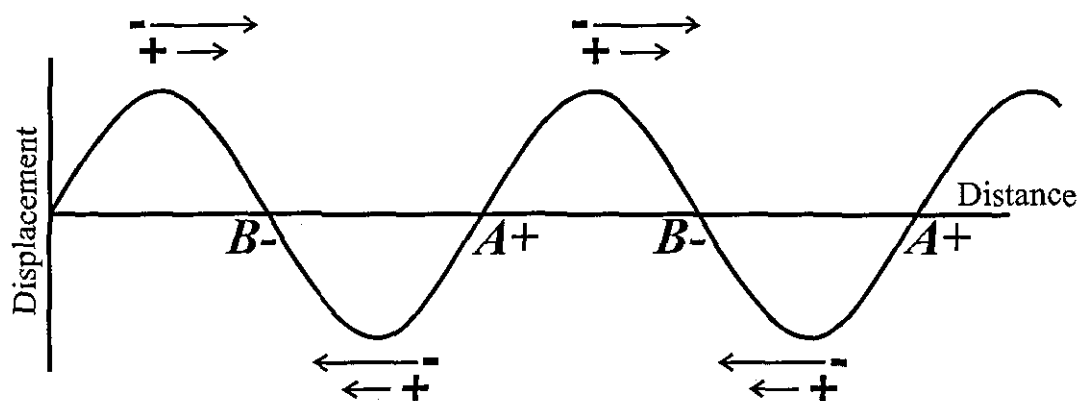
Figure 5-1: Schematic of IVP

In aqueous solutions, the measured IVP is independent of electrolyte concentrations over the range 10^{-3} M to 10^{-1} M. Below this range the IVP decreases with decreasing concentration. At these low concentrations care must be taken to avoid a 'false effect' resulting from the mounting of platinum electrodes (Zana and Yeager, 1982). This effect can even cause a signal to be measured in pure liquids, if the electrode mounting touches the test solution. The authors suggest that the easiest method of avoiding this effect is to position the probe at the centre of the cell, and by filling the cell to 1mm below the probe seal, any false readings are avoided. Jossinet *et al* (1998) state that this phenomenon is still not understood, and it is unclear why the position of the probe would have such an effect.

For salts containing large hydrophobic ions such as tetraalkylammonium, the IVP is dependent on concentration. The same occurs for other long chain salts such as alkyl carboxylates and amphiphiles in the concentration range where micelles form (Zana and Yeager, 1982). However for the small ions used here, these concentration effects should be less pronounced. Solvent viscosity also has little effect on IVP, which is shown by Zana and Yeager (1982) by comparing the IVP of a given salt in two solvents which have different viscosities, but in which the salt has similar ionic behaviour. For example, potassium iodide in water and ethylene glycol has similar ionic mobility values and transport numbers, even though the solvent viscosities are very different. The IVP values for the salt vary by only 0.1 μV s cm^{-1} in the two solvents.

5.1.3   The Colloid Vibration Potential (CVP)

Colloid vibration potentials are closely related to the IVP, but the potential generation involves displacement of the colloidal particles and their surrounding diffuse layers. These are generally larger than IVP's, of order magnitude 10^{-4} to 10^{-2} V s cm^{-1}; although the CVP is smaller if the mobilities of the anion and cation in the supporting electrolyte are unequal (Zana & Yeager, 1982). The ionic mobilities of some solvated ions are given in Table 5-1 (Jossinet *et al*, 1998). The mobilities quoted in Table 5-1 do indeed show that the CVP in the solutions used for these experiments could be lower than the respective IVP, because there is a large difference between the anion and cation mobilities of dissociated HCl and NaOH.

Cation	Ionic mobility, x 10^{-8} m^{2}s^{-1}V^{-1}	Anion	Ionic mobility, x 10^{-8} m^{2}s^{-1}V^{-1}
H_3O^+	36.3	OH^-	20.52
Na^+	5.19	Cl^-	7.91

Table 5-1: Ionic mobilities of solvated ions in water at 25°C

5.2   Experimental Design and Characterisation

An experiment to investigate the effect of ultrasonic irradiation on the conductivity of suspensions was carried out by Cataldo (1997, 1998). A conical flask containing the test suspension was immersed in an ultrasonic bath. A conductivity meter was placed in the flask and the conductivity measured during varying phases of ultrasonic activity. Based on this procedure, an experimental programme was devised to investigate the ultrasonic effect on dead end vacuum filtration. A number of experimental configurations were considered:

1. A method similar to Cataldo's; the placing of the test suspension and conductivity probe in a conical flask which is subsequently placed in an ultrasonic bath.

2. The use of a sonic horn directly into the flask containing the test suspension and probe. The advantage here is that there is no attenuation caused by the glass flask, and control of the ultrasonic amplitude and power is possible. However the close proximity of the sonic horn to the conductivity probe was considered likely to damage the probe due to the large acoustic forces associated with this type of sound

generation. The sonic horn type of transducer is different to that used in the filtration experiments, and has much higher intensity and pressure amplitude.

3. Use of the filtration cell as a vessel to conduct the experiments. The cell can be filled with any test suspension, simply by closing the filter cell drain valve. A known volume of suspension can be exposed to ultrasonic irradiation, and any changes in conductivity measured.

The third method was chosen due to the similarity of the experimental set up with that of the filtration experiments. The test suspension could easily be monitored for temperature and conductivity changes. The coupling of the ultrasound with the suspension would be exactly the same as in the filtration experiments. The only disadvantage of this method is that the suspension is static, and so is subject to any heating effects the ultrasound may cause, and does not therefore fully represent the experimental set up. Conductivity measurements were taken *in–situ* during filtration experiments to address this. It is well known that conductivity is a function of temperature and so it was also investigated whether temperature effects could be the reason for conductivity changes, by monitoring the bulk fluid temperature throughout.

In order to carry out the experiments two litres of test suspension were taken, and electrolyte added in the form of hydrochloric acid or sodium hydroxide. When the solution was at the required pH and/or conductivity, and well mixed, these values were noted and the vessel charged. A lid was fitted to the cell, which allowed positioning of the conductivity probe and thermometer in a known configuration relative to the ultrasonic transducer. The ultrasonic supply was turned on, and readings for the measured parameters were taken at 0, 5, 15, 30, 45 and 60 s and then every 30 s for 5 minutes. The supply was then switched off and the repeat measurements taken for the same time period. The supply was then re-started, and the cycle repeated 3 times.

A series of experiments was carried out for test suspensions of de-ionised water and MIPA dispersed rutile, using hydrochloric acid and sodium hydroxide as electrolytes for altering the initial conductivities.

5.3 Conductivity Measurement

In aqueous solutions ions carry the electrical current. For low salt concentrations, the higher the concentration of dissolved salts the higher the conductivity. The conductivity

increases to a maximum when the solution becomes overcrowded and the ability of ions to move in the solution is reduced. At this point the conductivity can diminish as ionic mobility falls. Some species ionise more completely than others, and so each salt has its own characteristic curve of conductivity against salt concentration. It is well known that an increase in an electrolyte solution's temperature decreases the solution viscosity and increases ion mobility. Temperature effects are different for each ion, because they carry different amounts of water with them. A typical variation in conductivity is 1-3% per ° C (WPA, 1999). Conductivity instruments measure the conductance of a suspension, and convert it to conductivity based on the properties of the probe.

5.4   Experimental Results and Discussion

Experiments were carried out as previously described, de-ionised water was used, and the pH (and thus conductivity) was altered using hydrochloric acid or sodium hydroxide. Characterisation of the electrolytic solution for changes in conductivity due to pH is shown in Figure 5-2.
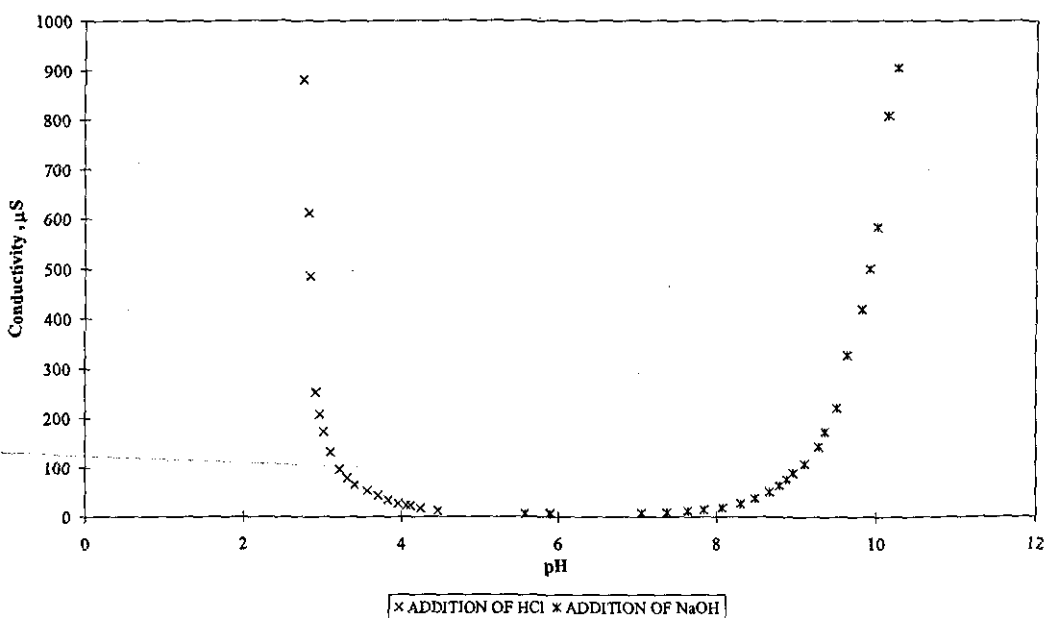
Figure 5-2: Characterisation of electrolyte solutions for conductivity.

Clearly, within the pH ranges being studied here (pH 4-10), the conductivity is no higher than 100 μS on the acid side, and is in general between 10 μS at pH 6 and 30 μS at pH 4. For the addition of base conductivities are higher, from a low of 10 μS at pH 6 to 600

µS at pH 10. At extremes of pH (pH 3 and 10), the conductivities of the electrolyte solutions rise rapidly, because of high ionic concentrations in the suspension. The solution contains a large number of ions and electrons can easily move around. Figure 5-3 shows similar results for rutile suspensions, with the electrolyte solution results plotted for comparison. The curves are similar shapes, with a slightly higher pH required to achieve similar conductivities to the electrolyte.

The filtration cell was then used as a vessel to examine the effect of the ultrasonic field on these suspensions. The measured conductivity was seen to rise, considerably in some cases, depending on the initial conductivity of the suspension. This increase in conductivity was always seen to various extents.
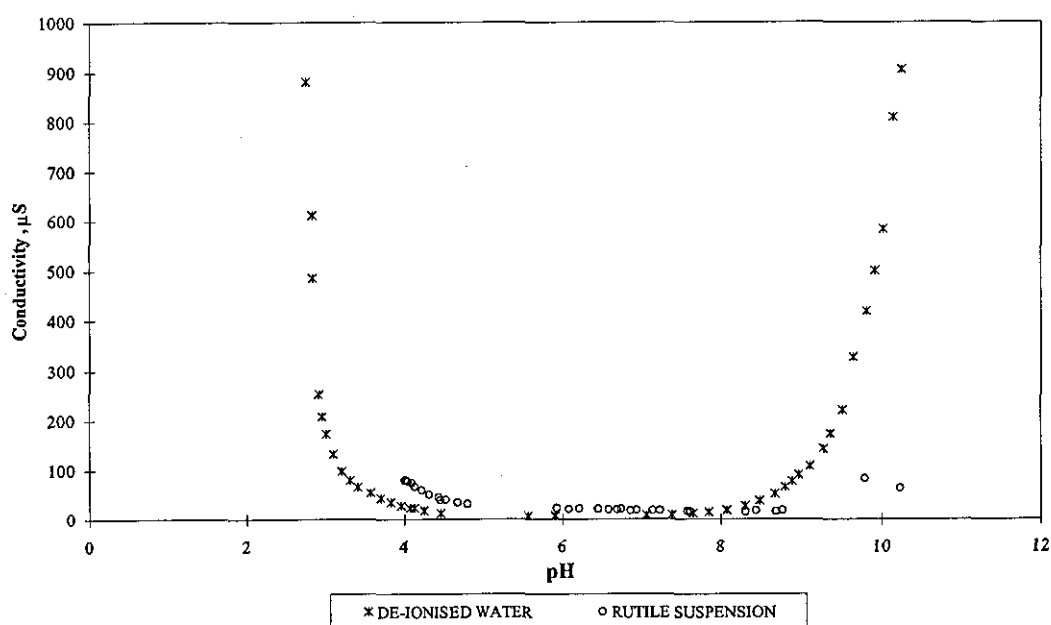
Figure 5-3: Characterisation curve for de-ionised water and Rutile.

5.4.1   Ultrasonic irradiation of electrolyte suspensions: conductivity effects

Figures 5-4 and 5-5 clearly show that, for suspensions with low initial conductivities (below 30 µS), ultrasonic irradiation markedly increases the conductivity of an electrolytic suspension. This increase may be attributed to the ultrasonic vibration effects, or is possibly due to cavitation in the solution causing high local temperatures

and pressures. The conductivity falls the moment the irradiation ceases, suggesting that the increase seen cannot be attributed to macroscopic effects such as bulk fluid heating. If these heating effects were the explanation for the changes seen, then there would be a relaxation time when irradiation ceased, rather than the almost instantaneous return to low levels when the source was switched off. Short relaxation times have also been observed by Cataldo (1997), in similar experiments, confirming that the large increases are not due solely to macroscopic heating. Changes in temperature of the bulk suspension were monitored throughout the experiments, at the end of each period of irradiation or relaxation. Over each 30 minute experiment the temperature increase was generally between 2-3 °C, with an average increase of 2.6 °C. The bulk temperature tended to remain constant during periods of relaxation. Use of the approximations given by WPA along with these temperature increases suggests the bulk solution increases in temperature by around 9%. Study of Figures 5-4 and 5-5 suggests that this is indeed the case. Although the conductivity that the suspension falls back to when irradiation ceases increases over the time of the experiment, it is always less than 110% of the original value by the end of the 30-minute experiment.

The effect on conductivity seen at low ionic concentrations in this study is similar to that carried out by others (for example, Cataldo, 1997 & 1998,). Jossinet *et al* (1998) proposed that the primary cause of these effects was the phenomena resulting from the periodic pressure changes due to wave propagation. This increase in pressure results in a compression of the medium, and the resulting temperature increase then causes expansion. No heat transfer takes place during the pressure cycle, because the period of an acoustic wave is short compared with the time for heat exchange between a given element and the surrounding medium. So the variation in volume of an element can be calculated by summing an isothermal compression followed by a thermal expansion.
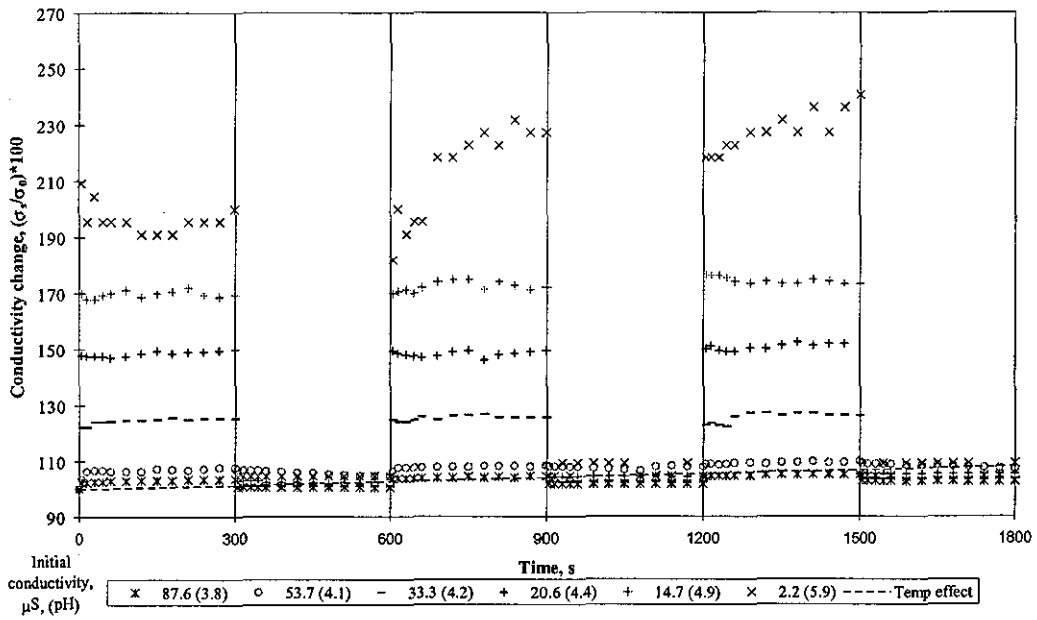
Figure 5-4: Effect of periodic ultrasonic irradiation on solutions of hydrochloric acid
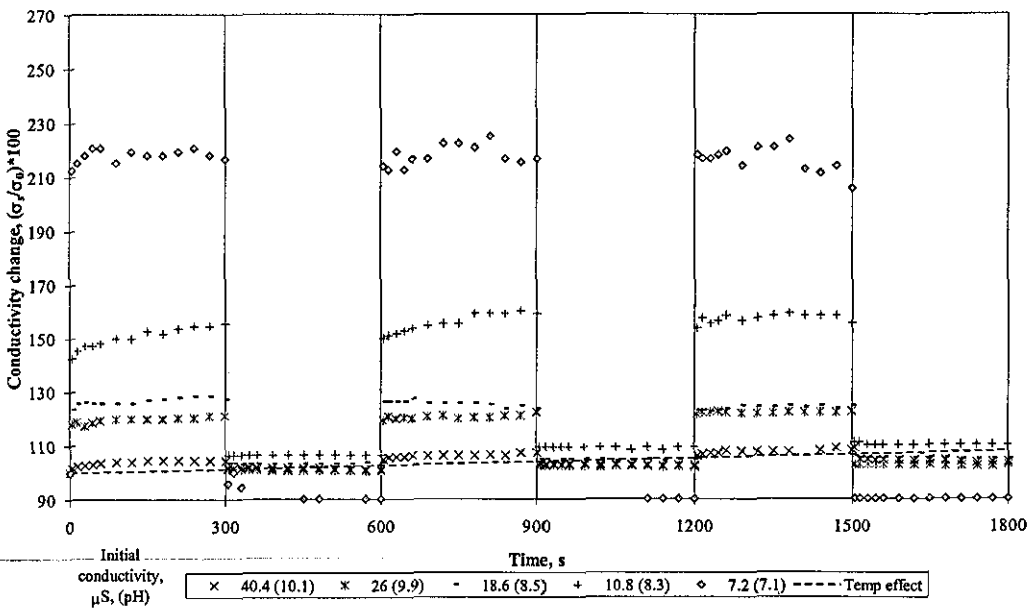
Figure 5-5: Effect of periodic ultrasonic irradiation on solutions of sodium hydroxide

For water the pressure increase is around 1.4×10^{-8} kPa^{-1}, suggesting a temperature increase of 10^{-3} K for the peak pressure amplitude of the acoustic source. This temperature change causes a change in the bulk compressibility. The compressibility coefficient (relative volume reduction per unit pressure) is given by β.

$$\beta = \frac{1}{v}\frac{\partial v}{\partial p} = \frac{1}{\rho}\frac{\partial \rho}{\partial p} \qquad\qquad 5\text{-}1$$

The number of ions per unit volume is inversely proportional to the volume of the element. Should a volume element of fluid be compressed, the ionic concentration of that element increases, increasing the electrical conductivity of the element.

From Stokes law, the force on a sphere in a viscous medium is inversely proportional to the medium viscosity. With ionic mobility being directly related to fluid viscosity by the Henry equation (equation 2-33), an increase in viscosity due to the acoustic pressure wave will result in a direct increase of the fluid viscosity. This is not however a bulk fluid effect and only affects the compressed part of the fluid as the wave propagates. As the conductivity of a solution is dependent on the concentration and mobilites of the ions present in a solution, variations in these parameters affect the conductivity. Above 4°C, the viscosity of water decreases with pressure. Periodic temperature changes as the wave propagates result in periodic (viscosity) ionic mobility and thus conductivity changes in addition to the pressure effect.

Temperature changes resulting from the adiabatic compression expansion cycle act as a secondary phenomenon. These periodic temperature changes result in periodic ionic mobility changes, and this is an additional effect to those directly caused by the periodic pressure variations. The apparent ionic concentration can also be altered by changes in the dissociation equilibrium constant of partially dissociated electrolytes, such as weak electrolytes or water. The influence of temperature and pressure on this coefficient can be determined by the Van't Hoff equation and by consideration of the Gibbs free energy respectively. As a result of these changes, the ionic mobility can vary due to viscosity changes in the solution caused by temperature and pressure changes.

5.4.2   Ultrasonic irradiation of rutile suspensions: conductivity effects

Figure 5-6 shows similar results for identical experiments, but using MIPA dispersed rutile as the test suspension. Although the increases in conductivity are still apparent during periods of ultrasonic irradiation, they are less striking than those shown in Figures 5-4 and 5-5.
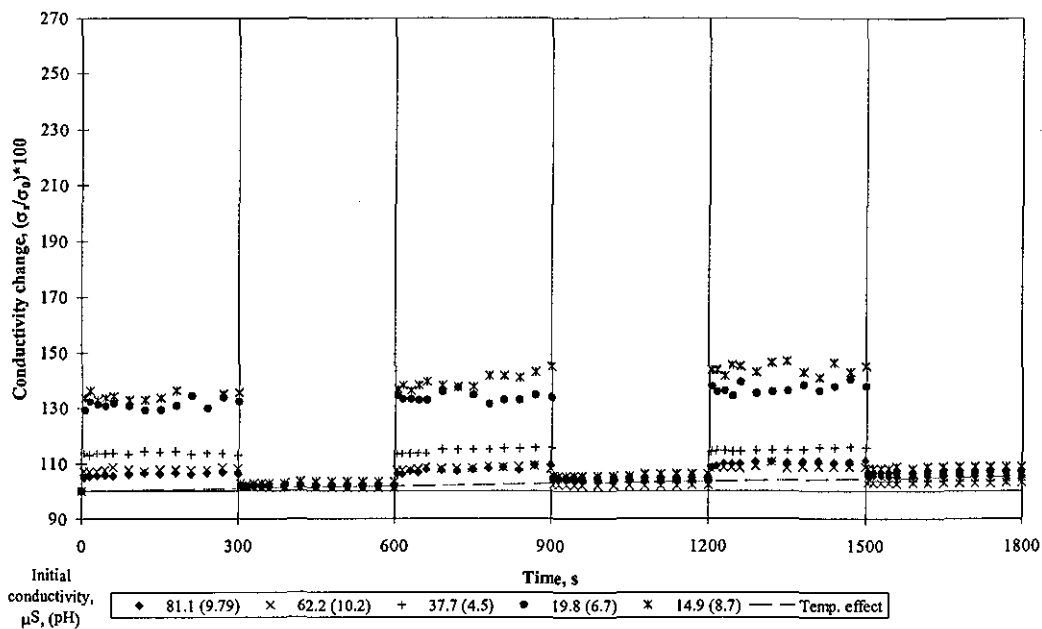
Figure 5-6: Ultrasonic effects on the conductivity of rutile suspensions.

In this study the differences in ionic mobility does appear to have affected the magnitude of the CVP. This is shown in Figure 5-7, between pHs 5 and 7, the ratio of magnitudes of the conductivity measured with and without ultrasound is much larger in the absence of suspended particulates.
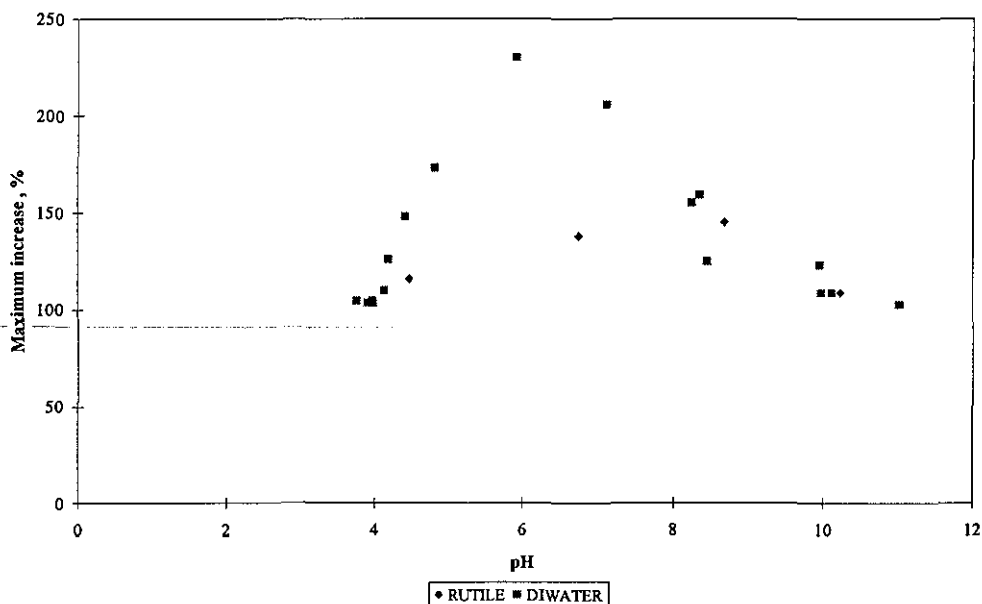
Figure 5-7: Larger IVP than CVP effects occur for electrolyte suspensions

It is interesting to note that irrespective of the ions present, or whether particles are present, the ratio of magnitudes is generally the same for any specific initial conductivity (Figure 5-8) and if the conductivity is over 50 μS, ultrasonic irradiation does not produce any change in the measured conductivity. At high conductivities, the double layer is compressed and the counter-ions are less able to move under the influence of the acoustic field. Thus there is less relative motion between fluid and double layer and the vibration potential is reduced.
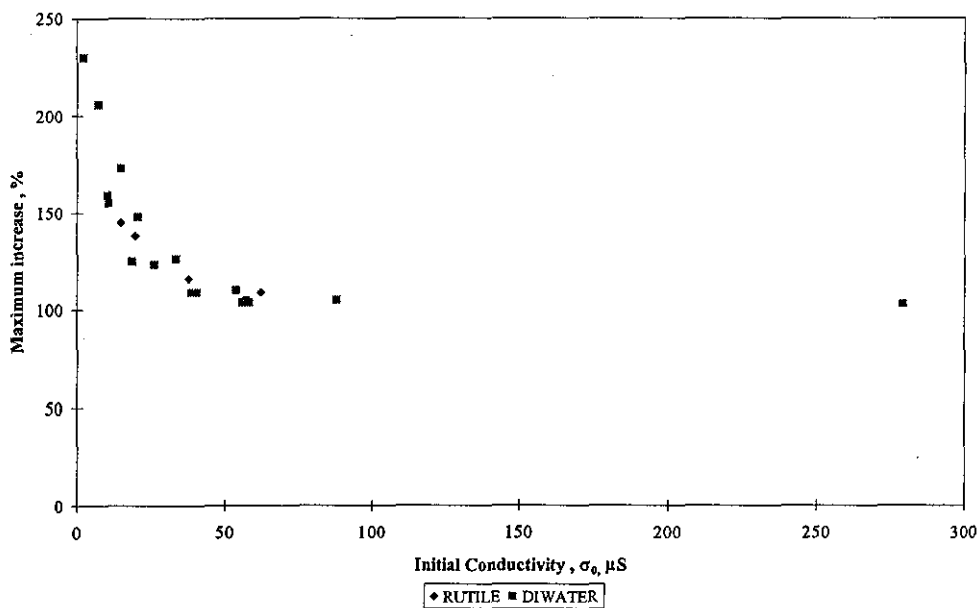
Figure 5-8: Shows maximum initial conductivity to cause a change in conductivity.

As can be seen in Figure 5-8 only those colloidal suspensions having an initial conductivity below 30 μS show an effect which can be attributed to phenomena other than macroscopic bulk heating. At these low conductivities, the electrolyte concentration is also low, and the zeta potential is of large magnitude. In these circumstances, the diffuse cloud around the rutile particle is large, and a large amount of relative motion between the particle and cloud can be achieved, as illustrated by the schematic of the CVP, Figure 5-9. This diffuse layer motion can be compared to the electrokinetic streaming potential. At higher ionic concentrations, the double layer is compressed, and motion of the diffuse cloud is much closer to the particle. In these

cases, the suspensions conductivity is not affected by the ultrasonic irradiation in the way described above, but there may be an effect from the IVP.
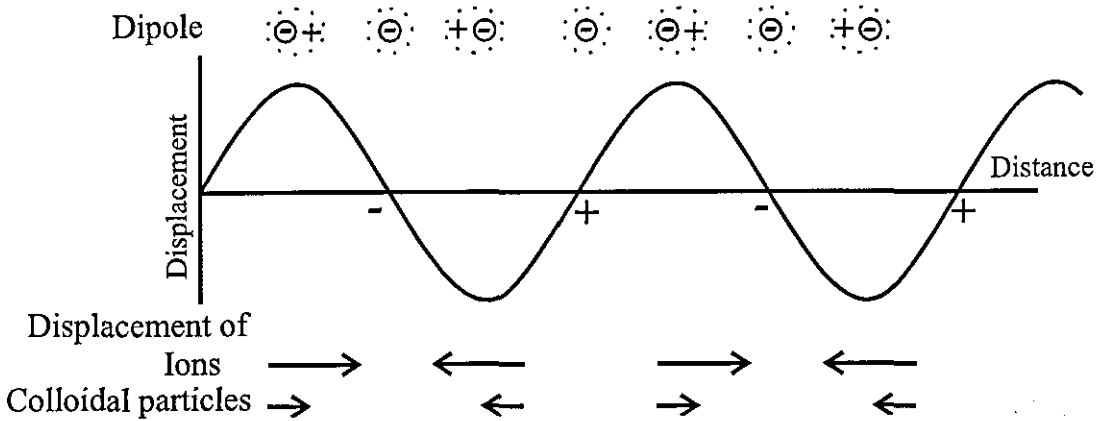
Figure 5-9: Colloid vibration potential. The arrows represent the difference in ionic and colloidal displacements

Filtration experiments were carried out using the procedure described in Chapter 2, with a conductivity probe fitted into the top of the filter cell. An example of the results achieved is shown in Figure 5-10.
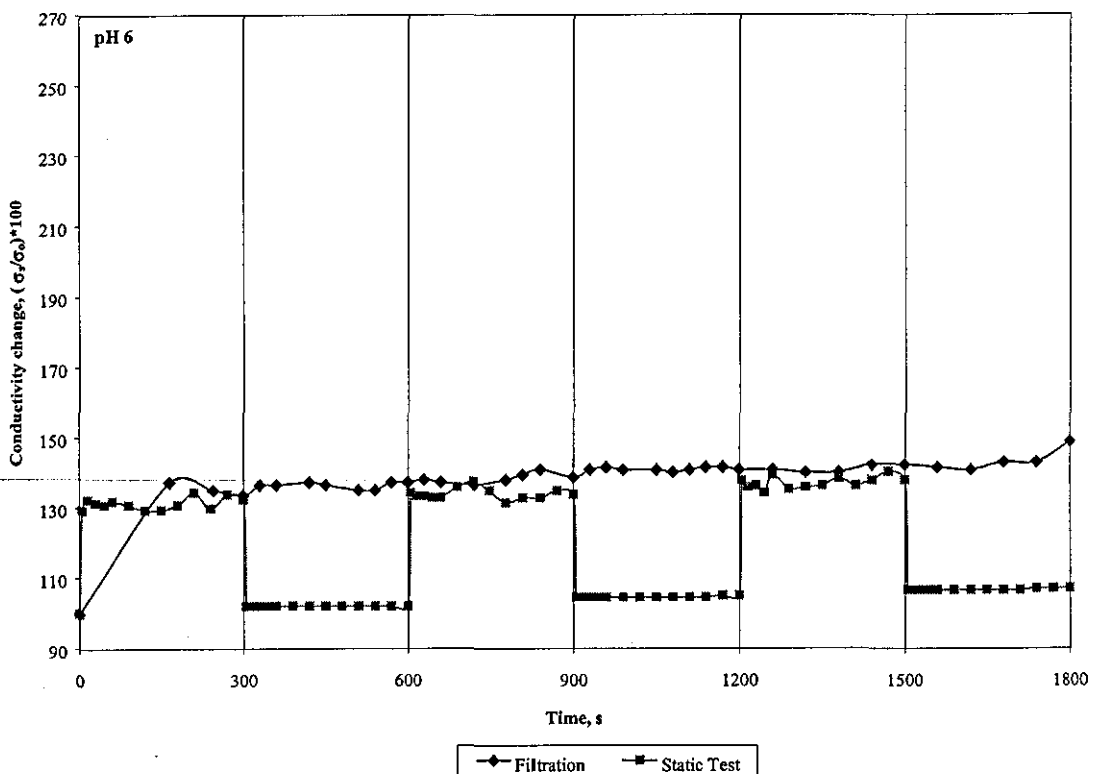
Figure 5-10: Conductivity changes during filtration

The results for suspension conductivity changes during acoustic filtration are given in Table 5-2. The magnitude of the CVP is indicated by quoting the relative change in conductivity during the duration of an experiment. Study of the data shown in Figure 5-10 shows that the percentage increases are similar under stationary conditions, and when the fluid is in motion. This supports the hypothesis that the conductivity effect is due to the application of the acoustic field, and not due to motion of the fluid through the filter causing distortion of the double layer.

	PH 4	PH 6	PH 8	PH 10
NO FIELDS	91.7	198.6	177.8	97.0
ACOUSTIC FIELD	113.0	148.9	151.2	116.0
ELECTRIC & ACOUSTIC FIELDS (20VCM^{-1})	119.9	237.6		
ELECTRIC & ACOUSTIC FIELDS (50VCM^{-1})	139.7	345.7		

Table 5-2: Increases in conductivity (%) during filtration of rutile suspensions

The CVP is much greater when a low voltage electric field gradient is applied in addition to the ultrasonic field, and greater still when a high voltage gradient is applied. It is well understood that the application of an electric field imparts a velocity to suspended particulates, and this motion causes the double layer to be more distorted than by motion due to the acoustic field alone, resulting in greater relative motion and a higher CVP. However this rise could also be due to increased heating of the bulk fluid.

At pH 4, the conductivity increases from CVP are small. The compression of the double layer close to the IEP prevents relative motion between the particle and diffuse cloud. Where the diffuse layer is large, at pHs 6 and 8 the CVP is much more pronounced as the cloud is easily moved. This enhanced CVP may be responsible for the increased electroacoustic filtration rates seen under some conditions during this study.

5.5 Conclusions

The propagation of an acoustic wave in an aqueous solution produces periodic pressure and temperature changes and an electric signal is produced, due to local modifications

of the conductivity (Jossinet *et al*, 1998). These ultrasonic vibration potentials (UVP) are always produced where ultrasonic waves propagate through solutions containing ionic species, including proteins or polyions in solutions of polyelectroyte, and can be ionic (IVP) or colloidal (CVP).

Dipoles occur as a consequence of the diffuse atmosphere being periodically distorted by the sound waves as the centre of charge moves away from that of the particle. The field generated is dependent on the same suspension parameters as the magnitude of particle-liquid displacement (equation 2-30); the magnitude of density differences, particle size and shape, sound wave frequency, and the geometry and type of ultrasonic device (Bolt and Heuter, 1955). The zeta potential, colloid concentration, apparent mass, nature and concentration of the supporting electrolyte also affect the CVP as they alter the diffuse layer surrounding the particle. The magnitude of the CVP is much greater at low ionic concentrations, particularly between pHs 6 and 8.

The CVP can be used to explain the enhanced filtration seen when electric and acoustic fields were applied to the filter system. The increased conductivity allows the electric field to act as if the field strength were greater than that actually applied via the generator. In turn this reduces the specific cake resistance, (Figures 3-21 to 3-24) and thus allows increased flow through the filter cake.

6   Conclusions and further work

This chapter briefly summarises the main findings of each of the areas researched. Conclusions are presented, and suggestions for further work are made.

Research was carried out to investigate the effects of combinations of electric and acoustic fields on dead end filtration. The test suspension was low concentration rutile, a well characterised material, which is known to be difficult to filter.

6.1   Summary of filtration experiments

The majority of this work was carried out to establish the effects of applied field on low concentration rutile suspensions. Comparison of conventional and acoustic filtration showed that, at concentrations greater than 1% by volume the acoustic field was attenuated almost immediately. This was backed up by a review of attenuation mechanisms. At higher concentrations, although the volumes of filtrate were similar, the nature of the cake and suspension changed. No conclusions could be drawn regarding the effect of applied vacuum on field assisted filtration.

The success of electric field application varied according to the pH of the suspension being filtered. At low pHs particulate agglomeration occurred and the critical field strength to suspend particles increased. This resulted in increased settling and faster filtration, overriding the electric field effect to produce a higher porosity cake. At high pHs, a well dispersed suspension was achieved, and improvements in the filtration process were seen as a result of electrophoresis.

Gains in filtration rate were observed over conventional filtration in most cases where an electric field was applied. If the applied field was close to the critical field strength, then the acoustic field acted to further increase filtrate volumes. At lower pHs, where the critical field strength was greater, addition of the acoustic field had little effect.

Measurement of cake porosity yielded the interesting result that whilst application of any magnitude electric field increased the cake porosity, the addition of an acoustic field reduced the porosity increase slightly, suggesting a compressive effect of ultrasound on the electrophoretically generated cake.

6.2   Summary of Acoustic force analysis

The effect of ultrasound on suspensions was reviewed, in order to establish what mechanisms might explain the experimental results. The filtration system was analysed to quantify the forces present on particles within the filtered suspension. It was shown that analysis based on standing waves can not describe the filter system adequately. It was beyond the scope of this thesis to study reflective wave analysis.

6.3   Summary of conductivity effects

The effect of the colloid vibration potential on rutile suspensions was investigated experimentally. Increases in the suspension's conductivity were seen, due to the CVP, when it was ultrasonically irradiated. These increases were shown to be due to mechanisms other than bulk heating of the fluid. By increasing the conductivity using CVP, similar effects to those seen by increasing ionic concentration were expected to occur. The CVP was not evident when filtration took place, due to particle motion as a result of fluid drag being greater than the CVP.

6.4   Conclusions

Additional fields can be used as a means of improving filtration rates, or changing the properties of the filter cake. Mechanisms such as cavitation and the colloid vibration potential acted to alter the characteristics of the suspension, although the synergy seen was much less than that by other authors. The power consumed by the electric field can offer sufficiently large improvements in filtration rates that in some cases it could be considered a technical improvement to filtration technology. However, the power consumed by the ultrasonic field is not sufficiently offset by increases in filter performance. The orientation of the sound field perpendicular to the filter medium resulted in compression of the filter cake. Fluid flow parallel to the transducer surface resulted in a reduction in the CVP induced by ultrasound.

6.5   Further work

As a result of the work described in this thesis, a number of areas could benefit from continued investigation. The following are suggestions to either improve the practical knowledge of field assisted filtration or to investigate the theory behind field assisted

filtration. They are based upon studying acoustic field assisted filtration, as electrofiltration is already well understood.

- *Re-consider filtration method*

  The experimental results described in this thesis were severely limited by the limitations of the filter design. For example it was difficult to obtain a representative cake sample without disturbing the formed cake, and the method developed may have removed some moisture from otherwise open cakes. Similar dead end filters are likely to come across related problems as excess feed suspension will always have to be removed, however it may be possible to study the effects on dead end filtration using candle filters. The results seen agreed with other authors work, showing that acoustic field application does not appear to be terribly beneficial to dead end filtration. For the above reasons it would seem to be of more practical use to extend the studies of field assisted crossflow filtration, which has previously shown some encouraging results.

- *Improve practical knowledge of acoustic effects on suspensions*

  There is a large amount of scope for further experimental work into the parameters which govern suspension behaviour in acoustic and electroacoustic filtration. Parameters such as test material density and size could be varied; the rutile used in this study moved with the fluid, varying of material properties is likely to result in a range of particle behaviours. Similarly acoustic parameters such as intensity and frequency could be varied to show these effects on materials. The design of the experimental rig, which has a large bearing on how the field affects the suspension should take into account the requirement of parameter and orientaion changes, allowing the relationship between filter medium and acoustic field to be changed.

- *In depth study of the forces present*

  Collaboration with acoustic experts may give more insight into the field- fluid-particle interactions present, resulting in better understanding and prediction of the filtration behaviour.

APPENDIX A

EXPERIMENTAL RESULTS

In the results that follow, although specific cake resistance, α, and medium resistance are quoted, they are meaningless in assisted filtration experiments due to the limitations of the calculation method. Comparable data is given by the slope of plot, K_1 as it indicates the relative magnitude of the specific cake resistance, although this cannot be calculated explicitly as the pressure is not, strictly speaking, constant during acoustic filtration due to the cyclic nature of the wave. Similarly K_2 gives an indication of the relative magnitude of the medium resistance. For further explanation see Section 3.7

NFPH4No1		
	Filtrate	Solid
Weight	*4995.0*	*21.3* g
Density, ρ	*1000*	*4260* kg m^{-3}
Volume	5.00E-03	5.00E-06 m^3
Total Mass	5.02 kg	
Total Volume	5.00E-03 m^3	
Solids conc^n	4.26 kg m^{-3}	
$\equiv$	0.10% v/v	
$\equiv$	0.42% w/w	
pH	4.00	
Applied field	0 V	
Separation	1.5 cm	
Field Strength	0 Vcm^{-1}	
Viscosity, μ	*0.001* Pa s	
Filter Area	6.22E-03 m^2	
Pressure drop	0.75 bar	
	75000 Pa	
Slope of plot	1.11E+09 sm^{-6}	
Intercept	2.30E+04 sm^{-3}	
R^2	0.995	

α	*1.508E+12*	m kg^{-1}
R_m	*1.071E+10*	m^{-1}

Volume @1800s	*1241* ml
Vol. per unit area	0.199 m^{3}m^{-2}

Mass of *wet* cake	*11.14* g
Mass of *dry* cake	*7.34* g
Mass of liquid	3.80 g
Volume of solid	1.72 cm^3
Volume of liquid	3.80 cm^3
Cake conc^n	65.89% (Mass)
Cake conc^n	31.20% (Volume)
ε	*0.688*
Moisture ratio, m	1.518
Effective c	4.27 kg m^{-3}
Slurry c	4.26 kg m^{-3}

NFPH4No2

	Filtrate	Solid	
Weight	4995.0	21.3	g
Density, ρ	1000	4260	kg m^{-3}
Volume	5.00E-03	5.00E-06	m^3
Total Mass	5.02		kg
Total Volume	5.00E-03		m^3
Solids conc^n	4.26		kg m^{-3}
$\equiv$	0.10%		v/v
$\equiv$	0.42%		w/w
pH	4.00		
Applied field	0		V
Separation	1.5		cm
Field Strength	0		Vcm^{-1}
Viscosity, μ	0.001		Pa s
Filter Area	6.22E-03		m^2
Pressure drop	0.75		bar
	75000		Pa
Slope of plot	1.45E+09		sm^{-6}
Intercept	2.74E+04		sm^{-3}
R^2	0.976		

α	1.976E+12	m kg^{-1}
R_m	1.276E+10	m^{-1}

Volume @1800s	916	ml
Vol. per unit area	0.147294	m^{3}m^{-2}

Mass of *wet* cake	14.91	g
Mass of *dry* cake	8.10	g
Mass of liquid	6.81	g
Volume of solid	1.90	cm^3
Volume of liquid	6.81	cm^3
Cake conc^n	54.33%	(Mass)
Cake conc^n	21.83%	(Volume)
ε	0.782	
Moisture ratio, m	1:841	
Effective c	4.28	kg m^{-3}
Slurry c	4.26	kg m^{-3}

NF001PH4

	Filtrate	Solid	
Weight	*4942.7*	*2.1*	g
Density, ρ	*1000*	*4260*	kg m^{-3}
Volume	4.94E-03	4.93E-07	m^3
Total Mass	4.94		kg
Total Volume	4.94E-03		m^3
Solids conc^n	0.42		kg m^{-3}
$\equiv$	0.01%		v/v
$\equiv$	0.04%		w/w
pH	3.60		
Applied field	0		V
Separation	1.5		cm
Field Strength	0		Vcm^{-1}
Viscosity, μ	*0.001*		Pa s
Filter Area	6.22E-03		m^2
Pressure drop	0.75		bar
	75000		Pa
Slope of plot	1.53E+08		sm^{-6}
Intercept	1.66E+05		sm^{-3}
R^2	0.999		

α	*2.087E+12*	m kg^{-1}
R$_m$	*7.727E+10*	m^{-1}

Volume @1800s	*2913*	ml
Vol. per unit area	4.68E-01	m^{3}m^{-2}

NFPH6NO1		
	Filtrate	**Solid**
Weight	*4995.0*	*21.4* g
Density, ρ	*1000*	*4260* kg m^{-3}
Volume	5.00E-03	5.02E-06 m^3
Total Mass	5.02 kg	
Total Volume	5.00E-03 m^3	
Solids conc^n	4.28 kg m^{-3}	
$\equiv$	0.10% v/v	
$\equiv$	0.43% w/w	
pH	5.40	
Applied field	0 V	
Separation	1.5 cm	
Field Strength	0 Vcm^{-1}	
Viscosity, μ	*0.001* Pa s	
Filter Area	6.22E-03 m^2	
Pressure drop	0.75 bar	
	75000 Pa	
Slope of plot	9.76E+08 sm^{-6}	
Intercept	1.51E+05 sm^{-3}	
R^2	0.994	

α	*1.322E+12*	m kg^{-1}
R_m	*7.044E+10*	m^{-1}

Volume @1800s	*1298* ml	
Vol. per unit area	0.209 m^{3}m^{-2}	

Mass of *wet* cake	*6.24* g	
Mass of *dry* cake	*4.70* g	
Mass of liquid	1.54 g	
Volume of solid	1.10 cm^3	
Volume of liquid	1.54 cm^3	
Cake conc^n	75.32%	(Mass)
Cake conc^n	41.74%	(Volume)
ε	*0.583*	
Moisture ratio, m	1.328	

Effective c	4.29 kg m^{-3}	
Slurry c	4.28 kg m^{-3}	

NFPH6NO2

	Filtrate	Solid	
Weight	*4995.0*	*21.1*	g
Density, ρ	*1000*	*4260*	kg m^{-3}
Volume	5.00E-03	4.95E-06	m^3
Total Mass		5.02	kg
Total Volume		5.00E-03	m^3
Solids conc^n		4.22	kg m^{-3}
$\equiv$		0.10%	v/v
$\equiv$		0.42%	w/w
pH		5.96	
Applied field		0	V
Separation		1.5	cm
Field Strength		0	Vcm^{-1}
Viscosity, μ		*0.001*	Pa s
Filter Area		6.22E-03	m^2
Pressure drop		0.75	bar
		75000	Pa
Slope of plot		3.45E+09	sm^{-6}
Intercept		2.56E+05	sm^{-3}
R^2		0.996	

α	*4.738E+12* m kg^{-1}
R_m	*1.197E+11* m^{-1}

Volume @1800s	*702*	ml
Vol. per unit area	1.13E-01	m^{3}m^{-2}

Mass of *wet* cake	*3.73*	g
Mass of *dry* cake	*2.77*	g
Mass of liquid	0.96	g
Volume of solid	0.65	cm^3
Volume of liquid	0.96	cm^3
Cake conc^n	74.26%	(Mass)
Cake conc^n	40.38%	(Volume)
ε	*0.596*	
Moisture ratio, m	1.347	
Effective c	4.23	kg m^{-3}
Slurry c	4.22	kg m^{-3}

	NF001NO1		
	Filtrate	**Solid**	
Weight	*1999.0*	*1.1*	g
Density, ρ	*1000*	*4260*	kg m^{-3}
Volume	2.00E-03	2.58E-07	m^3
Total Mass	2.00	kg	
Total Volume	2.00E-03	m^3	
Solids conc^n	0.55	kg m^{-3}	
$\equiv$	0.01%	v/v	
$\equiv$	0.05%	w/w	
Applied field	0	V	
Separation	1.5	cm	
Field Strength	0	Vcm^{-1}	
Viscosity, μ	*0.001*	Pa s	
Filter Area	6.22E-03	m^2	
Pressure drop	0.75	bar	
	75000	Pa	
Slope of plot	1.54E+08	sm^{-6}	
Intercept	1.33E+05	sm^{-3}	
R^2	0.997		

α	*1.629E+12*	m kg^{-1}
R$_m$	*6.193E+10*	m^{-1}

Volume @ 885s	*1966*	ml
Vol. per unit area	3.16E-01	m^{3}m^{-2}

NF001No2

	Filtrate	Solid	
Weight	*4886.3*	*2.2*	g
Density, ρ	*1000*	*4260*	kg m^{-3}
Volume	4.89E-03	5.16E-07	m^3
Total Mass	4.89		kg
Total Volume	4.89E-03		m^3
Solids conc^n	0.45		kg m^{-3}
$\equiv$	0.01%		v/v
$\equiv$	0.05%		w/w

Applied field	0	V
Separation	1.5	cm
Field Strength	0	Vcm^{-1}
Viscosity, μ	*0.001*	Pa s
Filter Area	6.22E-03	m^2
Pressure drop	0.75	bar
	75000	Pa
Slope of plot	1.23E+08	sm^{-6}
Intercept	1.07E+05	sm^{-3}
R^2	0.995	

α	*1.58E+12*	m kg^{-1}
R_m	*4.991E+10*	m^{-1}

Volume @1800s	*2270*	ml
Vol. per unit area	3.65E-01	m^{3}m^{-2}

NF001No3

	Filtrate	Solid	
Weight	*1999.8*	*0.9*	g
Density, ρ	*1000*	*4260*	kg m^{-3}
Volume	2.00E-03	2.00E-07	m^3
Total Mass	2.00		kg
Total Volume	2.00E-03		m^3
Solids conc^n	0.43		kg m^{-3}
$\equiv$	0.01%		v/v
$\equiv$	0.04%		w/w
Applied field	0		V
Separation	1.5		cm
Field Strength	0		Vcm^{-1}
Viscosity, μ	*0.001*		Pa s
Filter Area	6.22E-03		m^2
Pressure drop	0.75		bar
	75000		Pa
Slope of plot	1.39E+08		sm^{-6}
Intercept	1.78E+05		sm^{-3}
R^2	0.997		

α	*1.902E+12*	m kg^{-1}
R$_m$	*8.291E+10*	m^{-1}

Volume @ 870s	*1938*	ml
Vol. per unit area	3.11E-01	m^{3}m^{-2}

NF05No1

	Filtrate	Solid	
Weight	*495.0*	*10.7*	g
Density, ρ	*1000*	*4260*	kg m^{-3}
Volume	4.95E-04	2.50E-06	m^3
Total Mass	0.51	kg	
Total Volume	4.98E-04	m^3	
Solids conc^n	21.52	kg m^{-3}	
$\equiv$	0.50%	v/v	
$\equiv$	2.11%	w/w	

Applied field	0	V
Separation	1.5	cm
Field Strength	0	Vcm^{-1}
Viscosity, μ	*0.001*	Pa s
Filter Area	6.22E-03	m^2
Pressure drop	0.75	bar
	75000	Pa
Slope of plot	1.62E+11	sm^{-6}
Intercept	2.47E+06	sm^{-3}
R^2	0.895	

α	*4.369E+13*	m kg^{-1}
R_m	*1.152E+12*	m^{-1}

Volume @1800s	*100*	ml
Vol. per unit area	1.61E-02	m^{3}m^{-2}

	NF1No1	
	Filtrate	**Solid**
Weight	*495.0*	*21.3* g
Density, ρ	*1000*	*4260* kg m^{-3}
Volume	4.95E-04	5.00E-06 m^3
Total Mass	0.52 kg	
Total Volume	5.00E-04 m^3	
Solids conc^n	43.03 kg m^{-3}	
≡	1.00% v/v	
≡	4.13% w/w	
Applied field	0 V	
Separation	1.5 cm	
Field Strength	0 Vcm^{-1}	
Viscosity, μ	*0.001* Pa s	
Filter Area	6.22E-03 m^2	
Pressure drop	0.75 bar	
	75000 Pa	
Slope of plot	1.03E+11 sm^{-6}	
Intercept	8.75E+05 sm^{-3}	
R^2	0.965	

α	*1.389E+13*	m kg^{-1}
R$_m$	*4.081E+11*	m^{-1}

Volume @1800s	*124*	ml
Vol. per unit area	1.99E-02	m^{3}m^{-2}

	NF1No2		
	Filtrate	**Solid**	
Weight	*990.0*	*4.3*	g
Density, ρ	*1000*	*4260*	kg m^{-3}
Volume	9.90E-04	1.00E-06	m^3
Total Mass	0.99	kg	
Total Volume	9.91E-04	m^3	
Solids conc^n	4.30	kg m^{-3}	
$\equiv$	0.10%	v/v	
$\equiv$	0.43%	w/w	
Applied field	0	V	
Separation	1.5	cm	
Field Strength	0	Vcm^{-1}	
Viscosity, μ	*0.001*	Pa s	
Filter Area	6.22E-03	m^2	
Pressure drop	0.75	bar	
	75000	Pa	
Slope of plot	6.07E+10	sm^{-6}	
Intercept	1.07E+07	sm^{-3}	
R^2	0.769		

α	*8.187E+13*	m kg^{-1}
R$_m$	*4.993E+12*	m^{-1}

Volume @1800s	*107*	ml
Vol. per unit area	1.72E-02	m^{3}m^{-2}

	NF5No1	
	Filtrate	**Solid**
Weight	*475.0*	*106.5* g
Density, ρ	*1000*	*4260* kg m^{-3}
Volume	4.75E-04	2.50E-05 m^3
Total Mass	0.58 kg	
Total Volume	5.00E-04 m^3	
Solids conc^n	224.21 kg m^{-3}	
$\equiv$	**5.00%** v/v	
$\equiv$	**18.31%** w/w	
Applied field	0 V	
Separation	1.5 cm	
Field Strength	0 Vcm^{-1}	
Viscosity, μ	*0.001* Pa s	
Filter Area	6.22E-03 m^2	
Pressure drop	0.75 bar	
	75000 Pa	
Slope of plot	- sm^{-6}	
Intercept	- sm^{-3}	
R^2	-	

α	*#VALUE!*	m kg^{-1}
R_m	*#VALUE!*	m^{-1}

Volume @1800s	*5* ml	
Vol. per unit area	7.67E-04 m^{3}m^{-2}	

NF250PH8

	Filtrate	Solid	
Weight	*4995.1*	*21.1*	g
Density, ρ	*1000*	*4260*	kg m^{-3}
Volume	5.00E-03	4.96E-06	m^3
Total Mass	5.02		kg
Total Volume	5.00E-03		m^3
Solids conc^n	4.23		kg m^{-3}
$\equiv$	0.10%		v/v
$\equiv$	0.42%		w/w
pH	8.02		
Applied field	0		V
Separation	1.5		cm
Field Strength	0		Vcm^{-1}
Viscosity, μ	*0.001*		Pa s
Filter Area	6.22E-03		m^2
Pressure drop	0.25		bar
	25000		Pa
Slope of plot	9.28E+09		sm^{-6}
Intercept	5.56E+05		sm^{-3}
R^2	0.984		

α	*4.248E+12*	m kg^{-1}
R$_m$	*8.643E+10*	m^{-1}

Volume @1800s	*410*	ml
Vol. per unit area	6.60E-02	m^{3}m^{-2}

Mass of *wet* cake	2.65	g
Mass of *dry* cake	1.57	g
Mass of liquid	1.08	g
Volume of solid	0.37	cm^3
Volume of liquid	1.08	cm^3
Cake conc^n	59.25%	(Mass)
Cake conc^n	25.44%	(Volume)
ε	*0.746*	
Moisture ratio, m	1.688	
Effective c	4.24	kg m^{-3}
Slurry c	4.23	kg m^{-3}

NF500PH8

	Filtrate	Solid	
Weight	*4995.2*	*21.2*	g
Density, ρ	*1000*	*4260*	kg m^{-3}
Volume	5.00E-03	4.98E-06	m^3
Total Mass	5.02		kg
Total Volume	5.00E-03		m^3
Solids conc^n	4.24		kg m^{-3}
$\cong$	0.10%		v/v
$\cong$	0.42%		w/w
pH	8.00		
Applied field	0		V
Separation	1.5		cm
Field Strength	0		Vcm^{-1}
Viscosity, μ	*0.001*		Pa s
Filter Area	6.22E-03		m^2
Pressure drop	0.5		bar
	50000		Pa
Slope of plot	5.43E+09		sm^{-6}
Intercept	-1.54E+05		sm^{-3}
R^2	0.996		

α	*4.947E+12*	m kg^{-1}
R_m	*-4.8E+10*	m^{-1}

Volume @1800s	*582*	ml
Vol. per unit area	9.36E-02	m^{3}m^{-2}

Mass of *wet* cake	*3.29*	g
Mass of *dry* cake	*2.17*	g
Mass of liquid	1.12	g
Volume of solid	0.51	cm^3
Volume of liquid	1.12	cm^3
Cake conc^n	65.87%	(Mass)
Cake conc^n	31.18%	(Volume)
ε	*0.688*	
Moisture ratio, m	1.518	
Effective c	4.25	kg m^{-3}
Slurry c	4.24	kg m^{-3}

NF750PH8

	Filtrate	Solid	
Weight	4995.0	21.1	g
Density, ρ	1000	4260	kg m^{-3}
Volume	5.00E-03	4.95E-06	m^3
Total Mass	5.02		kg
Total Volume	5.00E-03		m^3
Solids conc^n	4.22		kg m^{-3}
$\equiv$	0.10%		v/v
$\equiv$	0.42%		w/w
pH	8.00		
Applied field	0		V
Separation	1.5		cm
Field Strength	0		Vcm^{-1}
Viscosity, μ	0.001		Pa s
Filter Area	6.22E-03		m^2
Pressure drop	0.75		bar
	75000		Pa
Slope of plot	5.46E+09		sm^{-6}
Intercept	1.68E+05		sm^{-3}
R^2	0.994		

α	7.51E+12	m kg^{-1}
R_m	7.861E+10	m^{-1}

Volume @1800s	554	ml
Vol. per unit area	8.90E-02	m^{3}m^{-2}

Mass of *wet* cake	3.03	g
Mass of *dry* cake	2.27	g
Mass of liquid	0.76	g
Volume of solid	0.53	cm^3
Volume of liquid	0.76	cm^3
Cake conc^n	74.92%	(Mass)
Cake conc^n	41.22%	(Volume)
ε	0.588	
Moisture ratio, m	1.335	
Effective c	4.23	kg m^{-3}
Slurry c	4.22	kg m^{-3}

	NF750p82		
	Filtrate	**Solid**	
Weight	*1926.5*	*8.2*	g
Density, ρ	*1000*	*4260*	kg m^{-3}
Volume	1.93E-03	1.92E-06	m^3
Total Mass	1.93	kg	
Total Volume	1.93E-03	m^3	
Solids conc^n	4.24	kg m^{-3}	
$\equiv$	0.10%	v/v	
$\equiv$	0.42%	w/w	
pH	8		
Applied field	0	V	
Separation	1.5	cm	
Field Strength	0	Vcm^{-1}	
Viscosity, μ	*0.001*	Pa s	
Filter Area	6.22E-03	m^2	
Pressure drop	0.75	bar	
	75000	Pa	
Slope of plot	6.60E+09	sm^{-6}	
Intercept	8.07E+05	sm^{-3}	
R^2	0.995		

α	*9.047E+12*	m kg^{-1}
R_m	*3.765E+11*	m^{-1}

Volume @1800s	*463*	ml
Vol. per unit area	7.44E-02	m^{3}m^{-2}

NF750P83

	Filtrate	Solid	
Weight	*1998.5*	*8.5*	g
Density, ρ	*1000*	*4260*	kg m^{-3}
Volume	2.00E-03	2.00E-06	m^3
Total Mass	2.01		kg
Total Volume	2.00E-03		m^3
Solids conc^n	4.25		kg m^{-3}
≡	0.10%		v/v
≡	0.42%		w/w
pH	8		
Applied field	0		V
Separation	1.5		cm
Field Strength	0		Vcm^{-1}
Viscosity, μ	*0.001*		Pa s
Filter Area	6.22E-03		m^2
Pressure drop	0.75		bar
	75000		Pa
Slope of plot	8.63E+09		sm^{-6}
Intercept	7.60E+05		sm^{-3}
R^2	0.978		

α	*1.179E+13*	m kg^{-1}
R$_m$	*3.544E+11*	m^{-1}

Volume @1800s	*410*	ml
Vol. per unit area	6.60E-02	m^{3}m^{-2}

NFPH10N1		
	Filtrate	**Solid**
Weight	*4995.0*	*21.3* g
Density, ρ	*1000*	*4260* kg m^{-3}
Volume	5.00E-03	5.00E-06 m^3
Total Mass	5.02 kg	
Total Volume	5.00E-03 m^3	
Solids conc^n	4.26 kg m^{-3}	
$\equiv$	0.10% v/v	
$\equiv$	0.42% w/w	
pH	10.01	
Applied field	0 V	
Separation	1.5 cm	
Field Strength	0 Vcm^{-1}	
Viscosity, μ	*0.001* Pa s	
Filter Area	6.22E-03 m^2	
Pressure drop	0.75 bar	
	75000 Pa	
Slope of plot	5.63E+09 sm^{-6}	
Intercept	1.48E+06 sm^{-3}	
R^2	0.965	

α	*7.669E+12*	m kg^{-1}
R_m	*6.927E+11*	m^{-1}

Volume @1800s	*453* ml
Vol. per unit area	7.29E-02 m^{3}m^{-2}

Mass of *wet* cake	*3.03* g	
Mass of *dry* cake	*2.19* g	
Mass of liquid	0.84 g	
Volume of solid	0.51 cm^3	
Volume of liquid	0.84 cm^3	
Cake conc^n	72.28%	(Mass)
Cake conc^n	37.97%	(Volume)
ε	*0.620*	
Moisture ratio, m	1.384	
Effective c	4.27 kg m^{-3}	
Slurry c	4.26 kg m^{-3}	

NFPH10N2

	Filtrate	Solid	
Weight	*4995.0*	*21.3*	g
Density, ρ	*1000*	*4260*	kg m^{-3}
Volume	5.00E-03	5.00E-06	m^3
Total Mass	5.02		kg
Total Volume	5.00E-03		m^3
Solids conc^n	4.26		kg m^{-3}
$\equiv$	0.10%		v/v
$\equiv$	0.42%		w/w
pH	9.99		
Applied field	0		V
Separation	1.5		cm
Field Strength	0		Vcm^{-1}
Viscosity, μ	*0.001*		Pa s
Filter Area	6.22E-03		m^2
Pressure drop	0.75		bar
	75000		Pa
Slope of plot	9.51E+09		sm^{-6}
Intercept	-3.90E+05		sm^{-3}
R^2	0.996		

α	*1.294E+13*	m kg^{-1}
R_m	*-1.82E+11*	m^{-1}

Volume @1800s	*458*	ml
Vol. per unit area	7.36E-02	m^{3}m^{-2}

Mass of *wet* cake	2.87	g
Mass of *dry* cake	*1.58*	g
Mass of liquid	1.29	g
Volume of solid	0.37	cm^3
Volume of liquid	1.29	cm^3
Cake conc^n	55.05%	(Mass)
Cake conc^n	22.33%	(Volume)
ε	*0.777*	
Moisture ratio, m	1.816	
Effective c	4.28	kg m^{-3}
Slurry c	4.26	kg m^{-3}

AC750PH4		
	Filtrate	Solid
Weight	*4995.0*	*21.2* g
Density, ρ	*1000*	*4260* kg m^{-3}
Volume	5.00E-03	4.98E-06 m^3
Total Mass	5.02 kg	
Total Volume	5.00E-03 m^3	
Solids conc^n	4.24 kg m^{-3}	
$\equiv$	0.10% v/v	
$\equiv$	0.42% w/w	
pH	4.07	
Applied field	0 V	
Separation	. 1.5 cm	
Field Strength	0 Vcm^{-1}	
Viscosity, μ	*0.001* Pa s	
Filter Area	6.22E-03 m^2	
Pressure drop	0.75 bar	
	75000 Pa	
Slope of plot	1.40E+09 sm^{-6}	
Intercept	1.05E+05 sm^{-3}	
R^2	0.995	

α	*1.909E+12*	m kg^{-1}
R_m	*4.911E+10*	m^{-1}

Volume @1800s	*1126* ml	
Vol. per unit area	1.81E-01	m^{3}m^{-2}

Mass of *wet* cake	*6.65* g	
Mass of *dry* cake	*4.34* g	
Mass of liquid	2.31 g	
Volume of solid	1.02 cm^3	
Volume of liquid	2.31 cm^3	
Cake conc^n	65.26%	(Mass)
Cake conc^n	30.61%	(Volume)
ε	*0.694*	
Moisture ratio, m	1.532	

Effective c	4.25 kg m^{-3}	
Slurry c	4.24 kg m^{-3}	

	AC01PH4	
	Filtrate	**Solid**
Weight	*4995.0*	*21.1* g
Density, ρ	*1000*	*4260* kg m^{-3}
Volume	5.00E-03	4.95E-06 m^3
Total Mass	5.02 kg	
Total Volume	5.00E-03 m^3	
Solids conc^n	4.22 kg m^{-3}	
≡	0.10% v/v	
≡	0.42% w/w	
pH	4.07	
Applied field	0 V	
Separation	1.5 cm	
Field Strength	0 Vcm^{-1}	
Viscosity, μ	*0.001* Pa s	
Filter Area	6.22E-03 m^2	
Pressure drop	0.75 bar	
	75000 Pa	
Slope of plot	1.04E+09 sm^{-6}	
Intercept	5.65E+05 sm^{-3}	
R^2	0.933	

α *1.431E+12*	m kg^{-1}
R$_m$ *2.634E+11*	m^{-1}

Volume @1800s	*3386*	ml
Vol. per unit area	5.44E-01	m^{3}m^{-2}

AC750PH6		
	Filtrate	Solid
Weight	*4995.0*	*21.0* g
Density, ρ	*1000*	*4260* kg m^{-3}
Volume	5.00E-03	4.93E-06 m^3
Total Mass	5.02 kg	
Total Volume	5.00E-03 m^3	
Solids conc^n	4.20 kg m^{-3}	
$\equiv$	0.10% v/v	
$\equiv$	0.42% w/w	
pH	6.00	
Applied field	0 V	
Separation	1.5 cm	
Field Strength	0 Vcm^{-1}	
Viscosity, μ	*0.001* Pa s	
Filter Area	6.22E-03 m^2	
Pressure drop	0.75 bar	
	75000 Pa	
Slope of plot	2.09E+09 sm^{-6}	
Intercept	2.13E+05 sm^{-3}	
R^2	0.997	

α	*2.893E+12*	m kg^{-1}
R$_m$	*9.936E+10*	m^{-1}

Volume @1800s	*883* ml	
Vol. per unit area	1.42E-01 m^{3}m^{-2}	

Mass of *wet* cake	*4.80* g	
Mass of *dry* cake	*3.50* g	
Mass of liquid	1.30 g	
Volume of solid	0.82 cm^3	
Volume of liquid	1.30 cm^3	
Cake conc^n	72.92% (Mass)	
Cake conc^n	38.73% (Volume)	
ε	*0.613*	
Moisture ratio, m	1.371	
Effective c	4.21 kg m^{-3}	
Slurry c	4.20 kg m^{-3}	

AC250PH8		
	Filtrate	**Solid**
Weight	*4995.7*	*21.1* g
Density, ρ	*1000*	*4260* kg m^{-3}
Volume	5.00E-03	4.95E-06 m^3
Total Mass	5.02 kg	
Total Volume	5.00E-03 m^3	
Solids conc^n	4.22 kg m^{-3}	
$\equiv$	0.10% v/v	
$\equiv$	0.42% w/w	
pH	8.00	
Applied field	0 V	
Separation	1.5 cm	
Field Strength	0 Vcm^{-1}	
Viscosity, μ	*0.001* Pa s	
Filter Area	6.22E-03 m^2	
Pressure drop	0.25 bar	
	25000 Pa	
Slope of plot	1.30E+10 sm^{-6}	
Intercept	8.19E+05 sm^{-3}	
R^2	0.993	

α	*5.936E+12*	m kg^{-1}
R_m	*1.274E+11*	m^{-1}

Volume @1800s	*334* ml	
Vol. per unit area	5.37E-02 m^{3}m^{-2}	

Mass of *wet* cake	*1.75* g	
Mass of *dry* cake	*1.29* g	
Mass of liquid	0.46 g	
Volume of solid	0.30 cm^3	
Volume of liquid	0.46 cm^3	
Cake conc^n	73.71% (Mass)	
Cake conc^n	39.70% (Volume)	
ε	*0.603*	
Moisture ratio, m	1.357	
Effective c	4.23 kg m^{-3}	
Slurry c	4.22 kg m^{-3}	

AC500PH8		
	Filtrate	**Solid**
Weight	*4995.6*	*21.2* g
Density, ρ	*1000*	*4260* kg m^{-3}
Volume	5.00E-03	4.98E-06 m^3
Total Mass	5.02 kg	
Total Volume	5.00E-03 m^3	
Solids conc^n	4.24 kg m^{-3}	
≡	0.10% v/v	
≡	0.42% w/w	
pH	8.00	
Applied field	0 V	
Separation	1.5 cm	
Field Strength	0 Vcm^{-1}	
Viscosity, μ	*0.001* Pa s	
Filter Area	6.22E-03 m^2	
Pressure drop	0.5 bar	
	50000 Pa	
Slope of plot	6.45E+09 sm^{-6}	
Intercept	3.00E+05 sm^{-3}	
R^2	0.991	

α	*5.878E+12*	m kg^{-1}
R$_m$	*9.325E+10*	m^{-1}

Volume @1800s	*506* ml	
Vol. per unit area	8.13E-02 m^{3}m^{-2}	

Mass of *wet* cake	*3.14* g	
Mass of *dry* cake	*2.08* g	
Mass of liquid	1.06 g	
Volume of solid	0.49 cm^3	
Volume of liquid	1.06 cm^3	
Cake conc^n	66.24% (Mass)	
Cake conc^n	31.54% (Volume)	
ε	*0.685*	
Moisture ratio, m	1.510	
Effective c	4.25 kg m^{-3}	
Slurry c	4.24 kg m^{-3}	

AC750PH8

	Filtrate	Solid	
Weight	*4995.0*	*21.0* g	
Density, ρ	*1000*	*4260* kg m^{-3}	
Volume	5.00E-03	4.93E-06 m^3	
Total Mass	5.02	kg	
Total Volume	5.00E-03	m^3	
Solids conc^n	4.20	kg m^{-3}	
$\equiv$	0.10%	v/v	
$\equiv$	0.42%	w/w	
pH	8.04		
Applied field	0	V	
Separation	.1.5	cm	
Field Strength	0	Vcm^{-1}	
Viscosity, μ	*0.001*	Pa s	
Filter Area	6.22E-03	m^2	
Pressure drop	0.75	bar	
	75000	Pa	
Slope of plot	3.87E+09	sm^{-6}	
Intercept	-7.14E+04	sm^{-3}	
R^2	0.998		

α	*5.35E+12*	m kg^{-1}
R_m	*-3.33E+10*	m^{-1}

Volume @1800s	*692*	ml
Vol. per unit area	1.11E-01	m^{3}m^{-2}

Mass of *wet* cake	*3.55*	g
Mass of *dry* cake	*2.54*	g
Mass of liquid	1.01	g
Volume of solid	0.60	cm^3
Volume of liquid	1.01	cm^3
Cake conc^n	71.55%	(Mass)
Cake conc^n	37.12%	(Volume)
ε	*0.629*	
Moisture ratio, m	1.398	
Effective c	4.21	kg m^{-3}
Slurry c	4.20	kg m^{-3}

AC750P82

	Filtrate	Solid	
Weight	4995.1	21.3	g
Density, ρ	1000	4260	kg m^{-3}
Volume	5.00E-03	5.00E-06	m^3
Total Mass		5.02	kg
Total Volume		5.00E-03	m^3
Solids conc^n		4.26	kg m^{-3}
$\equiv$		0.10%	v/v
$\equiv$		0.42%	w/w
pH		8.00	
Applied field		0	V
Separation		1.5	cm
Field Strength		0	Vcm^{-1}
Viscosity, μ		0.001	Pa s
Filter Area		6.22E-03	m^2
Pressure drop		0.75	bar
		75000	Pa
Slope of plot		8.66E+09	sm^{-6}
Intercept		6.68E+05	sm^{-3}
R^2		0.989	

α	1.18E+13	m kg^{-1}	
R_m	3.119E+11	m^{-1}	

Volume @1800s	425	ml
Vol. per unit area	6.83E-02	m^{3}m^{-2}

Mass of *wet* cake	1.33	g
Mass of *dry* cake	0.83	g
Mass of liquid	0.50	g
Volume of solid	0.19	cm^3
Volume of liquid	0.50	cm^3
Cake conc^n	62.41%	(Mass)
Cake conc^n	28.04%	(Volume)
ε	0.720	
Moisture ratio, m	1.602	
Effective c	4.28	kg m^{-3}
Slurry c	4.26	kg m^{-3}

	AC750		
	Filtrate	**Solid**	
Weight	*1998.5*	*8.5*	g
Density, ρ	*1000*	*4260*	kg m^{-3}
Volume	2.00E-03	2.00E-06	m^3
Total Mass	2.01	kg	
Total Volume	2.00E-03	m^3	
Solids conc^n	4.25	kg m^{-3}	
$\cong$	0.10%	v/v	
$\cong$	0.42%	w/w	
pH	8		
Applied field	0	V	
Separation	1.5	cm	
Field Strength	0	Vcm^{-1}	
Viscosity, μ	*0.001*	Pa s	
Filter Area	6.22E-03	m^2	
Pressure drop	0.75	bar	
	75000	Pa	
Slope of plot	6.66E+09	sm^{-6}	
Intercept	1.79E+06	sm^{-3}	
R^2	0.948		

α	*9.091E+12*	m kg^{-1}
R_m	*8.349E+11*	m^{-1}

Volume @1800s	*396*	ml
Vol. per unit area	6.37E-02	m^{3}m^{-2}

	AC750_2		
	Filtrate	**Solid**	
Weight	*1998.0*	*8.5*	g
Density, ρ	*1000*	*4260*	kg m^{-3}
Volume	2.00E-03	2.00E-06	m^3
Total Mass	2.01	kg	
Total Volume	2.00E-03	m^3	
Solids conc^n	4.26	kg m^{-3}	
$\equiv$	0.10%	v/v	
$\equiv$	0.42%	w/w	
pH	8		
Applied field	0	V	
Separation	1.5	cm	
Field Strength	0	Vcm^{-1}	
Viscosity, μ	*0.001*	Pa s	
Filter Area	6.22E-03	m^2	
Pressure drop	0.75	bar	
	75000	Pa	
Slope of plot	1.00E+10	sm^{-6}	
Intercept	6.93E+05	sm^{-3}	
R^2	0.991		

α	*1.366E+13*	m kg^{-1}
R_m	*3.232E+11*	m^{-1}

Volume @1800s	*391*	ml
Vol. per unit area	6.29E-02	m^{3}m^{-2}

AC750_3

	Filtrate	Solid	
Weight	*4999.1*	*22.3*	g
Density, ρ	*1000*	*4260*	kg m^{-3}
Volume	5.00E-03	5.23E-06	m^3
Total Mass	5.02		kg
Total Volume	5.00E-03		m^3
Solids conc^n	4.46		kg m^{-3}
$\equiv$	0.10%		v/v
$\equiv$	0.44%		w/w
pH	8		
Applied field	0		V
Separation	1.5		cm
Field Strength	0		Vcm^{-1}
Viscosity, μ	*0.001*		Pa s
Filter Area	6.22E-03		m^2
Pressure drop	0.75		bar
	75000		Pa
Slope of plot	4.27E+09		sm^{-6}
Intercept	3.74E+05		sm^{-3}
R^2	0.996		

α	*5.563E+12*	m kg^{-1}
R_m	*1.743E+11*	m^{-1}

Volume @1800s	*620*	ml
Vol. per unit area	9.97E-02	m^{3}m^{-2}

	AC750_4		
	Filtrate	**Solid**	
Weight	*1982.9*	*7.4*	g
Density, ρ	*1000*	*4260*	kg m^{-3}
Volume	1.98E-03	1.74E-06	m^3
Total Mass	1.99	kg	
Total Volume	1.98E-03	m^3	
Solids conc^n	3.75	kg m^{-3}	
≅	0.09%	v/v	
≅	0.37%	w/w	
pH	*8*		
Applied field	0	V	
Separation	1.5	cm	
Field Strength	0	Vcm^{-1}	
Viscosity, μ	*0.001*	Pa s	
Filter Area	6.22E-03	m^2	
Pressure drop	0.75	bar	
	75000	Pa	
Slope of plot	4.78E+09	sm^{-6}	
Intercept	2.43E+05	sm^{-3}	
R^2	0.995		

α	*7.413E+12*	m kg^{-1}
R_m	*1.136E+11*	m^{-1}

Volume @1560s	*577*	ml
Vol. per unit area	9.28E-02	m^{3}m^{-2}

AC750_5		
	Filtrate	**Solid**
Weight	*4999.1*	*22.3* g
Density, ρ	*1000*	*4260* kg m^{-3}
Volume	5.00E-03	5.23E-06 m^3
Total Mass	5.02 kg	
Total Volume	5.00E-03 m^3	
Solids conc^n	4.46 kg m^{-3}	
$\equiv$	0.10% v/v	
$\equiv$	0.44% w/w	
pH	8	
Applied field	0 V	
Separation	1.5 cm	
Field Strength	0 Vcm^{-1}	
Viscosity, μ	*0.001* Pa s	
Filter Area	6.22E-03 m^2	
Pressure drop	0.75 bar	
	75000 Pa	
Slope of plot	1.76E+09 sm^{-6}	
Intercept	5.85E+05 sm^{-3}	
R^2	0.738	

α	*2.299E+12*	m kg^{-1}
R$_m$	*2.73E+11*	m^{-1}

Volume @1800s	*1632* ml
Vol. per unit area	2.62E-01 m^{3}m^{-2}

	AC750P10		
	Filtrate	**Solid**	
Weight	*4995.4*	*21.6*	**g**
Density, ρ	*1000*	*4260*	**kg m^{-3}**
Volume	5.00E-03	5.07E-06	**m^3**
Total Mass	5.02		**kg**
Total Volume	5.00E-03		**m^3**
Solids conc^n	4.32		**kg m^{-3}**
≡	**0.10%**		**v/v**
≡	**0.43%**		**w/w**
pH	**9.99**		
Applied field	0		**V**
Separation	1.5		**cm**
Field Strength	**0**		**Vcm^{-1}**
Viscosity, μ	*0.001*		**Pa s**
Filter Area	6.22E-03		**m^2**
Pressure drop	**0.75**		**bar**
	75000		**Pa**
Slope of plot	**6.37E+09**		**sm^{-6}**
Intercept	**3.30E+05**		**sm^{-3}**
R^2	0.996		

α	*8.554E+12*	**m kg^{-1}**
R$_m$	*1.538E+11*	**m^{-1}**

Volume @1800s	*506*	**ml**
Vol. per unit area	8.13E-02	**m^{3}m^{-2}**

Mass of *wet* cake	*1.90*	**g**
Mass of *dry* cake	*1.28*	**g**
Mass of liquid	0.62	**g**
Volume of solid	0.30	**cm^3**
Volume of liquid	0.62	**cm^3**
Cake conc^n	67.37%	**(Mass)**
Cake conc^n	32.64%	**(Volume)**
ε	*0.674*	
Moisture ratio, m	1.484	
Effective c	4.33	**kg m^{-3}**
Slurry c	4.32	**kg m^{-3}**

	AC001	
	Filtrate	**Solid**
Weight	*4905.5*	*2.2* g
Density, ρ	*1000*	*4260* kg m^{-3}
Volume	4.91E-03	5.16E-07 m^3
Total Mass	4.91 kg	
Total Volume	4.91E-03 m^3	
Solids conc^n	0.45 kg m^{-3}	
$\equiv$	0.01% v/v	
$\equiv$	0.04% w/w	
Applied field	0 V	
Separation	1.5 cm	
Field Strength	0 Vcm^{-1}	
Viscosity, μ	*0.001* Pa s	
Filter Area	6.22E-03 m^2	
Pressure drop	0.75 bar	
	75000 Pa	
Slope of plot	2.56E+08 sm^{-6}	
Intercept	8.93E+04 sm^{-3}	
R^2	0.977	

α	*3.32E+12*	m kg^{-1}
R_m	*4.164E+10*	m^{-1}

Volume @1800s	*2655*	ml
Vol. per unit area	4.27E-01	m^{3}m^{-2}

	AC05		
	Filtrate	Solid	
Weight	495.0	10.7	g
Density, ρ	1000	4260	kg m^{-3}
Volume	4.95E-04	2.50E-06	m^3
Total Mass	0.51	kg	
Total Volume	4.98E-04	m^3	
Solids conc^n	21.52	kg m^{-3}	
$\equiv$	0.50%	v/v	
$\equiv$	2.11%	w/w	
Applied field	0	V	
Separation	1.5	cm	
Field Strength	0	Vcm^{-1}	
Viscosity, μ	0.001	Pa s	
Filter Area	6.22E-03	m^2	
Pressure drop	0.75	bar	
	75000	Pa	
Slope of plot	3.62E+10	sm^{-6}	
Intercept	5.44E+05	sm^{-3}	
R^2	0.976		

α	9.768E+12	m kg^{-1}
R_m	2.539E+11	m^{-1}

Volume @1800s	224	ml
Vol. per unit area	3.60E-02	m^{3}m^{-2}

	AC05_2		
	Filtrate	**Solid**	
Weight	*1990.0*	*42.6*	g
Density, ρ	*1000*	*4260*	kg m^{-3}
Volume	1.99E-03	1.00E-05	m^3
Total Mass	2.03		kg
Total Volume	2.00E-03		m^3
Solids conc^{n}	21.41		kg m^{-3}
$\equiv$	0.50%		v/v
$\equiv$	2.10%		w/w
Applied field	0		V
Separation	1.5		cm
Field Strength	0		Vcm^{-1}
Viscosity, μ	*0.001*		Pa s
Filter Area	6.22E-03		m^2
Pressure drop	0.75		bar
	75000		Pa
Slope of plot	1.81E+11		sm^{-6}
Intercept	1.24E+07		sm^{-3}
R^2	0.929		

α	*4.912E+13*	m kg^{-1}	
R$_m$	*5.797E+12*	m^{-1}	

Volume @1800s	72	ml
Vol. per unit area	1.15E-02	m^{3}m^{-2}

	ACI		
	Filtrate	**Solid**	
Weight	*1980.0*	*85.2*	g
Density, ρ	*1000*	*4260*	kg m^{-3}
Volume	1.98E-03	2.00E-05	m^3
Total Mass	2.07	kg	
Total Volume	2.00E-03	m^3	
Solids conc^n	43.03	kg m^{-3}	
$\equiv$	1.00%	v/v	
$\equiv$	4.13%	w/w	
Applied field	0	V	
Separation	1.5	cm	
Field Strength	0	Vcm^{-1}	
Viscosity, μ	*0.001*	Pa s	
Filter Area	6.22E-03	m^2	
Pressure drop	0.75	bar	
	75000	Pa	
Slope of plot	4.95E+10	sm^{-6}	
Intercept	1.37E+07	sm^{-3}	
R^2	0.841		

α	*6.674E+12*	m kg^{-1}
R_m	*6.402E+12*	m^{-1}

Volume @1800s	*95*	ml
Vol. per unit area	1.53E-02	m^{3}m^{-2}

	AC5		
	Filtrate	Solid	
Weight	*1900.0*	*426.0*	g
Density, ρ	*1000*	*4260*	kg m^{-3}
Volume	1.90E-03	1.00E-04	m^3
Total Mass	2.33	kg	
Total Volume	2.00E-03	m^3	
Solids conc^n	224.21	kg m^{-3}	
$\equiv$	5.00%	v/v	
$\equiv$	18.31%	w/w	
Applied field	0	V	
Separation	1.5	cm	
Field Strength	0	Vcm^{-1}	
Viscosity, μ	*0.001*	Pa s	
Filter Area	6.22E-03	m^2	
Pressure drop	0.75	bar	
	75000	Pa	
Slope of plot	-	sm^{-6}	
Intercept	-	sm^{-3}	
R^2	-		

α	#*VALUE!*	m kg^{-1}
R_m	#*VALUE!*	m^{-1}

Volume @ 900s	*10*	ml
Vol. per unit area	1.53E-03	m^{3}m^{-2}

ACSP01_1

	Filtrate	Solid	
Weight	*2955.4*	*12.2*	g
Density, ρ	*1000*	*4260*	kg m^{-3}
Volume	2.96E-03	2.86E-06	m^{3}
Total Mass	2.97		kg
Total Volume	2.96E-03		m^{3}
Solids conc^{n}	4.13		kg m^{-3}
$\equiv$	0.10%		v/v
$\equiv$	0.41%		w/w
pH	8		
Applied field	0		V
Separation	1.5		cm
Field Strength	0		Vcm^{-1}
Viscosity, μ	*0.001*		Pa s
Filter Area	6.22E-03		m^{2}
Pressure drop	0.75		bar
	75000		Pa
Slope of plot	5.68E+09		sm^{-6}
Intercept	2.53E+05		sm^{-3}
R^{2}	0.984		

α	*7.983E+12*	m kg^{-1}
R_m	*1.18E+11*	m^{-1}

Volume @1800s	*554*	ml
Vol. per unit area	8.90E-02	m^{3}m^{-2}

Mass of *wet* cake	*6.60*	g
Mass of *dry* cake	*4.57*	g
Mass of liquid	2.03	g
Volume of solid	1.07	cm^{3}
Volume of liquid	2.03	cm^{3}
Cake conc^{n}	69.24%	(Mass)
Cake conc^{n}	34.57%	(Volume)
ε	*0.654*	
Moisture ratio, m	1.444	
Effective c	4.14	kg m^{-3}
Slurry c	4.13	kg m^{-3}

ACSP01_2

	Filtrate	Solid	
Weight	*2957.7*	*12.7*	g
Density, ρ	*1000*	*4260*	kg m^{-3}
Volume	2.96E-03	2.98E-06	m^3
Total Mass	2.97		kg
Total Volume	2.96E-03		m^3
Solids conc^n	4.30		kg m^{-3}
$\equiv$	0.10%		v/v
$\equiv$	0.43%		w/w
pH	8		
Applied field	0		V
Separation	1.5		cm
Field Strength	0		Vcm^{-1}
Viscosity, μ	*0.001*		Pa s
Filter Area	6.22E-03		m^2
Pressure drop	0.75		bar
	75000		Pa
Slope of plot	2.30E+09		sm^{-6}
Intercept	2.46E+05		sm^{-3}
R^2	0.997		

α	*3.113E+12* m kg^{-1}
R_m	*1.149E+11* m^{-1}

Volume @1800s	*830*	ml
Vol. per unit area	1.33E-01	m^{3}m^{-2}

Mass of *wet* cake	*5.10*	g
Mass of *dry* cake	*3.50*	g
Mass of liquid	1.60	g
Volume of solid	0.82	cm^3
Volume of liquid	1.60	cm^3
Cake conc^n	68.63%	(Mass)
Cake conc^n	33.93%	(Volume)
ε	*0.661*	
Moisture ratio, m	1.457	
Effective c	4.31	kg m^{-3}
Slurry c	4.30	kg m^{-3}

EFP4V20		
	Filtrate	Solid
Weight	*4994.9*	*20.6* g
Density, ρ	*1000*	*4260* kg m^{-3}
Volume	4.99E-03	4.84E-06 m^3
Total Mass	5.02 kg	
Total Volume	5.00E-03 m^3	
Solids conc^n	4.13 kg m^{-3}	
$\equiv$	0.10% v/v	
$\equiv$	0.41% w/w	
pH	4.03	
Applied field	30 V	
Separation	1.5 cm	
Field Strength	20 Vcm^{-1}	
Viscosity, μ	*0.001* Pa s	
Filter Area	6.22E-03 m^2	
Pressure drop	0.75 bar	
	75000 Pa	
Slope of plot	1.21E+09 sm^{-6}	
Intercept	8.19E+04 sm^{-3}	
R^2	0.990	

α	*1.697E+12*	m kg^{-1}
R_m	*3.82E+10*	m^{-1}

Volume @1800s	*1222*	ml
Vol. per unit area	1.96E-01	m^{3}m^{-2}

Mass of *wet* cake	*14.86*	g
Mass of *dry* cake	8.97	g
Mass of liquid	5.89	g
Volume of solid	2.11	cm^3
Volume of liquid	5.89	cm^3
Cake conc^n	60.36%	(Mass)
Cake conc^n	26.33%	(Volume)
ε	*0.737*	
Moisture ratio, m	1.657	
Effective c	4.14	kg m^{-3}
Slurry c	4.13	kg m^{-3}

EFP4V50

	Filtrate	Solid	
Weight	*4995.5*	*21.1*	g
Density, ρ	*1000*	*4260*	kg m^{-3}
Volume	5.00E-03	4.95E-06	m^3
Total Mass		5.02	kg
Total Volume		5.00E-03	m^3
Solids conc^n		4.22	kg m^{-3}
$\equiv$		0.10%	v/v
$\equiv$		0.42%	w/w
pH		4.07	
Applied field		75	V
Separation		1.5	cm
Field Strength		50	Vcm^{-1}
Viscosity, μ		*0.001*	Pa s
Filter Area		6.22E-03	m^2
Pressure drop		0.75	bar
		75000	Pa
Slope of plot		3.57E+08	sm^{-6}
Intercept		2.22E+05	sm^{-3}
R^2		0.997	

α	*4.909E+11*	m kg^{-1}
R$_m$	*1.034E+11*	m^{-1}

Volume @1800s	*1957*	ml
Vol. per unit area	3.15E-01	m^{3}m^{-2}

Mass of *wet* cake	*22.70*	g
Mass of *dry* cake	*12.57*	g
Mass of liquid	10.13	g
Volume of solid	2.95	cm^3
Volume of liquid	10.13	cm^3
Cake conc^n	55.37%	(Mass)
Cake conc^n	22.56%	(Volume)
ε	*0.774*	
Moisture ratio, m	1.806	
Effective c	4.24	kg m^{-3}
Slurry c	4.22	kg m^{-3}

EFP6V20		
	Filtrate	**Solid**
Weight	*4995.0*	*20.9* g
Density, ρ	*1000*	*4260* kg m^{-3}
Volume	5.00E-03	4.90E-06 m^3
Total Mass	5.02 kg	
Total Volume	5.00E-03 m^3	
Solids conc^n	4.18 kg m^{-3}	
≡	0.10% v/v	
≡	0.42% w/w	
pH	6.00	
Applied field	30 V	
Separation	1.5 cm	
Field Strength	20 Vcm^{-1}	
Viscosity, μ	*0.001* Pa s	
Filter Area	6.22E-03 m^2	
Pressure drop	0.75 bar	
	75000 Pa	
Slope of plot	5.94E+08 sm^{-6}	
Intercept	6.41E+05 sm^{-3}	
R^2	0.992	

α	*8.259E+11*	m kg^{-1}
R$_m$	*2.992E+11*	m^{-1}

Volume @1800s	*1279* ml	
Vol. per unit area	2.06E-01 m^{3}m^{-2}	

Mass of *wet* cake	*13.78* g	
Mass of *dry* cake	*6.73* g	
Mass of liquid	7.05 g	
Volume of solid	1.58 cm^3	
Volume of liquid	7.05 cm^3	
Cake conc^n	48.84% (Mass)	
Cake conc^n	18.31% (Volume)	
ε	*0.817*	
Moisture ratio, m	2.048	
Effective c	4.20 kg m^{-3}	
Slurry c	4.18 kg m^{-3}	

EFP6V50		
	Filtrate	*Solid*
Weight	*4996.6*	*20.6* g
Density, ρ	*1000*	*4260* kg m^{-3}
Volume	5.00E-03	4.84E-06 m^3
Total Mass	5.02 kg	
Total Volume	5.00E-03 m^3	
Solids conc^n	4.12 kg m^{-3}	
$\equiv$	0.10% v/v	
$\equiv$	0.41% w/w	
pH	6.06	
Applied field	75 V	
Separation	1.5 cm	
Field Strength	50 Vcm^{-1}	
Viscosity, μ	*0.001* Pa s	
Filter Area	6.22E-03 m^2	
Pressure drop	0.75 bar	
	75000 Pa	
Slope of plot	2.87E+08 sm^{-6}	
Intercept	4.46E+05 sm^{-3}	
R^2	0.994	

α	*4.044E+11*	m kg^{-1}
R$_m$	*2.079E+11*	m^{-1}

Volume @1800s	*1842*	ml
Vol. per unit area	2.96E-01	m^{3}m^{-2}

Mass of *wet* cake	*18.42*	g
Mass of *dry* cake	*9.16*	g
Mass of liquid	9.26	g
Volume of solid	2.15	cm^3
Volume of liquid	9.26	cm^3
Cake conc^n	49.73%	(Mass)
Cake conc^n	18.84%	(Volume)
ε	*0.812*	
Moisture ratio, m	2.011	
Effective c	4.14	kg m^{-3}
Slurry c	4.12	kg m^{-3}

	EFP8V20	
	Filtrate	**Solid**
Weight	*4995.2*	*21.0* g
Density, ρ	*1000*	*4260* kg m^{-3}
Volume	5.00E-03	4.92E-06 m^3
Total Mass	5.02 kg	
Total Volume	5.00E-03 m^3	
Solids conc^n	4.19 kg m^{-3}	
$\cong$	0.10% v/v	
$\cong$	0.42% w/w	
pH	8.03	
Applied field	30 V	
Separation	1.5 cm	
Field Strength	20 Vcm^{-1}	
Viscosity, μ	*0.001* Pa s	
Filter Area	6.22E-03 m^2	
Pressure drop	0.75 bar	
	75000 Pa	
Slope of plot	1.67E+09 sm^{-6}	
Intercept	6.01E+05 sm^{-3}	
R^2	0.956	

α	*2.313E+12*	m kg^{-1}
R$_m$	*2.805E+11*	m^{-1}

Volume @1800s	*912* ml
Vol. per unit area	1.47E-01 m^{3}m^{-2}

Mass of *wet* cake	*4.90* g
Mass of *dry* cake	*3.24* g
Mass of liquid	1.66 g
Volume of solid	0.76 cm^3
Volume of liquid	1.66 cm^3
Cake conc^n	66.12% (Mass)
Cake conc^n	31.42% (Volume)
ε	*0.686*
Moisture ratio, m	1.512
Effective c	4.20 kg m^{-3}
Slurry c	4.19 kg m^{-3}

EFP8V50

	Filtrate	Solid
Weight	*4995.0*	*21.3* g
Density, ρ	*1000*	*4260* kg m^{-3}
Volume	5.00E-03	4.99E-06 m^3
Total Mass	5.02 kg	
Total Volume	5.00E-03 m^3	
Solids conc^n	4.26 kg m^{-3}	
$\equiv$	0.10% v/v	
$\equiv$	0.42% w/w	
pH	8.00	
Applied field	75 V	
Separation	1.5 cm	
Field Strength	50 Vcm^{-1}	
Viscosity, μ	*0.001* Pa s	
Filter Area	6.22E-03 m^2	
Pressure drop	0.75 bar	
	75000 Pa	
Slope of plot	2.17E+08 sm^{-6}	
Intercept	3.83E+05 sm^{-3}	
R^2	0.997	

α	*2.964E+11* m kg^{-1}
R_m	*1.785E+11* m^{-1}

Volume @1800s	*2109* ml	
Vol. per unit area	3.39E-01 m^{3}m^{-2}	

Mass of *wet* cake	*17.06* g	
Mass of *dry* cake	*9.72* g	
Mass of liquid	7.34 g	
Volume of solid	2.28 cm^3	
Volume of liquid	7.34 cm^3	
Cake conc^n	56.98% (Mass)	
Cake conc^n	23.72% (Volume)	
ε	*0.763*	
Moisture ratio, m	1.755	
Effective c	4.27 kg m^{-3}	
Slurry c	4.26 kg m^{-3}	

EFP10V20		
	Filtrate	Solid
Weight	*4994.9*	*20.6* g
Density, ρ	*1000*	*4260* kg m^{-3}
Volume	4.99E-03	4.84E-06 m^3
Total Mass	5.02 kg	
Total Volume	5.00E-03 m^3	
Solids conc^n	4.13 kg m^{-3}	
$\equiv$	0.10% v/v	
$\equiv$	0.41% w/w	
pH	10.00	
Applied field	30 V	
Separation	1.5 cm	
Field Strength	20 Vcm^{-1}	
Viscosity, μ	*0.001* Pa s	
Filter Area	6.22E-03 m^2	
Pressure drop	0.75 bar	
	75000 Pa	
Slope of plot	5.06E+08 sm^{-6}	
Intercept	6.50E+05 sm^{-3}	
R^2	0.970	

α	*7.116E+11*	m kg^{-1}
R_m	*3.034E+11*	m^{-1}

Volume @1800s	*1370* ml
Vol. per unit area	2.20E-01 m^{3}m^{-2}

Mass of *wet* cake	7.08 g
Mass of *dry* cake	4.75 g
Mass of liquid	2.33 g
Volume of solid	1.12 cm^3
Volume of liquid	2.33 cm^3
Cake conc^n	67.09% (Mass)
Cake conc^n	32.37% (Volume)
ε	*0.676*
Moisture ratio, m	1.491
Effective c	4.14 kg m^{-3}
Slurry c	4.13 kg m^{-3}

EFP10V50		
	Filtrate	**Solid**
Weight	*4995.0*	*21.2* g
Density, ρ	*1000*	*4260* kg m^{-3}
Volume	5.00E-03	4.97E-06 m^3
Total Mass	5.02 kg	
Total Volume	5.00E-03 m^3	
Solids conc^n	4.24 kg m^{-3}	
$\cong$	0.10% v/v	
$\cong$	0.42% w/w	
pH	10.00	
Applied field	75 V	
Separation	1.5 cm	
Field Strength	50 Vcm^{-1}	
Viscosity, μ	*0.001* Pa s	
Filter Area	6.22E-03 m^2	
Pressure drop	0.75 bar	
	75000 Pa	
Slope of plot	9.40E+07 sm^{-6}	
Intercept	4.94E+05 sm^{-3}	
R^2	0.994	

α	*1.287E+11* m kg^{-1}
R_m	*2.304E+11* m^{-1}

Volume @1800s	*2479* ml	
Vol. per unit area	3.98E-01 m^{3}m^{-2}	

Mass of *wet* cake	*17.14* g	
Mass of *dry* cake	*10.23* g	
Mass of liquid	6.91 g	
Volume of solid	2.40 cm^3	
Volume of liquid	6.91 cm^3	
Cake conc^n	59.69% (Mass)	
Cake conc^n	25.79% (Volume)	
ε	*0.742*	
Moisture ratio, m	1.675	
Effective c	4.25 kg m^{-3}	
Slurry c	4.24 kg m^{-3}	

EF250PH8

	Filtrate	Solid	
Weight	*4995.3*	*21.1*	g
Density, ρ	*1000*	*4260*	kg m^{-3}
Volume	5.00E-03	4.95E-06	m^3
Total Mass	5.02		kg
Total Volume	5.00E-03		m^3
Solids conc^n	4.22		kg m^{-3}
$\equiv$	0.10%		v/v
$\equiv$	0.42%		w/w
pH	8.00		
Applied field	75		V
Separation	1.5		cm
Field Strength	50		Vcm^{-1}
Viscosity, μ	*0.001*		Pa s
Filter Area	6.22E-03		m^2
Pressure drop	0.25		bar
	25000		Pa
Slope of plot	2.01E+08		sm^{-6}
Intercept	4.75E+05		sm^{-3}
R^2	0.959		

α	*9.221E+10*	m kg^{-1}
R_m	*7.38E+10*	m^{-1}

Volume @1800s	*1990*	ml
Vol. per unit area	3.20E-01	m^{3}m^{-2}

Mass of *wet* cake	*10.89*	g
Mass of *dry* cake	*5.75*	g
Mass of liquid	5.14	g
Volume of solid	1.35	cm^3
Volume of liquid	5.14	cm^3
Cake conc^n	52.80%	(Mass)
Cake conc^n	20.80%	(Volume)
ε	*0.792*	
Moisture ratio, m	1.894	
Effective c	4.24	kg m^{-3}
Slurry c	4.22	kg m^{-3}

EF500PH8

	Filtrate	Solid
Weight	4995.2	21.2 g
Density, ρ	1000	4260 kg m^{-3}
Volume	5.00E-03	4.98E-06 m^3
Total Mass	5.02 kg	
Total Volume	5.00E-03 m^3	
Solids conc^n	4.24 kg m^{-3}	
$\equiv$	0.10% v/v	
$\equiv$	0.42% w/w	
pH	8.03	
Applied field	75 V	
Separation	1.5 cm	
Field Strength	50 Vcm^{-1}	
Viscosity, μ	0.001 Pa s	
Filter Area	6.22E-03 m^2	
Pressure drop	0.5 bar	
	50000 Pa	
Slope of plot	2.52E+08 sm^{-6}	
Intercept	3.90E+05 sm^{-3}	
R^2	0.998	

α	2.298E+11	m kg^{-1}
R_m	1.214E+11	m^{-1}

Volume @1800s	2014	ml
Vol. per unit area	3.24E-01	m^{3}m^{-2}

Mass of *wet* cake	11.68	g
Mass of *dry* cake	6.42	g
Mass of liquid	5.25	g
Volume of solid	1.51	cm^3
Volume of liquid	5.25	cm^3
Cake conc^n	54.99%	(Mass)
Cake conc^n	22.29%	(Volume)
ε	0.777	
Moisture ratio, m	1.818	
Effective c	4.26	kg m^{-3}
Slurry c	4.24	kg m^{-3}

EF500850		
	Filtrate	Solid
Weight	*4995.2*	*21.2* g
Density, ρ	*1000*	*4260* kg m^{-3}
Volume	5.00E-03	4.98E-06 m^3
Total Mass	5.02 kg	
Total Volume	5.00E-03 m^3	
Solids conc^n	4.24 kg m^{-3}	
$\equiv$	0.10% v/v	
$\equiv$	0.42% w/w	
pH	8.03	
Applied field	75 V	
Separation	1.5 cm	
Field Strength	50 Vcm^{-1}	
Viscosity, μ	*0.001* Pa s	
Filter Area	6.22E-03 m^2	
Pressure drop	0.5 bar	
	50000 Pa	
Slope of plot	2.50E+08 sm^{-6}	
Intercept	3.93E+05 sm^{-3}	
R^2	0.997	

α	*2.279E+11*	m kg^{-1}
R_m	*1.223E+11*	m^{-1}

Volume @1800s	*2014* ml
Vol. per unit area	3.24E-01 m^{3}m^{-2}

Mass of *wet* cake	*11.68* g
Mass of *dry* cake	*6.42* g
Mass of liquid	5.25 g
Volume of solid	1.51 cm^3
Volume of liquid	5.25 cm^3
Cake conc^n	54.99% (Mass)
Cake conc^n	22.29% (Volume)
ε	*0.777*
Moisture ratio, m	1.818
Effective c	4.26 kg m^{-3}
Slurry c	4.24 kg m^{-3}

EF750V20

	Filtrate	Solid	
Weight	*4879.4*	*19.9*	g
Density, ρ	*1000*	*4260*	kg m^{-3}
Volume	4.88E-03	4.67E-06	m^3
Total Mass		4.90	kg
Total Volume		4.88E-03	m^3
Solids conc^n		4.08	kg m^{-3}
$\cong$		0.10%	v/v
$\cong$		0.41%	w/w
pH		8	
Applied field		30	V
Separation		1.5	cm
Field Strength		20	Vcm^{-1}
Viscosity, μ		*0.001*	Pa s
Filter Area		6.22E-03	m^2
Pressure drop		0.75	bar
		75000	Pa
Slope of plot		7.33E+08	sm^{-6}
Intercept		7.84E+05	sm^{-3}
R^2		0.995	

α	*1.044E+12*	m kg^{-1}
R$_m$	*3.658E+11*	m^{-1}

Volume @1800s	*1131*	ml
Vol. per unit area	1.82E-01	m^{3}m^{-2}

EF750V20_2

	Filtrate	Solid	
Weight	*3996.0*	*17.0*	g
Density, ρ	*1000*	*4260*	kg m^{-3}
Volume	4.00E-03	4.00E-06	m^3
Total Mass	4.01		kg
Total Volume	4.00E-03		m^3
Solids conc^n	4.26		kg m^{-3}
$\equiv$	0.10%		v/v
$\equiv$	0.42%		w/w
pH	8		
Applied field	30		V
Separation	1.5		cm
Field Strength	20		Vcm^{-1}
Viscosity, μ	*0.001*		Pa s
Filter Area	6.22E-03		m^2
Pressure drop	0.75		bar
	75000		Pa
Slope of plot	8.31E+08		sm^{-6}
Intercept	8.24E+05		sm^{-3}
R^2	0.986		

α	*1.131E+12*	m kg^{-1}
R_m	*3.846E+11*	m^{-1}

Volume @1800s	*1060*	ml
Vol. per unit area	1.70E-01	m^{3}m^{-2}

EF750V30		
	Filtrate	**Solid**
Weight	*4882.8*	*25.6* g
Density, ρ	*1000*	*4260* kg m^{-3}
Volume	4.88E-03	6.01E-06 m^3
Total Mass	4.91 kg	
Total Volume	4.89E-03 m^3	
Solids conc^n	5.24 kg m^{-3}	
$\equiv$	**0.12%** v/v	
$\equiv$	**0.52%** w/w	
pH	8	
Applied field	45 V	
Separation	1.5 cm	
Field Strength	30 Vcm^{-1}	
Viscosity, μ	*0.001* Pa s	
Filter Area	6.22E-03 m^2	
Pressure drop	0.75 bar	
	75000 Pa	
Slope of plot	6.06E+08 sm^{-6}	
Intercept	3.42E+05 sm^{-3}	
R^2	0.986	

α	*6.711E+11*	m kg^{-1}
R_m	*1.595E+11*	m^{-1}

Volume @1800s	*1499*	ml
Vol. per unit area	2.41E-01	m^{3}m^{-2}

EF750V33

	Filtrate	Solid	
Weight	*2985.0*	*12.8*	g
Density, ρ	*1000*	*4260*	kg m^{-3}
Volume	2.99E-03	3.00E-06	m^3
Total Mass	3.00		kg
Total Volume	2.99E-03		m^3
Solids conc^n	4.28		kg m^{-3}
$\equiv$	0.10%		v/v
$\equiv$	0.43%		w/w
pH	8		
Applied field	50		V
Separation	1.5		cm
Field Strength	33.3		Vcm^{-1}
Viscosity, μ	*0.001*		Pa s
Filter Area	6.22E-03		m^2
Pressure drop	0.75		bar
	75000		Pa
Slope of plot	6.39E+08		sm^{-6}
Intercept	4.80E+05		sm^{-3}
R^2	0.988		

α	*8.661E+11*	m kg^{-1}
R_m	*2.239E+11*	m^{-1}

Volume @1800s	*1375*	ml
Vol. per unit area	2.21E-01	m^{3}m^{-2}

EF750V46		
	Filtrate	Solid
Weight	2987.4	12.4 g
Density, ρ	1000	4260 kg m^{-3}
Volume	2.99E-03	2.92E-06 m^3
Total Mass	3.00 kg	
Total Volume	2.99E-03 m^3	
Solids conc^n	4.16 kg m^{-3}	
$\equiv$	0.10% v/v	
$\equiv$	0.41% w/w	
pH	7.70	
Applied field	70 V	
Separation	1.5 cm	
Field Strength	46.7 Vcm^{-1}	
Viscosity, μ	0.001 Pa s	
Filter Area	6.22E-03 m^2	
Pressure drop	0.75 bar	
	75000 Pa	
Slope of plot	2.97E+08 sm^{-6}	
Intercept	3.25E+05 sm^{-3}	
R^2	0.978	

α	4.147E+11	m kg^{-1}
R_m	1.516E+11	m^{-1}

Volume @1800s	2033	ml
Vol. per unit area	3.27E-01	m^{3}m^{-2}

EFP8V60		
	Filtrate	Solid
Weight	*4995.1*	*21.3* g
Density, ρ	*1000*	*4260* kg m^{-3}
Volume	5.00E-03	5.00E-06 m^3
Total Mass	5.02 kg	
Total Volume	5.00E-03 m^3	
Solids conc^n	4.26 kg m^{-3}	
$\equiv$	0.10% v/v	
$\equiv$	0.42% w/w	
pH	8.02	
Applied field	90 V	
Separation	1.5 cm	
Field Strength	60 Vcm^{-1}	
Viscosity, μ	*0.001* Pa s	
Filter Area	6.22E-03 m^2	
Pressure drop	0.75 bar	
	75000 Pa	
Slope of plot	1.27E+08 sm^{-6}	
Intercept	3.77E+05 sm^{-3}	
R^2	0.997	

α	*1.733E+11*	m kg^{-1}
R$_m$	*1.757E+11*	m^{-1}

Volume @1800s	*2559* ml
Vol. per unit area	4.11E-01 m^{3}m^{-2}

Mass of *wet* cake	*9.36* g
Mass of *dry* cake	*5.71* g
Mass of liquid	3.65 g
Volume of solid	1.34 cm^3
Volume of liquid	3.65 cm^3
Cake conc^n	61.00% (Mass)
Cake conc^n	26.86% (Volume)
ε	*0.731*
Moisture ratio, m	1.639
Effective c	4.28 kg m^{-3}
Slurry c	4.26 kg m^{-3}

EAPH3V20

	Filtrate	Solid	
Weight	*4996.0*	*21.3*	g
Density, ρ	*1000*	*4260*	kg m^{-3}
Volume	5.00E-03	5.00E-06	m^3
Total Mass	5.02		kg
Total Volume	5.00E-03		m^3
Solids conc^n	4.26		kg m^{-3}
$\equiv$	0.10%		v/v
$\equiv$	0.42%		w/w
pH	3.10		
Applied field	30		V
Separation	1.5		cm
Field Strength	20		Vcm^{-1}
Viscosity, μ	*0.001*		Pa s
Filter Area	6.22E-03		m^2
Pressure drop	0.75		bar
	75000		Pa
Slope of plot	7.56E+08		sm^{-6}
Intercept	1.17E+05		sm^{-3}
R^2	0.993		

α	*1.029E+12*	m kg^{-1}
R$_m$	*5.462E+10*	m^{-1}

Volume @1800s	*1470*	ml
Vol. per unit area	2.36E-01	m^{3}m^{-2}

Mass of *wet* cake	*3.47*	g
Mass of *dry* cake	*2.67*	g
Mass of liquid	0.80	g
Volume of solid	0.63	cm^3
Volume of liquid	0.80	cm^3
Cake conc^n	76.95%	(Mass)
Cake conc^n	43.93%	(Volume)
ε	*0.561*	
Moisture ratio, m	1.300	
Effective c	4.27	kg m^{-3}
Slurry c	4.26	kg m^{-3}

EApH4V20		
	Filtrate	**Solid**
Weight	*5000.3*	*21.3* g
Density, ρ	*1000*	*4260* kg m^{-3}
Volume	5.00E-03	5.00E-06 m^{3}
Total Mass	5.02 kg	
Total Volume	5.01E-03 m^{3}	
Solids conc^{n}	4.26 kg m^{-3}	
$\equiv$	0.10% v/v	
$\equiv$	0.42% w/w	
pH	4.00	
Applied field	30 V	
Separation	1.5 cm	
Field Strength	20 Vcm^{-1}	
Viscosity, μ	*0.001* Pa s	
Filter Area	6.22E-03 m^{2}	
Pressure drop	0.75 bar	
	75000 Pa	
Slope of plot	1.58E+09 sm^{-6}	
Intercept	-8.85E+03 sm^{-3}	
R^{2}	0.995	

α	*2.161E+12*	m kg^{-1}
R$_{m}$	*-4.13E+09*	m^{-1}

Volume @1800s	*1098* ml	
Vol. per unit area	1.76E-01 m^{3}m^{-2}	

Mass of *wet* cake	*11.80* g	
Mass of *dry* cake	7.70 g	
Mass of liquid	4.10 g	
Volume of solid	1.81 cm^{3}	
Volume of liquid	4.10 cm^{3}	
Cake conc^{n}	65.25% (Mass)	
Cake conc^{n}	30.60% (Volume)	
ε	*0.694*	
Moisture ratio, m	1.532	

Effective c	4.27 kg m^{-3}	
Slurry c	4.26 kg m^{-3}	

EApH4V50#2

	Filtrate	Solid	
Weight	*9989.9*	*42.2*	g
Density, ρ	*1000*	*4260*	kg m^{-3}
Volume	9.99E-03	9.91E-06	m^3
Total Mass	10.03		kg
Total Volume	1.00E-02		m^3
Solids conc^n	4.22		kg m^{-3}
$\equiv$	0.10%		v/v
$\equiv$	0.42%		w/w
pH	4.01		
Applied field	75		V
Separation	1.5		cm
Field Strength	50		Vcm^{-1}
Viscosity, μ	*0.001*		Pa s
Filter Area	6.22E-03		m^2
Pressure drop	0.75		bar
	75000		Pa
Slope of plot	2.23E+08		sm^{-6}
Intercept	2.39E+05		sm^{-3}
R^2	0.998		

α	*3.063E+11*	m kg^{-1}
R_m	*1.113E+11*	m^{-1}

Volume @1800s	*2344*	ml
Vol. per unit area	3.77E-01	m^{3}m^{-2}

Mass of *wet* cake	*15.50*	g
Mass of *dry* cake	*9.89*	g
Mass of liquid	5.61	g
Volume of solid	2.32	cm^3
Volume of liquid	5.61	cm^3
Cake conc^n	63.81%	(Mass)
Cake conc^n	29.27%	(Volume)
ε	*0.707*	
Moisture ratio, m	1.567	
Effective c	4.23	kg m^{-3}
Slurry c	4.22	kg m^{-3}

EApH6V20		
	Filtrate	**Solid**
Weight	*4995.0*	*21.2* g
Density, ρ	*1000*	*4260* kg m^{-3}
Volume	4.99E-03	4.96E-06 m^3
Total Mass	5.02 kg	
Total Volume	5.00E-03 m^3	
Solids conc^n	4.23 kg m^{-3}	
$\equiv$	0.10% v/v	
$\equiv$	0.42% w/w	
pH	5.99	
Applied field	30	
Separation	1.5 cm	
Field Strength	20 Vcm^{-1}	
Viscosity, μ	*0.001* Pa s	
Filter Area	6.22E-03 m^2	
Pressure drop	0.75 bar	
	75000 Pa	
Slope of plot	4.60E+08 sm^{-6}	
Intercept	7.25E+05 sm^{-3}	
R^2	0.983	

α	*6.311E+11* m kg^{-1}
R$_m$	*3.381E+11* m^{-1}

Volume @1800s	*1346* ml
Vol. per unit area	2.16E-01 m^{3}m^{-2}

Mass of *wet* cake	*14.30* g	
Mass of *dry* cake	7.86 g	
Mass of liquid	6.44 g	
Volume of solid	1.85 cm^3	
Volume of liquid	6.44 cm^3	
Cake conc^n	54.97%	(Mass)
Cake conc^n	22.27%	(Volume)
ε	*0.777*	
Moisture ratio, m	1.819	
Effective c	4.25 kg m^{-3}	
Slurry c	4.23 kg m^{-3}	

EApH6V50		
	Filtrate	**Solid**
Weight	*4995.2*	*20.8* g
Density, ρ	*1000*	*4260* kg m^{-3}
Volume	5.00E-03	4.88E-06 m^3
Total Mass	5.02 kg	
Total Volume	5.00E-03 m^3	
Solids conc^n	4.16 kg m^{-3}	
$\equiv$	0.10% v/v	
$\equiv$	0.41% w/w	
pH	6.00	
Applied field	75 V	
Separation	1.5 cm	
Field Strength	50 Vcm^{-1}	
Viscosity, μ	*0.001* Pa s	
Filter Area	6.22E-03 m^2	
Pressure drop	0.75 bar	
	75000 Pa	
Slope of plot	2.57E+08 sm^{-6}	
Intercept	3.34E+05 sm^{-3}	
R^2	0.942	

α	*3.593E+11*	m kg^{-1}
R_m	*1.559E+11*	m^{-1}

Volume @1800s	*2043* ml
Vol. per unit area	3.28E-01 m^{3}m^{-2}

Mass of *wet* cake	*23.24* g	
Mass of *dry* cake	*13.16* g	
Mass of liquid	10.08 g	
Volume of solid	3.09 cm^3	
Volume of liquid	10.08 cm^3	
Cake conc^n	56.63%	(Mass)
Cake conc^n	23.46%	(Volume)
ε	*0.765*	
Moisture ratio, m	1.766	

Effective c	4.17 kg m^{-3}
Slurry c	4.16 kg m^{-3}

EAP8V20		
	Filtrate	**Solid**
Weight	*4864.5*	*20.6* g
Density, ρ	*1000*	*4260* kg m^{-3}
Volume	4.86E-03	4.84E-06 m^3
Total Mass	4.89 kg	
Total Volume	4.87E-03 m^3	
Solids conc^n	4.23 kg m^{-3}	
$\equiv$	0.10% v/v	
$\equiv$	0.42% w/w	
pH	**8.10**	
Applied field	30 V	
Separation	1.5 cm	
Field Strength	20 Vcm^{-1}	
Viscosity, μ	*0.001* Pa s	
Filter Area	6.22E-03 m^2	
Pressure drop	0.75 bar	
	75000 Pa	
Slope of plot	6.24E+08 sm^{-6}	
Intercept	9.81E+05 sm^{-3}	
R^2	0.987	

α	*8.549E+11*	m kg^{-1}
R_m	*4.578E+11*	m^{-1}

Volume @1800s	*1079* ml
Vol. per unit area	6.75E-02 m^{3}m^{-2}

Mass of *wet* cake	*5.20*	g
Mass of *dry* cake	*3.74*	g
Mass of liquid	1.46	g
Volume of solid	0.88	cm^3
Volume of liquid	1.46	cm^3
Cake conc^n	71.92%	(Mass)
Cake conc^n	37.55%	(Volume)
ε	*0.624*	
Moisture ratio, m	1.390	
Effective c	4.24	kg m^{-3}
Slurry c	4.23	kg m^{-3}

EAPH8P250V50

	Filtrate	Solid	
Weight	4995.8	21.2	g
Density, ρ	1000	4260	kg m^{-3}
Volume	5.00E-03	4.98E-06	m^3
Total Mass	5.02		kg
Total Volume	5.00E-03		m^3
Solids conc^n	4.24		kg m^{-3}
$\equiv$	0.10%		v/v
$\equiv$	0.42%		w/w
pH	8.02		
Applied field	75		V
Separation	1.5		cm
Field Strength	50		Vcm^{-1}
Viscosity, μ	0.001		Pa s
Filter Area	6.22E-03		m^2
Pressure drop	0.25		bar
	25000		Pa
Slope of plot	1.82E+08		sm^{-6}
Intercept	4.93E+05		sm^{-3}
R^2	0.997		

α	8.294E+10 m kg^{-1}
R_m	7.674E+10 m^{-1}

Volume @1800s	2086	ml
Vol. per unit area	3.35E-01	m^{3}m^{-2}

Mass of *wet* cake	12.64	g
Mass of *dry* cake	6.41	g
Mass of liquid	6.24	g
Volume of solid	1.50	cm^3
Volume of liquid	6.24	cm^3
Cake conc^n	50.67%	(Mass)
Cake conc^n	19.43%	(Volume)
ε	0.806	
Moisture ratio, m	1.973	
Effective c	4.26	kg m^{-3}
Slurry c	4.24	kg m^{-3}

EApH8P500V50

	Filtrate	Solid
Weight	*4995.8*	*21.2* g
Density, ρ	*1000*	*4260* kg m^{-3}
Volume	5.00E-03	4.98E-06 m^3
Total Mass	5.02 kg	
Total Volume	5.00E-03 m^3	
Solids conc^n	4.24 kg m^{-3}	
$\cong$	0.10% v/v	
$\cong$	0.42% w/w	
pH	8.02	
Applied field	75 V	
Separation	1.5 cm	
Field Strength	50 Vcm^{-1}	
Viscosity, μ	*0.001* Pa s	
Filter Area	6.22E-03 m^2	
Pressure drop	0.5 bar	
	50000 Pa	
Slope of plot	1.83E+08 sm^{-6}	
Intercept	4.66E+05 sm^{-3}	
R^2	0.996	

α	*1.67E+11*	m kg^{-1}
R_m	*1.449E+11*	m^{-1}

Volume @1800s	*2112* ml
Vol. per unit area	3.40E-01 m^{3}m^{-2}

Mass of *wet* cake	13.09 g
Mass of *dry* cake	6.51 g
Mass of liquid	6.58 g
Volume of solid	1.53 cm^3
Volume of liquid	6.58 cm^3
Cake conc^n	49.77% (Mass)
Cake conc^n	18.87% (Volume)
ε	*0.811*
Moisture ratio, m	2.009

Effective c	4.26 kg m^{-3}
Slurry c	4.24 kg m^{-3}

EApH8V50

	Filtrate	Solid	
Weight	*4995.0*	*21.3*	g
Density, ρ	*1000*	*4260*	kg m^{-3}
Volume	5.00E-03	5.00E-06	m^3
Total Mass		5.02	kg
Total Volume		5.00E-03	m^3
Solids conc^n		4.26	kg m^{-3}
$\equiv$		0.10%	v/v
$\equiv$		0.42%	w/w
pH		7.99	
Applied field		75	V
Separation		1.5	cm
Field Strength		50	Vcm^{-1}
Viscosity, μ		*0.001*	Pa s
Filter Area		6.22E-03	m^2
Pressure drop		0.75	bar
		75000	Pa
Slope of plot		1.81E+08	sm^{-6}
Intercept		5.23E+05	sm^{-3}
R^2		0.997	

α	*2.462E+11*	m kg^{-1}
R_m	*2.442E+11*	m^{-1}

Volume @1800s	*2014*	ml
Vol. per unit area	0.00E+00	m^{3}m^{-2}

Mass of *wet* cake	*12.92*	g
Mass of *dry* cake	*7.46*	g
Mass of liquid	5.45	g
Volume of solid	1.75	cm^3
Volume of liquid	5.45	cm^3
Cake conc^n	57.78%	(Mass)
Cake conc^n	24.32%	(Volume)
ε	*0.757*	
Moisture ratio, m	1.731	
Effective c	4.28	kg m^{-3}
Slurry c	4.26	kg m^{-3}

EApH8V20#2

	Filtrate	Solid	
Weight	*4884.4*	*20.4*	g
Density, ρ	*1000*	*4260*	kg m^{-3}
Volume	4.88E-03	4.79E-06	m^3
Total Mass	4.90		kg
Total Volume	4.89E-03		m^3
Solids conc^n	4.18		kg m^{-3}
≡	0.10%		v/v
≡	0.42%		w/w
pH	8		
Applied field	30		V
Separation	1.5		cm
Field Strength	20		Vcm^{-1}
Viscosity, μ	*0.001*		Pa s
Filter Area	6.22E-03		m^2
Pressure drop	0.75		bar
	75000		Pa
Slope of plot	5.30E+08		sm^{-6}
Intercept	9.80E+05		sm^{-3}
R^2	0.975		

α	*7.369E+11*	m kg^{-1}
R$_m$	*4.574E+11*	m^{-1}

Volume @1800s	*1136*	ml
Vol. per unit area	1.83E-01	m^{3}m^{-2}

EApH8V46

	Filtrate	Solid	
Weight	*4923.4*	*20.3*	g
Density, ρ	*1000*	*4260*	kg m^{-3}
Volume	4.92E-03	4.77E-06	m^3
Total Mass	4.94		kg
Total Volume	4.93E-03		m^3
Solids conc^n	4.12		kg m^{-3}
$\equiv$	0.10%		v/v
$\equiv$	0.41%		w/w
pH	7.90		
Applied field	70		V
Separation	1.5		cm
Field Strength	46.67		Vcm^{-1}
Viscosity, μ	*0.001*		Pa s
Filter Area	6.22E-03		m^2
Pressure drop	0.75		bar
	75000		Pa
Slope of plot	2.68E+08		sm^{-6}
Intercept	5.25E+05		sm^{-3}
R^2	0.975		

α	*3.774E+11*	m kg^{-1}
R$_m$	*2.45E+11*	m^{-1}

Volume @1800s	*1804*	ml
Vol. per unit area	2.90E-01	m^{3}m^{-2}

EA PH10V20

	Filtrate	Solid	
Weight	4995.3	21.1	g
Density, ρ	1000	4260	kg m^{-3}
Volume	5.00E-03	4.96E-06	m^3
Total Mass	5.02		kg
Total Volume	5.00E-03		m^3
Solids conc^n	4.23		kg m^{-3}
$\cong$	0.10%		v/v
$\cong$	0.42%		w/w
pH	10.01		
Applied field	30		V
Separation	1.5		cm
Field Strength	20		Vcm^{-1}
Viscosity, μ	0.001		Pa s
Filter Area	6.22E-03		m^2
Pressure drop	0.75		bar
	75000		Pa
Slope of plot	1.74E+08		sm^{-6}
Intercept	1.04E+06		sm^{-3}
R^2	0.946		

α	2.388E+11	m kg^{-1}
R_m	4.834E+11	m^{-1}

Volume @1800s	1413	ml
Vol. per unit area	2.27E-01	m^{3}m^{-2}

Mass of _wet_ cake	4.90	g
Mass of _dry_ cake	3.50	g
Mass of liquid	1.40	g
Volume of solid	0.82	cm^3
Volume of liquid	1.40	cm^3
Cake conc^n	71.43%	(Mass)
Cake conc^n	36.98%	(Volume)
ε	0.630	
Moisture ratio, m	1.400	

Effective c	4.23	kg m^{-3}
Slurry c	4.23	kg m^{-3}

EApH10V50#1

	Filtrate	Solid	
Weight	*3996.0*	*17.0*	g
Density, ρ	*1000*	*4260*	kg m^{-3}
Volume	4.00E-03	4.00E-06	m^3
Total Mass	4.01		kg
Total Volume	4.00E-03		m^3
Solids conc^n	4.26		kg m^{-3}
$\equiv$	0.10%		v/v
$\equiv$	0.42%		w/w
pH	10.10		
Applied field	100		V
Separation	2		cm
Field Strength	50		Vcm^{-1}
Viscosity, μ	*0.001*		Pa s
Filter Area	6.22E-03		m^2
Pressure drop	0.75		bar
	75000		Pa
Slope of plot	1.07E+08		sm^{-6}
Intercept	2.94E+05		sm^{-3}
R^2	0.976		

α	*1.456E+11*	m kg^{-1}
R_m	*1.371E+11*	m^{-1}

Volume @1800s	*2925*	ml
Vol. per unit area	4.70E-01	m^{3}m^{-2}

EApH10V50#2

	Filtrate	Solid	
Weight	4936.4	21.3	g
Density, ρ	1000	4260	kg m^{-3}
Volume	4.94E-03	4.99E-06	m^3
Total Mass	4.96		kg
Total Volume	4.94E-03		m^3
Solids conc^n	4.31		kg m^{-3}
$\equiv$	0.10%		v/v
$\equiv$	0.43%		w/w
pH	10.00		
Applied field	100		V
Separation	2		cm
Field Strength	50		Vcm^{-1}
Viscosity, μ	0.001		Pa s
Filter Area	6.22E-03		m^2
Pressure drop	0.75		bar
	75000		Pa
Slope of plot	8.54E+07		sm^{-6}
Intercept	3.15E+05		sm^{-3}
R^2	0.989		

α	1.15E+11	m kg^{-1}
R_m	1.471E+11	m^{-1}

Volume @1800s	3113	ml
Vol. per unit area	5.00E-01	m^{3}m^{-2}

Mass of *wet* cake	10.02	g
Mass of *dry* cake	6.91	g
Mass of liquid	3.11	g
Volume of solid	1.62	cm^3
Volume of liquid	3.11	cm^3
Cake conc^n	68.96%	(Mass)
Cake conc^n	34.28%	(Volume)
ε	0.657	
Moisture ratio, m	1.450	
Effective c	4.32	kg m^{-3}
Slurry c	4.31	kg m^{-3}

EAPH10V50#3

	Filtrate	Solid	
Weight	*4917.0*	*21.9*	g
Density, ρ	*1000*	*4260*	kg m^{-3}
Volume	4.92E-03	5.13E-06	m^3
Total Mass	4.94		kg
Total Volume	4.92E-03		m^3
Solids conc^n	4.45		kg m^{-3}
$\equiv$	0.10%		v/v
$\equiv$	0.44%		w/w
pH	10.10		
Applied field	100		V
Separation	2		cm
Field Strength	50		Vcm^{-1}
Viscosity, μ	*0.001*		Pa s
Filter Area	6.22E-03		m^2
Pressure drop	0.75		bar
	75000		Pa
Slope of plot	1.48E+08		sm^{-6}
Intercept	4.34E+05		sm^{-3}
R^2	0.991		

α *1.928E+11*	m kg^{-1}
R$_m$ *2.026E+11*	m^{-1}

Volume @1800s	*2321*	ml
Vol. per unit area	3.73E-01	m^{3}m^{-2}

Mass of *wet* cake	*24.70*	g
Mass of *dry* cake	*16.69*	g
Mass of liquid	8.01	g
Volume of solid	3.92	cm^3
Volume of liquid	8.01	cm^3
Cake conc^n	67.57%	(Mass)
Cake conc^n	32.85%	(Volume)
ε	*0.672*	
Moisture ratio, m	1.480	
Effective c	4.46	kg m^{-3}
Slurry c	4.45	kg m^{-3}

APPENDIX B

PUBLICATIONS

i. The use of acoustic fields as a filtration and dewatering aid, M.C.Smythe & R.J. Wakeman, Ultrasonics 38 (2000) 657-661

ii. Clarifying filtration of fine particle suspensions aided by electrical and acoustic fields, R.J. Wakeman & M.C. Smythe, Trans IchemE, Vol 78, Part A, Jan 2000, 125-135

iii. Experiments on electroacoustic vacuum filtration, M.C.Smythe & R.J. Wakeman, IchemE Research event abstracts, 1998, 80-85

The use of acoustic fields as a filtration and dewatering aid

M.C. Smythe, R.J. Wakeman *

Department of Chemical Engineering, Loughborough University, Loughborough LE11 3TU, UK

Abstract

An experimental rig has been developed to study the effects of electric and acoustic field combinations on the filtration rate of titanium dioxide suspensions. Ultrasound energy is applied tangentially to the filter medium. Electric field strengths, suspension characteristics and process parameters can all be varied independently. Results from an experimental programme demonstrate that the use of ultrasound across the cake surface can decrease the specific cake flow resistance and increase the filtration rates of low-concentration rutile suspensions (0.1% v/v). Changes in the conductivity induced by ultrasonic irradiation affect the suspension such that the application of an electrical field is enhanced, giving an equivalent electric field strength higher than that applied. © 2000 Elsevier Science B.V. All rights reserved.

Keywords: Electricity; Electroacoustic; Filtration; Ultrasound

1. Introduction

The separation of liquids from fine particle suspensions can be difficult and costly, yet they play an important role in commercial processing. Slurries are often deliquored by filtration methods, requiring a vacuum or pressure driving force. As filter cake forms, resistance to fluid flow increases, and filtrate flow rate is reduced. The effect of particles blocking the filter medium can be reduced by a number of methods, including mechanical removal of the cake, reduction of the cake resistance by chemical methods, or the prevention of cake formation. Assisted separations, using electrical, magnetic or sonic fields, have emerged as potential alternatives to conventional filtration. Magnetically enhanced filtration has been widely used in the mining industry, and the use of electric fields as an additional driving force has recently become more viable with advances in suitable electrode materials. Acoustic fields have been used to dewater sludges, coals and food dispersions. They are particularly useful in the removal of bound water which cannot be removed by conventional filtration, allowing closer packing of the particles and thus a drier cake, which may be more important than filtration time if a solid product is being made. In turn, this removes the need for prolonged

thermal drying, attractive in both energy terms and for materials that are heat-sensitive. Combinations of fields have been investigated by Muralidhara et al. [1] and Wakeman and Tarleton [2], particularly the combination of electric and acoustic fields.

2. Filtration experiments

Filtration experiments have been conducted using aqueous rutile suspensions as the test material. An experimental filter cell was designed and built, based on a conventional dead-end vacuum filter with the filter medium support acting as a cathode and a variable position anode suspended parallel to the support. An ultrasonic transducer was attached to one side of the filter cell and ultrasonic energy (provided by a Telsonic NSM 220 supply) applied tangentially to the filter surface, with a contact area of 91.68 cm^2. The ultrasonic transducer position was fixed, and the frequency was constant at 23 kHz with a power output of 300 W. A stabilized d.c. power supply (Sorensen model DCR 150-12B) allowed application of a constant voltage across the electrodes. A field gradient of 50 V cm^{-1} was used for the results quoted in this paper, with an electrode separation distance of 1.5 cm. In the filtration experiments, Sartorious cellulose nitrate membranes with a pore size rating of 0.2 μm were used. These membranes had been characterized previously [3], and

* Corresponding author. Fax: +44-1509-2239231.
E-mail address: r.j.wakeman@lboro.ac.uk (R. Wakeman)
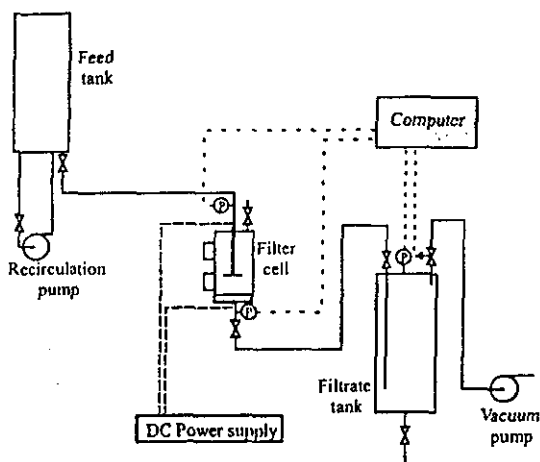
Fig. 1. Flow diagram of the experimental apparatus; the filter cell has a diameter of 9.9 cm and a volume of 1.9 l. The effective filtration area is 62.2 cm².

show a negative zeta potential for $2 < pH < 12$. A new membrane was used for each filtration test.

The experimental flow circuit (Fig. 1) comprised a feed reservoir with recirculation pump to ensure that the feed remained completely mixed during the course of an experiment. The feed flowed into the filter cell, and pressure transducers monitored the pressure drop across the cell. A host computer controlled the pressure difference across the filter. Experiments were carried out at a constant vacuum. On commencement of a filtration experiment, the fields required were switched on; the suspension was under the influence of the fields for the duration of the experiment. The filtrate volume collected was measured at different filtration times.

3. Measurement of ultrasonic effects on solution conductivity

The basic rig was also used as a vessel to carry out experiments on the effects of ultrasonic energy on the conductivity of rutile suspensions. The experimental method is based on earlier work by Cataldo [4]. To measure the effect on the suspension under the same conditions as the filtration experiments, the filter cell was filled with test suspension and the initial pH and conductivity measured. The conductivity was measured as a function of time and the bulk temperature was monitored throughout the experiment. Investigations were carried out using deionized water, with HCl or NaOH added to alter the initial conductivity. Further tests using rutile suspensions were carried out to evaluate effects of the presence of suspended particles.

4. Modification of the classical filtration equation

The form of plot in Fig. 2 follows that often used to report conventional filtration data, from which an effective specific cake resistance can be calculated. Following the simplifications used by Yukawa et al. [5] to derive a relationship for electrofiltration, a similar equation was used to describe the effects of ultrasound. A conventional plot (reciprocal flow rate vs. cumulative volume of filtrate) of the data should yields a straight line with gradient K_1 and intercept K_2. Table 1 gives values of K_1 for the data from a range of filtration experiments; since K_1 is directly proportional to the product of specific cake flow resistance and feed suspension concentration, which may both vary with the applied fields, it provides an insight into how this parameter varies with the applied fields. The data in Table 1 show that whilst the application of fields to assist filtration does have an effect, the field combinations act differently at the pHs studied.

5. Porosity effects

The porosities of the filter cakes formed are listed in Table 1. These have been calculated from gravimetric mesurements of wet and dried samples of the cakes, and give an indication of variations in cake structure. These data generally indicate that a cake formed in an acoustic field from better dispersed (higher pH) suspensions is more porous than that formed without added fields, but
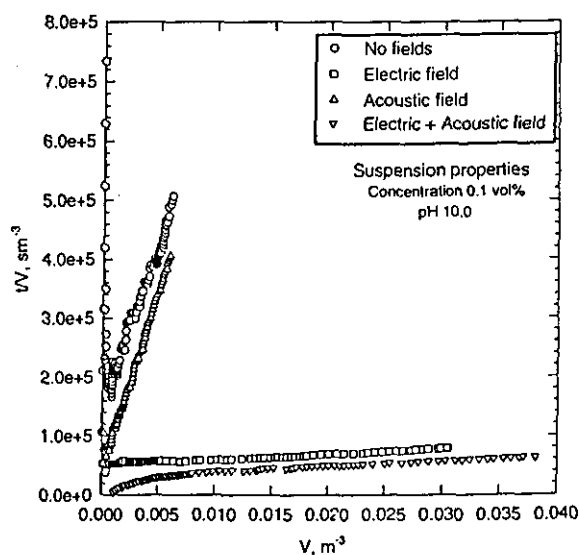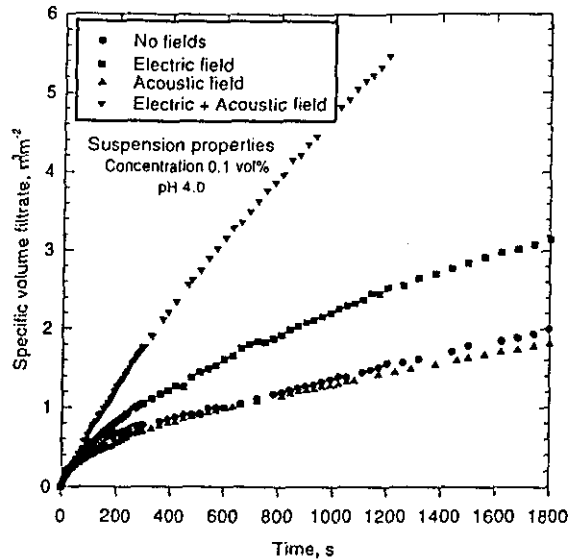

Fig. 2. Plots of t/V vs. V showing the effects of electric and acoustic fields and their combinations on the filtration of pH 10 rutile suspensions of concentration 0.1% v/v. (Electric field strength 50 V cm⁻¹, acoustic frequency 23 kHz.)

659

Table 1

Effect of electric and acoustic fields on the rate of filtration, and porosity, of 0.1% v/v rutile suspensions at $\Delta p = 75$ kPa

	$K_j \times 10^{-6}$ m^6 s^{-1}				Porosity			
	pH 4	pH 6	pH 8	pH 10	pH 4	pH 6	pH 8	pH 10
Number of fields	13	10	57	56	0.68	0.58	0.59	0.62
Acoustic field (23 kHz)	14	20	40	62	0.69	0.61	0.71	0.67
Electric field (50 V cm^{-1})	4	3	2	0.9	0.77	0.81	0.76	0.74
Electric and acoustic fields (50 V cm^{-1}, 23 kHz)	0.4	2	2	0.8	0.69	0.76	0.75	0.66

as the pH moves closer to the iso-electric point (IEP), there is an effect of ultrasound on cake porosity. The electric field causes formation of a more open cake structure at all pH values, and combining the fields causes the cake to become less porous. At low pH, with no added fields, a higher porosity is expected due to the particle aggregation; unlike in the work of Kowalska et al. [6,7], the porosity data here suggest that the ultrasound intensity used in the filter is not great enough to disperse all of the aggregates.

6. Conductivity effects

Results from irradiating solutions of various initial conductivities are shown in Figs. 3 and 4 and indicate that the electrolyte solution conductivity increases from the moment the solution is subjected to ultrasonic irradiation. Normalizing the data with the initial conductivity of the solution gives an indication of the magnitude of the conductivity change with the largest changes

Fig. 4. Effect of periodic ultrasonic irradiation on NaOH solutions of different initial conductivity and pH. Ultrasonic irradiation periods as in Fig. 3.

being shown for solutions with low initial conductivities (σ_0), irrespective of whether the solution is acidic or basic. The temperature increase over the period of each experiment was 4°C. As an approximation, the increase in conductivity due to temperature is 2% per°C; thus, an increase of 8% is likely over the duration of the experiment. For $\sigma_0 > 50$ µS, the magnitude of the change is small (below 10% increase in σ). At lower initial conductivities, the increase is much greater than 8% during ultrasonic exposure, but when irradiation is ceased, the conductivity falls back to levels close to σ_0, and there is generally less than an 8% increase from the original value. Therefore, the conductivity increase is not, in this case, due solely to an increase in temperature of the solution.

Fig. 5 shows the results of the similar experiments using a 0.1% v/v rutile suspension dispersed by MIPA. The initial conductivity was altered in the same way as in the previous experiments. Increases in conductivity are around 40% for σ_0 between 15 and 20 µS, which can

Fig. 3. Effect of periodic ultrasonic irradiation on HCl solutions of different initial conductivity (and pH). Ultrasonic irradiation was during the periods 0–300 s, 600–900 s and 1200–1500 s.
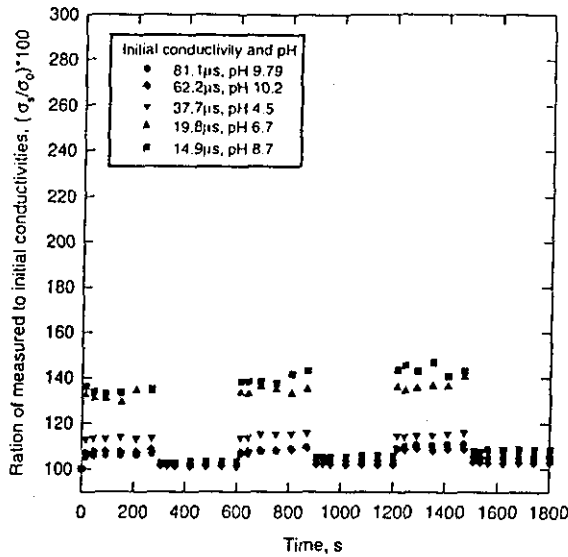
Fig. 5. Effect of periodic ultrasonic irradiation on 0.1% v/v rutile suspensions of different initial conductivity (and pH), pH altered with HCl or NaOH. Ultrasonic irradiation as in Fig. 3.

Fig. 7. Effect of electric and acoustic field combinations on the filtration of pH 4 rutile suspensions of concentration 0.1% v/v. (Electric field strength 50 V cm^{-1}, acoustic frequency 23 kHz).

be compared with 50–70% for HCl solutions and 20–30% for NaOH solutions.

The variation of the conductivity increase with initial conductivity is shown on Fig. 6 for all suspensions investigated. At higher ionic strengths, the double layer is compressed, and the percentage increase in conductivity is smallest. Compression of the double layer restricts movement of the diffuse cloud, and the particle and diffuse layer oscillate together. At low conductivities,

ultrasound is seen to increase the apparent conductivity approximately the same amount as for electrolyte solutions. This is because the diffuse layer is large and easily distorted, and there is relative motion between the particle and the layer. Cataldo [4] explained the increase in conductivity of electrolyte solutions by calculating the maximum temperatures and pressures inside bubbles at the point of collapse. This 'hot spot' theory based on the collapse of cavitation bubbles provides a possible explanation of the conductivity effects.

The apparent synergy between electrical and acoustic fields to enhance filtration tends to appear at lower (Fig. 7) and, to a lesser extent, higher pH values. It seems likely that the synergism is due to two main factors. Closer to the IEP, ultrasound causes some of the aggregates to disperse, reducing the effective particle size and increasing the electrophoretic mobility of the particles in the electric field. Far from the IEP, the particles are well dispersed, the double layer is compressed, the particles and diffuse layer oscillate together in the ultrasonic field, and the particles and diffuse layer migrate together in the electric field.

Fig. 6. Relationship between initial conductivity of a suspension and the maximum conductivity increase shown by that suspension when it is irradiated using a 23 kHz acoustic field.

7. Conclusion

Assisting filtration by the application of electrical or acoustic fields leads to the production of a more open cake, with a higher porosity and lower specific cake resistance. The rate of filtration is reduced by sole

application of acoustic fields but is considerably increased when combined fields are used. Application of an acoustic field has been shown to significantly increase the measured conductivity of electrolytic and rutile suspensions. Ultrasound thus enhances the effect of an applied electric field close to the isoelectric point of the suspension by reducing the effective particle size and increasing electrophoretic velocities.

Acknowledgement

References

[1] H.S. Muralidhara, B. Parekh, N. Senapati, Solid liquid separation process for fine particle suspensions by an electric and ultrasonic field. US Patent 4,561,953, 1985.

[2] R.J. Wakeman, E.S. Tarleton, Chem. Eng. Res. Des. 69 (5) (1991) 386.

[3] E.S. Tarleton, R.J. Wakeman, Trans IChemE, Part A 72 (1994) 521.

[4] F. Cataldo, J. Electroanal. Chem. 431 (1997) 61.

[5] H. Yukawa, K. Kobayashi, Y. Tsukui, S. Yamano, M. Iwata, J. Chem. Eng. Jpn 9 (5) (1976) 396.

[6] E. Kowalska, J. Bien, E. Zielewicz, Acustica 40 (1978) 99.

[7] E. Kowalska, W. Kowalski, J. Bien, Acustica 43 (1979) 260.

IChem^E

CLARIFYING FILTRATION OF FINE PARTICLE SUSPENSIONS AIDED BY ELECTRICAL AND ACOUSTIC FIELDS

R. J. WAKEMAN (FELLOW) and M. C. SMYTHE (ASSOCIATE MEMBER)

Department of Chemical Engineering, Loughborough University, Loughborough, UK

An experimental rig has been developed to study the effects of electric and acoustic fields on constant pressure filtration. The filter is designed with the medium support acting as a cathode, and with a variable height anode located in the feed suspension inducing an electric field normal to the filter medium. A flat plate ultrasonic transducer attached to the side of the filter applied ultrasonic energy tangentially to the medium. Electric and acoustic fields, suspension characteristics and process parameters can all be varied independently.

Experimental results demonstrate that acoustic fields have little or no effect on the dewatering of suspensions of concentrations higher than 1% by volume. Changes in the conductivity induced by ultrasonic irradiation are pH dependent and may affect the suspension such that application of an electrical field is enhanced. Electric fields enhance filtration rates but form filter cakes with higher porosities. The power consumed by the ultrasonic field is large; the power consumed by the electric field is much smaller and is more effective at improving filtration characteristics.

Keywords: electroacoustic; ultrasound; electricity; filtration; dewatering; colloids

INTRODUCTION

Assisted separations have become more important in recent years as the demand for higher purity products has increased. In terms of the filtration of finer particle suspensions, the production of a drier cake can lead to a more economical process when compared with the energy costs of thermal drying and there are advantages if the batch time for cake formation can be shortened. Improvements to the filtration process have been demonstrated by the exploitation of phenomena such as electrokinetic, acoustic, magnetic and centrifugal forces (Muralidhara[1]). A combined fields approach enables limitations to the degree of separation, purity and yield imposed by conventional filtration to be overcome. Electroacoustic dewatering (EAD) has been used as a means of dewatering sludges, producing a higher solids content than attainable using electric, or acoustic fields separately (Muralidhara *et al.*[2]). This technology has been extended to crossflow microfiltration (Wakeman and Tarleton[3]).

The use of electric fields to improve separations has been studied little in depth until recently by, for example, Moulik *et al.*[4], Moulik[5], Yukawa *et al.*[6,7] and Wakeman[8]. The processes require continuous application of electric fields and as such are energy intensive. Electrofiltration has not been widely exploited, but recent advances in electrode materials have enabled the technology to be used to improve filtrate flux, and as an alternative to backwashing as a method of membrane cleaning.

Ultrasonics has been shown by many authors to be a potentially economical means of removing water from products to relatively low levels (Kowalska *et al.*[9,10]), and to decrease fouling of membranes (Tarleton[11]). Research to date largely implies that ultrasound is a potential aid to cake deliquoring rather than a filtration technique, but whichever it may be it is important to understand how the mechanisms associated with ultrasound affect the suspension characteristics. However, it may be that the ultrasonic energy can provide an additional driving force, in a similar way to an electric field, during either cake formation or cake deliquoring operations. That is, ultrasound may act to aid filtration, and by facilitating a more open cake may improve mass transfer through the filter medium.

Electric fields can be generated in an electrolytic suspension by the application of an ultrasonic field. Ultrasonic vibration potentials are produced when ultrasonic waves are propagated through ionic media, and can be ionic or colloidal. Ionic vibration potentials (IVP) occur as a result of sound waves passing through an electrolytic solution generating relative motion between the ions and the liquid. The differences in amplitudes and phases of the displacement of anions and cations result in a potential of the order of $10\,\mu$V (Yeager *et al.*[12]). The magnitude of this motion depends on the particle and suspending liquid density differences, particle size and shape, and the sound wave frequency (Heuter and Bolt[13]). The colloidal vibration potential (CVP) is a similar effect with the fields arising from the diffuse layer around the colloidal particles. The potentials arising in this way are greater than for IVP. As a result of this relative motion of the particles and the

126   WAKEMAN and SMYTHE

diffuse layer, the ionic atmosphere around the colloidal
particle distorts, resulting in a displacement of the centre
of charge away from that of the particle (in the same way
as the electrophoretic relaxation effect). Each particle
generates an alternating electric field, and an overall effect
occurs in the form of a macroscopic electric field, alter-
nating at the frequency of the sound wave (O'Brien[14]). The
field generated is dependent on the same suspension
parameters as the magnitude of the particle-liquid displace-
ment, and also the geometry and type of ultrasonic device.

This idea of sound waves generating electric fields was
first noted by Debye[15]. Calculation of these vibration poten-
tials has been limited to the dilute case (Enderby[16]; Booth
and Enderby[17]) until recently. Electroacoustic effects in
suspensions of arbitrary concentration can be calculated,
provided the particles are small compared with the sound
wavelength (O'Brien[14,18]). Equations describing micro-
scopic variations in ion density, electrical potential, velocity
and pressure are used as a starting point to produce a set
of macroscopic equations linking the electrical field gene-
rated by a sound wave, and conversely the sound waves
generated by an electric field. The effect of alternating
electric fields producing an ultrasonic wave was discovered
by Cannon et al.[19]. O'Brien and White[20] and Sherwood[21]
gave the initial detailed mathematical derivations, which
are solved for a dilute suspension[14] and for arbitrary
concentrations[18].

This paper describes the results from an experimental
programme that was carried out to determine the effects
of using electrical and ultrasonic force fields, either alone
or in combination, on cake formation in deadend filters.

EXPERIMENTAL PROCEDURES

The experimental programme consisted mainly of filtra-
tion experiments, using aqueous rutile suspensions as the
test material. The suspension was characterized by mea-
suring the particle size, zeta potential and conductivity
variations with pH. The particle size was determined using
a Malvern Mastersizer and the zeta potential using a
Malvern Zetamaster. The conductivity was monitored using
a WPA portable conductivity meter, together with an epoxy
resin conductivity probe.

The test suspension was prepared by dispersing rutile
in a solution of 0.15% by weight (based on the mass of
TiO₂) monoisopropanolamine (MIPA) in deionized (DI)
water. The suspension was homogenized with a high shear
mixer for 8 minutes at 2000 rpm and a Malvern Master-
sizer was used to ensure a mean particle size of 0.3 μm.
The stock suspension was made up at 50% (w/w) of TiO₂
as this concentration was found to give the best and most
reproducible dispersion.

Filtration Experiments

An experimental filter cell was designed and built, based
on a conventional dead end vacuum filter (Figure 1); the
filter had a diameter of 89 mm and was located in a perspex,
cylindrical housing. In these experiments the filter medium
support acted as a cathode, and any cake that formed
did so on the medium but below the anode. A variable
position anode was suspended parallel to the support, and
the separation distance could be varied. The electric field
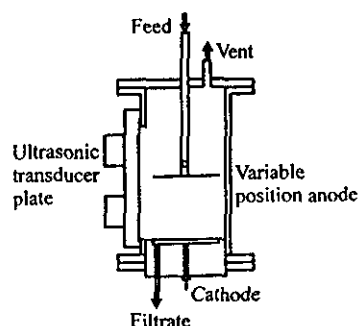
Figure 1. Filter cell schematic.

was thus applied normal to the filter surface. An ultrasonic
transducer was attached to one side of the filter cell and
ultrasonic energy applied tangentially to the filter surface.
A stabilized d.c. power supply (Sorensen model DCR
150-12B) provided an electric field gradient between the
electrodes and the ultrasonic energy was provided by a
Telsonic NSM 220 supply. The d.c. power supply allowed
application of a constant, stabilized voltage across the
electrodes. The field gradient was varied from one experi-
ment to the next by altering the separation distance between
the electrodes or by applying a different voltage. The
ultrasonic transducer position could not be altered and
the frequency was fixed at 23 kHz (the power input to the
transducers was 3 Wcm⁻²). The transducer plate had a
contact area with the suspension of 91.68 cm². In the
filtration experiments, Sartorious cellulose nitrate mem-
branes with a pore size rating of 0.2 μm were used. These
membranes have been extensively characterized pre-
viously (Tarleton and Wakeman[22]; Wakeman[23]), and show
a negative zeta potential for 2 < pH < 12 with a measured
mean (flow) pore size of 0.51 μm and a thickness of
130 μm. A new membrane was used for each filtration test.

The experimental flow circuit (Figure 2) comprised a
feed reservoir with recirculation pump to ensure the feed
remained completely mixed during the course of an experi-
ment. The feed flowed into the filter cell, and the pressure
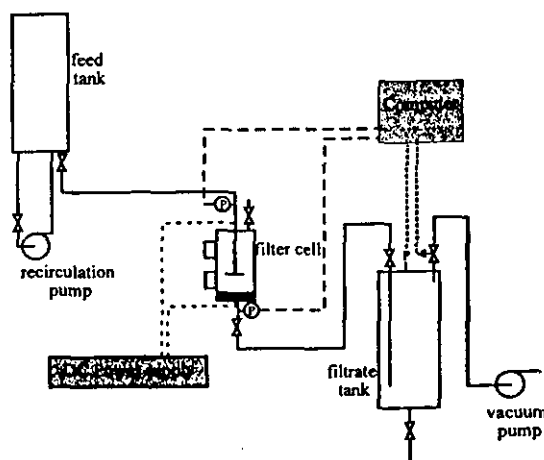

Figure 2. Flowsheet of the experimental apparatus.

FILTRATION OF FINE PARTICLE SUSPENSIONS AIDED BY ELECTRICAL AND ACOUSTIC FIELDS 127

drop across the cell was monitored by pressure transducers. A host computer controlled the vacuum held in the filtrate tank in order to control the pressure difference across the filter. Experiments were carried out at constant vacuum. The pressure drop across the cell was recorded and the filtrate volume collected was measured at different filtration times.

Before commencing a filtration experiment a test suspension was made to a known concentration by dilution of the stock suspension described above with double distilled water. The suspension was re-circulated around the flow circuit until a homogenous mixture was achieved. The pH of the resulting suspension was monitored, and if necessary altered to the desired value using dilute HCl or NaOH. A sample of the suspension was then taken for particle size analysis. The initial conductivity and temperature was noted. At commencement of the experiment, the feed cell valve was opened, and the suspension allowed to fill the filter cell. At this point the fields required for the particular test were switched on, such that the suspension was under the influence of the fields for the entire duration of the experiment.

Figure 3. Particle size and zeta potential variations with pH for the rutile used in the experimental programme.

Measurement of Ultrasonic Effects on Solution Conductivity

The basic rig was also used as a vessel to carry out experiments on the effects of ultrasonic energy on the conductivity of rutile suspensions, to investigate the mechanisms that may explain the effects of the acoustic field. The experimental method is based on earlier works (Cataldo[24,25]) for measuring changes in the conductivity of halide salts. To measure the effect on the suspension under the same conditions as the filtration experiments, the filter cell was filled with test suspension and the initial pH and conductivity measured. The conductivity was measured as a function of time with the ultrasonic field being turned on and off at 5 minute intervals. Measurements were taken at 15 second intervals for the first minute of each period, and every 30 seconds thereafter for each 'on' or 'off' period. This cycle was repeated 3 times in each experiment. The bulk temperature was monitored to assess whether any changes in conductivity were due to the temperature increase due to energy input. Investigations were carried out using DI water, with HCl or NaOH added to alter the initial conductivity. Further tests using rutile suspensions were carried out to evaluate effects of the presence of suspended particles.

RESULTS AND DISCUSSION

Measurements of the zeta potential showed an isoelectric point (IEP) in the vicinity of pH ≈ 3.3. Around this pH the particles agglomerated and the mean particle size was larger than at higher pH values (Figure 3). At pH > 6 the suspension was well dispersed, and the mean particle size was 0.3 μm. At the IEP the mean particle size was between 2 and 3 μm, and the suspension settled rapidly. The zeta potential of suspended particles has a large effect on the success of electrofiltration (Wakeman[26]); where the magnitude of zeta potential is large the particles have greater electrophoretic mobilities than those close to the IEP, and a greater response is obtained from the particles when an electric field is superimposed across the suspension.
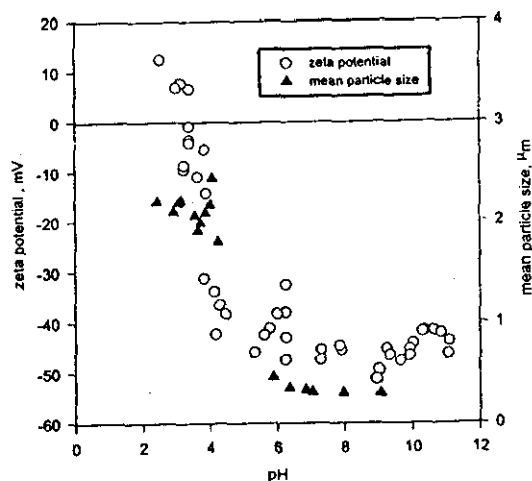
Electrofiltration Experiments

Typical filtrate volume versus filtration time curves measured for deadend filtration of 0.1% v/v rutile suspensions, pH 8, under various applied electric field strengths are shown on Figure 4. It is clear that the overall rate of filtration increases as the electric field gradient is increased. It can also be seen that as the electric field strength is increased the rate of decline in filtrate flux is reduced. This reduced decline in flux is a result of reduced cake formation due to electrophoresis, an effect that has been previously observed by Moulik et al.[4] and Wakeman[26]. It has been shown[6] that there exists a critical voltage gradient at which point the induced electrophoretic velocity, v_e, is equal to the local fluid velocity, v, and suspended particles become stationary, assuming zero slip between the liquid and the suspended solids. This critical voltage gradient, E_{CR}, is
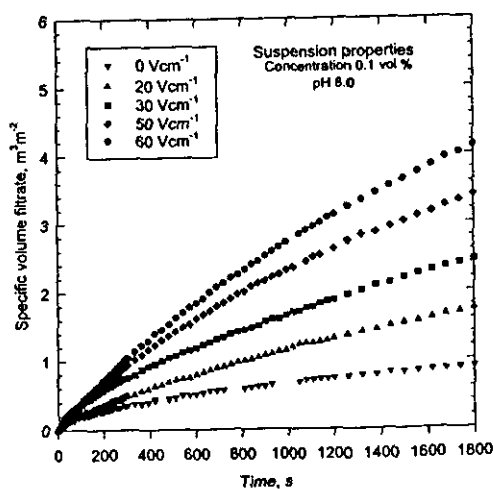

Figure 4. The effect of increasing electric field strength on the filtration of 0.1% v/v rutile suspensions at pH 8.

128   WAKEMAN and SMYTHE

given by:

$$E_{CR} = \frac{3\mu v}{2\varepsilon_0 D\zeta} \tag{1}$$

where μ, D, ε_0 and ζ are the viscosity and dielectric constant of the fluid, permittivity of a vacuum and the zeta potential, respectively. On Figure 4, the initial filtrate flux is of the order $0.004\,\text{ms}^{-1}$: to avoid deposition altogether, equation (1) suggests that a critical field of about $1.8\,\text{kV cm}^{-1}$ would need to be applied. As the applied fields are well below this value some cake formation or suspension thickening is to be expected and is responsible for the fall in filtrate flux. As the flux falls, so an equilibrium condition is approached where the cake or suspension thickness becomes constant—for the $60\,\text{V cm}^{-1}$ data shown on Figure 4 this would occur when the filtrate flux had dropped to $0.00013\,\text{ms}^{-1}$. From similar data at pHs 4 and 10 the corresponding initial fluxes are about 0.009 and $0.003\,\text{ms}^{-1}$, indicating critical fields of 10 and $1.4\,\text{kV cm}^{-1}$ respectively.

Experimental results obtained by filtering suspensions of the same feed concentration but different pHs show that the applied field enhances the rate of filtration by an extent dependent on the zeta potential: at a higher zeta potential there is more enhancement of the rate of filtration, with larger volumes of filtrate being produced in any given time. Also, there is a smaller decline of filtrate flux when the zeta potential is greater. These phenomena have been observed is crossflow filtration studies (Wakeman and Tarleton[27]; Wakeman and Sabri[28]; Akay and Wakeman[29,30]; Wakeman[23]) and are now well established effects of electric fields on filtration.

Acoustic Effects on Filtration

Woodside *et al.*[31] measured the magnitude and direction of the ultrasonic radiation forces acting on individual polystyrene latex particles in a standing wave field using a microscope based imaging system. They showed that the axial primary radiation force varied sinusoidally with axial position and the local acoustic energy density, and the magnitude of the transverse primary force was about 100-fold weaker than the axial force. Attenuation of sound in suspensions of particles has been well documented, together with the effect of concentration and the dependence of the attenuation coefficient on volume concentration (Harker and Temple[32]). Wakeman and Tarleton[3] showed that a 23 kHz sound field attenuated over increasingly shorter distances as the feed suspension concentration in a crossflow microfilter was increased and observed a total loss of any effect of ultrasound for concentration >4% v/v.

In the experimental filter cell, the ultrasonic transducer was orientated so that the primary radiation force was tangential to the filtering surface. The transducer surface was arranged so that the sound field irradiated the volume of solid/liquid mixture (whether this be a filter cake or a suspension lying above the cake) up to about 10 cm above the filter medium. Thus any particles depositing onto the surfaces of the medium or formed cake had experienced the sonic radiation force. Whilst the particle existed in the suspension it experienced a velocity parallel to the filtering surface induced by the sound field, but as the suspension thickened (during the cake formation process) the sound

field had a decreasing effect on the motion of the particles. Wakeman and Bailey[33] showed that the velocity of a $1\,\mu\text{m}$ particle in a low concentration suspension was about $12\,\text{ms}^{-1}$ at the surface of a 20 kHz transducer and was about $2\,\text{ms}^{-1}$ at a distance of 10 cm from the surface. The finer particles used in this work could be expected to have a similar or greater velocity close to the transducer when they were in the feed suspension. Their crossflow motion at the surface of the forming cake would act in similar way to the suspension flowing through a crossflow microfilter in so far as it will slow the rate of cake growth (Wakeman[34]), but unlike a crossflow filter the cake thickness will not be limited. The cake thickness will be determined by the balance between the drag and hydraulic forces acting on the particles. Whereas the trajectory of the particles is affected by the sound field, there is comparatively little direct effect of the radiation pressure on the direction of motion of the liquid.

It has been shown that the primary radiation force, F_z, acting on a particle in the z direction can be represented by[33]:

$$F_z = A\cos(Bz) \tag{2}$$

where A and B are dependent on the wave number, the particle size, the acoustic energy density and the acoustic contrast factor. In the case of neutrally buoyant or very small particles, A and B are known from radiation field theories that consider the acoustic energy density and the time-averaged potential and kinetic energy densities of the incident field (see for example, Yosioka and Kawasima[14], Woodside *et al.*[31]). The extent of the influence of the sound field on particle motions in this work are quite different for four main reasons:

(i) When the particles close to the transducer have a velocity imparted to them by displacement of the transducer, they move away from the transducer surface primarily in the axial direction. If the fluid were displaced axially by the transducer as a 'plug', then the particle velocity relative to the fluid would be zero. (During the reverse part of the cycle of the transducer displacement fluid is dragged into the zone immediately in front of the transducer surface, which imparts a retarding drag force on any particle still close to the surface.) However, in reality the fluid also has a transverse motion component across the transducer surface; this also creates a relative velocity between the fluid and particle in the axial direction, which leads to a retarding drag force acting on the particle.

(ii) At distances farther from the transducer surface localized recirculation currents are set up that slow the particles.

(iii) The particles have a density significantly greater than the liquid, so they will not accumulate close to the node points (if they exist within the filter) in the sound wave in the fluid. Once a particle has acquired its velocity, it will decelerate as it approaches the node but its momentum will carry it through the node.

(iv) The geometry of the filter cell confines the suspension and the sound field, causing recirculation of the particles (and to some extent of the fluid displaced by the flowing particles) in the volume above the forming filter cake.

Typical filtrate volume versus filtration time curves

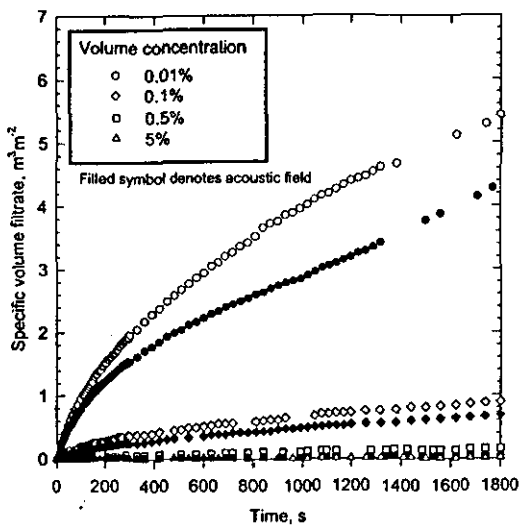FILTRATION OF FINE PARTICLE SUSPENSIONS AIDED BY ELECTRICAL AND ACOUSTIC FIELDS   129

Figure 5. The effect of feed concentration and of the application of a 23 kHz acoustic field on the filtration of 0.1% v/v rutile suspensions at pH 8. (The open symbols are data measured without an acoustic field, and the filled symbols are when an acoustic field is applied.)

measured for deadend filtration of pH 8 rutile suspensions of various volume concentrations under an applied acoustic field are shown on Figure 5, and compared with curves measured for filtration of the same suspensions in the absence of ultrasound. The sound field reduces the rate of filtration. The overall rate of filtration increases as the concentration decreases, with or without the sound field. The difference between the filtration curves (comparing those measured with sound to those without) also increases as the feed suspension concentration decreases, apparently due to the increased attenuation of sound as the proportion of solids in the feed is increased. At 5% v/v solids the effect of the ultrasound has disappeared, which is in precise agreement with the results obtained in a crossflow microfilter[3]. The underlying mechanism leading to this result is considered to be the sonically induced velocity imparted to the particles tangential to the filtering surface reducing their tendency to form a cake, but when they do so the particles pack to a higher density leading to a lower permeability cake (this is the mechanism observed previously in crossflow microfiltration[34]). This result is likely to be specific to the orientation of the sound field: if the field were normal to the filtering surface it is unlikely that any effects of the ultrasound would be observable, unless the feed were flocculated. In the case of a polyelectrolyte flocculated feed it has been shown that the specific resistance of the cake is increased and its the final moisture is reduced (Kowalska *et al.*[36]). However, in cases of polyelectrolyte flocculation the bulk volume of the filter cake is increased by floc formation, which is broken down by ultrasound. Such is not the case in the experiments in this work; although there is aggregation closer to the IEP, the size of the aggregates is rather smaller than would be expected if polyelectrolytes were used so little change in specific resistance caused by the sound field would be expected in the results reported here.

Electroacoustic Filtration

The effect of the application of combinations of electrical and acoustic fields on the filtration of 0.1% v/v rutile suspensions at pH 4, 8 and 10 is shown on Figures 6, 7 and 8 respectively. On Figures 6 and 7 the data are plotted as filtrate volume (V) versus filtration time (t), and on Figure 8 as t/V versus V. Figures 6 and 7 both indicate that use of the acoustic field with conventional filtration actually reduces the filtration rate slightly, whilst use of an electric field increases the filtration rate. When the electrical and acoustic fields are applied simultaneously, at pH 4 a substantial increase in flux is observed above that obtained with the electric field alone, as though there is a synergy working between the two force fields. At pH 8, the flux increase using the combined acoustic and electrical fields is much smaller. The reasons for this observed phenomenon could be several and are further investigated and discussed in the next section of this paper.

The form of plot on Figure 8 follows that often used to report conventional filtration data, from which an effective specific cake resistance can be calculated. Following the simplifications used by Yukawa *et al.*[6] and Wakeman[26] to derive a relationship for electrofiltration, a similar equation can be formed to include the effects of ultrasound. The result of modifying the classical filtration equation based on Darcy's law is simply expressed as:

$$\frac{dt}{dV} = \frac{\mu \alpha c^* V}{A^2 \Delta p} + \frac{\mu R}{A \Delta p} \qquad (3)$$

where c^* is the effective concentration of the feed suspension. In these experiments, the electrical and/or acoustic forces change the effective concentration of the suspension that actually forms the filter cake so that it is different from that which obtains in the slurry feed (as do gravitational effects in a conventional filtration of coarser particles onto upwards or downwards facing filter media). The pressure across the filter, Δp, is given by the sum of the pressure differences across the cake and the medium; this
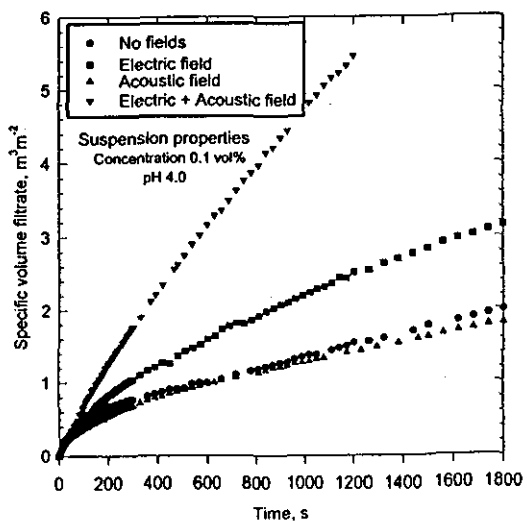

Figure 6. Effect of electric and acoustic field combinations on the filtration of pH 4 rutile suspensions of concentration 0.1% v/v. (Electric field strength 50 Vcm⁻¹, acoustic frequency 23 kHz.)
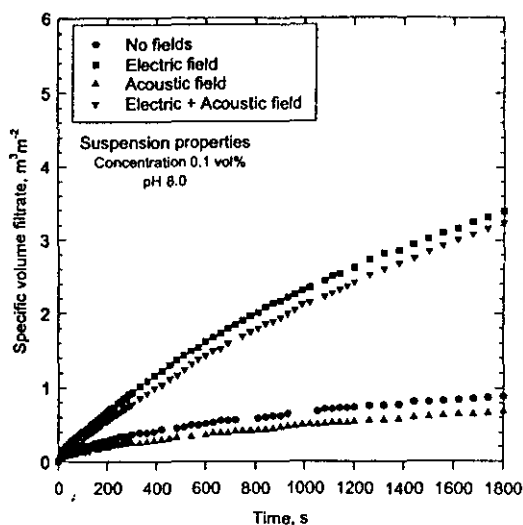
130   WAKEMAN and SMYTHE

Figure 7. Effect of electric and acoustic field combinations on the filtration of pH 8 rutile suspensions of concentration 0.1% v/v. (Electric field strength 50 Vcm^{-1}, acoustic frequency 23 kHz.)

includes contributions from the hydraulic (p_h), electro-osmotic (p_e) and acoustic (p_a) pressures, that is:

$$\Delta p = \Delta p_h + \Delta p_e + \Delta p_a \qquad (4)$$

The electroosmotic pressure difference arises from electro-osmotic flow of liquid through the filter medium and any cake or thickened suspension that is formed; assuming this and the acoustic pressure difference are small compared with the hydraulic pressure difference derived from the vacuum, Δp is constant to a first approximation and equation (3) can be integrated at constant pressure difference to give:

$$\frac{t}{V} = \frac{\alpha c^* \mu}{2 A^2 \Delta p} V + \frac{\mu R}{A \Delta p} = K_1 V + K_2 \qquad (5)$$
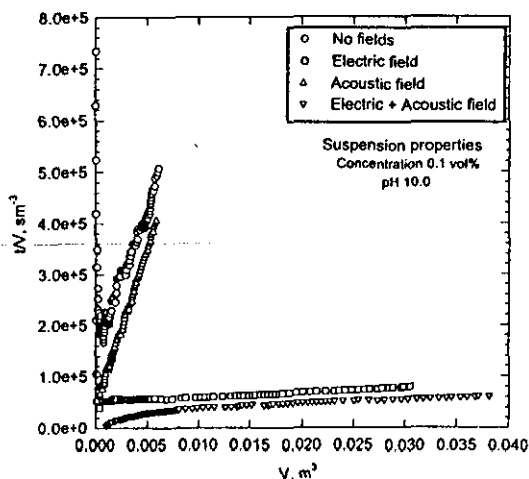
Figure 8. Plots of t/V vs V showing the effects of electric and acoustic fields and their combinations on the filtration of pH 10 rutile suspensions of concentration 0.1% v/v. (Electric field strength 50 Vcm^{-1}, acoustic frequency 23 kHz.)

A conventional t/V versus V plot of the data should there-fore yield a straight line with gradient K_1 and intercept K_2. Table 1 gives values for the gradient, K_1, of the data shown on Figures 6, 7 and 8; since K_1 is directly proportional to the product (αc^*), which may both vary with the applied fields, it provides an insight into how this parameter varies with the applied fields. The data in Table 1 show that whilst the application of fields to assist filtration does have an effect, the field combinations act differently at the pHs studied.

The porosity of the filter cakes formed is difficult to measure *in situ* and it is recognized that a porosity measured gravimetrically on the cake after formation may not be the same as that in the forming cake; nonetheless, a porosity measured at the end of filtration does give an indication as to whether different cake structures are likely to have developed. The porosities of the filter cakes formed are shown in Table 2. These data generally indicate that a cake formed in an acoustic field from better dispersed (higher pH) suspensions is more porous that one formed without any added fields, but as the pH moves closer to the IEP there is effect of ultrasound on cake porosity. The electric field causes formation of a more open cake structure at all pH values, and then combining the fields causes the cake to become less porous. At low pH, with no added fields, a higher porosity would be expected due to the particle aggregation; unlike in the work of Kowalska *et al.*[9,10,36] where polyelectrolyte flocculation was used, the porosity data here suggests that the ultrasound intensity used in the filter is not great enough to disperse the aggregates.

Figure 6 shows that there is no practical change in the filtrate flux when an acoustic field is applied, but that an electric field causes a considerable increase. A particularly curious result occurs when both electric and ultrasonic fields are applied simultaneously, as there appear to be considerable synergy between the two fields leading to a marked increase in flux. Such a synergy has been reported previously in deliquoring[2] and crossflow microfiltration[3] studies, but no explanation of the phenomenon was offered.

Comparison of Figure 7 with 6 indicates little synergy between the two fields at higher pH values. Suspensions at pH 8 are well dispersed, particle aggregation and settling do not occur and the large magnitude of zeta potential coupled with a lower critical field strength (relative to the applied field) means that strong electrokinetic effects are expected to be observed in both Figures 6 and 7. This is also reflected by the lower K_1 values in Table 1 when an electric field is applied. However, the same synergy is not observed between the two added fields on Figure 7. The data on Figure 8 at pH 10 also show little synergy between the

Table 1. The effect of electric and acoustic fields on the rate of filtration of 0.1% v/v rutile suspensions at $\Delta p = 75$ kPa.

	$K_1 \times 10^{-6}$ m^6 s^{-1}			
	pH 4	pH 6	pH 8	pH 10
No fields	13	10	57	56
Acoustic field (23 kHz)	14	20	40	62
Electric field (50 Vcm^{-1})	4	3	2	0.9
Electric and acoustic fields (50 Vcm^{-1}, 23 kHz)	0.4	2	2	0.8

FILTRATION OF FINE PARTICLE SUSPENSIONS AIDED BY ELECTRICAL AND ACOUSTIC FIELDS 131

Table 2. The effect of electric and acoustic fields on the porosity of cakes formed by filtration of 0.1% v/v rutile suspensions at $\Delta p = 75$ kPa.

	Cake porosity			
	pH 4	pH 6	pH 8	pH 10
No fields	0.68	0.58	0.59	0.62
Acoustic field (23 kHz)	0.69	0.61	0.71	0.67
Electric field (50 Vcm⁻¹)	0.77	0.81	0.76	0.74
Electric and acoustic fields (50 Vcm⁻¹, 23 kHz)	0.69	–	0.75	0.66

simultaneously applied fields. At pH 6, there was more synergy than at pHs 8 and 10 but not as much as at pH 4. The respective values of K_1 in Table 1 are indicative of this trend.

Taking into account previous work[26] it is reasonable to assume from Table 1 that the electric field reduced the specific résistance of the filter, due to induced electrophoretic velocities of the particles towards the anode together with electroosmotic flow through the membrane and any filter cake that has been formed. At pH 4 the acoustic field further reduced the specific resistance. A further variable requiring investigation is the different conductivities of the feed suspensions; at pH 4, 6, 8 and 10 these were 40, 15, 18 and 70 μS respectively. The data on Table 1 from the filtration experiments suggest that combinations of electrical and acoustic fields have a greater effect where the suspension conductivity is highest; this is further investigated below.

Energy Consumption

Energy consumption in separation processes must always be considered when taking a practical viewpoint; the consumptions corresponding to the experiments reported in Table 1 are shown in Table 3. Because of the differing filtrate flow rates obtained under different conditions, for comparative purposes it is most appropriate to look at specific energy consumption figures. These show that least energy is consumed by a conventional filtration (that is, by the pump) at all pH values; the addition of either field increases the energy consumed, with far and away the greatest amount taken by the ultrasonic field.

In making these comparisons, the increased filtrate rates also need to be considered as this affects either the time to accomplish the filtration of a given volume of suspension or the size of equipment required to achieve the separation. The corresponding flow rate data after 600 s of filtration are given in Table 4. The increased flux as a result of adding the fields is apparent, but also the data indicate that the electric field is more effective at increasing the flux than is the acoustic field. In some applications it may be acceptable to consider using the electric field as a way of shortening the filtration time, albeit with the penalty of an increased energy consumption. But for industrial use it is unlikely that ultrasound would be contemplated to increase filtration rates, with or without an electric field, as the penalty in higher energy consumption is likely to be always too high.

THE ELECTRO-ACOUSTIC SYNERGISM

The apparent synergy (see Table 4 and Figure 6, for example) between electrical and acoustic fields to enhance filtration requires explanation, particularly as it tends to show itself at lower, and to a lesser extent at higher, pH values. The literature indicates that conductivity changes of irradiated aqueous solutions are primarily due to the acoustic pressure inducing changes in the solvent viscosity, thermal effects due to the adiabatic compression-expansion cycle and the bulk compressibility of the medium (Jossinet *et al.*[37]). A decrease in the viscosity of a solution as it increases in temperature causes an increase in the ionic mobility. Ionic mobilities of electrolytes and particles are typically of the same order, so the electrolyte contribution is only significant if the electrolyte mass is

Table 3. Power consumption data for the experiments reported in Table 1; to provide comparable figures the filtrate rates after 600 s of filtration are used in data.

	Power consumption, W			
	pH 4	pH 6	pH 8	pH 10
No fields	0.8 + 0 + 0 = 0.8	0.9 + 0 + 0 = 0.9	0.3 + 0 + 0 = 0.3	0.2 + 0 + 0 = 0.2
Acoustic field (23 kHz)	0.8 + 275 + 0 = 275.8	0.6 + 275 + 0 = 275.6	0.2 + 275 + 0 = 275.2	0.3 + 275 + 0 = 275.3
Electric field (50 Vcm⁻¹)	1.3 + 0 + 3.2 = 4.5	0.8 + 0 + 5.5 = 6.3	0.9 + 0 + 3.5 = 4.4	0.9 + 0 + 4.4 = 5.3
Electric and acoustic fields (50 Vcm⁻¹, 23 kHz)	2.5 + 275 + 5.4 = 282.9	0.9 + 275 + 4.1 = 280	0.8 + 275 + 2.5 = 278.3	1.3 + 275 + 2.5 = 278.8

The data above show the contributions from each source of power consumption as:
(Pump energy + ultrasonic field + electric field)

	Power per unit volume of filtrate per unit area of filter, W/(m³ m⁻²) Specific energy consumption, kWh m⁻³							
	pH 4		pH 6		pH 8		pH 10	
No fields	0.8	0.02	0.8	0.02	0.6	0.02	0.6	0.02
Acoustic field (23 kHz)	281	7.5	372	10.0	834	22.3	626	16.8
Electric field (50 Vcm⁻¹)	2.8	0.08	4.7	0.13	2.7	0.08	3.3	0.09
Electric and acoustic fields (50 Vcm⁻¹, 23 kHz)	89.5	2.4	177	4.7	199	4.7	125	3.3

132   WAKEMAN and SMYTHE

Table 4. The filtrate flux averaged over the first 600 s of filtration for the experiments in Table 1.

	Average flux of filtrate up to 600 s, $m^3 m^{-2} h^{-1}$			
	pH 4	pH 6	pH 8	pH 10
No fields	5.88	6.72	2.94	1.98
Acoustic field (23 kHz)	5.88	4.44	1.98	2.64
Electric field (50 Vcm^{-1})	9.48	8.10	8.40	9.78
Electric and acoustic fields (50 Vcm^{-1}, 23 kHz)	18.96	9.48	9.60	13.38

comparable to the particle mass, thus in most cases the particles provide the dominant electroacoustic effect[18].

Results from irradiating solutions of various initial conductivities are shown in Figures 9 and 10 and indicate that the conductivity of electrolyte solutions increases the moment the solution is subjected to ultrasonic irradiation. The initial conductivity of the solution gives an indication of the magnitude of the conductivity change with the largest changes being shown for solutions with low initial conductivities (σ_0), irrespective of whether the solution is acidic or basic. For $\sigma_0 > 50 \mu S$, the magnitude of the change is small (below 10% increase in σ). The temperature increase over the period of each experiment was 4°C. As an approximation an increase in conductivity due to temperature causes a 2% increase per °C, thus an increase of 8% is likely over the duration of the experiment; this is shown in the figures by a broken line. While the solution is being irradiated the conductivity increase is much greater than 8%, but when irradiation is ceased the conductivity falls back to levels close to σ_0 and generally follows the temperature base line plotted. So the conductivity increase is not due solely to an increase in temperature of the solution. Figures 9 and 10 also show that the ionic species present affect the magnitude of the conductivity increase.

Figure 11 shows the results of the similar experiments using a 0.1% v/v suspension of rutile, dispersed using

Figure 10. Effect of periodic ultrasonic irradiation on NaOH solutions of different initial pH (and conductivity).

MIPA. The initial conductivity was again altered with HCl or NaOH. The effect of ultrasound on the conductivity appears to be similar. Increases in conductivity here are around 40% for σ_0 between 15 and 20 μS, which can be compared with 50 to 70% for HCl solutions and 20 to 30% for NaOH solutions.

The variation of the conductivity increase with pH is shown on Figure 12 for rutile suspensions and NaOH and HCl solutions, and with initial conductivity on Figure 13. At higher ionic strengths the double layer is compressed, and the percentage increase in conductivity is smallest. Compression of the double layer restricts movement of the diffuse cloud, and the particle and diffuse layer oscillate together. At low conductivities however, ultrasound is seen to increase the apparent conductivity
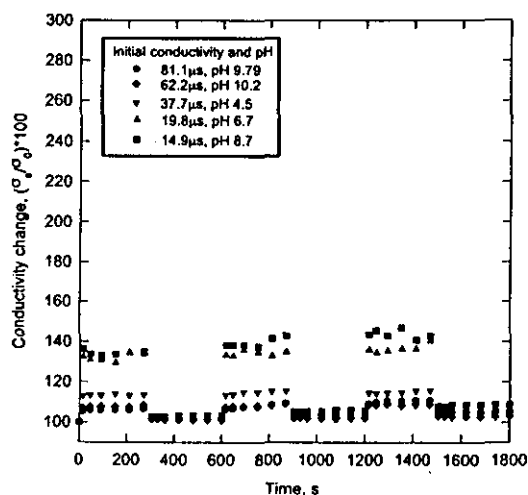
Figure 9. Effect of periodic ultrasonic irradiation on HCl solutions of different initial conductivity (and pH).

Figure 11. Effect of periodic ultrasonic irradiation on 0.1% v/v rutile suspensions of different initial conductivity (and pH), pH altered with HCl or NaOH.

FILTRATION OF FINE PARTICLE SUSPENSIONS AIDED BY ELECTRICAL AND ACOUSTIC FIELDS   133
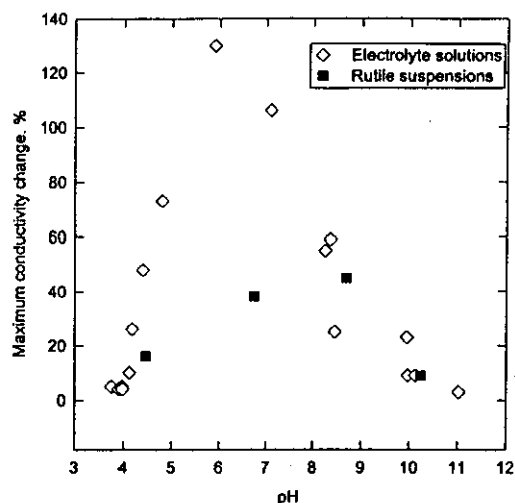

Figure 12. Relationship between the pH of a suspension and the maximum conductivity increase shown by that suspension when it is irradiated using a 23 kHz acoustic field.

approximately the same amount as for electrolyte solutions. This is because the diffuse layer is large and easily distorted and there is relative motion between the particle and the layer.

Cataldo[24] explains the increase in conductivity of electrolyte solutions by calculating the maximum temperatures and pressures inside bubbles at the point of collapse. The temperatures and pressures calculated are high, and the hot spot theory accounts for the high conductivities shown. The sonochemical effects of ultrasound have been well documented[38,39]. The 'hot spot' theory based on the collapse of cavitation bubbles provides a possible explanation of the conductivity effects seen. For an aqueous solution the maximum pressure and temperature inside the

Figure 13. Relationship between initial conductivity of a suspension and the maximum conductivity increase shown by that suspension when it is irradiated using a 23 kHz acoustic field.

collapsing bubble can be estimated using the following expressions[40]:

$$T_m = T_0 \left\{ \frac{P'(\gamma - 1)}{P_v} \right\} \tag{6}$$

$$P_m = P_v \left\{ \frac{P'(\gamma - 1)}{P_v} \right\}^{\left(\frac{\gamma}{\gamma - 1}\right)} \tag{7}$$

Values for T_m and P_m can be calculated for pure water and for electrolytes. The addition of colloidal particles to a solution will not significantly alter the vapour pressure, and values for T_m and P_m for an aqueous colloidal suspension will be similar to those for water. Addition of a solute, however, lowers the vapour pressure which raises T_m and P_m.

Using equations (15) and (16) for the systems in this work suggest values of for T_m and P_m of 3810°C and 980 atm respectively at the point of bubble collapse. The equations used by Cataldo[24] however are for transient cavitation (intensities greater than 10 Wcm^{-2}). For the lower intensity ultrasound used in this work stable cavitation is likely to be dominant (and was observed during the experiments. Under these conditions, cavitation bubbles oscillate about an equilibrium size for a number of cycles and the time for which they exist is sufficiently long for diffusive processes to take place. If mass transfer rates across the gas-liquid vapour interface are unequal, the bubble will grow and rectified diffusion occurs. The bubble may grow until it becomes unstable and collapses, but the violence of the implosion is less as the internal gases act as a cushion. The maximum temperature which develops in the bubble is much lower than for transient cavitation. The bubble may alternatively pass this point and grow until it becomes sufficiently buoyant to rise in the liquid, but this depends on the pressure amplitude of the acoustic wave.

Figures 12 and 13 show the effect of ionic strengths on this conductivity change. The changes are least at high ionic concentrations (extremes of pH). The ultrasound provides energy at the low concentrations for the dissociation of water. At higher ionic concentrations, the energy pushes the dissociation equilibrium in the opposite direction and the conductivity remains close to its initial value. At low initial conductivities the observed increase in conductivity enhances the electrophoretic migration velocity of the particles in an electric field and hence increases effects of the electric field across the filter.

The conductivity and the filtration characteristics measured in this work are properties of the bulk solution or suspension, but the preceding discussion is concerned with effects that arise as a result of phenomena taking place at or near the surface of the particles, making it essential to develop a model that examines the current carried by the ions in the double layer. It seems likely that the synergism is due to two main factors. Closer to the IEP, ultrasound causes the aggregates to disperse, reducing the effective particle size and increasing the mobility of the particles in the electric field. The electric field by itself does not seem to cause break-up of the aggregates. Far from the IEP, the particles are well dispersed and the double layer is compressed, the particles and diffuse layer oscillate together
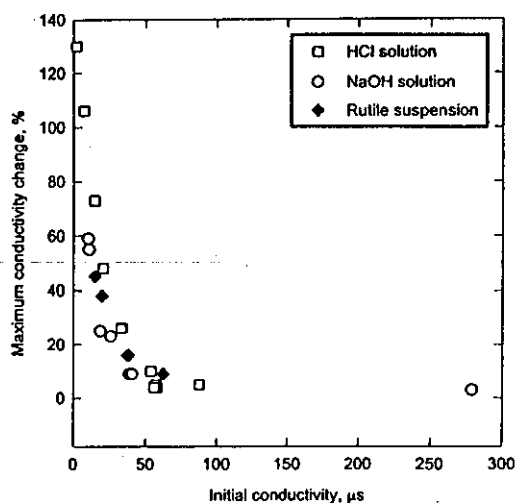
134   WAKEMAN and SMYTHE

in the ultrasonic field and the particles and diffuse layer
migrate together in the electric field.

γ   ratio of specific heats
μ   viscosity of the liquid, Pa s
ζ   zeta potential, V

CONCLUSIONS

Electrical and acoustic force fields can improve rates of
filtration, but the extent of improvement is dependent on
complex interactions between microscopic properties of the
constituents of the suspension and the macroscopic forces
applied. In some instances acoustic fields actually reduce
filtration rates. The experimental results show:

(i) Acoustic fields have little effect on filtration rates
close to the suspension isoelectric point, produce a minor
improvement in filtration rate at high pH, but have a
deleterious effect at intermediate pHs.

(ii) Electric fields enhance filtration rates, apparently
by *reducing the cake specific resistance; the extent of*
enhancement varies with the magnitude of the field applied.

(iii) Above a critical voltage gradient a constant rate of
filtration can be achieved, although once the suspension has
thickened too much immediately above the filter medium
the rate decreases.

(iv) Acoustic and electric fields applied simultaneously
produce an increased rate of filtration; synergy exists
between *the two fields closer to the IEP and at high pHs.*

(v) Both electric and acoustic fields tend to increase the
porosity of the filter cakes formed.

(vi) The power consumed by the ultrasonic field is not
sufficiently offset by increased performance of the filter,
making it unlikely that ultrasound would be a viable force
field to use to improve cake formation rates.

(vii) The power consumed by the electric field can offer
sufficiently large improvements in filtration rates that in
some cases it may be considered as a technical improvement
to filtration technology.

The conductivity of low conductivity solutions increases
when irradiated by ultrasound, but other phenomena occur
simultaneously. A possible explanation is offered for the
apparent synergy between electrical and ultrasonic fields,
based on dispersion effects closer to the isoelectric point
and compression of the double layer at pHs well away from
the IEP.

NOMENCLATURE

A	filtration area, m^2, or a coefficient (in equation (2))
B	coefficient in equation (2)
c^*	effective solids concentration in the feed suspension, $kg\ m^{-3}$
D	dielectric constant of the liquid phase
E_{cx}	critical electric field gradient, Vm^{-1}
F_z	primary radiation force acting on a particle on the axis from the transducer, N
K_1, K_2	constants in equation (5)
Δp	pressure difference over the filter, Pa
P	pressure, Pa
R	resistance of the filter medium, m^{-1}
t	time, s
T	temperature, K
v	electrophoretic velocity, ms^{-1}
V	filtrate, volume, m^3
z	axial distance from the acoustic transducer surface, m

Greek letters

α	specific resistance of the filter cake, $m\ kg^{-1}$
ε_0	permittivity of a vacuum, $C^2 J^{-1} m^{-1}$

REFERENCES

1. Muralidhara, H. S., 1994, Enhance separations with electricity, *Chemtech*, 5: 36.
2. Muralidhara, H. S., Parekh, B. and Senapati, N., 1985, Solid liquid separation process for fine particle suspensions by an electric and ultrasonic field, *US Patent 4,561,953.*
3. Wakeman, R. J. and Tarleton, E. S., 1991, An experimental study of electroacoustic crossflow microfiltration, *Chem Eng Res Des*, 69(5): 386.
4. Moulik, S. P., Cooper, F. C. and Bier, M., 1967, Forced-flow electrophoretic filtration of clay suspensions, *J Colloid Interface Sci*, 24(4): 427.
5. Moulik, S. P., 1971, Physical aspects of electrofiltration, *Env Sci and Technol*, 5(9): 771–776.
6. Yukawa, H., Kobayashi, K., Tsukui, Y., Yamano, S. and Iwata, M., 1976, Analysis of batch electrokinetic filtration, *J Chem Eng Japan*, 9(5): 396.
7. Yukawa, H., Yoshida, H., Kobayashi, K. and Hakoda, M., 1978, Electro-osmotic dewatering of sludge under condition of constant voltage, *J Chem Eng Japan*, 11(6): 475.
8. Wakeman, R. J., 1986, Electrofiltration- microfiltration plus electrophoresis, *The Chemical Engineer*, 426: 65.
9. Kowalska, E., Bien, J. and Zielewicz, E., 1978, The influence of ultrasound on the thickening of the sludge from some municipal and industrial wastes, *Acustica*, 40: 99.
10. Kowalska, E., Chmura, K. and Bien, J., 1978, Ultrasonics in the dehydration process of sludge, *Ultrasonics*, 16(4): 183.
11. Tarleton, E. S., 1988, How electric and ultrasonic fields assist membrane filtration, *Filtration and Separation*, 25(6): 402.
12. Yeager, E., Bugosh, J., Hovorka, F. and McMarty, J., 1949, The application of ultrasonic waves to the study or electrolytic solutions, *J Chem Phys*, 17: 411.
13. Heuter, T. F. and Bolt, R. H., 1955, *Sonics: Techniques for the Use of Sound and Ultrasound in Engineing and Science*, (J Wiley and Sons, New York).
14. O'Brien, R. W., 1988, Electro-acoustic effects in a dilute suspension of spherical particles, *J Fluid Mech*, 190: 71.
15. Debye, P., 1933, A method for the determination of the mass of electrolyte ions, *J Chem Phys*, 1: 13.
16. Enderby, J. A., 1951, On electrical effects due to sound waves in colloidal suspensions, *Proc Royal Soc A*, 207: 329.
17. Booth, F. and Enderby, J. A., 1952, On electrical effects due to sound waves in colloidal suspensions, *Proc Phys Soc A*, 65: 321.
18. O'Brien, R. W., 1990, The electroacoustic equations for a colloidal suspension, *J Fluid Mech*, 212: 81.
19. Cannon, D. W., Oja, T. and Petersen, G. L., 1985, A method for measuring the electrokinetic properties of a solution, *US Patent 4497207.*
20. O'Brien, R. W. and White, L. R., 1978, The electrophoretic mobility of a spherical colloidal particle, *J Chem Soc Faraday Trans*, 2 74: 1607.
21. Sherwood, J. D., 1980, The primary electroviscous effect in a suspension of spheres, *J Fluid Mech*, 101: 609.
22. Tarleton, E. S. and Wakeman, R. J., 1994, Understanding flux decline in crossflow microfiltration: Part III-Effects of membrane morphology, *Trans IChemE, Part A*, 72(A4): 521.
23. Wakeman, R. J., 1998, Electrically enhanced microfiltration of albumin suspensions, *Trans IChemE, Part C*, 76(C1): 53.
24. Cataldo, F., 1997, Effects of ultrasound on the electrolytic conductivity of simple halide salts, *J Electroanal Chem*, 431: 61.
25. Cataldo, F., 1998, Erratum to 'Effects of ultrasound on the electrolytic conductivity of simple halide salts', *J Electroanal Chem*, 445: 225.
26. Wakeman, R. J., 1982, Effects of solids concentration and pH on electrofiltration, *Filtration and Separation*, 19(4): 316.
27. Wakeman, R. J. and Tarleton, E. S., 1986, Membrane fouling prevention in crossflow microfiltration by the use of electric fields, *Chem Eng Sci*, 42: 829.
28. Wakeman, R. J. and Sabri, M. N., 1995, Utilizing pulsed electric fields in crossflow microfiltration of titania suspensions, *Trans IChemE, Part A*, 73(A4): 455.
29. Akay, G. and Wakeman, R. J., 1996, Electric field intensification of

FILTRATION OF FINE PARTICLE SUSPENSIONS AIDED BY ELECTRICAL AND ACOUSTIC FIELDS   135

surfactant mediated separation processes, *Trans IChemE, Part A*, 74(A): 517.

30. Akay, G. and Wakeman, R. J., 1997, Electric field enhanced crossflow microfiltration of hydrophobically modified water soluble polymers, *J Mem Sci*, 131: 229.

31. Woodside, S. M., Bowen, B. D. and Piret, J. M., 1997, Measurement of ultrasonic forces for particle-liquid separations, *AIChEJ*, 43: 1727.

32. Harker, A. H. and Temple, J. A. G., 1988, Velocity and attenuation of ultrasound in suspensions of particles in fluids, *J Phys D: Appl Phys*, 21: 1576.

33. Wakeman, R. J. and Bailey, A. J. L'., 1999, Sonothickening: Continuous in-line concentration/ clarification of fine particle suspensions by power ultrasound, *Trans IChemE*, (submitted).

34. Wakeman, R. J., 1994, Visualisation of cake formation in crossflow microfiltration, *Trans IChemE, Part A*, 72(A4): 530.

35. Yosioka, K. and Kawasima, Y., 1955, Acoustic radiation pressure on a compressible sphere, *Acustica*, 5: 167.

36. Kowalska, E., Kowalski, W. and Bien, J., 1979, Changes of some physical properties of sonated suspensions, *Acustica*, 43: 260.

37. Jossinet, J., Lavandier, B. and Cathignol, D., 1998, The phenomenology of acousto-electric interaction signals in aqueous solutions of electrolytes, *Ultrasonics*, 36: 607.

38. Suslick, K. S., 1988, *Ultrasound: Its Chemical, Physical and Biological Effects*, (VCH, Weinheim).

39. Mason, T. J., 1993, Sonochemistry: A technology for tomorrow, *Chem & Ind*, January, 47.

40. Mason, T. J. and Lorimer, J. P., 1988, *Sonochemistry: Theory, Applications and Uses of Ultrasound in Chemistry*, (Ellis Horwood, Chichester).

41. Bailey, A. J. L'. and Wakeman, R. J., 1998, Measurement of ultrasonically induced particle velocities in suspensions, *Proc 1998 IChemE research event, Newcastle-upon-Tyne* (The Institution of Chemical Engineers), CD Rom Rec No 9236, ISBN 0 85295 400X.

ACKNOWLEDGEMENTS

ADDRESS

Correspondence concerning this paper should be addressed to Professor R. J. Wakeman, Department of Chemical Engineering, Loughborough University, Loughborough, Leicestershire LE11 3TU, UK. (E-mail: R.J.Wakeman@lboro.ac.uk).

EXPERIMENTS ON ELECTROACOUSTIC VACUUM FILTRATION

M.C. Smythe and R.J. Wakeman
Dept. of Chemical Engineering, Loughborough University, Loughborough, UK

An experimental apparatus has been developed to study the effects of electric, acoustic and electroacoustic fields on filtration. The filter utilises an electrical force acting normal to the filtration surface, and an ultrasonic force acting tangentially.

Initial experiments have demonstrated that both acoustic and electric fields, used separately or in combination, increase the rate of filtration of TiO_2 suspensions that are close to their isoelectric point.

Keywords: electroacoustic, ultrasonic, electrofiltration, filtration

INTRODUCTION

Assisted separations have become more important in recent years as the demand for higher purity products has increased. In terms of filtration, the production of a drier cake is cost effective when compared with the energy costs of thermal drying Improvements to the filtration process have been demonstrated by the exploitation of phenomena such as electrokinetic, acoustic, magnetic, and centrifugal forces[1]. A combined fields approach enables limitations to the degree of separation, purity, and yield imposed by conventional filtration to be overcome. Electroacoustic dewatering (EAD) has been used as a means of dewatering sludges, producing a higher solids content than attainable using electric, or acoustic fields separately[2]. This technology has been extended to cross flow filtration[3]. The major cost of these technologies is electricity, but the cost is an order of magnitude less than evaporative drying, because preliminary liquid removal leads to smaller thermal energy requirements.

The use of electric fields to improve separations is a well known technology. The processes require continuous application of electric fields and as such are energy intensive. Electrofiltration has not been exploited, but recent advances in electrode materials have enabled the technology to be used both to improve filtrate flux, and as an alternative to backwashing as a method of membrane cleaning .

Ultrasonics has been shown by many authors to be a potentially economical means of removing water from products to relatively low levels, and to decrease fouling of membranes. It is implied however, that this is a dewatering, rather than a filtration technique, and thus the mechanisms proposed focus on how ultrasound affects suspension characteristics. It may be that the ultrasonic energy provides an additional driving force, in a similar way to an electric field. That is, ultrasound should be considered an aid to filtration, and by facilitating a more open cake may improve mass transfer through the filter medium.

EXPERIMENTATION

An experimental rig has been designed and built based on a conventional dead end vacuum filter (Figure 1). The filter medium support acts as a cathode. A variable position anode is suspended parallel to the support, and the separation distance can be varied. The electric field is thus applied normal to the filter surface. An ultrasonic transducer is attached to one side of the filter cell, and ultrasonic energy is applied tangentially to the filter surface. The filter medium used is a Sartorious 0.2μm cellulose nitrate membrane; this has a measured mean pore size of 0.51μm, a thickness of 130μm and is reported to carry a zero or negative surface charge over the pH range 2-12[4]. The test suspension used was uncoated rutile, which was dispersed using monoisopropanolamine (MIPA) at a concentration of 0.15% by weight on the

mass of TiO_2. The suspension was then homogenised for 8 minutes at 2000rpm and a Malvern Mastersizer was used to ensure a mean particle size of $0.3\mu m$.
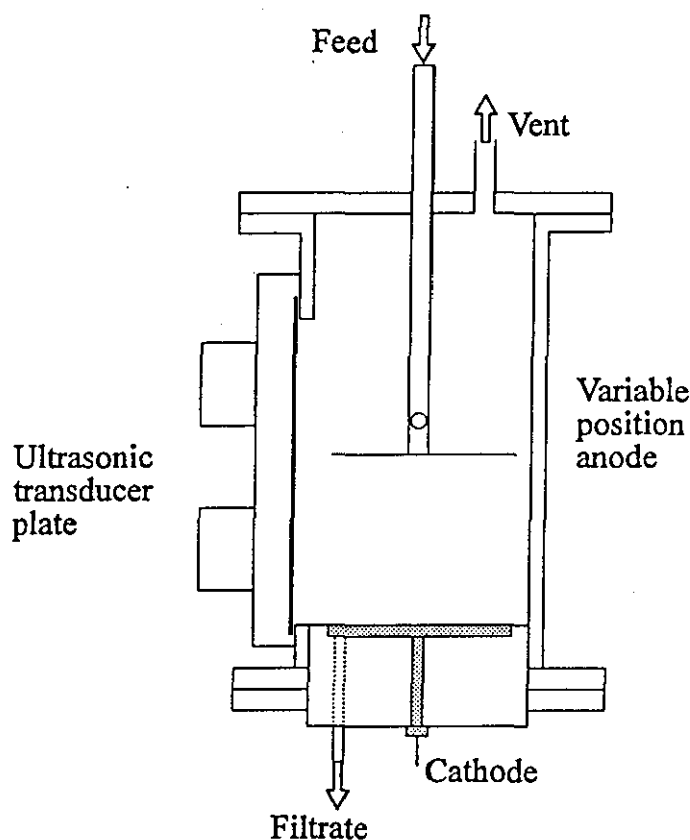

Figure 1: Filter cell schematic

The flow circuit (Figure 2) comprises a feed reservoir with recirculation pump to ensure the feed is completely mixed. The feed flows into the filter cell, and the pressure drop across the cell is monitored by pressure transducers. The system is controlled by a host computer which controls the vacuum held in the filtrate tank in order to control the pressure difference across the filter. Experimental runs were carried out at constant vacuum. The pressure drop across the cell was recorded and the filtrate volume collected is measured at different filtration times. Run lengths were between 30 and 60 minutes, as the initial effects of the fields are thought to be most significant. A typical filtered volume is approximately 2 litres. The DC power supply allows application of a constant, stabilised voltage across the electrodes. The field gradient can be changed from one experiment to the next by altering the separation distance between the electrodes, or by applying a different voltage. The ultrasonic transducer position cannot be altered, and the frequency is fixed at 23 kHz.
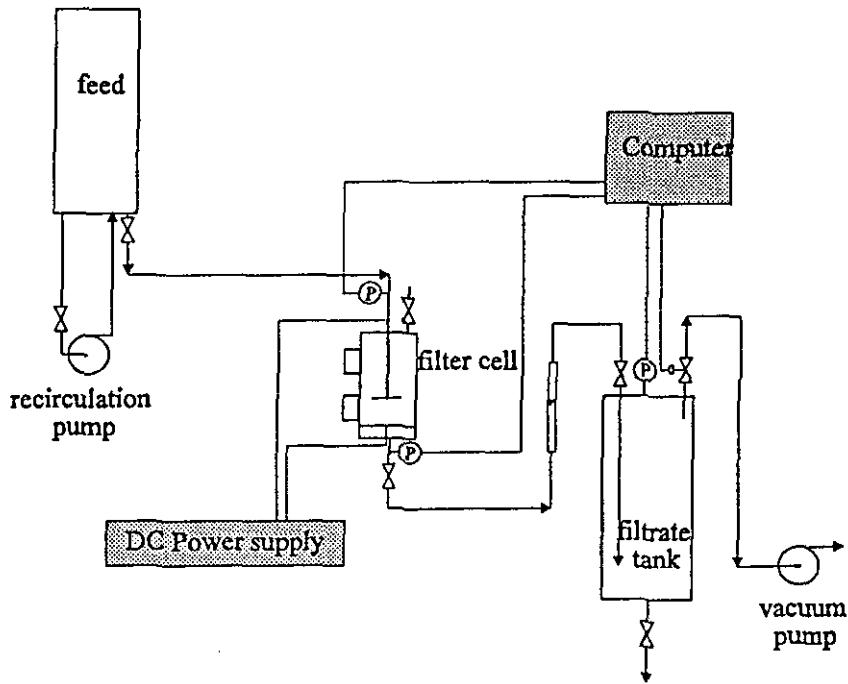
Figure 2: Experimental flowsheet

RESULTS AND DISCUSSION

The titanium dioxide suspension has been characterised for zeta potential variations with pH. The isoelectric point is clearly shown at a pH of around 7 which is similar to the 'natural' pH of the suspension.
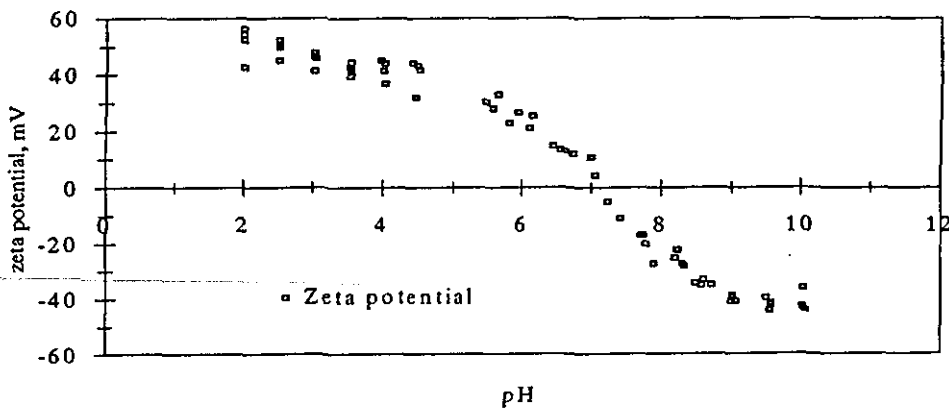

Figure 3: Suspension characterisation

A number of experiments have been carried out using electric and ultrasonic fields separately. To minimise the initial number of variables the pH of the suspension was kept at its natural value of 7.1. The suspension concentration was varied to establish the effect of particle concentration on the filter performance. A series of tests using the ultrasonic field as a filtration

aid were carried out. These results are compared with dead end vacuum filtration in Figure 4. The acoustic field is only seen to have a positive effect on filtration at very low concentrations. A volume concentration higher than 1% (4.2% by mass) shows little effect due to ultrasound, and a 5% suspension shows no effect. The higher particle concentrations cause increased attenuation as scattering losses increase; the majority of sound absorption is however due to the frictional losses caused by the viscosity of the suspending fluid[5]. The intensity of the sound wave is inversely related to the density of the medium it is travelling in. As the concentration is increased, either through a higher initial concentration or as the filtration progresses and the suspension thickens, the effect of the sound field diminishes, as seen in the figure below.
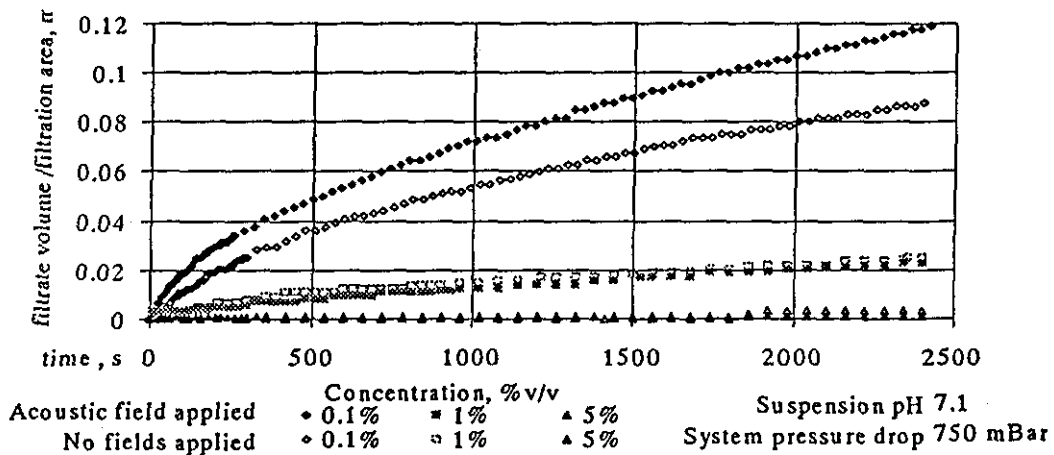
Figure 4: The effect of concentration on ultrasonic filtration performance

The principal concentration used for the remaining experiments is 0.1% by volume (0.42 % by mass). A series of electrically assisted filtrations have been carried out, varying the applied voltage and keeping the electrode separation distance constant at 1.5 cm. For the given concentration, the filter performance is improved by increasing the voltage across the electrodes. The 0V case is equivalent to conventional filtration and provides a base against which comparisons can be made. When an electric field is applied, the flow rate is higher than for conventional filtration. Electrophoresis reduces the rate of cake formation, and electroosmosis increases the filtrate flowrate. The cake resistance under an applied electric field can be expressed as [6,7]:

$$R_c = \alpha v_o \left(\frac{E_{CR} - E}{E_{CR}} \right) \frac{V}{A} \tag{1}$$

E_{CR} is the critical voltage where suspended particles become stationary because the electrophoretic velocity equals to the velocity of filtrate flow. As the voltage across the electrodes is increased, towards E_{CR} the filtration resistance of the cake tends to zero. The specific cake resistance produced decreases with increasing voltage difference. This is shown in Table 1.

Applied Voltage, V	Specific Cake Resistance, mkg^{-1}
0	$9.18x10^{12}$
30	$1.05 x10^{12}$
50	$0.75 x10^{12}$
70	$0.32 x10^{12}$

Table 1: Variation in specific cake resistance with voltage

The filtration rate is increased as shown in Figure 5. The increase in filtrate production rate is most encouraging as it is acheived with only a small potential on the surface of the particles (Figure 3). At a higher (or lower) pH greater filtrate rates could be expected at the voltages shown in figure 5.

Voltage across electrodes   ◆ 0V   ■ 30V   ▲ 50V   × 70V   Suspension pH 7.1
                                                            System pressure drop 750 mBar
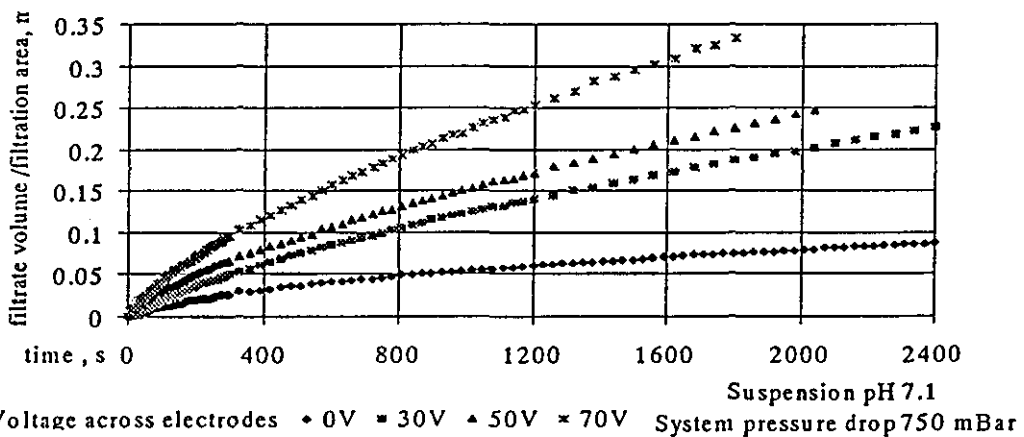
Figure 5: The effect of voltage on electrofiltration performance

Experiments have been carried out using a combination of electric and acoustic fields, and these show a slight improvement over the use of an electric field alone. A continued improvement is seen over the duration of the experiment.
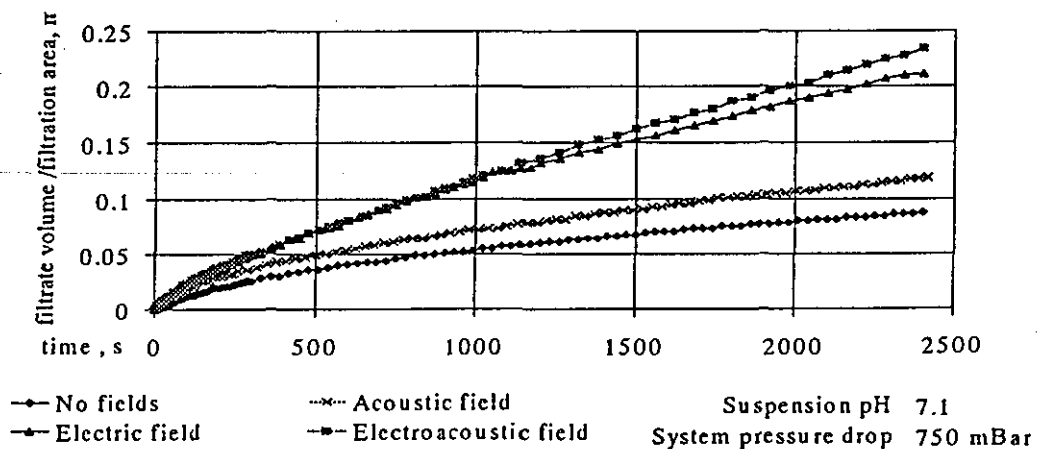

—◆— No fields   ---×--- Acoustic field   Suspension pH   7.1
—▲— Electric field   —■— Electroacoustic field   System pressure drop   750 mBar

Figure 6: The effect of field combinations on filtration performance.

CONCLUSION

An experimental vacuum filter has been developed which incorporates an electrical field acting in a direction normal to the filtering surface, and an acoustic field acting tangentially. The acoustic field appears to be effectively fully attenuated at a suspension concentration between 0.1 and 1%v/v, limiting its enhancement potential to the filtration of lower concentration fields. Nonetheless, this has practical significance because such lower concentration fields are often more difficult to filter due to their tendency to blind filter media.

The electric field is demonstrated to enhance greatly the rate of filtration, but this is at the expense of putting additional energy into the filter. It remains to be assessed as to whether or not, and for what conditions this added rate represents a rise or fall in energy consumption per unit volume of filtrate produced.

Evidence of synergy between the electric and acoustic fields has been found. However the experimental programme of variation of field combinations and suspension concentrations is to continue, with the programme being extended to encompass variation of other parameters such as system pressure drop, feed material and pH.

NOMENCLATURE

A	Filtration Area	m^2
E	Electric field strength	Vcm^{-1}
E_{CR}	Critical field strength	Vcm^{-1}
R_C	Filter cake resistance	mkg^{-1}
V	Filtrate Volume	m^3
α	Average specific filtration resistance	mkg^{-1}
υ_o	Dry cake mass per unit volume of filtrate	kgm^{-3}

REFERENCES
1. Muralidhara, H.S., 1994, Enhance separations with electricity, *Chemtech*, 5:36-41
2. Muralidhara, H.S. *et al*, 1985, Solid liquid separation process for fine particle suspensions by an electric and ultrasonic field. US Patent 4,561,953
3. Wakeman R.J., and Tarleton E.S., An experimental study of electroacoustic crossflow microfiltration, *Trans IChemE*, Part A,69:386-397
4. Tarleton E.S., Wakeman R.J.,1994, Understanding flux decline in crossflow microfiltration: Part III-Effects of membrane morphology, *Trans IChemE*, 72, Part A:521-529
5. Urick R.J., 1948, The absorption of sound in suspensions of irregular particles *J Acoust Soc Am*. 20 (3):283-288
6. Yukawa H., Studies of electrically enhanced sedimentation, filtration and dewatering processes. 1977, in R.J. Wakeman ed. *Progress in filtration and separation* Volume 1:83-112
7. Wakeman R.J., 1982, Effects of solids concentration and pH on electrofiltration , *Filtration and Separation*, 19:316-319

REFERENCES

Ahuja, A.S., Hendee W.R., 1978, Effects of particle shape and orientation on propagation of sound in suspensions, *J. Acoust. Soc. Am*, **63** (4)

Akay, G., Wakeman, R.J.,1996, Electric field intensification of surfactant mediated separation processes, *Trans IChemE*, **74** (A), 517

Allegra, J.R., Hawley, S.A., 1972, Attenuation of sound in suspensions and emulsions: Theory and Experiments, *J. Acoust. Soc. Am*, **51** (5:2)

Bailey, A.J.L'., Wakeman R.J., 1998, Measurement of ultrasonically induced particle velocities in suspensions, *IChemE research event abstracts*, 85

Beard, R.E., Muralidhara, H.S., 1985, Mechanistic considerations of acoustic dewatering techniques. Proceedings Ultrasonics symposium, 1072

Benes, E., Hager, F., Bolek, W., *et al*, 1991, Separation of dispersed particles by drifting ultrasonic resonance fields, 1991 Ultrasonics International conference, (UI91), *Ultrasonics international*, 167

Benes *et al* 1993, Method and apparatus for separating particles, U.S. Patent No. 5225089

Bernhardt, C., 1994, Dispersion of Solids in liquids, *In*: Particle size analysis:classification & sedimentation methods, Chapman & Hall, London.

Blake JR, Keen GS, Tong RP, *et al.*, 1999, Acoustic cavitation: the fluid dynamics of non-spherical bubbles Philos. T. Roy. Soc.,A **357**: (1751), 251

Blitz, J., 1971, Ultrasonics: Methods and applications, Butterworths, London

Blue, J.E., Mcleroy, E.G., 1968, Attenuation of sound in suspensions and gels, *J.Acoust. Soc. Am.*, **44**

Bolt, R.H., Heuter T.F., 1955,*Sonics*, John Wiley & Sons Inc., NY,

Bratby, J., 1980, Colloids and Interfaces, *In:* Coagulation and Flocculation, Uplands Press Ltd.

Brown, B., Goodman, J.E. 1965, Magnetostrictive and piezo electric transducers in high intensity ultrasonics, Iliffe books Ltd, London

Cannon, D.W., Oja, T., Petersen G.L., 1985, A method for measuring the electrokinetic properties of a suspension, U.S. Patent No. 4497207

Cataldo, F., 1997, Effects of ultrasound on the electrolytic conductivity of simple halide salts, *J. Electroanalytical Chem.* **431**, 61

Cataldo, F., 1998, Erratum to "Effects of ultrasound on the electrolytic conductivity of simple halide salts, *J. Electroanalytical Chem.* **431** 1997, pp 61-65", *J. Electroanalytical Chem.* **445**, 225

Chauhan, S.P., Muralidhara, H.S., Senapati, N., 1986, A technical note on electroacoustic dewatering, Battelle Columbus

Chou K.H., Lee, P.S., Shaw, D.T., 1981, Aerosol agglomeration in high intensity acoustic fields, *J. Coll. Int. Sci,* **83** (2),

Chow, J.C.F., 1964, Attenuation of acoustical aves in dilute emulsions and suspensions, J. Acoust. Soc. Am., **36**, 2395

Crum, L.A., 1984, Acoustic cavitation series. 5. Rectified diffusion, *Ultrasonics*, **22** (5), 215

Dassie, G., Reali, M., 1996, Dynamics of an oscillating spherical gas/vapor bubble, *J.Acoust. Soc. Am.*, **100** (5),3088

Davis, M.C., 1979, Attenuation of sound in highly concentrated suspensions and emulsions, *J. Acoust. Soc. Am*, **65** (2)

Debye, P., 1933, A method for the determination of the mass of electrolyte ions, *J. Chem. Phys.*, **1**, 13

Enderby, J.A., 1951,On electrical effects due to sound waves in colloidal suspensions, *Proc. Roy. Soc.*, **A207**, 329

Epstein P.S., Carhart, R.R., 1953, The absorption of sound in suspensions and emulsions. I. Water fog in air, *J.Acoust. Soc. Am.*, **20**, 553

Fairbanks, H.V. 1973, Use of ultrasound to increase filtration rate, Presented at the International Ultrasonics conference, London,

Fairbanks, H.V., Cheng, W.I., 1969, Influence of ultrasonics upon liquid flow through porous media, *Ultrasonics,*

Fairbanks, H.V., Morton, W., Wallis J., 1986, Separation processes aided by ultrasound, *Filtration and Separation*

Gooberman, G.L., 1968, Ultrasonics theory and application, English Universities Press,

Gor'kov L.P., 1962, On the forces acting on a small particle in an acoustical field in an ideal fluid, *Soviet Physics Doklady*, **6** (9), 773

Gregory, J., 1993, The role of colloid interactions in solid-liquid separation, *Env. Sci. Tech*, **27** (10),

Hager, F., Benes, E., 1991, A summary of all forces acting on spherical particles in a sound field, Ultrasonics International 91 Conference Proceedings, 283

Hall, D.E., Acoustics: A preliminary acquaintance, _In_: Basic Acoustics, Krieger Pub. Co., Florida, 1993

Hamaker, H.C., 1937,The London-van der waals attraction between spherical particles, _Physica_, **4**,

Hänel, R., Mues, A., Sobotta, R., 1996, Description of ultrasound transducers through wave parameters, _Ultrasonics_, **34**,

Harker A.H., Temple J.A.G., 1988, Velocity and attenuation of ultrasound in suspensions of particles in fluids, _J.Phys. D: Appl. Phys._, **21**,

Higashitani, K., Fukushima, M., Matsuno, Y., 1981, Migration of suspended particles in plane stationary ultrasonic field, _Chem. Eng. Sci_, **36** (12),

Hunter, R.J., 1993, Introduction to modern colloid science, Oxford U.P., New York,

Hunter,R. J., 1981, Zeta potential in colloid science: principles and applications London:Academic Press,

Jossinet, J., Lavandier, B., Cathignol, D., 1998, The phenomenology of acousto-electric interaction signals in aqueous solutions of electrolytes, _Ultrasonics_, **36**, 607

King, L.V., 1934, On the acoustic radiation pressure on spheres, _Proc. Roy. Soc. A._, **147**, 212

Kinsler, L.E., Frey, A.R., Fundamentals of Acoustics, John Wiley & Sons, 1962

Kinsler, L.E., Frey, A.R., Coppers, A.B., Sanders, J.V.,The acoustic wave equation and simple solutions, _In_ : Fundamentals of Acoustics, Third Edition, John Wiley & Sons, 1982

Kowalska, Bién, J., Zielewicz, E., 1978, The influence of ultrasound on the thickening of the sludge from some municipal and industrial wastes, _Acustica_, 40,99

Kowalska, E., Kowalski, W., Bien, J., 1979, Changes of some physical properties of sonated suspensions, _Acustica_, **43**, 260

Lamb, H., 1945, Hydrodynamics, Sixth Edition, Cambridge U.P.,

Lee, C.H., Gidaspow, D., Wasan, D.T., 1980, Cross-flow electrofilter for nonaqueous slurries, _Ind. Eng. Chem. Fundam._, **19**,

Majmudar A.A., Manohar, C., 1994, Electrophoretic separation of dilute TiO_2 suspension, _Separation science and Technology_, **29** (7),

Marchant, J.Q., The crossflow microfiltration of concentrated titania dispersions, PhD thesis, Loughborough university, UK, 1999

Mason, T.J., Paniwynk, L., Lorimer, J.P., 1996, The uses of ultrasound in food technology, _Ultrasonics sonochemistry_, **3**,

Mason, T.J.,Cordemans, E.D., 1996, Ultrasonic intensification of chemical processing and related operations, _Trans IChemE_, **74** (A), 511

Matsumoto, Y., Miwa, T., Nakao, S. Kimura, S., 1996, Improvement of membrane permeation performance by ultrasonic microfiltration, _J. Chem. Eng. Japan_, **29** (4),

Moulik, S.P., Cooper, F.C., Bier, M., 1967, Forced flow electrofiltration of clay suspensions, J.Coll. Int. Sci., 24,427

Moulik, S.P., Physical aspects of electrofiltration, 1971, _Env. Sci & Tech._ **5** (9), 771

Muralidhara, H.S., 1985, The combined fields approach to separations, Chemtech, 229

Muralidhara, H.S., Senapati, N., Parekh, B.K., 1985, Solid-liquid separation process for fine particle suspensions by an electric and ultrasonic field, U.S. Patent No. 4561953,

Muralidhara, H.S., Ensminger, D., Putnam, A., 1985, Acoustic dewatering and drying (low and high frequency) :state of the art review, _Drying Technology_, **3** (4), 529

Muralidhara H.S., Senapati, N., Beard, R.B., 1986, A novel electroacoustic separation process for fine particle suspenaions, _In:_ Editor H.S. Muralidhara, Advances in solid liquid separation, Battelle Press, 335

Muralidhara, H.S., Beard, R.B., Senapati, N., 1987, Mechanisms of ultrasonic agglomeration for dewatering colloid suspensions, _Filtration and Separation_,

Muralidhara, H.S., 1994, Enhance separations with electricity, _Chemtech_, 36

Nadh Jagannah, S., Muralidhara, H.S., 1996, Electrokinetics methods to control membrane fouling, _Ind. Eng. Chem. Res._, **35**,1133

Neppiras, E.A., 1980, Acoustic Cavitation, _Physics Reports (Review section of Physics letters)_, **61** (3),159

O'Brien R.W., 1990, The electroacoustic equations for a colloidal suspension _J. Fluid Mech._, **212**,

O'Brien R.W., White, L.R., 1978, The electrophoretic mobility of a spherical colloidal particle, _J.Chem. Soc. Faraday Trans. 2_, **74**, 1607

O'Brien, R.W., 1988, Electro-acoustic effects in a dilute suspension of spherical particles, _J. Fluid Mech._, **190**,

Ohl, C.D., Kurz, T., Geisler, R., *et al.*, 1999, Bubble dynamics, shock waves and sonoluminescence, *Philos. T. Roy. Soc.*, **A 357**: (1751), 269

Prosperetti, A., 1997, A new mechanism for sonoluminescence, *J.Acoust. Soc. Am.*, **101** (4), 2003

Rushton, A., Hosseini, M., Hassan, I., 1978, The effects of velocity and concentration on filter cake resistance, *Proc. Symp. on solid-liquid separation practice*, Yorkshire Branch of IchemE.

Scott Fogler, 1971, Recent advances in sonochemical engineering, *Chem. Eng. Progr. Symposium series*, **67** (109)

Sewell, C.T.J., 1910, On the extinction of sound in a viscous atmosphere by small obstacles of cylindrical and spherical form, *Phil. Trans. Roy. Soc. London*, **210**, 239

Shaw D.J. 1992, Charged interfaces, *In*: Introduction to colloid and surface chemistry, Fourth Edition, Butterworth Heinemann,

Shaw D.T. 1978, Acoustic agglomeration of Aerosols *In*: Ed. D.T. Shaw, Recent developments in aerosol science, Wiley Press,

Sollner, K., 1950, Colloidal effects of ultrasonics, Ultrasonic symposium series No. 1, 28

Suslick, K.S., 1989, The chemical effects of ultrasound, *Sci. Am.*, **260** (2),80

Svarovsky L., 1981, Solid-liquid separation, 2nd ed, Butterworths monographs in chemistry and chemical engineering, London:Butterworths,

Tarleton, E.S, 1986, A study of electrically assisted microfiltration, PhD Thesis, Exeter University, UK

Tarleton, E.S, Wakeman, R.J., 1988, Prevention of Flux Decline in Electrical Microfiltration, *Int. J. Drying Technol.*, 6(3), 547.

Tarleton, E.S., 1988, How electric and ultrasonic fields assist membrane filtration, *Filtration & Separation*, 402

Tarleton, E.S., 1988, The Influence of Electric Fields and Ultrasound on the Membrane Filtration of Aqueous Colloidal Suspensions, Filtr. and Sepn, 25(6), 402.

Tarleton, E.S., Wakeman, R.J., 1990, Microfiltration enhancement by electrical and ultrasonic force fields, Filtration & Separation, 192

Tarleton, E.S., 1992, The Role of Field Assisted Techniques in Solid/Liquid Separation, Filtr. and Sepn, 29(3), 246.

Tarleton, E.S., Wakeman, R.J., 1992, Electroacoustic Crossflow Microfiltration, *Filtr. and Sepn*, 29(5), 425.

Tarleton, E.S., Wakeman, R.J., 1994, Understanding flux decline in crossflow microfiltration: Part III Effect of membrane morphology, Trans. IChemE, 72 (4),521

Tarleton , E.S., Willmer S.A., 1997, The effects of scale up and process parameters in cake filtration, Chem. Eng. Res. Des., 75 (A5), 497

Telsonic Ltd, Personal Communication, 1999

Temkin, S., 1981, Elements of Acoustics, John Wiley & Sons, NY,

Tiller, F.M., Crump, J.R., 1977, Solid-liquid separation: An overview, Chem. Eng. Prin., 65

Urick R.J., 1948, The absorption of sound in suspensions of irregular particles, *J. Acoust. Soc. Am.*, 20 (3),

Urick R.J., 1975, Principles of underwater sound for engineers, Revised edition, McGraw Hill Inc.,

Wakeman, R.J. and Holdich, R.G., 1982, The Use of Electrical Measurements to Elucidate the Theory of Gravity Thickening, *Proceedings 271st EFCE Event Symposium on Water Filtration*, Koninklijke Vlaamse Ingenieursvereniging, Antwerp, 6.47.

Wakeman, R.J., 1982, Effects of solids concentration and pH on electrofiltration, *Filtration & Separation,*

Wakeman, R.J., 1986, Electrofiltration: microfiltration plus electrophoresis, *Chemical Engineer*, 65

Wakeman, R.J. , Tarleton, E.S., 1986, Experiments Using Electricity to Prevent Fouling in Membrane Filtration, *Filtration and Separation*, 23(3), 174

Wakeman, R.J. ,Tarleton, E.S., 1986, Modelling Crossflow Electro- and Micro-Filtrations, *Proceedings 4th World Filtration Congress*, Technologisch Instituut-Koninklijke Vlaamse Ingenieusvereniging , Ostend, 11.1 .

Wakeman, R.J., Tarleton, E.S., 1987, Membrane Fouling Prevention in Crossflow Microfiltration by the Use of Electric Fields, *Chem. Engng Sci.*, 42(4), 829.

Wakeman, R.J., Tarleton, E.S., 1991, An Experimental Study of Electroacoustic Crossflow Microfiltration, Trans Instn Chem. Engrs , 69 (A), 386.

Wakeman, R.J., Bailey, A.J.L'., 2000, Sonothickening: Continuous in line concentration/clarification of fine particle suspensions by power ultrasound, *Chem. Eng. Res & Design*, **78** (4),651

Wiersema, P.H., Loeb, A.L., Overbeek, J.TH.G., 1966, Calculation of the electrophoretic mobility of a spherical colloid particle, *J.Coll. Int. Sci.*, **22**,

Wilson, Introduction to theory and design of sonar transducers, Peninsula publishing, 1988

Woodside, S.M., Bowen, B.D., Piret, J.M., 1997, Measurement of ultrasonic forces for particle-liquid separations, *AIChE Journal*, **43** (7), 1727

WPA, 1999,Walden Precision Apparatus Ltd, The Old Station, Linton, Cambridge, CB1 6NW, Personal communication with Peter R Watson.

Yosioka, K., Kawasima, Y., 1955, Acoustic radiation pressure on a compressible sphere, *Acustica*, **3**,167

Young, F. R., 1989, Cavitation, London:McGraw-Hill,

Yukawa, H., Yoshida, H., Kobayashi, K., Hakoda, M., 1976, Fundamental study on electroosmotic dewatering of sludge at constant electric current, *J. Chem. Eng. Japan*, **9** (5), 402

Yukawa H., Yoshida, H., Kabayashi, K, Hakoda, M., 1978, Electro-osmotic dewatering of sludge under conditions of constant voltage, *J. Chem. Eng. Japan*, **11** (6), 475

Yukawa, H., Kobayashi, K., Yoshida, H., Iwata, M., 1979, Studies of electrically enhanced sedimentation, filtration and dewatering processes, *In:* Editor R.J. Wakeman, Progress in filtration and separation, Volume 1, Elsevier, Amsterdam, 83

Zana R., Yeager, E.B., 1982, Ultrasonic vibration potentials In: Editors J.O'M Bockris, B.E. Conway, R.E. White, *Modern aspects of electrochemistry*, **14**, Plenum Press, NY & London,